DEVELOPMENT OF NOVEL POLYMERIC CARRIERS FOR GENE THERAPY

A Thesis Submitted to
the Graduate School of
İzmir Institute of Technology
in Partial Fulfillments of the Requirements for the Degree of

DOCTOR OF PHILOSOPHY

in Bioengineering

by
Aykut ZELÇAK

June, 2021

İZMİR

ACKNOWLEDGMENTS

Firstly, I would like to express my sincere gratitude to my supervisor Prof. Dr. Volga BULMUŞ for her valuable advice and important comments. Her scientific knowledge and guidance made this study possible.

I acknowledge Council of Higher Education for funding me in abroad through YOK-YUDAB scholarship and The Scientific and Technological Research Council of Turkey (TUBITAK) for funding our work (the grant# 115R301).

I sincerely thank Prof. Dr. Tom DAVIS for inviting me to MIPS (Monash Institute of Pharmacy and Pharmaceutical Sciences) and for supporting me, Dr. Kristian KEMPE for having me in his group, Dr. Meike LEISKE and Dr. Joshua McCARROLL for their support and help. I thank to KEMPE group members and CBNS (The ARC Centre of Excellence in Bio-Nano Science and Technology) staff and students.

I also would like to thank my committee members Prof. Dr. Gülgün OKTAY and Assoc. Prof. Dr. Ayben TOP for their support and Assoc. Prof. Dr. Gülistan MEŞE and Yağmur Ünal for PCR experiments.

I would like to thank to the staff of Biotechnology and Bioengineering Application and Research Centre, Evrim PAŞIK, Yekta GÜNAY OĞUZ, Dane RUSÇUKLU, and Özgür YILMAZER, and the staff of The Center for Materials Research (CMR).

I thank to my labmates, Gürbüz DURSUN, Damla TAYKOZ, Cansu SÖYLEMEZ, Aysel TOMAK, Ecem ÖNAL, Alper ULUBAŞ, Şebnem KILIÇ for their friendships.

Lastly, I would like to extend my endless appreciations and thanks to my family. I am grateful to them for everything. I dedicate this thesis to my mother Nebahat ZELÇAK for her limitless love, support, and kind help.

ABSTRACT

DEVELOPMENT OF NOVEL POLYMERIC CARRIERS FOR GENE THERAPY

The development of effective delivery systems is a limiting step in gene therapy. In this work, new linear block copolymers and star polymers were synthesized, and their siRNA delivery abilities were investigated. For this aim, diblock copolymers consisting of alternative "stealth" polymer blocks (PEG, P(OEGMA) (Poly(oligo(ethylene glycol) methyl ether methacrylate)) or P(OEtOxMA) (Poly(oligo(2-ethyl-2-oxazoline) methacrylate))); and same cationic polymer block (P(AEAEMA) (Poly(2-((2-aminoethyl)amino)ethyl methacrylate))), have been prepared via RAFT polymerization or combination of CROP and RAFT polymerizations. Additionally, to demonstrate the effect of polymeric architecture, P(OEGMA)/P(AEAEMA) miktoarm star polymers have also been synthesized via RAFT polymerization. Polymers were characterized by SEC, NMR and DLS.

siRNA complexation was investigated by gel electrophoresis, DLS, SEM and TEM. Compared to star polymers, linear block copolymers could bind the siRNA molecules easier and tighter due to their more flexible natures and sterically accessible amine groups. The diameter of star polymer-siRNA complexes at N/P of 50 was found to be approximately 20 nm. Compared to this, linear block copolymers formed smaller particles (≈ 10 nm) at the same N/P ratio. The viability of linear block copolymer-treated cells was found to be 50% or better at the polymer concentration of 5 μM. In contrast, star polymers showed more detrimental effects at the same polymer concentrations. P(OEGMA)$_{43}$-*b*-P(AEAEMA)$_{45}$-siRNA complexes at N/P of 50 were taken up by 63.5% and 74.1% of H460 and MDA-MB-231 cells, respectively. In contrast, P(AEAEMA)$_{40}$-*b*-P(OEtOxMA)$_{38}$ complexes showed much lower uptake profile at the same conditions. Remarkably, P(OEGMA)$_{43}$-*b*-P(AEAEMA)$_{45}$-siRNA complexes showed potent gene silencing effect on MDA-MB-231 cells as shown by luciferase and RT-qPCR assays. Overall, it has been found that "stealth" polymers and polymeric architecture have a very significant effect on siRNA delivery.

ÖZET

GEN TERAPİSİ İÇİN YENİ POLİMERİK TAŞIYICILARIN GELİŞTİRİLMESİ

Etkili taşıyıcı sistemlerinin geliştirilmesi, gen terapisinde sınırlayıcı bir adımdır. Bu çalışmada, yeni lineer blok kopolimerler ve yıldız polimerler sentezlenmiş ve bunların siRNA taşıma yetenekleri araştırılmıştır. Bu amaçla, PEG, P(OEGMA) (Poli(oligo(etilen glikol)metil eter metakrilat)) veya P(OEtOxMA) (Poli(oligo(2-etil-2-oksazolin) metakrilat)) gibi alternatif "gizli" polimer bloklardan ve aynı P(AEAEMA) (Poli(2-((2-aminoetil)amino)etil metakrilat)) katyonik polimer bloğundan oluşan diblok kopolimerler, RAFT polimerizasyonu veya CROP ve RAFT polimerizasyonlarının kombinasyonu yoluyla hazırlanmıştır. Ek olarak, polimer mimarisinin etkisini göstermek için, P (OEGMA) / P (AEAEMA) miktoarm yıldız polimerleri de RAFT polimerizasyonu yoluyla sentezlenmiştir. Polimerler SEC, NMR ve DLS ile karakterize edilmiştir.

siRNA kompleks oluşumu jel elektroforezi, DLS, SEM ve TEM ile araştırılmıştır. Yıldız polimerlere kıyasla lineer blok kopolimerler, daha esnek yapıları ve sterik olarak erişilebilir amin grupları nedeniyle siRNA moleküllerini daha kolay ve daha sıkı bağlayabilmişlerdir. Yıldız polimer-siRNA komplekslerinin çapı N/P 50'de yaklaşık olarak 20 nm olarak bulunmuştur. Buna kıyasla, lineer blok kopolimer-siRNA kompleksleri aynı N/P oranında daha küçük yapılar (<10 nm) oluşturmuştur. 5 μM polimer konsantrasyonunda lineer blok kopolimer ile muamele edilmiş hücrelerin canlılığı %50 veya daha iyi olarak bulunmuştur. Buna karşılık, yıldız polimerler aynı polimer konsantrasyonlarında daha zararlı etkiler göstermiştir. $P(OEGMA)_{43}$-*b*-$P(AEAEMA)_{45}$-siRNA kompleksleri sırasıyla H460 ve MDA-MB-231 hücrelerinin %63,5 ve %74,1'i tarafından alınmıştır. Buna karşın, $P(AEAEMA)_{40}$-*b*-$P(OEtOxMA)_{38}$ kompleksleri aynı koşullarda çok daha düşük alım profili göstermiştir. Önemli olarak, $P(OEGMA)_{43}$-*b*-$P(AEAEMA)_{45}$-siRNA kompleksleri, lusiferaz ve RT-qPCR deneyleriyle gösterildiği üzere MDA-MB-231 hücreleri üzerinde güçlü bir gen susturma etkisi göstermiştir. Genel olarak, "gizli" polimerlerin ve polimer mimarisinin siRNA taşınımı üzerinde çok önemli bir etkiye sahip olduğu görülmüştür.

TABLE OF CONTENT

LIST OF FIGURES

Figure **Page**

Figure **Page**

Figure **Page**

Figure **Page**

Figure **Page**

Figure **Page**

Figure **Page**

LIST OF TABLES

Table **Page**

CHAPTER 1

INTRODUCTION

Nucleic acid therapeutics are an emerging class of medicines that can be used in the treatment of genetic, neurodegenerative, or viral diseases as well as cancer. However, for the successful clinical applications, these macromolecules often require rationally designed delivery systems. With the advancement of material science and molecular biology, the delivery problems have been solved for the treatment of some diseases and target organs and these therapeutics have already taken an important place in the market. On the other hand, there are still many diseases that cannot be treated with the current delivery systems due to the limited accessibility/applicability of these platforms to the most other target tissues/organs. The development of new and alternative systems is still the major goal in gene therapy.

As in many biomedical applications, polymers play an important role in drug delivery as well. These materials are often preferable delivery systems as they are versatile, can easily be modified and tailored for desired purposes. Starting from 1990s, modification of nanoparticles with stealth polymers such as PEG or preparation of PEG-drug conjugates have been a solid strategy to increase the stability and blood circulation time of the parent drugs or nanoparticles. However, the intense usage of PEG in cosmetics, food and drug industries have led to increase in immunogenic effects and formation of anti-PEG antibodies against PEG-containing formulations. Moreover, PEG is known to trigger hypersensitivity on some occasions. Since this scenario can get even worse in the near future, the investigation of PEG-alternatives and demonstration of the biological effects of other stealth polymers are crucial for the field of drug delivery. Although P(OEGMA) (Poly(oligo(ethylene glycol) methyl ether methacrylate)) and Poly(2-oxazoline)s (POx) are prominent stealth polymers, their biological behavior and usability in gene delivery are still not as well reported as PEG.

Beside linear polymer blocks, it has become easier to prepare more sophisticated and complex structures with the advancement of RDRP (Reversible-Deactivation Radical Polymerization) techniques. Polymers with star architecture in example, could be easily

synthesized via these techniques thereby, the polymer toolbox in gene delivery have expanded. The unique structures of star-shaped polymers offer unique biological effects. The low viscosity, good solubility and other unique physicochemical properties of these well-defined structures make them competitive compared to their linear counterparts. The successful gene delivery applications of star polymers in recent years have exhibited the potential of these systems.

In this thesis, novel polymeric carriers with varying stealth polymer blocks or architectures have been prepared and their siRNA delivery potential has been evaluated *in vitro*. For this aim, diblock copolymers consisting of alternative stealth polymer blocks (PEG, P(OEGMA) or P(OEtOxMA) (Poly(oligo(2-ethyl-2-oxazoline) methacrylate))); and same cationic polymer block (P(AEAEMA) (Poly(2-((2-aminoethyl)amino)ethyl methacrylate))), have been prepared via RAFT (Reversible Addition-Fragmentation Chain Transfer) polymerization or combination of CROP (Cationic Ring-Opening Polymerization) and RAFT polymerizations. Additionally, to demonstrate the effect of polymeric architecture, P(OEGMA)/P(AEAEMA) miktoarm star polymers have also been synthesized via RAFT polymerization. As a cationic and endosome disruptive polymer block, P(AEAEMA) has been chosen as this novel structure was shown to be a viable alternative to gold standard PEI in our previous studies. Commonly used stealth polymer PEG or PEG alternatives; comb-type (brush) PEG (P(OEGMA)) or P(EtOxMA), have also been incorporated to polymeric structures to particularly increase the biocompatibility and stability of the prepared systems. The polymers have been characterized using analytics like SEC (Size Exclusion Chromatography), NMR (Nuclear Magnetic Resonance Spectroscopy) and DLS (Dynamic Light Scattering).

siRNA delivery potential of the prepared polymers has been determined by various in vitro assays. Because of its broad therapeutic potential and successful clinical translation, siRNA has been chosen as the nucleic acid drug. The siRNA complex formation ability of the polymers was investigated using gel retardation assay. The size, morphology, and surface charge of polymer-siRNA complexes (polyplexes) has been determined by DLS, SEM (Scanning Electron Microscopy), TEM (Transmission Electron Microscopy) and ELS (Electrophoretic Light Scattering). The release of siRNA has been investigated by heparin competition assay. Serum stability of the complexes was examined by gel electrophoresis. Cytotoxicity of the polymers were determined via MTT assay. The cell association, uptake, and intracellular distribution of the polymers or

polyplexes was investigated by FACS (Fluorescence-Activated Cell Sorting) and CLSM (Confocal Laser Scanning Microscopy). Last of all, gene silencing efficiency of the formulations was determined by luciferase assay and RT-qPCR (Quantitative Reverse Transcription PCR). Overall, this study reports the preparation of various block copolymers (PEG-*b*-P(AEAEMA), P(OEGMA)-*b*-P(AEAEMA) and P(AEAEMA)-*b*-P(EtOxMA)) and miktoarm star polymers (P(OEGMA)/P(AEAEMA)), investigates the siRNA delivery potential of these newly synthesized polymers, discusses the effect of stealth polymers and polymeric architecture on siRNA delivery.

CHAPTER 2

LITERATURE REVIEW

2.1. Gene Therapy

Gene therapy is a relatively new class of treatment that mainly aims at the replacement of defective genes with their functional copies, the introduction of new genes or suppression the pathological genes to treat diseases (Dunbar et al., 2018). Theoretically, many inherited disorders or non-hereditary diseases can be treated by manipulating/introducing genetic materials. While gene therapy has tremendous potential at the clinical stage, the development of successful therapies is extremely challenging due to low efficacy or safety concerns (Dunbar et al., 2018; Vandamme, Adjali, & Mingozzi, 2017). Nevertheless, discoveries, and progress in genetics and material sciences have enabled the successful clinical translation of some of these new therapeutics (Akinc et al., 2019; de Paula Brandão, Titze-de-Almeida, & Titze-de-Almeida, 2020; Prasad, 2018; Wood, 2018).

Modified adeno-associated viruses (AAV) and retroviruses are the very first gene delivery systems that have been used to facilitate the transfection of human somatic cells (Kotterman, Chalberg, & Schaffer, 2015). Although these viral systems mediate the addition of a gene of interest, they cannot edit or alter the defective gene. In contrast, some other recently discovered strategies allow gene ablation and correction and offer a new way of genome editing (Reyon et al., 2012). As an example, clustered regularly interspace short palindromic repeat-CRISPR associated 9 (CRISPR-Cas 9) nucleases technology has enabled a very simple way of genome editing by employing specific short guide RNAs designed against the DNA of interest. Due to simplicity and potential applicability, CRISPR-Cas 9 opened a new window in genome editing (Cong et al., 2013; Doudna & Charpentier, 2014). However, ethical reasons and the potential unknown effects such as off-targeting and immunogenicity may complicate the clinical translation of this new technology (Brokowski & Adli, 2019; Chew et al., 2016).

RNA interference (RNAi), antisense oligonucleotides and ribozymes are some other tools of gene therapy which can be utilized to suppress the expression of a gene of interest (Dias & Stein, 2002; Doherty & Doudna, 2001; Hannon, 2002). Among these gene silencing technologies, RNAi stands out as a safer and effective technique which generally employs rationally designed 21-23 base pair double stranded RNA (dsRNA) molecules namely small (or short) interfering RNAs (siRNAs). Artificially designed siRNAs can trigger a cellular machinery which already exists in the mammalian cells and eventually lead to the reduction in target gene expression (Reynolds et al., 2004). Compared to existing and more recently discovered techniques, RNAi is simple, less complicated, effective, and well-developed technology presenting the huge potential for the treatment of many different diseases in a safe manner. Indeed, the less complex nature of RNAi mechanism and strategic advances in drug delivery has led to the approval of several siRNA drugs by Food and Drug Administration (FDA) and with the FDA approval, RNAi is now a proven technology (Garber, 2018; Ledford, 2018).

The increase in the number of FDA approved gene therapy products has shown the potential of gene therapy in therapeutic applications (Byrne, Cullinan, Mintzes, & Smith, 2020; F. Wang, Zuroske, & Watts, 2020). Despite these rapid technological developments, the major goal in gene therapy remains to be same: safe and effective delivery of these nucleic acid-based drugs to the target tissues (Dunbar et al., 2018).

Table 2.1. List of FDA approved siRNA drugs.

Drug	**Brand Name**	**Carrier System**	**Target disease**	**Company**	**Approved Year (Reference)**
Patisiran	Onpattro	Lipid Nanoparticle	hereditary transthyretin-mediated amyloidosis (hATTR)	Alnylam	2018 (Ledford, 2018)
Givosiran	Givlaari	GalNAc conjugate	Acute hepatic porphyria (AHP)	Alnylam	2019 (Scott, 2020)

(cont. on next page)

Table 2.1. (Cont.)

Lumasiran	Oxlumo	GalNAc conjugate	primary hyperoxaluria type 1	Alnylam	2020 (F. Wang et al., 2020)
Inclisiran	Leqvio	GalNAc conjugate	hypercholesterolemia	Novartis-Alnylam	Late stage- EU Approved (Byrne et al., 2020)

2.1.2. siRNA Mediated Gene Silencing

The discovery of RNAs that can interfere with gene expression has led to tremendous progress in gene function research and therapeutical applications. RNAi has been identified by Andrew Fire and Craig Mello and the researchers have received the Nobel Prize for Physiology or Medicine in 2006 (Bernards, 2006). Fire et al. have discovered that injection of double stranded RNA molecules leads to "specific and potent interference" in *Caenorhabditis elegans* (Fire et al., 1998). Previous and later studies have revealed that post transcriptional gene silencing is a naturally existing, evolutionary conserved mechanism and can be observed in many organisms such as fungi, plants, and animals (Gheysen & Vanholme, 2007; Gordon & Waterhouse, 2007; Romano & Macino, 1992). Subsequent research in the field of RNAi has demonstrated that double stranded long RNA molecules are processed by a specific endonuclease and this leads to the formation of shorter RNA fragments (Zamore, Tuschl, Sharp, & Bartel, 2000). With the addition of more research, the biochemical players of RNAi have been identified and the mechanism of RNAi has been understood in details (Bernstein, Caudy, Hammond, & Hannon, 2001; Hannon, 2002) (Figure 2.1).

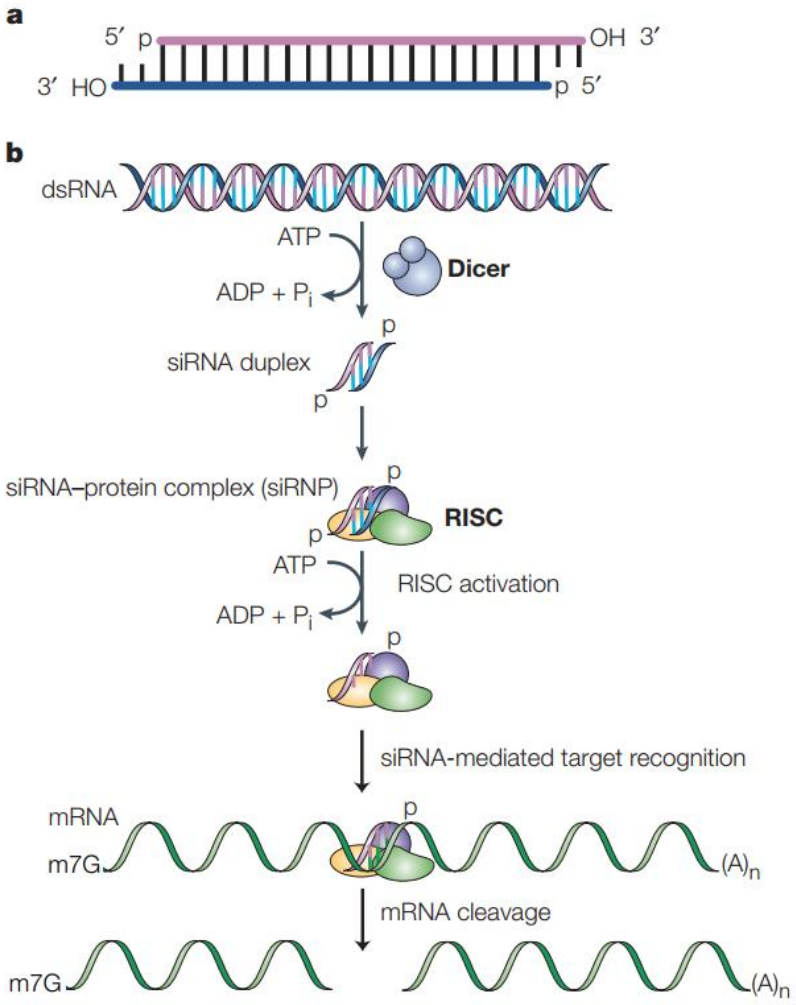

Figure 2.1. The schematic structure of siRNA (a) and the mechanism of siRNA induced gene silencing (b).
(Source: Dykxhoorn, Novina, & Sharp, 2003)

The first step of RNAi, in case siRNA is not delivered exogenously, is a cleavage of long dsRNA molecules by Dicer. Dicer is an endonuclease, an RNase III enzyme, which very characteristically can cleave the dsRNA molecules into shorter fragments. Formed shorter (21-23 nucleotides) dsRNA molecules, siRNAs, typically have unpaired two nucleotides at 3 prime end (overhangs) and 5'-phosphate (Dykxhoorn, Novina, & Sharp, 2003). Dicer is shown to have dsRNA-binding domain, an RNA helicase domain and two RNase III motifs (Bass, 2000). Dicer does not only take the role in the formation of siRNAs, but it also can process hairpin RNAs (longer RNA molecules having loop structure) in a similar fashion (Grishok et al., 2001). In addition, research has revealed that RNA molecules processed by Dicer are incorporated to RNA-induced silencing

complex (RISC) system more efficiently compared to unprocessed RNA molecules (Hutvágner & Zamore, 2002). Moreover, Dicer processing is believed to facilitate the correct strand selection (antisense strand) later on (Snead et al., 2013). However, it is known that Dicer processing is not mandatory for the RNAi mechanism. Small siRNAs or analogs can bypass the Dicer processing and can be incorporated to RISC with the help of TAR RNA binding protein (TRBP) (Cifuentes et al., 2010; H. Y. Lee, Zhou, Smith, Noland, & Doudna, 2013). Importantly, bypassing the Dicer process provides researchers with the opportunity to substantially modify the entire siRNA molecules for desired purposes (Parmar et al., 2016).

siRNAs that undergo via Dicer-mediated or non-Dicer-mediated pathways binds to a protein complex consisting of Ago2 (Argonaute 2), TRBP and RHA (RNA helicase A) and forms RISC (Robb & Rana, 2007; Setten, Rossi, & Han, 2019) (Figure 2.2). It has been found that 5' phosphate is essential for the RISC loading and RNAi activity (Lima et al., 2012; Nykänen, Haley, & Zamore, 2001). Indeed, siRNAs that have no phosphate at 5' were found to be phosphorylated with the help of a kinase (Schwarz, Hutvágner, Haley, & Zamore, 2002). RISC is activated with the selection of one of the strands of double stranded siRNA. Both strands of siRNA (sense or antisense) can be incorporated into the RISC however, it is known that the driving force behind the strand selection is thermodynamic stability (Khvorova, Reynolds, & Jayasena, 2003). Therefore, rational design of siRNA sequences can allow the correct strand (antisense strand) incorporation to the RISC and can eliminate the off-target effects (Reynolds et al., 2004). It has been shown that the weaker base pairing at 5' end potentially increases the RISC loading possibility for that strand (Khvorova et al., 2003). In other words, siRNA sequence with more adenine and uracil bases at 5' end will be preferably selected for the RISC. Notably, in addition to the nucleotide composition, the different modifications and design strategies were shown to have a significant effect on strand selection (Setten et al., 2019). Sano et al. have examined the effect of siRNAs with (a)symmetric blunt ends or overhangs and they have found that siRNA with 2 nucleotides overhangs on 3' antisense strand and blunt end (no overhang) at 3'sense strand decreased the gene expression more compared to standard siRNA with 2 nucleotides overhang at each 3' end (Sano et al., 2008). Together with some other reports, this work indicates that overhangs at 3' end antisense strand are highly desirable for potent gene silencing and terminal end groups play an important role in strand selection (Hohjoh, 2004; Vermeulen et al., 2005).

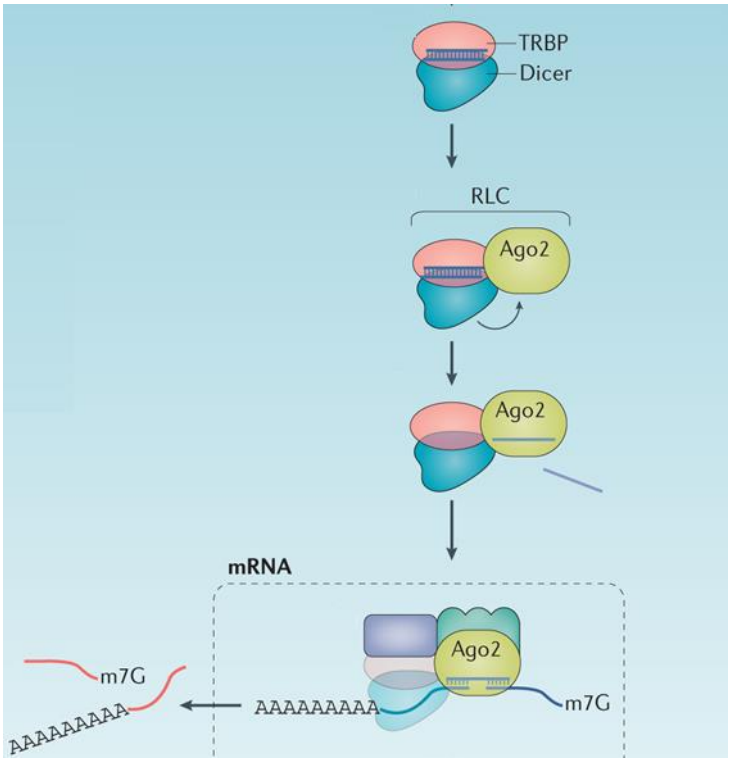

Figure 2.2. The binding of siRNA to RNAi proteins, TRBP and Dicer, and subsequent degradation of target mRNA.
(Source: Setten et al., 2019)

Ago2 is one of the most important enzymes taking the role in RNAi and it is responsible for the cleavage of target mRNA in mammals (J. Liu et al., 2004). Ago2 is known to be bound to the guide strand (antisense strand) at 5' and contact the backbone (Ipsaro & Joshua-Tor, 2015; Y. Wang et al., 2009). Also, PAZ domain of Ago2 binds to 3' hydroxyl (Ipsaro & Joshua-Tor, 2015; Y. Wang et al., 2009). Together with TRBP, Ago2 also requires double-stranded A-form RNA for efficient binding (Rettig & Behlke, 2012). Therefore, any modification performed on siRNA structure might affect the RISC loading efficiency (Dowdy, 2017). In addition to catalytic activity, Argonaute proteins have significant roles in increasing the binding stability and finding the correct target (Chandradoss, Schirle, Szczepaniak, MacRae, & Joo, 2015). Salomon et al. have shown that these proteins organize the bases of the guide strand so that they show high binding affinity to the target sequence (Salomon, Jolly, Moore, Zamore, & Serebrov, 2015). The authors have pointed out that Argonautes change the classical nucleic acid hybridization into a different interaction so that guide strand loaded RISC behaves more like RNA-

binding protein rather than free nucleic acid looking for its complementary sequence (Salomon et al., 2015). This brings potent silencing ability and specificity to RNAi mechanism.

The seed region of guide strand siRNA (2-8 nucleotides from 5' end) display perfect base pairing with the target mRNA sequence (Lewis, Burge, & Bartel, 2005). Upon guide strand-target mRNA hybridization, the cleavage of target mRNA occurs between 10^{th} and 11^{th} nucleotides from the 5' end of the guide siRNA strand (Elbashir, Lendeckel, & Tuschl, 2001).

Theoretically any endogenous mRNA displaying a full match with the seed region (consisting of seven nucleotides) of siRNA's guide strand can potentially be silenced with the introduced siRNAs. Although this situation raises questions about the specificity of siRNA drugs, it has been known that the successful Ago2 dicing activity requires more extensive base pairing (Song, Smith, Hannon, & Joshua-Tor, 2004). Nevertheless, off-target effects seem to be a major problem among other concerns (Janas et al., 2018; Setten et al., 2019; Zlatev et al., 2018). Janas et al. have investigated the liver toxicity profile of GalNac-conjugated siRNAs at exaggerated doses in the rat (Janas et al., 2018). They have evaluated the hepatotoxicity of different siRNAs with the same chemical modifications and found out that siRNAs show different hepatotoxicity even though a comparable amount of siRNAs have been found in the liver and RISC in each case. Moreover, they have shown that changing the sequence of seed region, blocking the RISC loading process or the activity of loaded RISC have altered the observed toxicity profile. Collectively, their results indicate that the major reason for hepatotoxicity is not the chemical modifications on siRNA or saturation of RNAi machinery but sequence-related off-targeting (Janas et al., 2018). Another reason supporting the off-target concerns is the potential miRNA-like behavior of siRNAs. It was shown that RISC-loaded siRNAs can trigger translational repression even in the case of partial base pairing (Birmingham et al., 2006; Jackson et al., 2003; Jackson et al., 2006).

The chemical modifications, carrier systems and their degradation products are other factors that can potentially lead to toxicity (Janas et al., 2018; Setten et al., 2019; Zuckerman & Davis, 2015). Research has shown that modifications might heavily contribute to in vitro and in vivo toxicity profiles (Crooke, Wang, Vickers, Shen, & Liang, 2017; Frazier, 2015). Especially in the case of single stranded oligonucleotides it was shown that heavy phosphorothioate modifications may result in non-specific protein

binding (Liang, Sun, Shen, & Crooke, 2015). The interaction of chemical entities with cellular proteins may damage the structure and function of the protein and eventually lead to toxicity (Liang et al., 2015).

Accumulation of introduced siRNAs in unintended tissues could result in toxicity as well. Although it is known that the knock-down of many genes such as MYC transcription factor can have positive effects in tumor cells, it creates undesired side effects in healthy cells (Soucek et al., 2013). This situation prevents many genes from being used as targets. It has been stated that this issue can be eliminated with the active targeting of desired tissue, selecting only disease-related genes as targets, or choosing appropriate drug administration routes (Setten et al., 2019).

siRNAs longer than 30 bp might lead to immunogenic reactions (Setten et al., 2019). Protein Kinase R (PKR), Toll-like receptor 3 (TLR3) and TLR7 can sense the siRNAs and activation of innate immunity can eventually lead to non-specific toxicity (D.-H. Kim et al., 2005; Kleinman et al., 2008). On the other hand, siRNAs shorter than 15 bp can bypass the RISC loading process (Setten et al., 2019). However, it has been reported that using appropriately modified ~21 nt siRNA greatly helps to overcome the immunogenicity problem (Robbins et al., 2007). Often, 2′ ribose sugar of siRNA is modified to 2′-O-methyl (O-Me), 2′-fluoro (F), 2′-methoxyethyl (MOE) or 2′,4′ locked nucleic acid (LNA) to decrease the immunogenicity and/or increase the stability against nucleases (Dowdy, 2017) (Figure 2.3). The native phosphodiester backbone of siRNA is also commonly modified to phosphorothioate (PS), phosphotriester, morpholino and peptide nucleic acid to cover (shield) the charge of siRNA and/or increase the hydrophobicity (Iwamoto et al., 2017; Nielsen, Egholm, & Buchardt, 1994).

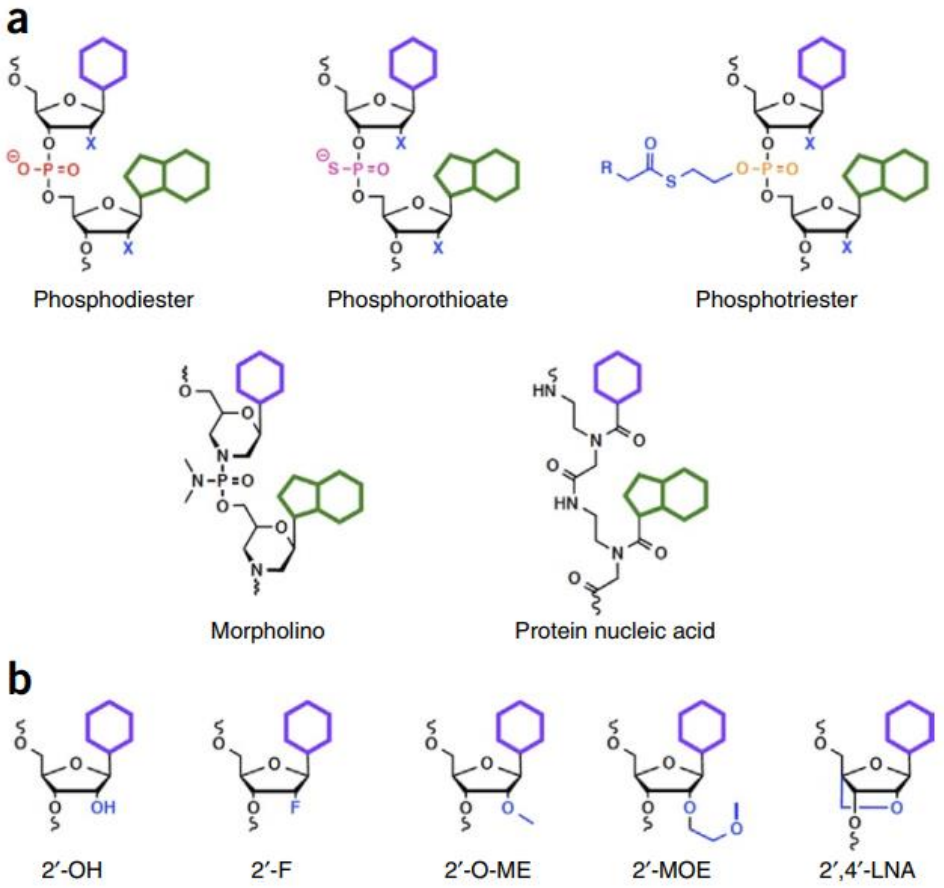

Figure 2.3. Modifications commonly used in siRNA phosphate backbone (a) and 2′ ribose sugar (b).

(Source: Dowdy, 2017)

Since RNAi machinery requires a defined siRNA structure, any modification made on siRNA might affect the gene silencing potency. Early efforts have shown that 2′-O-Me modifications could reduce the immunogenicity while keeping the gene silencing activity at similar levels; however, serum stability of siRNA was still found to be low (Collingwood et al., 2008). Later, it was found that serum protection can be achieved when 2′-F modification was employed together with 2′-O-Me (Bramsen et al., 2009; Khvorova & Watts, 2017). Researchers at Alnylam Pharmaceuticals have developed the enhanced stability chemistry (ESC) which utilizes PS backbone at the ends of siRNA and defined 2′-F and 2′-O-Me modifications along with the sense and antisense sequence. It has been reported that these defined modifications lead to a very large reduction in the introduced siRNA doses (Nair et al., 2017; Ray et al., 2017; Willoughby et al., 2018). Moreover, the duration of siRNA activity was found to be improved due to

enhanced stability and potency (Nair et al., 2017; Ray et al., 2017; Willoughby et al., 2018).

Dowdy and his colleagues have introduced siRNA with phosphotriester backbone, namely, short-interfering ribonucleic neutral (siRNN) molecules, which lacks the negative charges coming from the native phosphodiester backbone (Hamil & Dowdy, 2016; Meade et al., 2014). siRNN has been reported to be converted into siRNA thanks to intracellular enzymes. The authors have stated that this strategy could be used to mask the negative charge of siRNA which ultimately results in the longer systemic circulation, higher stability, and robust RNAi activity (Hamil & Dowdy, 2016; Meade et al., 2014).

2.2. Cellular Barriers and Nanoparticle-Cell Interactions

Effective siRNA therapies require overcoming many hurdles, both physically and biologically (Figure 2.4). These nucleic acid drugs face with several problems such as shear stress, rapid elimination, protein adsorption (Wilhelm et al., 2016). The administration route, target disease, target organ/tissue and patient itself are the factors that generally affects the extent of these problems (Blanco, Shen, & Ferrari, 2015). Local administration can avoid some of these problems however not all parts of biological systems are accessible, and this type of delivery require invasive procedures (Gehr & Zellner, 2019). In contrast, systemic administration is more favorable since it enables the introduction of nanoparticles directly to the bloodstream.

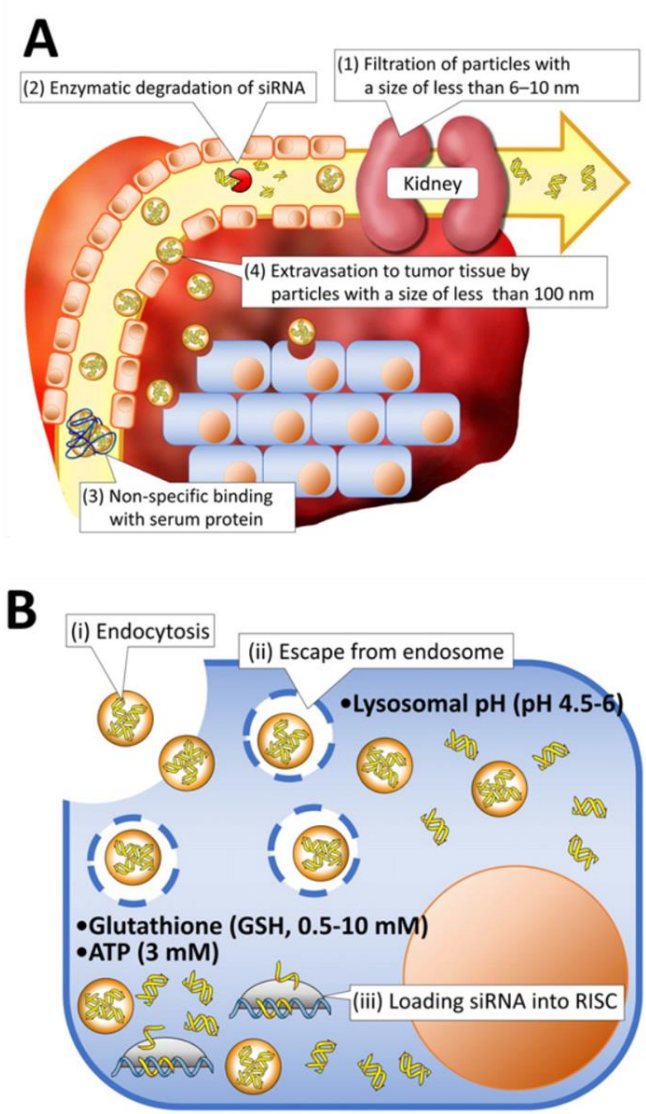

Figure 2.4. Extracellular (A) and intracellular (B) barriers in siRNA delivery. (Source: Kim et al, 2016)

Different from small drug molecules, nucleic acid drugs are large (approximately 14 kDa), hydrophilic, and strongly negatively charged molecules which necessitates a special handling. These molecules are susceptible to nuclease degradation and cannot be taken up by cells without a delivery system or special modification. Additionally, small size of siRNAs (length = 7nm, diameter = 2 nm) result in rapid elimination through kidney glomeruli upon administration (S. Gao et al., 2009; Schroeder, Levins, Cortez, Langer, & Anderson, 2010). Whereas, nanoparticles with a size of 10-100 nm can avoid rapid renal clearance and additionally provide enhanced accumulation in the tumor cells via so called enhanced permeability and retention (EPR) effect (Matsumura & Maeda, 1986). However

it is reported that nanoparticles larger than 200 nm can activate the complement system (Hoshyar, Gray, Han, & Bao, 2016). Cationic particles tend to interact with serum proteins and lipids which eventually result in rapid elimination from the circulation. Whereas neutral or slightly negatively charged nanoparticles are retained in the circulation for longer periods (Blanco et al., 2015; Kou et al., 2018). Large particles are known to orient to the vessel walls in a higher extent than smaller ones (Cooley et al., 2018). Ellipse- and rod-like structures can localize to blood vessels better than the spherical particles (Da Silva-Candal et al., 2019; Uhl, Gao, Zhou, & Liu, 2018). Stiff nanoparticles are known to be removed by mononuclear phagocytic system (MPS) more rapidly (Key et al., 2015).

MPS interaction not only result in the liver and spleen accumulation of the nanoparticles but additionally, it can also lead to other unintended effects such as immune response and toxicity (von Roemeling, Jiang, Chan, Weissman, & Kim, 2017). To avoid MPS elimination, nanoparticles are commonly coated or modified with PEG. PEG brings stealth properties to the nanoparticles and increases the stability both during storage and in circulation (Akinc et al., 2019). PEG prevents the aggregation of the nanoparticles via steric effects however it also often limits the cellular uptake (Itaka & Kataoka, 2009). To overcome this, targeting ligands such as folate, RGD peptides, antibodies have been conjugated to the delivery systems (Bertrand, Wu, Xu, Kamaly, & Farokhzad, 2014). Or, in more rational designs, PEG can be removed by protein corona formation from the nanoparticle prior to cellular uptake (Akinc et al., 2019). More information on PEG and other stealth polymers is given in the section entitled “stealth polymers” in this thesis.

Nucleic acid drugs should be taken up by the cells and cell membrane is one of the bigger barriers in cellular level. The complex, heterogenous and varying properties (negative charge, stiffness, fluidity) of the cell membrane makes the cell-nanoparticle interaction complicated (Behzadi et al., 2017). Same nanoparticle may interact with the different regions of the cell membrane which eventually result in different internalization behavior (Mitchell et al., 2020). Anionic nanoparticles are repelled by the cell membrane via repulsive forces while cationic nanoparticles tend to attach cell membrane easier because of attractive forces. However, cationic nanoparticles can strongly interact with the cell membrane which can cause to membrane damage and toxicity. Nanoparticles are majorly internalized into the cells via endocytosis. The utilized endocytic pathways are determined by several factors such as cell type, nanoparticle size shape, charge, rigidity

and receptor interactions (Mitchell et al., 2020). Phagocytosis or micropinocytosis are the dominant pathways for the uptake of nanoparticles larger than 200 nm. For nanoparticles smaller than 100 nm, size becomes less important factor since internalization of these nanoparticles is geometrically possible via different routes (Rennick, Johnston, & Parton, 2021). When nanoparticles are introduced to the biological media, serum proteins attach to the surface of the nanoparticles and forms a corona around it. This interaction might differ the nanoparticle size and affect the internalization pathway (Rennick et al., 2021). Additionally, the composition of the corona might trigger the binding to a specific cell receptor which in turn differs the cellular uptake pathway of the nanoparticles (Caracciolo et al., 2013). Among endocytic routes, clathrin-mediated endocytosis is the best understood and the most common route for the uptake of nanoparticles in mammals (Behzadi et al., 2017). Although controversial results are reported in the literature, it is generally shown that stiff and rigid nanoparticles are taken up by cells easier (Foroozandeh & Aziz, 2018).

Internalized nanoparticles should escape from the endo-lysosomal pathway (early endosome (pH 6.5), late endosome (pH 6.0), and lysosome (pH 4.5–5.0)) otherwise they are entrapped in the acidic vesicles, digested, and removed from the cells via exocytosis. Polymers having protonable groups at endolysosomal pH can escape from the endosome via so called proton sponge theory (H. J. Kim, Kim, Miyata, & Kataoka, 2016). The buffering capacity of the material leads to increased influx of proton and chloride ions which eventually result in the diffusion of water and osmotic swelling. The endosome membrane ruptures and disrupts upon swelling and nanoparticles are released to the cell cytosol. PEI is a very well-known polymer which triggers the endosomal escape via proton sponge theory (Boussif et al., 1995). In general, structures having diaminoethane (DET) motif are known to exhibit proton sponge effect and show potent transfection efficiency (H. J. Kim et al., 2016). While DET containing polymers are semi-protonated at physiological pH, they become fully protonated at acidic pH (H. J. Kim et al., 2016). Therefore, they do not interact with the cell membrane heavily, but they show high buffering capacity and membrane destabilizing effect once they are inside the endosomes. In addition to proton sponge effect, polycations are also believed to disrupt membrane integrity which in turn result in effective cytosolic release (Miyata et al., 2008). Different from polycations, lipid nanoparticles employ ionizable lipid molecules which interact with negatively charged endosomal membrane and destabilize the endosomal lipid

bilayer. 1,2-dilinoleyl-N,N-dimethyl-3-aminopropane (DLinDMA) is used as a benchmark ionizable lipid, later on next generations have been developed and they are found to be much more effective at destabilizing the endosomal membranes (Akinc et al., 2019).

Once siRNA is in the cytosol, it can trigger RNAi machinery. Effective dissociation of siRNA from its carrier might be crucial for potent gene silencing activity. For this aim, redox responsive carriers have been developed and used successfully since they are able to disassemble to smaller components after reduction in the cell cytosol (H. J. Kim et al., 2016). As a similar approach, siRNA conjugates formed via disulfide bonds can be reducible in the cell cytosol thanks to glutathione peptides (Kanasty, Dorkin, Vegas, & Anderson, 2013). These rational designs enable the successful release of siRNA from its carrier. Although siRNA acts in cell cytosol, for other drugs cell organelles might be the target. In these cases, there might be additional intracellular barriers that need to be overcome. In case of pDNA delivery in example, nuclear membrane stands as an additional barrier.

2.3. Non-Viral Carriers in Gene Therapy

Among nucleic acid-based drugs, RNA therapeutics such as microRNAs (miRNAs) small-interfering RNAs (siRNAs), short hairpin RNAs (shRNAs), antisense oligonucleotides, messenger RNAs (mRNAs), aptamers, ribozymes, and CRISPR/Cas-9 occupy an important place as they have potential in the treatment of cancer, neurodegenerative diseases, viral infections etc. However, this class of medicines often requires a delivery system (vectors) which enables the introduction of the corresponding genetic material to the target tissue/cells effectively. Even though viral vectors are known to be effective transfection tools, the use of such systems raises safety concerns along as viral carriers have been shown to trigger an immune response, create toxicities and organ failure and even fatal effects. Alternatively, non-viral carriers such as polymers, lipids, inorganic nanoparticles stand out as safer vehicles and offers modifiability for desired applications which makes them versatile delivery platforms. Low effectiveness on the other hand is the major disadvantage of these systems.

2.3.1. Polymers

Polymers occupy one of the biggest places among non-viral carrier systems as they offer countless advantages (Arnold, Czupiel, & Shoichet, 2017; B. Kim, Park, & Sailor, 2019). With the advancement of controlled polymerization techniques, polymer class has begun to grow rapidly and the applications in the biomedical field have diversified exponentially (Dong, Siegwart, & Anderson, 2019; Smith, Holley, & McCormick, 2011). Tailorability and modifiability of the polymers, enable the preparation of tremendous architectures (star-shape, branched, brush-shape etc.) with versatile properties (size, shape, charge, hydrophobicity etc.) (Averick et al., 2012; Siegwart, Oh, & Matyjaszewski, 2012). Relatively high stability of these systems compared to lipids, can be counted as another biggest advantage of this class (Rideau, Dimova, Schwille, Wurm, & Landfester, 2018).

Polymers, especially cationic polymers, have found applications in nucleic acid delivery since they can condense the genetic materials effectively, increase the serum stability of the nucleic acids, facilitate the cellular uptake, and enhance the cytosolic release by providing endosomal escaping ability (Bholakant et al., 2020; Cavallaro, Sardo, Craparo, Porsio, & Giammona, 2017). Different types of polymeric structures such as micelles, solid nanoparticles, polymer-nucleic acid conjugates, nanogels, dendrimers have been employed for nucleic acid delivery (Dong et al., 2019). However, polyplexes (cationic polymer-siRNA complexes) stand out among those thanks to their complex formation capability with nucleic acids via simple electrostatic interactions (Dong et al., 2019).

Different natural and synthetic polymers such as PEI (Polyethylene imine), P(DMAEMA) (Poly(2-(N,Ndimethylamino)ethyl methacrylate), PLL (Poly(L-lysine), PLGA (Poly(lactic-co-glycolic acid)), PAMAM (Poly(amido amide), cyclodextrin-based polymers, and chitosan have been widely employed for nucleic acid delivery (Bono, Ponti, Mantovani, & Candiani, 2020; de Ilarduya, Sun, & Düzgüneş, 2010) (Figure 2.5)

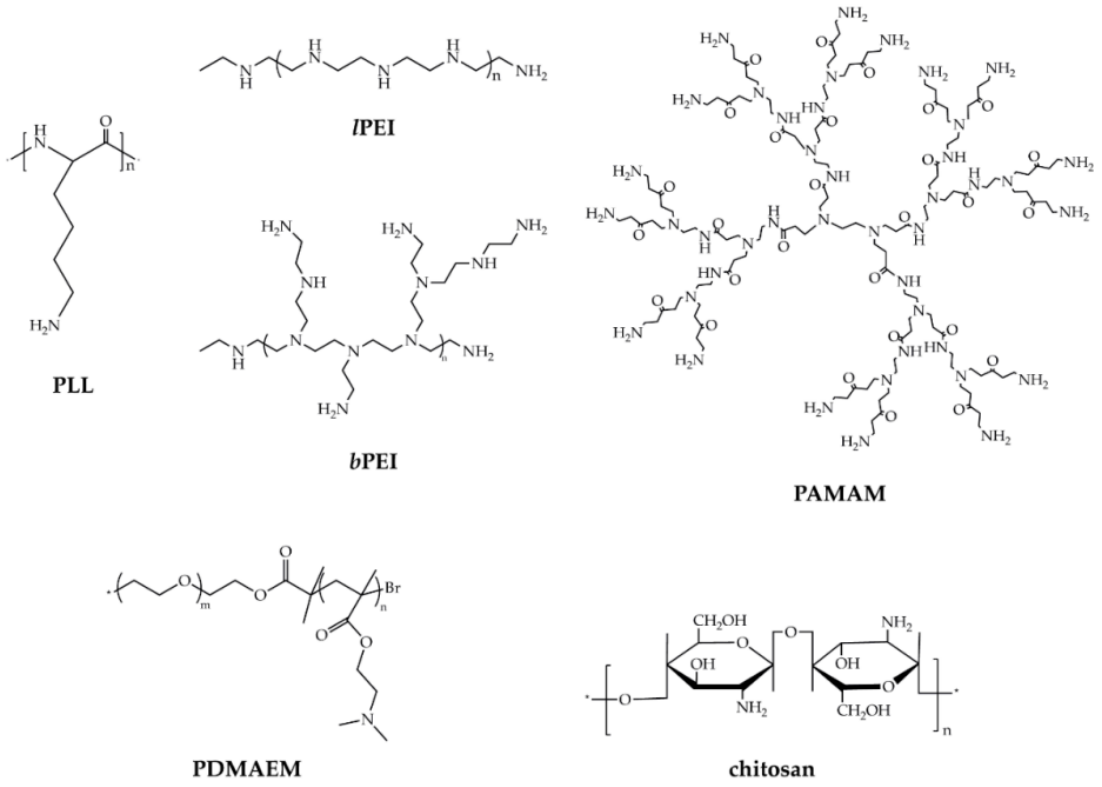

Figure 2.5. Commonly used polymeric carriers in gene delivery.
(Source: Bono et al, 2020)

Chitosan is a polysaccharide that displays low immunogenicity and because of its cationic nature and functional groups (amine and hydroxyl) it has been widely utilized in gene delivery applications. On the other hand, the low in vivo solubility, low buffering capacity and unspecific interactions with red blood cells of these polymers limits their applications (C. Yang, Gao, Dagnæs-Hansen, Jakobsen, & Kjems, 2017). Several different strategies like PEGylation for better solubility, polypeptide modification for enhanced cell uptake, antibody conjugation for targeted delivery have been employed to develop effective chitosan-based carrier systems (X. Chen et al., 2018; Sun et al., 2017). Although these modifications have been reported to decrease the non-specific interactions, increase the endosomal escape and/or target cell uptake and improve the gene silencing efficiency, it has been stated that these platforms still need to be improved to address all requirements necessary for clinical translation (Gu, Al-Bayati, & Ho, 2017; B. Kim et al., 2019).

PLL is another cationic polymer that especially stands out for its biodegradability properties (Choi et al., 1998; Harada-Shiba et al., 2002). However, it has been reported

that PLL displays similar toxicity with bPEI (Navarro, Pan, & Torchilin, 2015). Additionally, PLL shows poor transfection efficiency due to limited buffering capacity and short circulatory half-life time due to susceptibility to protease degradation (Navarro et al., 2015). siRNA transfection efficiency of PLL and PEGylated PLL polyplexes was found to be affected by the percentage serum content of the medium (Buyens et al., 2010). These polymers are known to be capable of delivering plasmid DNA (pDNA) however they are not able to deliver siRNA effectively in serum containing media. This is attributed to the low stability of PLL-siRNA polyplexes in serum containing media (Cavallaro et al., 2017). Patil et al. have prepared a triblock copolymer consisting of PEG, poly(amido amine) (PAMAM) and PLL and evaluated siRNA transfection ability of this polymer (Patil, Zhang, & Minko, 2011). Their results have shown that gene silencing efficiency substantially decreases when PAMAM is not present in the polymeric carrier thus, indicating the ineffectiveness of PLL when it is employed without another cationic block (Patil et al., 2011).

PLGA is an FDA approved biocompatible polyester which makes it favorable for drug delivery applications including nucleic acid delivery. The degradation time of PLGA can be fine-tuned by changing the molecular weight and copolymer ratio (lactic acid: glycolic acid). However, PLGA often requires another polymer to condense the nucleic acids since PLGA is negatively charged at physiological pH. LODER^{TM} is a PLGA based polymeric matrix developed by Silenseed Ltd. for local treatments of solid tumors (Shemi, Khvalevsky, Gabai, Domb, & Barenholz, 2015). It has been stated that *siG12D*-LODER^{TM} can provide slow and prolonged siRNA release and protect the siRNA against enzymatic degradation over months (Khvalevsky et al., 2013). The combinatorial effect of *siG12D*-LODER^{TM} and chemotherapy against patients with locally advanced pancreatic cancer has been shown to be well-tolerated and beneficial (Golan et al., 2015).

P(DMAEMA) is a tertiary amine containing polymer with a methacrylate backbone that can be synthesized via reversible-deactivation radical polymerization (RDRP) techniques such as ATRP (Atom Transfer Radical Polymerization) and RAFT (Reversible Addition-Fragmentation Chain Transfer) Polymerization (Convertine et al., 2010). Thanks to RDRP, the polymer structure can be combined with another monomer, stealth polymer, targeting ligand etc. (Convertine et al., 2010; Malcolm et al., 2017; Nelson et al., 2013). The sterically available amine groups of the polymer make it favorable for siRNA complexation, cell uptake and endosomal escape (Kargaard, Sluijter,

& Klumperman, 2019). However, like other cationic polymers, P(DMAEMA) also displays significant toxicity (Cheng et al., 2016; Schallon et al., 2010).

PEI is a very well-known cationic polymer in the field of gene delivery. Different forms of PEI; branched (bPEI), linear (lPEI), low molecular weight (typically below 25kDa) etc. have been investigated as gene delivery vehicles (Pezzoli, Giupponi, Mantovani, & Candiani, 2017). The high effectiveness of PEI comes from the high complexation ability and buffering capacity of the polymer. Like some other cationic polymers with protonable amine groups at endosomal pH (PAMAM, poly(aspartamide) derivatives bearing 1,2-diaminoethane side chains (PAsp(DET)), p(DMAEMA)), it is known that PEI escapes from the endosome via the proton sponge theory (Boussif et al., 1995). The protonation ability of PEI over a wide pH range makes it an ideal nucleic acid carrier as it provides required cationity for complexation and further buffering capacity for endosomal escape (Boussif et al., 1995). Although very controversial results regarding the most efficient form/architecture of PEI have been reported in the literature, PEI can be considered as the gold standard polymer in pDNA delivery (Grayson, Doody, & Putnam, 2006; Pezzoli et al., 2017). In contrast, siRNA delivery potential of PEI has been reported to be limited due to structural differences of siRNA- and pDNA-PEI complexes (Scholz & Wagner, 2012). The biggest disadvantage of PEI is the high toxicity of the polymer especially seen at the high molecular weights and branched architecture (Beyerle, Irmler, Beckers, Kissel, & Stoeger, 2010; Zintchenko, Philipp, Dehshahri, & Wagner, 2008).

Several strategies have been suggested to address problems of PEI such as high toxicity and low siRNA transfection efficiency (Scholz & Wagner, 2012). Modification of PEI with hydrophobic units is shown to offer higher stability due to presence of hydrophobic interactions, improved endosomal escaping ability due to the enhanced polyplex-endosomal membrane interactions and lower cytotoxicity due to decreased charge density (P. Y. Teo et al., 2013). Eventually, all these improvements lead to higher transfection efficiency. Shen et al. have prepared a library consisting of alkane, cycloalkane or fluoroalkane modified bPEI-25kDa (Shen et al., 2016). They have evaluated the siRNA transfection efficiency of these different polymers on a model cell line, stably luciferase expressing HeLa. They have reported that siRNA transfection efficiency of unmodified bPEI was only 14% and 80% of modified bPEIs in the library were more effective than unmodified bPEI. Their data revealed that siRNA knockdown efficiency increased with an increasing amount of functionalization (modification).

Moreover, fluoroalkylated PEIs were found to be more effective compared to alkylated and cycloalkylated PEI. The authors attributed this to unique lipophobic, and hydrophobic properties of fluorocarbons and they have shown that fluoroalkylated PEIs were taken up more compared to other modified bPEI analogous in the library. Higher cell uptake has been stated to be the reason for higher transfection efficiency (Shen et al., 2016).

2.3.1.1. Stealth Polymers

When nanoparticles are administered to a biological system, they are exposed to serum protein that can eventually cause the rapid elimination of the introduced nanoparticles without showing any therapeutic effect. Protein interactions, more specifically, binding of immunoglobulins, complement proteins and blood clotting factors (collectively called opsonins) to the surface of the nanoparticles is known to trigger mononuclear phagocytic system (MPS) which ultimately removes the nanoparticles from the bloodstream (Frank & Fries, 1991; Moghimi, Hunter, & Murray, 2001). Elimination of the interaction between nanoparticles and opsonin proteins leads to prolonged blood circulation (Gref et al., 1994; Kaul & Amiji, 2002). Some polymers, called stealth polymers, are discovered to prevent this interaction and lead to higher efficacy due to mentioned shielding effect (Amoozgar & Yeo, 2012; Fam et al., 2020; Moghimi et al., 2001; Salmaso & Caliceti, 2013). Poly(ethylene glycol) (PEG), poly(vinyl pyrrolidone) (PVP), poly(zwitterion)s, poly[N-(2-hydroxypropyl) methacrylamide] (PHPMA), poly(2-oxazoline)s (POx) are some important stealth polymers (Figure 2.6 and 2.7).

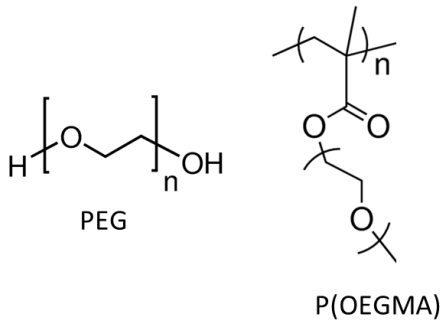

Figure 2.6. Chemical structures of PEG and P(OEGMA).

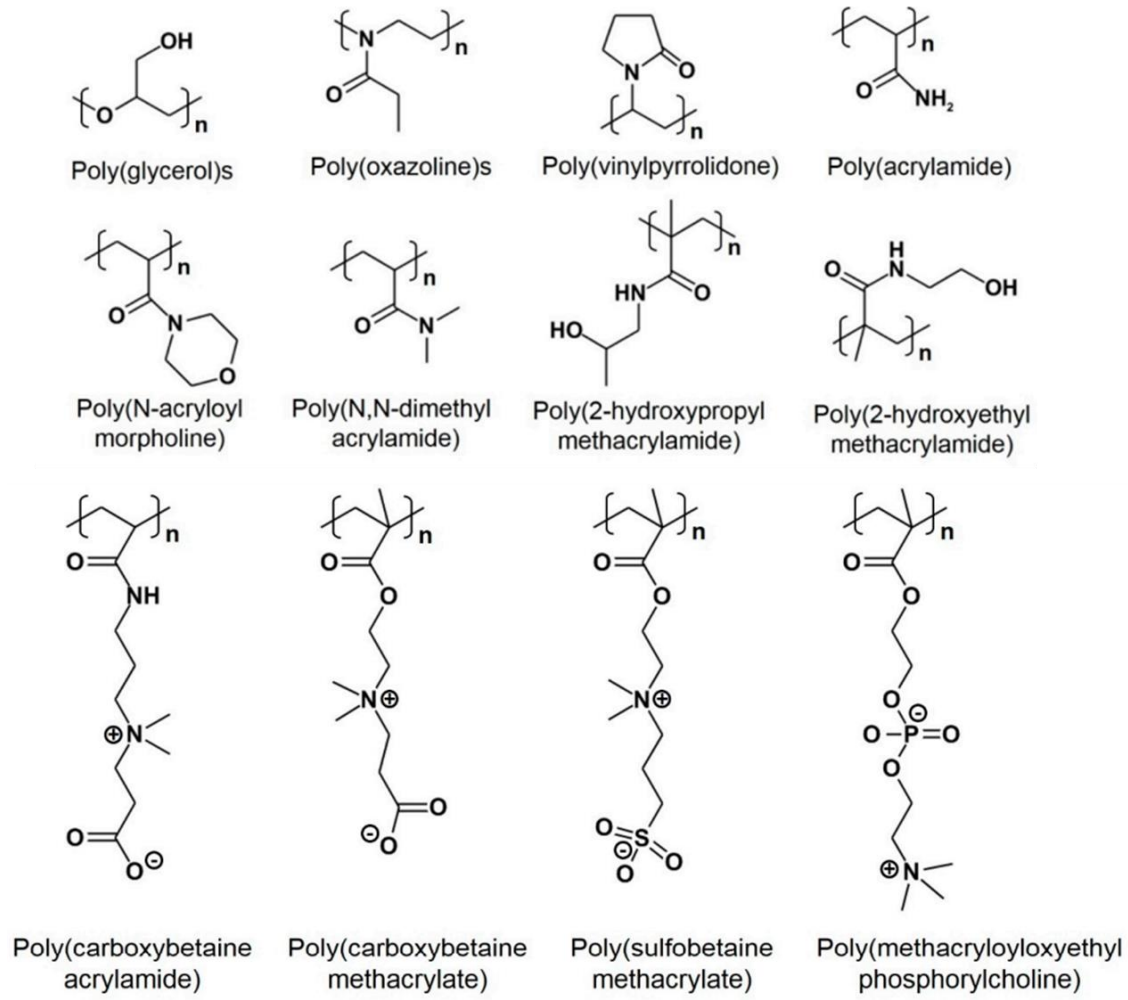

Figure 2.7. Chemical structures of PEG alternatives.
(Source: Hoang Thi et al., 2020)

PEG is a hydrophilic, neutral and non-toxic stealth polymer and heavily used in surface coating and drug conjugation. FDA approvement and commercial availability of varying PEGs with versatile properties make it gold standard among the other stealth polymers (Alconcel, Baas, & Maynard, 2011; Suk, Xu, Kim, Hanes, & Ensign, 2016; Veronese & Pasut, 2005). PEG is known to reduce the molecular recognition and protein adsorption and increase the solubility and stability of the attached nanoparticle/drug (D'souza & Shegokar, 2016). It is well accepted that hydrophobic and charged molecules attracts the opsonin molecules more (Carrstensen, Mueller, & Müller, 1992; Gessner et al., 2000; Roser, Fischer, & Kissel, 1998). Since PEG chains are neutral, flexible, and hydrophilic; it prevents the opsonin attraction. PEG is believed to form hydrated cloud

and display extended conformation in solution. Once it is exposed to opsonins, PEG is proposed to change its extended conformation to higher energy conformation -compressed- which in return overcomes the opsonin binding thereby PEG avoids MPS (Owens III & Peppas, 2006). Modification density, molecular weight, dispersity, and conformation of PEG is known to affect the extent of exhibited stealth property (Fam et al., 2020). Generally, PEG having 2 kDa or higher molecular weight is found to be effective at preventing the protein adsorption (Owens III & Peppas, 2006). However, some controversial studies have been also reported. It has been stated that if the grafting density of PEG is high enough ($\geq$ 1.2 PEG/nm^2), low molecular weight PEG (559 Da) also can prevent the protein adsorption (Q. Yang et al., 2014). In addition, Zhang et al. showed that monodisperse PEG with molecular weight of 752 Da can reduce the non-specific protein/cell interactions on planar surfaces (Peiyu Zhang, Zhang, Wang, Hao, & Cui, 2020). Similar effect could be obtained with polydisperse PEG with molecular weight of 2 kDa indicating that low molecular weight PEG is sufficient to obtain non-fouling surfaces when it is monodisperse (Peiyu Zhang et al., 2020). In addition to mentioned advantages, PEG also increases the hydrodynamic diameter of the attached drug or nanoparticle, therefore limits the renal clearance and access of proteases, antibodies etc. (Peng Zhang, Sun, Liu, & Jiang, 2016).

Although PEG offers many advantages for nanomedicine and biomedical applications, it suffers from several aspects. PEG is synthetic and non-biodegradable; therefore, high molecular weight PEG (more than 60 kDa) cannot be filtrated through the kidneys and accumulates in the liver and lysosomes which can cause macromolecular syndrome (Veronese & Pasut, 2005). Also, PEG can substantially decrease the cellular uptake which decrease the efficacy of the drug. Moreover, PEG is found to be immunogenic -contrary to the previous non-immunogenicity claims- (Garay, El-Gewely, Armstrong, Garratty, & Richette, 2012). Particularly anti-PEG immunoglobulin M (IgM) was shown to cause to the rapid clearance of the PEGylated drugs at repeated administrations (Sebak, 2018). Association of anti-PEG IgM with the PEGylated compounds is known to trigger the Kupffer cells and activate the complement system which leads to rapid elimination via a phenomenon known as accelerated blood clearance (M. Li, Al-Jamal, Kostarelos, & Reineke, 2010; Lila, Kiwada, & Ishida, 2013). This rapid clearance decreases the bioavailability and efficacy of PEGylated drugs especially at repeated dosages. In addition, anti-PEG IgM has been even found in the healthy people

who have never been treated with PEGylated drugs (Neun, Barenholz, Szebeni, & Dobrovolskaia, 2018; Park, 2018). Although very small number of healthy donors (0.2%) were known to have anti-PEG antibodies in the beginnings of 1980s, this number has reached to 25% (Armstrong, 2009; Richter & Åkerblom, 1984). Intense use of PEG in cosmetic and food industry seems to change the old non-immunogenic profile of PEG (Garay et al., 2012). On-going heavy consumption of PEG might possibly make the scenario even worse. Therefore, PEG alternatives might be highly necessary in the near future for the food, cosmetic and pharmaceutical industries.

Chilkoti, his group and others have introduced and heavily used the comb-type (or bottlebrush) PEG, namely; Poly(oligo(ethylene glycol) methyl ether methacrylate (P(OEGMA)) as a stealth polymer alternative to commonly used linear PEG (P. W. Lee et al., 2017; M. Liu, Johansen, Zabel, Leroux, & Gauthier, 2014; Qi et al., 2016). This methacrylate polymer bears oligoethylene glycol units with varying length in its side chains and it is shown to exhibit similar or superior pharmacokinetic properties compared to PEG. Drug conjugate of P(OEGMA) having nine ethylene glycol units is found to be less antigenic compared to two FDA approved PEG-protein conjugates, Krystexxa and Adagen (Qi et al., 2016). The number of ethylene glycol units in P(OEGMA) can be fine-tuned and have strong impact on the behavior of the polymer (Joh et al., 2019). Joh et al. have demonstrated that P(OEGMA) with ethylene glycol units of 2-3 is effective at eliminating the binding of anti-PEG antibodies and minimizing the adsorption of BSA and fibroblast cells (Joh et al., 2019). Collectively, studies on P(OEGMA) showing that these bottlebrush polymers with short ethylene glycol units are offering favorable non-fouling and non-antigenic features without compromising the pharmacokinetic properties.

Poly(2-Oxazoline)s (POx) are emerging stealth polymers alternative to PEG. It is synthesized via cationic ring-opening polymerization (CROP) of 2-oxazoline monomers, and the employed synthetic route enables the formation of well-defined polymers with functional end groups (Glassner, Vergaelen, & Hoogenboom, 2018). With the selection of desired/proper initiator and terminating agents, readily modifiable POx could be obtained. POx systems can be hydrophilic or hydrophobic and can also exhibit temperature-responsive behavior based on the polymer's pendant group (Glassner et al., 2018). Poly(2-methyl-2-oxazoline) (PMeOx) and poly(2-ethyl-2-oxazoline) (PEtOx) are the most used POx systems in the biomedical field (Luxenhofer & Jordan, 2016). PMeOx

is highly hydrophilic whereas PEtOx is relatively more hydrophobic due to additional methyl group residue in the side chain. Similar to PEGylation, POxylation also enhances the circulation time of the nanoparticles in the bloodstream (Chapman et al., 2000). POx is also found to be highly biocompatible and non-toxic (Luxenhofer et al., 2012; Victor, 2014). Moreover *in vivo* studies revealed that POx is non-immunogenic even after repeated administrations (Moreadith et al., 2017). However, POx synthesis is relatively difficult and not very cost-effective. There are also concerns regarding the impurities. The biological effects of POx are not known as much as PEG due to limited number of studies with this polymeric structure (Hadjesfandiari & Parambath, 2018; Hoang Thi et al., 2020; Khutoryanskiy, 2018).

POx systems have been used successfully in some gene delivery applications (Cabral, Miyata, Osada, & Kataoka, 2018; B. S. Kim et al., 2019; J. Li & Kataoka, 2020; Peng & Wagner, 2019). Gaspar et al. have synthesized a triblock copolymer, poly(2-ethyl-2-oxazoline)–poly(L-lactide) grafted with bioreducible polyethylenimine (PEtOx–PLA-g–PEI-SS) for combinatorial delivery of minicircle DNA (mcDNA) and Doxorubicin (Dox) (Gaspar et al., 2015). PEtOx is preferred as a non-fouling polymer to provide colloidal stability to the polymeric carrier. PEI was employed to complex mCDNA and PLA was used to form hydrophobic core for Dox encapsulation. The obtained bioreducible polymer was able to show potent gene delivery efficiency in *in vitro* tumor spheroid models. The gene expression was found to be detectable up to 8 days upon intratumoral administration. Moreover, the prepared polymeric drug delivery system was able to reduce the tumor volume in employed tumor bearing mice (Gaspar et al., 2015). In another study, Soo Kim et al. have prepared a triblock copolymer consisting of PEtOx, poly(2-n-propyl-2-oxazoline) (PnPrOx) and poly(l-lysine) (PLL), (PEtOx-*b*-PnPrOx-*b*-PLL) (B. S. Kim, Osawa, Yum, Naito, & Miyata, 2020). PnPrOx was preferred as thermoswitchable hydrophobic block and PLL was used as a cationic block. The obtained block copolymer was able to form unimer polymer-siRNA complexes with a diameter of approximately 10 nm. The block copolymer with hydrophobic PnPrOx block, $PEtOx_{116}$-*b*-$PnPrOx_{56}$-*b*-PLL_{42}, was able to show higher cell uptake and gene silencing efficiency compared to control block copolymer, $PEtOx_{175}$-*b*-PLL_{42}. It has been found that the hydrophobic PnPrOx block leads to the stronger cell binding through hydrophobic interactions between the polymer and the cell membrane (B. S. Kim et al., 2020).

2.3.1.2. Star Polymers

Star polymers are complex star-shaped polymeric structures with unique physical, chemical, and biological behavior thanks to their distinct architecture. Many advantages of star polymers make them ideal for biomedical applications (Ren et al., 2016; Wu, Wang, & Li, 2015). Star polymers usually exhibit good solubility and low viscosity. They offer three-dimensional structure with terminal functional groups which enable the conjugation of targeting ligands, drugs, and other moieties (i.e., radiolabels, gadolinium chelates, fluorescent dyes) (Cho et al., 2013; Duong et al., 2014; S. J. Kim, Ramsey, Boyer, Davis, & McAlpine, 2013). They can be obtained with low dispersity, defined molecular weight and size using RDRP techniques (Wu et al., 2015). They can be produced at high quantity in a reproducible manner and obtained cost-effectively which favors the clinical translation (Wu et al., 2015). In addition to their unique solution behavior, it has been shown that they can also be used for gene delivery applications (Cho et al., 2013; Pafiti, Mastroyiannopoulos, Phylactou, & Patrickios, 2011).

Different methodologies, arm-first, core-first, grafting-onto, have been employed up to date to prepare star polymers (Figure 2.8). “Arm-first” is one of the most commonly used approach in which linear polymer arms are fist synthesized and later cross-linked via cross-linking polymerization or coupling reaction (Georgiou, 2014). This route enables the incorporation of pre-determined and pre-characterized polymer arms into a core structure to yield star polymer. Arms having different structures, compositions and architectures can be incorporated to the star polymer structure easily via this route (Georgiou, 2014; Ren et al., 2016). In case of using biodegradable cross-linker, the star polymer can be degraded to smaller fragments in biological medium which is known to lead decreased toxicity (Georgiou, 2014). Arm-first star polymers also have distinct cross-linked core -network- structure which enables the chemical attachment or physical entrapment of functional compounds (Spiniello, Blencowe, & Qiao, 2008; Sulistio, Widjaya, Blencowe, Zhang, & Qiao, 2011). These compounds can be shielded/protected from the environment thanks to adjacent arms. The unique core structure brings many potentials to the biomedical applications (Helms et al., 2005; Terashima, Nomura, Ito, Ouchi, & Sawamoto, 2011). However, star polymers produced via this route usually have undefined arm number and relatively high dispersity (Đ) (Ren et al., 2016). Additionally, the yield of star formation can be low meaning that unreacted arms remain in the solution

at the end of the cross-linking reaction (Ren et al., 2016). The unincorporated arms need to be removed using a proper purification technique such as dialysis, chromatography and/or precipitation (Ren et al., 2016). The chemical structure and molecular weight of arms, the cross-linker type, the ratio between the cross linker and the arm and the employed polymerization technique are reported to be the main factors affecting the arm number and the yield (H. Gao & Matyjaszewski, 2009; Shibata, Kanaoka, & Aoshima, 2006). Arm-first star polymers can be synthesized via three different routes - macroinitiator, macromonomer and self-assembly cross-linking- as described elsewhere (Ren et al., 2016). All these routes can be utilized to obtain star polymers consisting of different arm species called miktoarm stars.

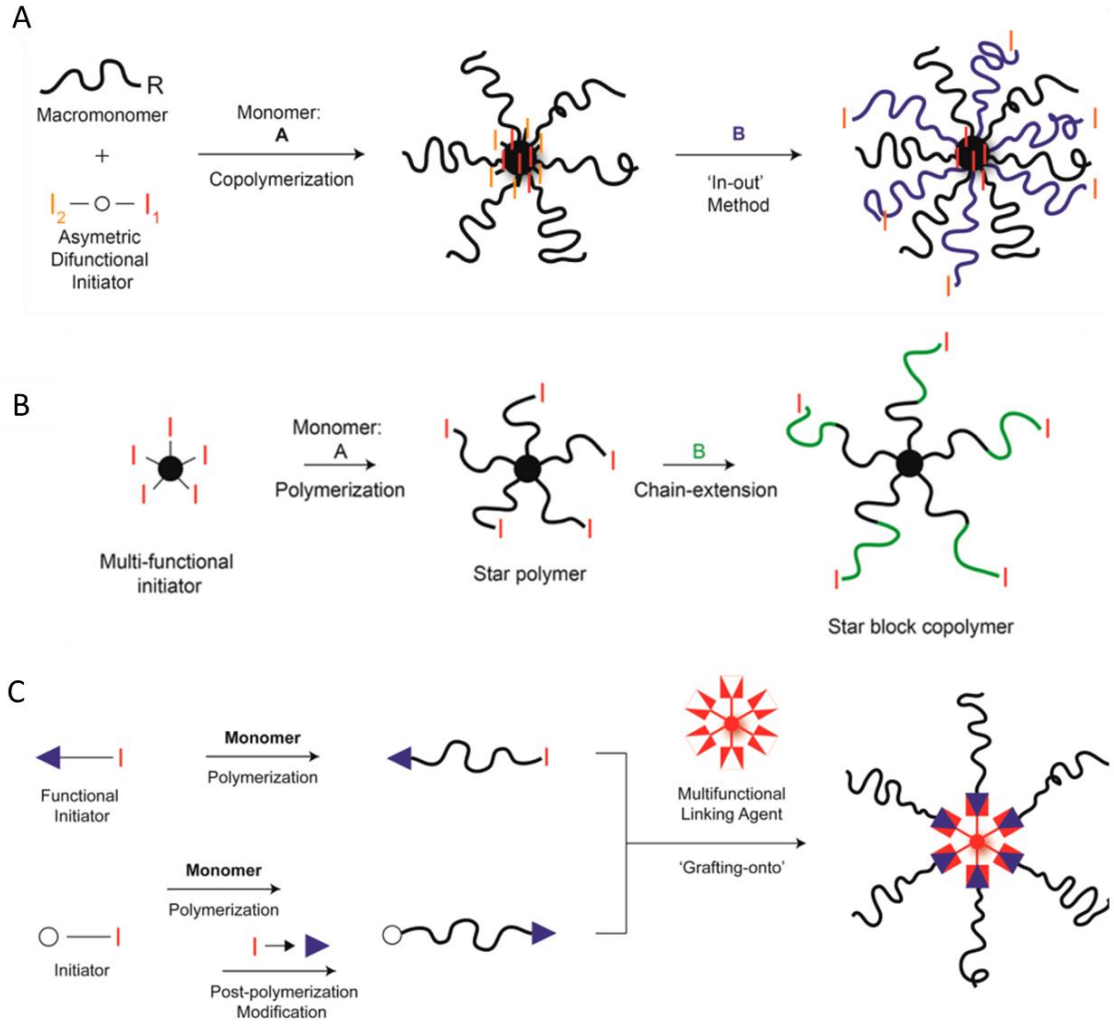

Figure 2.8. Schematical illustration of star synthesis via arm-first (A), core-first (B) and grafting-onto (C) approaches.
(Source: Ren et al., 2016)

Core-first approach is another method used for the preparation of star-shape polymers. As the name implies, this time arms are grown from a pre-employed multi-functional initiator molecule (core) by polymerization (Ren et al., 2016). In this case, the functional initiator must be capable of offering same reactivity for each initiation site so that, each arm will have equal opportunity to grow. At the end of the polymerization, depending on the polymerization technique and multifunctional initiator efficiency and reactivity, star polymers with pre-determined arm numbers and defined molecular weights could be obtained (Georgiou, 2014). Since arms are grown from a core structure, there will be no unreacted free arm at the end of the polymerization, unlike arm-first approach. This brings advantages for purification as the only impurities are small monomeric units or molecules that can be removed by simple precipitation. However, the characterization of arms is problematic in this method. It cannot be directly characterized unlike the arm-first route (Blencowe, Tan, Goh, & Qiao, 2009). Additionally, the arm number of these stars is most of the time limited with the functionality of the core unit. Since the core unit is mostly a small molecule, it can offer only a few functional sites, and this leads to the formation of star polymers with low arm numbers (typically 3-8 arm) (Ren et al., 2016). Moreover, this route is not the preferred method to prepare miktoarm stars though it is possible with specially designed core compounds (Tunca, Ozyurek, Erdogan, & Hizal, 2004).

Alternative to arm-first and core-first approaches, star polymers can be prepared via grafting-onto approach in which pre-synthesized arms are incorporated to a core via a coupling reaction. This approach combines the advantages and disadvantages of the other two methods. Low arm number, steric hindrance and purification are usually the problems however better characterized star polymers with defined structure/arm number could be obtained with this method (Ren et al., 2016).

Star polymers have been successfully used for gene delivery applications. Xu et al. have synthesized star polymers consisting of cyclodextrin core and P(DMAEMA) arms via ATRP (Xu et al., 2009). They have reported that star polymers were able to show higher pDNA transfection efficiency and lower toxicity on HEK293 cell line compared to P(DMAEMA) homopolymer (arm) (Xu et al., 2009). Boyer et al. have also prepared P(DMAEMA) star polymers via RAFT polymerization using arm-first approach. They could obtain core-degradable star polymers with low dispersity (Đ = 1.15). They found out that the star polymers were able to complex with siRNA at 8:1 and 10: 1 (w/w) ratio optimally. The size of the complexes was found to be approximately 40 nm and star

polymers displayed positive zeta potential before and after complexation with siRNA. The size of the star polymers did not change significantly after complexation however, the charge of the polymers has decreased from 50 mV to 29 mV upon complexation. They have used fluorescently labeled siRNA and investigated the uptake and intracellular distribution using flow cytometry and confocal microscopy. Their data showed that star polymers were able to carry siRNA (100 nM) to the MiaPaCa-2 (pancreatic cancer) and H460 (nonsmall cell lung cancer) successfully without showing any toxicity. Furthermore, they have tested gene silencing efficiency of star polymers on luciferase expressing MiaPaCa-2 and green fluorescent protein (GFP) expressing H460. RT-qPCR results revealed that star polymers were able to decrease the target mRNA expression to 50% and 20% in MiaPaCa-2 and H460 cells, respectively compared to star polymers complexed to non-silencing siRNA. Protein expression levels were also showed good correlation with mRNA expression levels. In the next study, Teo et al. have synthesized several different miktoarm star polymers consisting of varied amounts of P(DMAEMA) and P(OEGMA) arms (J. Teo et al., 2016). They have evaluated *in vitro* and *in vivo* siRNA delivery potential of three different star polymers, "Star 1 (48 mol %POEGMA with short-cationic side arms), Star 2 (51 mol % POEGMA with long-cationic side arms), and Star 3 (12.5 mol % POEGMA with long-cationic side arms)". The agarose gel electrophoresis results revealed that star polymers were able to complex with siRNA regardless of the cationic arm length, but the interaction was found to be affected by POEGMA amount. The viability of the non-POEGMA containing star polymer treated pancreatic cancer cells, MiaPaCa-2, was found to be drastically lower compared to POEGMA containing star polymer treated cells. The authors reported that star polymers were internalized by cells via different endocytosis mechanisms. The intracellular uptake mechanism of star 1-siRNA complexes was found to be clathrin-independent endocytosis whereas star 3-siRNA complexes were majorly taken up by clathrin-dependent endocytosis indicating that the physicochemical behavior of the star polymers have direct effect on the endocytosis pathway. The authors also evaluated the gene silencing ability of star 3-siRNA complexes in orthotopic pancreatic tumors in mice. They have demonstrated that systemic administration of star 3-siRNA complexes led to significant decrease (>80%) in βIII-tubulin gene expression (J. Teo et al., 2016).

CHAPTER 3

MATERIALS AND METHODS

3.1. Materials

N-(2-Hydroxyethyl)ethylenediamine, di-tert-butyl dicarbonate, anhydrous DCM (dichloromethane), triethylamine and methacrylic anhydride were purchased from Sigma-Aldrich for synthesis of the monomer, 2-((tert-butoxycarbonyl) (2-((tert-butoxycarbonyl) amino)ethyl)amino)ethyl methacrylate, (BocAEAEMA). 2-Ethyl-2-oxazoline (EtOx, >99%, Sigma-Aldrich) was distilled to dryness over barium oxide (BaO), Methyl tosylate (98%, Aldrich, MeTos) was distilled under reduced pressure and stored under nitrogen. Acetonitrile (ACN) (anhydrous, Sigma) was stored under nitrogen. Methacrylic acid (99%) was obtained from Sigma. EtOx, MeTos and following chemicals were used for the synthesis of the monomer, oligo(2-ethyl-2-oxazoline)methacrylate (OEtOxMA).

For polymerizations, Poly(ethylene glycol) methyl ether methacrylate (M_n 500), RAFT agents; (4-cyano-4-(phenylcarbonothioylthio) pentanoic acid) (CPADB), (4-Cyano-4-[(dodecylsulfanylthiocarbonyl)sulfanyl]pentanoic acid) (CDTPA), 2-Cyano-2-propyl benzodithioate (CPBD) were purchased from Sigma-Aldrich. Anisole (anhydrous, 99.7%), butyl acrylate, cross-linker (N,N′-Bis(acryloyl)cystamine) (BAC) were purchased from Sigma-Aldrich. 2,2′-Azobis(2-methylpropionitrile) (AIBN) was used after recrystallization three times in methanol.

For chemical synthesis and purification, basic aluminum oxide and (60-80 °C) silica for column chromatography was obtained from Sigma-Aldrich. Petroleum benzine was purchased from Merck. Ethyl acetate, toluene, dichloromethane (DCM), trifluoroacetic acid, deuterium oxide (D_2O), deuterium chloroform ($CDCl_3$), triethylamine (TEA), hexylamine, TFA (trifluoro acetic acid), diethylether, methanol and N'N-dimethylacetamide (DMAc, HPCL grade ≥ %99.9) were purchased from Sigma.

For cell culture studies and in vitro assays, RPMI 1640 with L-glutamine, DMEM (Dulbecco's Modified Eagle's Medium), HEPES and phenol red, Dulbecco's Phosphate

Buffered Saline (PBS), Hanks' Balanced Salt solution (HBSS) were purchased from thermoFisher Scientific. FBS (Fetal Bovine Serum) was purchased from Biowest. Pen-strep, non-essential amino acids and Trypsin-EDTA were obtained from Sigma. alamarBlue™ Cell Viability Reagent and Propidium Iodide (PI) was purchased from Invitrogen. 3-(4,5-dimethylthiazol-2-yl)-2,5-diphenyl tetrazolium bromide (MTT), dimethyl sulfoxide (DMSO) was purchased from Sigma. Luciferase assay system and luciferase cell culture lysis 5X reagent was purchased from Promega. Lipofeactamine RNAimax was purchased from Life Technologies. siRNAs targeting the luciferase sequence (sense: 5′-GCUAUGGGCUGAAUACAAAUU-3′; antisense: 5′-UUUGUAUUCAGCCCAUAGCUU-3′) was purchased from IDT-DNA. siRNA targeting the vimentin (sense: 5'-GAAUGGUACAAAUCCAAGUdTdT-3' ; anti-sense: 5'-ACUUGGAUUUGUACCAUUCdTdT-3') was purchased from Dharmacon. Non-targeting siRNA (siGENOME Non-targeting siRNA #3) was purchased from Dharmacon. 5′-Alexa Fluor 488 conjugated siRNA was purchased from Qiagen. LysoTracker™ Red DND-99 was purchased from Invitrogen Thermofisher. Hoechst 33342 Solution (20mM) was purchased from Life Technologies. MDA-MB-231-luc2-gfp (stably luciferase expressing human breast cancer cell line) was kindly provided by Dr. Özgür Şahin (Bilkent University, Ankara). H460-luc2 (stably luciferase expressing human lung cancer cell line) was kindly provided by Assoc. Prof. Dr. Joshua McCarroll (University of New South Wales, Sydney).

3.2. Instruments

3.2.1. Size Exclusion Chromatography (SEC)

Molar mass and dispersity (Đ) of the polymers were determined by SEC. Several different SEC systems with slightly different configurations were used for the analyses of the synthesized polymers.

Shimadzu modular system comprising a DGU-12A degasser, an SIL-20AD automatic injector, a 5.0 μm bead-size guard column (50 x 7.8 mm) followed by three KF-805L columns (300 x 8 mm, bead size: 10 μm, pore size maximum: 5000 Å), a SPD-

20A ultraviolet detector, and an RID-10A differential refractive index detector. A CTO-20A oven was used to maintain the columns at 40 °C. *N*, *N*-dimethylacetamide (DMAc) with 0.03% w/v LiBr was used as the mobile phase. Samples were run at 1 mL min^{-1}. Polystyrene standards (0.5 to 2000 kg mol-1) were used for calibration. 2-3 mg of polymer samples were dissolved in 1 ml of DMAc and filtered through 0,45 μm PTFE filters.

For some analyses, SEC system equipped with different column set (either PSS Gram 30 Å and 100 Å (10 μM, 8x300 mm) columns or Waters Styragel guard, HR4 (5 kDa-600 kDa) and HR3 (500 Da-30 kDa) columns) was employed.

3.2.2. Nuclear Magnetic Resonance Spectroscopy (NMR)

^{1}H NMR spectroscopy (Varian, VNMRJ 400 spectrometer or Bruker AVANCE III HD 400 MHz spectrometer) was used to determine the chemical structure of synthesized compounds, the reaction yields and the conversion of the monomers to polymers. Deuterium oxide (D_2O) and chloroform ($CDCl_3$) were used as NMR solvents. For NMR analysis, samples were dissolved at 6 mg/ml concentration in 600 μl deuterated NMR solvents.

3.2.3. Flash Chromatography System

Reveleris® X2 flash chromatography system equipped with ELSD and UV detectors was used to purify the monomer, BocAEAEMA. Petroleum benzine and ethyl acetate was used as a mobile phase. The sample was dissolved in DCM and injected as a liquid.

3.2.4. Dynamic Light Scattering (DLS) and Electrophoretic Light Scattering (ELS)

Malvern Zetasizer Nano ZS or NanoPlus DLS Nano Particle Size and Zeta Potential Analyzer is used to determine the hydrodynamic diameter and zeta potential of the polymers and polyplexes.

Dynamic Light Scattering (DLS) measurements were performed after an equilibration time of 120 s. Disposable small volume (40 µl) cuvettes were employed for measurements. 3 runs were carried out at 25 °C. Each measurement was performed in triplicate.

Electrophoretic Light Scattering (ELS) was used to determine surface charge (ζ-potential) of the particles. Smoluchowski equation was used to calculate zeta potential from the electrophoretic mobility. 6 runs were carried out for each measurement. Each experiment was performed in triplicate at 25 °C.

3.2.5. Scanning Electron Microscopy (SEM) and Transmission Electron Microscopy (TEM)

FEI Tecnai G^2 T20 TEM equipped with 200kV; LaB6 emitter; Twin lens; 5-axis compustage; column isolation valves for rapid sample exchange; Orius SCD200D wide-angle CCD camera (diffraction capable); Orius SC600 high-resolution CCD camera; Bruker 30mm^2 ultra-thin window SDD and Quantax analysis system; single tilting holder; 3-position single tilting holder; beryllium (low background) double-tilting analytical sample holder was used to analyze morphology and size of the polyplexes.

FEI QUANTA 250 FEG was used for SEM analysis. Prepared samples (2-3µl) were dropped on a pre-cleaned silicon wafers and left to dry at room temperature. Particles were analyzed after gold coating.

3.2.6. Plate Reader

Thermo Electron Corporation Varioskan microplate reader was used to measure absorbance and luminescence for MTT and luciferase assays, respectively. LumiSTAR Omega instrument (BMG Labtech, Ortenberg, Germany) was also used for luminescence measurements.

3.2.7. Fluorescence Spectrometer

Shimadzu RF-5301PC Fluorescence spectrometer was used to determine the fluorescence intensity of Cy5 labeled polymers.

3.2.8. Agarose Gel Electrophoresis System

Shimadzu Thermo Scientific Owl™ EasyCast™ B1 mini gel system was used in siRNA complex formation, release and serum protection assays.

3.2.9. Flow Cytometer

BD FACSCanto™ II was used to determine the cell association profile of polymers and polyplexes. Cy5 was detected with a 633 nm excitation and emission collected between 650-670 nm. Alexa Fluor-488 was detected with a 488 nm excitation and emission collected between 515-545 nm.

3.2.10. Confocal Laser Scanning Microscopy (CLSM)

Intracellular distribution profile of siRNA and polyplexes was investigated by SP8 LIGHTINING confocal microscope (Leica microsystems). Live cell imaging was performed using 63X HC PL APO CS2 objective and corresponding lasers (depending on the fluorochrome) were used in a sequential order for imaging. ibiTreat 8-well μ-Slide was used as a chambered coverslip.

3.3. Methods

3.3.1. Synthesis of Monomers

3.3.1.1 Synthesis of 2-((Tert-butoxycarbonyl) (2-((tert-butoxy carbonyl) amino) ethyl) amino) ethyl Methacrylate (BocAEAEMA)

The monomer 2-((tert-butoxycarbonyl) (2-((tert-butoxy carbonyl) amino) ethyl) amino) ethyl methacrylate (BocAEAEMA) was synthesized by adapting a previously reported procedure (Kurtulus et al., 2014) (Figure 3.1). The synthesis consists of two steps. In the first step of the reaction, the amine groups of the starting compound, N-(2-hydroxyethyl) ethylenediamine, was protected to prevent possible side-reactions at the next step. The Boc protection also allowed to perform the polymerizations in mild and convenient conditions. In the second step of the reaction, Boc-protected compound was reacted with methacrylic anhydride to obtain final methacrylated monomer structure.

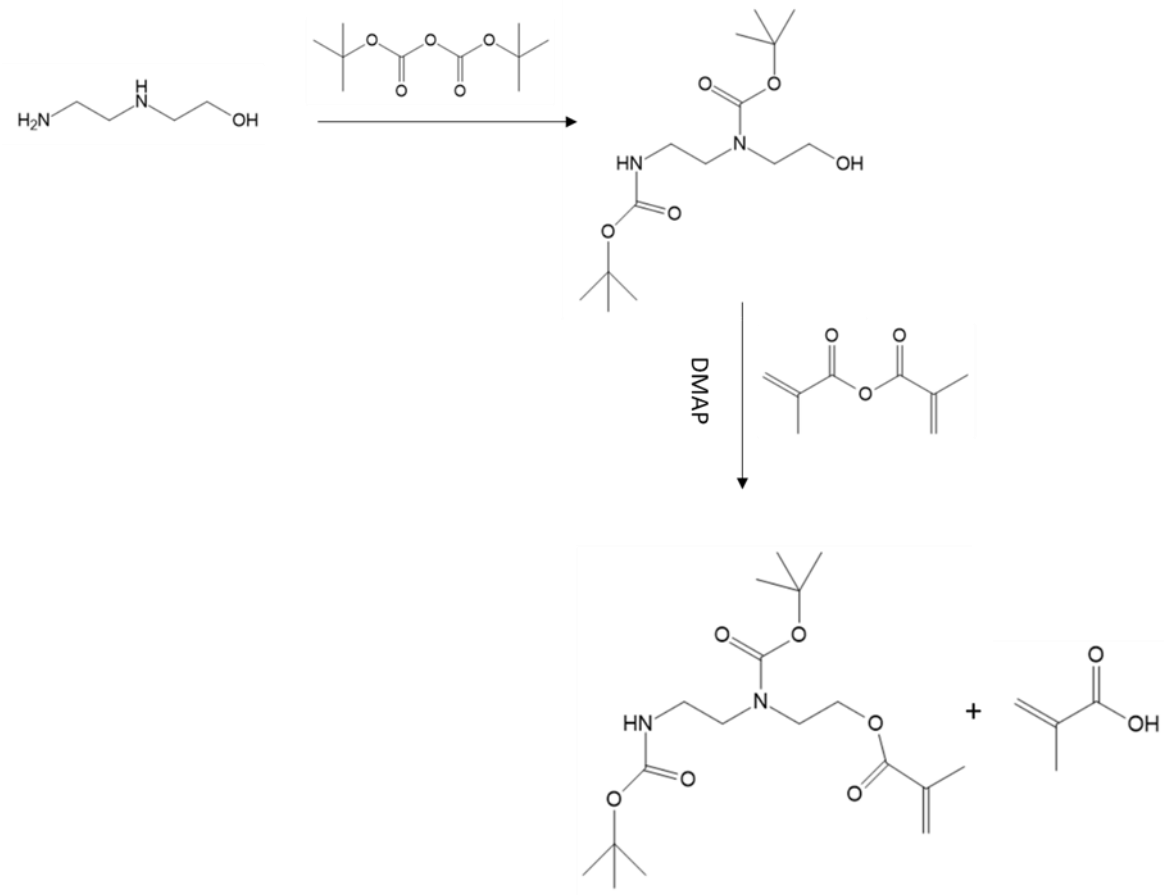

Figure 3.1. The scheme of BocAEAEMA synthesis.

To able to obtain Boc-protected, tert-butyl-2-(((tert-butoxycarbonyl) amino)ethyl)(2-hydroxyethyl)carbamate) (BocAEAE), first, 5 g (4,86 ml) of N-(2-hydroxyethyl) ethylenediamine (0.048 mole) was dissolved in 80 ml of dry DCM in ice bath. In a different round bottom flask, 21 g of di-tert-butyl dicarbonate (0.096 mol) was dissolved in 80 ml of dry DCM. Dissolved di-tert-butyl dicarbonate, was dropwise added to N-(2-hydroxyethyl) ethylenediamine under nitrogenous atmosphere in ice-bath. The reaction was allowed to stir for 1h in ice-bath while purging with nitrogen. After 1h, ice-bath is removed, and the reaction was stirred for 24 h at room temperature. After the reaction side-product was filtrated. To remove unreacted compounds water-DCM extraction was performed more than 3 times. Solution was concentrated using rotary evaporator. Flash chromatography system (mobile phase: petroleum benzine-ethyl acetate (30% ethyl acetate)) was further used to remove remaining unreacted compounds. Solvent was evaporated using rotary evaporator. Anhydrous magnesium sulphate was

added in order to remove water from organic phase completely. Amine groups-blocked BocAEAE was obtained at the end of the reaction and by ^{1}H-NMR analysis the formation of the product and purification was verified.

At the next step, BocAEAE was reacted with methacrylic anhydride to obtain BocAEAEMA, monomer. BocAEAE (14g, 0.046 mole) was dissolved in dry DCM (60 ml). Methacrylic anhydride (10.22 ml, 0.069 mole) was added dropwise to dissolved BocAEAEMA solution under nitrogenous atmosphere. The solution was allowed to stir for 15 min. Afterwards, DMAP (0.167g, 0.0014 mole) was dissolved in dry DCM (10 ml) and added dropwise to the solution. The reaction refluxed at 40 °C and was allowed to stir for further 16 h. At the end of the reaction, brine-DCM and then water-DCM extraction was performed three times. Organic phase was collected, and solvent was evaporated using rotary evaporator. The mixture was further purified by flash chromatography using petroleum benzine and ethyl acetate (10% and 20% ethyl acetate) solvent mixture.

3.3.1.2 Synthesis of Oligo(2-ethyl-2-oxazoline) Methacrylate (OEtOxMA)

The macromonomer, OEtOxMA, was synthesized via cationic ring opening polymerization (CROP) by adapting the method reported by Weber et al. (Weber, Becer, Hoogenboom, & Schubert, 2009) (Figure 3.2). Briefly, 2-ethyl 2-oxazoline (EtOx) (5g, 50.4 mmol) and Methyl p-toluenesulfonate (MeTos) (1.17g, 6.3 mmol) were transferred to the pre-dried reaction vessel under inert conditions. Dry Acetonitrile was added to the vessel (6.57 ml) (EtOx concentration: 4 mol/L). Reaction vessel was caped and immersed into the oil bath at 80 °C. After 1h, reaction vessel was removed from the oil bath and 1.5-fold excess methacrylic acid (9.5 mmol) and 2-fold excess triethyl amine (12.6 mmol) was added to the reaction vessel via syringe and the mixture was put into the oil bath at 60 °C overnight. Reaction mixture was analyzed by ^{1}H-NMR.

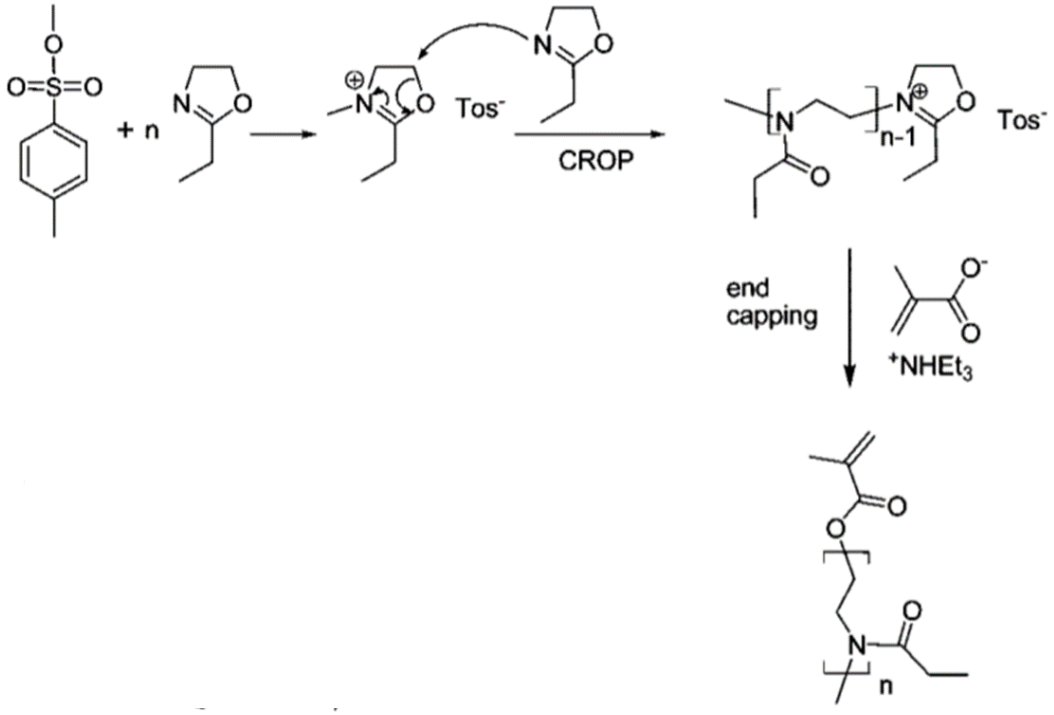

Figure 3.2. Synthesis of oligo(2-ethyl-2-oxazoline) methacrylate via CROP.
(Source: Weber et al., 2009)

For the purification of O(EtOxMA), acetonitrile was removed using rotary evaporator. Later, chloroform – sodium hydrogen carbonate (x3) and afterwards brine extraction (x3) was performed. After treatment with magnesium sulphate, pure O(EtOxMA) was analyzed by ^{1}H-NMR. Purification was verified and DP of the macromonomer was calculated via NMR spectrum.

3.3.2. Synthesis of Linear Block Copolymers

3.3.2.1. Synthesis of Poly(oligo(ethylene glycol) methyl ether methacrylate)-*b*-poly(2-((tert-butoxycarbonyl) (2-((tert-butoxycarbonyl) amino) ethyl) amino) ethyl methacrylate) (P(OEGMA)-*b*-P(BocAEAEMA))

In order to yield P(OEGMA)-*b*-P(BocAEAEMA), first P(OEGMA) with varied molecular weights have been synthesized by RAFT polymerization (Figure 3.3 and Table 3.1). For this aim, monomer concentration was set as 1 or 1.2 M and Monomer/RAFT agent/Initiator ratio was kept as 100/1/0.25 or 50/1/0.25. Initiator (AIBN), RAFT agent (CPADB) and monomer (OEGMA (Mn:500 g/mol)) were dissolved in acetonitrile separately. The reaction medium was purged with nitrogen for 25 min. and the mixtures were put in oil bath at 65°C. At the end of the polymerizations, the mixtures were treated with air and immersed in ice bath. Acetonitrile was removed under air flow. NMR samples were taken to determine the monomer conversion. P(OEGMA) polymers was purified by precipitating in cold diethyl ether or dialysis depending on the molecular weight. Pure polymers were analyzed by SEC and ^{1}H-NMR.

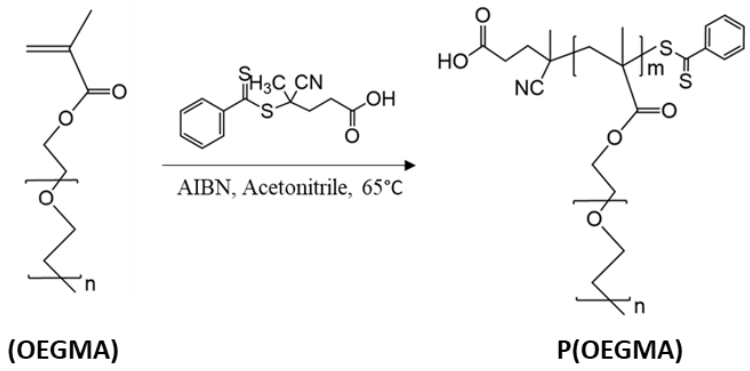

Figure 3.3. The scheme of P(OEGMA) synthesis.

Table 3.1. The polymerization conditions for P(OEGMA) synthesis.

[OEGMA] (mol/l)	$[OEGMA]_0/[CPDAB]_0/[AIBN]_0$	Time (min)
1	50/1/0.25	100
1	50/1/0.25	165
1.2	100/1/0.25	180

Chain extension of P(OEGMA) was performed to obtain block copolymer, P(OEGMA)-*b*-P(BocAEAEMA) (Figure 3.4 and Table 3.2). Synthesized P(OEGMA)s were used as macroRAFT agents. MacroRAFT agent, the monomer BocAEAEMA and AIBN were dissolved in acetonitrile ([BocAEAEMA = 1 M and [BocAEAEMA]/ [P(OEGMA)]/ [AIBN] ratio was 100/ 1/ 0.25). The reaction solution was purged with nitrogen for 25min., then immersed into an oil bath at 65 °C and polymerized for varied time periods. Polymerization was terminated by treating the mixture to air and immersing the vial to ice bath. Obtained block copolymers were purified from the crude by precipitating in hexane. Copolymers were characterized by ^{1}H-NMR and SEC analyses.

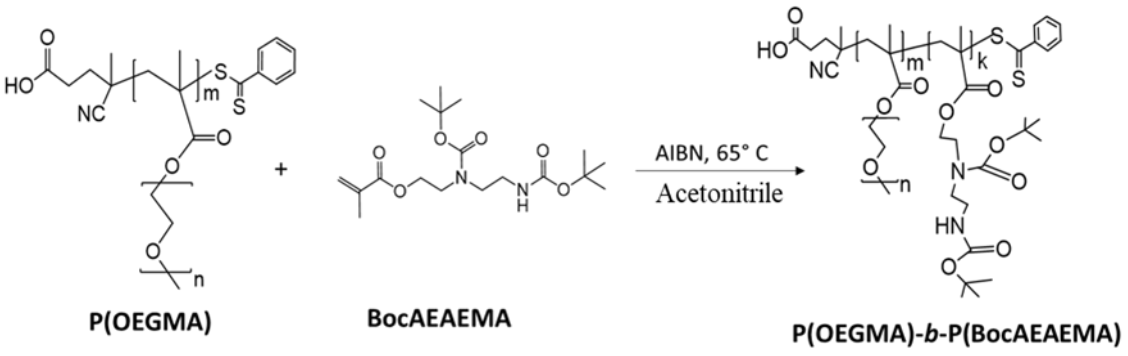

Figure 3.4. The scheme of P(OEGMA)-*b*-P(BocAEAEMA) synthesis.

Table 3.2. The polymerization conditions for P(OEGMA)-*b*-P(BocAEAEMA) synthesis.

$[BocAEAEMA]_0/[P(OEGMA)]_0/[AIBN]_0$	MakroRAFT Mn (SEC) (g/mol)	Time (min)
100/1/0.25	15 kDa	105
100/1/0.25	15 kDa	210
100/1/0.25	15 kDa	240
100/1/0.25	15 kDa	315
100/1/0.25	15 kDa	420
100/1/0.25	15 kDa	720
100/1/0.25	10 kDa	720
100/1/0.25	5 kDa	960

After polymerizations, (tert-butyloxycarbonyl) (Boc) groups were removed from the polymers by using trifluoroacetic acid (TFA). Briefly, polymers (4.35 μmol) were dissolved in DCM (1 ml). Drop by drop TFA (0.5 ml) was added into the solutions at 0 °C. The solution was allowed to stir for 1 h at room temperature. At the end of the reaction, solvent was evaporated under nitrogen flow. The reaction mixture was washed with diethyl ether for three times. The deprotected polymers were dried and characterized by ^{1}H-NMR spectroscopy in D_2O.

Thiocarbonylthio RAFT-end group of polymers was also removed to prevent possible cytotoxic effects. Briefly, polymers were reacted with methyl methacrylate (MMA) in the presence of hexylamine (HEA) and triethylamine (TEA) for 3 hours under nitrogen atmosphere at room temperature ([P(AEAEMA)]/ [HEA]/ [TEA]/ [MMA] = 1/ 50/ 50/ 3). The polymers were precipitated in diethyl ether and further purified by dialysis against distilled water (MWCO 1000 Da). The polymers were dried using freeze-dryer and characterized by ^{1}H-NMR spectroscopy.

3.3.2.2. Synthesis of Poly(ethylene glycol)-*b*-poly(2-((tert-butoxycarbonyl) (2-((tert-butoxycarbonyl) amino) ethyl) amino) ethyl methacrylate) (PEG-*b*-P(BocAEAEMA))

RAFT functionalized PEG (Poly(ethylene glycol) methyl ether (4-cyano-4-pentanoate dodecyl trithiocarbonate) (Mn 5400) was used to yield PEG-*b*-P(BocAEAEMA) (Figure 3.5). For this, PEG-RAFT agent, AIBN (initiator) and BocAEAEMA (monomer) was dissolved in acetonitrile ([BocAEAEMA]/ [PEG-RAFT]/ [AIBN] = 100/ 1/ 0.25 and [BocAEAEMA] = 1 M). The solution was degassed with nitrogen for 30 min and left to polymerization (4 h) in oil bath at 65°C. The solution was exposed to air and cooled down in ice to end the reaction. The polymer was purified, deprotected, and characterized as described in P(OEGMA)-*b*-P(AEAEMA) synthesis (Section 3.3.2.1).

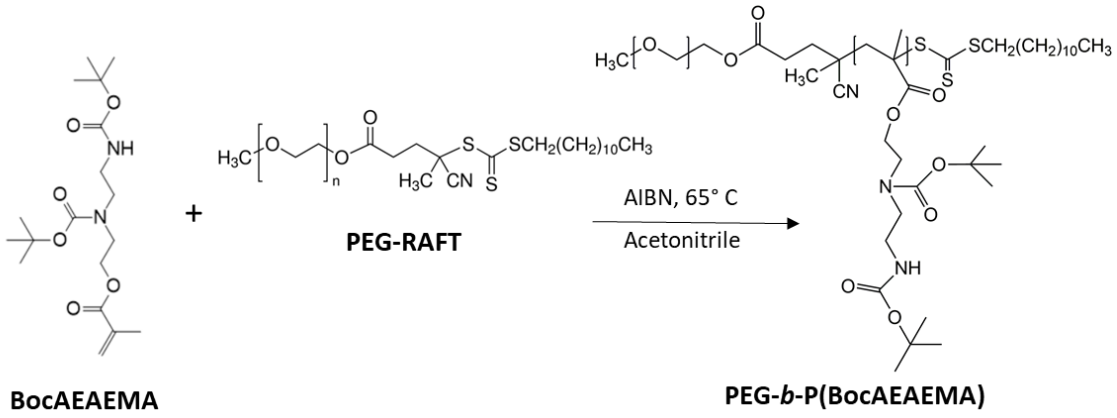

Figure 3.5. The scheme of PEG-*b*-P(BocAEAEMA) synthesis.

3.3.2.3. Synthesis of Poly(2-((tert-butoxycarbonyl) (2-((tert-butoxycarbonyl) amino)ethyl) amino) ethyl methacrylate-*b*-poly(oligo(2-ethyl-2-oxazoline) methacrylate) (P(BocAEAEMA)-*b*-P(OEtOxMA))

To yield P(AEAEMA)-*b*-P(OEtOxMA), first; BocAEAEMA was polymerized by RAFT polymerization (Figure 3.6) and the obtained P(BocAEAEMA) was used as a macroRAFT agent. For this aim, monomer (BocAEAEMA), RAFT agent (2-Cyano-2-propyl benzodithioate) and initiator (AIBN) was dissolved separately in toluene (M/R/I =60/1/0.125, monomer concentration: 1 M). The mixture was degassed for 25 min. and put in oil bath at 70°C for 5 h 15 min. Reaction was stopped by exposing the mixture to air and immersing the reaction vessel to ice bath. Mixture was analyzed by ^{1}H-NMR and conversion was calculated. Polymer (P(BocAEAEMA) was purified by precipitating the mixture into petroleum benzine and purified polymer was analyzed by SEC and ^{1}H-NMR.

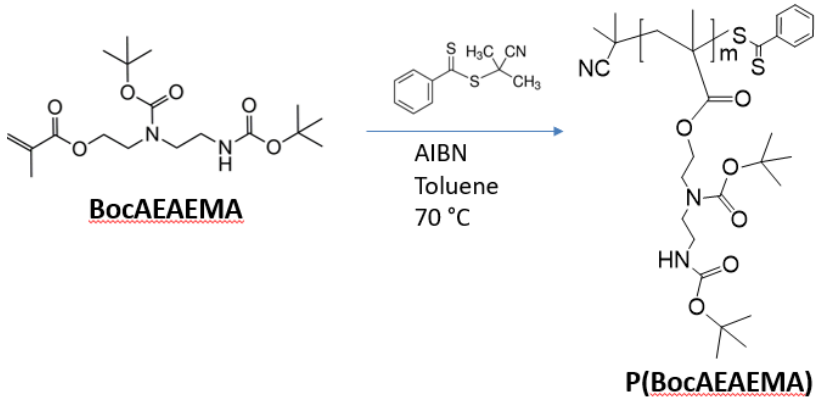

Figure 3.6. The scheme of P(BocAEAEMA) synthesis.

Synthesized P(BocAEAEMA) was used as macro-RAFT agent and polymerized in the presence of OEtOxMA (as monomer), and AIBN (as initiator) (Figure 3.7). Acetonitrile was used as reaction solvent. Monomer concentration was kept at 0.37 and M/R/I ratio was 50/1/0.25. 0.5% (v/v) anisole was added to reaction mixture as a reference

material and sample was taken before degassing. After purging with nitrogen, polymerization was carried out for 3 h 40 min at 70°C. Reaction mixture was analyzed by ^{1}H-NMR to find out the conversion. Polymer was purified from the mixture by precipitating it into diethyl ether (x1). Afterwards mixture was washed with diethyl ether more than 3 times. The purified polymer was analyzed by ^{1}H-NMR and SEC.

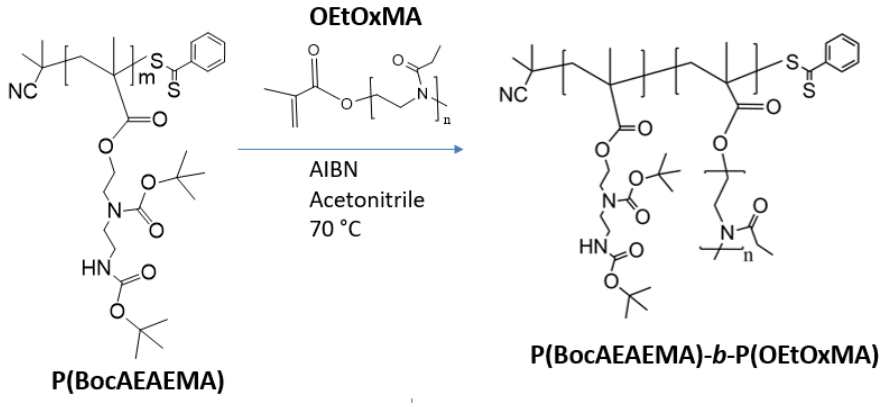

Figure 3.7. The scheme of P(BocAEAEMA)-*b*-P(OEtOxMA) synthesis.

P(BocAEAEMA)-*b*-P(OEtOxMA) was deprotected, aminolysed and purified as described previously (Section 3.3.2.1).

3.3.3. Synthesis of Star Polymers

Arm-first method was used to obtain the miktoarm star polymers. For this aim, first arms of the star polymers (P(OEGMA) and P(BocAEAEMA)) were synthesized and afterwards obtained arms were crosslinked in the presence of butyl acrylate. The feed ratio of macroRAFT agents (P(OEGMA):P(BocAEAEMA)) was differed to obtain star polymers with different compositions.

Synthesis of P(OEGMA) arm: OEGMA (Mn: 500 g/mol) was polymerized via RAFT polymerization (Figure 3.8). OEGMA, CDTPA, AIBN and acetonitrile was used as

monomer, RAFT agent, initiator and reaction solvent, respectively. Reaction was carried out at 70°C for 2 h and 45 min ([M]/ [R] [I] = 70/1/0.125 and [M]: 1.2 M). After the polymerization, reaction mixture was analyzed by ^{1}H-NMR to determine the monomer conversion. Polymer was purified by dialyzing against water (MWCO: 3.5kDa). Purification was confirmed by ^{1}H-NMR and SEC analysis. Mn and Đ was determined by SEC.

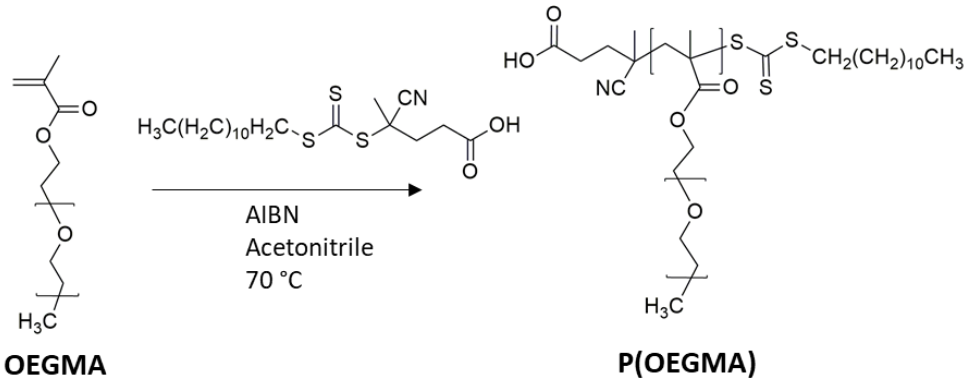

Figure 3.8. The scheme of P(OEGMA) arm synthesis.

Synthesis of P(BocAEAEMA) arm: Similar to P(OEGMA), RAFT polymerization was used for the synthesis (Figure 3.9). BocAEAEMA, CDTPA, AIBN and toluene was used as monomer, RAFT agent, initiator and reaction solvent, respectively. Reaction was carried out at 70°C for 7 h ([M]/ [R]/ [I] = 50/1/0.125 and [M]: 1 M). After the polymerization, reaction mixture was analyzed by ^{1}H-NMR to determine the monomer conversion. Polymer was purified by precipitating in petroleum benzine (more than 3 times). Purification was confirmed by ^{1}H-NMR and SEC analysis. Mn and Đ was determined by SEC.

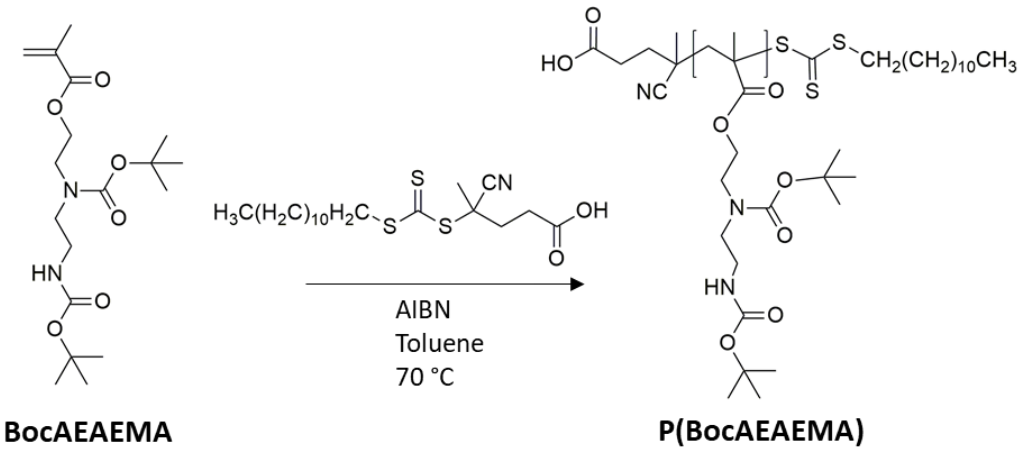

Figure 3.9. The scheme of P(BocAEAEMA) arm synthesis.

Synthesis of P(OEGMA)/P(BocAEAEMA) Miktoarm Stars: Purified arms, P(OEGMA) and P(BocAEAEMA) were cross-linked to obtain the star architecture. A redox reactive cross-linker, N,N′-Bis(acryloyl)cystamine (BAC), and a hydrophobic monomer (butyl acrylate) was used as core-forming units. P(BocAEAEMA), P(OEGMA), butyl acrylate (BA), BAC and AIBN (initiator), were mixed in anisole (1 ml) ([P(BocAEAEMA)]/ [P(OEGMA)]/ [BA]/ [BAC]/ [AIBN] = 0.5/0.5/4/8/0.33). The mixture was degassed for 30 min. under nitrogen on ice. After degassing, polymerized for 24 h in oil bath set at 70 °C. Reaction was stopped by exposing the reaction vessel to the air and immersing to the ice-bath. For purification, mixture was precipitated in petroleum benzine (1 time) then dissolved in methanol and centrifuged using centrifugal concentrator (MWCO: 100 kDa). Centrifugation was repeated for several times (5-6 times) by pouring the filtrated solution and topping the centrifuge tube up with methanol. Purification was confirmed by SEC analysis. Mn and Đ were determined by SEC. Composition of the star polymer was determined by ^{1}H-NMR.

In order to obtain another miktoarm star having high cationic content, the feed ratio of P(BocAEAEMA)]/ [P(OEGMA) was changed to 0.8:0.2 and all other process were repeated.

Miktoarm star polymers were deprotected by using TFA as described previously.

Synthesis of P(OEGMA) Homo-arm Star: Same procedure with miktoarm star synthesis were applied to homoarm star synthesis. In this case, only P(OEGMA) used as

macroRAFT agent ([P(OEGMA)]/ [BA]/ [BAC]/ [AIBN] = 1/4/8/0.33)). And instead of petroleum benzine, reaction mixture was precipitated into diethyl ether for purification.

3.3.4. Fluorescent Dye Labeling of Linear Block Copolymers

In order to determine cell association of the polymers and nanoparticles via flow cytometer and to observe intracellular distribution profile via confocal microscopy, block copolymers were labeled using a fluorescent dye, Cy5-NHS ester. The activated ester, Cy5-NHS was reacted with the block copolymer via its free amine groups. For this aim, 10 mg of $P(OEGMA)_{43}$-*b*-$P(AEAEMA)_{45}$ (and $P(AEAEMA)_{40}$-*b*-$P(OEtOxMA)_{38}$ at same mole equivalent) was dissolved in 810 µl of water and 90 µl of 1 M $NaHCO_3$ was added to the polymer solution. Separately 1 mg of Cy5-NHS was dissolved in 100 µl of DMSO. 33.38 µl of dye solution was transferred into separate vial and diluted with 66.62 µl of DMSO. Diluted dye solution was added to polymer solution. The mixture vortexed and incubated overnight. The conjugate was purified from unreacted dye and other organic impurities (N-hydroxysuccinimide, NHS ester, acid produced by hydrolysis) by dialyzing against DMF, then brine (1 M NaCl) and later mili-Q water. Labeling degree of the polymers were determined by UV-measurements according to Lambert-Beer law (accepting the molar extinction coefficient ε, 250000 $L \cdot mol^{-1} \cdot cm^{-1}$, provided by the manufacturer). Samples were freeze-dried and used for cell culture experiments (confocal microscopy and flow cytometry).

3.3.5. Preparation and Characterization of Polymer-siRNA Complexes

Polymer-siRNA formulations at varied N/P (N/P = moles of amine (polymer)/ moles of phosphate (siRNA)) were prepared and formed complexes characterized by gel electrophoresis, DLS, ELS, SEM and TEM.

The ability of the carriers to form polyplexes with siRNA has been investigated via gel electrophoresis. To determine the amount of polymer required to fully complex

the siRNA, varying amounts of polymers has been complexed with siRNA at a fixed concentration. The polymers were dissolved in 10 mM phosphate buffer at pH 6 to yield a polymer stock solution of 10^{-1} mM. Separately, siRNA was dissolved in RNase-free water at a concentration of 10 μM. Corresponding amounts of polymers were added to 0.04 nmol siRNA to obtain complexes at varying nitrogen/phosphate (N/P) ratios (1, 2, 3, 4, 5 and 50). The siRNA-polymer solutions were incubated at room temperature for 30 minutes. The solutions were then mixed with 6X loading dye and loaded into 3% agarose gel stained with 0.5 μg/ml ethidium bromide. The gel was run at 100 V for 25 minutes in 1X TAE running buffer and analyzed with UV illumination.

The change of hydrodynamic diameter of the complexes with respect to N/P was investigated by DLS. For this, siRNA concentration is fixed to 4 μM and polyplexes were prepared at N/P of 2,10 and 50 as described above. Average diameters were determined in PBS. To The zeta potential of the same complexes was analyzed by ELS.

The size and morphology of the polyplex was also investigated by TEM and SEM. As described, polyplexes were prepared (at N/P of 2 and 50) and 2-5 μl of the sample was applied to TEM grids (EM carbon grid, square, 200 mesh -copper, standard-). Before sample treatments, grids were treated to oxygen plasma. After sample treatment, the grids were dried using mild nitrogen-flow. SEM was also employed for the same reason. Complexes were prepared as described and 2 μl of the sample was dropped on pre-cleaned silicon wafers. Complexes left to dry in room temperature and coated with gold before SEM analysis.

3.3.6. Investigation of Serum Stability of the Polyplexes

The siRNA protection ability of the polymers against serum nucleases has been investigated by agarose gel electrophoresis. The polyplexes were prepared at N/P of 50 as previously described and incubated with equal volume of fetal bovine serum (FBS) at 37 °C for predetermined times (0 h, 0.5 h, 2 h, 8 h, and 24 h). At the end of the corresponding incubation times, the aliquots (0.08 nmole siRNA) were taken and immediately treated with 0.5 M EDTA to stop the degradation. Aliquots were frozen and kept at -20°C until the time of analysis. Before the analysis, heparin has been added to

the polyplex solutions in order to displace the siRNA from the complex and the final solution analyzed by 3% agarose gel electrophoresis (100 V, 25 min.). The serum stability of naked siRNA has been determined by applying the same procedure.

3.3.7. Investigation of siRNA Release

Heparin competition assay was performed to investigate the release profile of siRNA from the complexes.

Polymer-siRNA complexes (siRNA concentration = 0.04 nmol) were prepared at N/P of 50 as described before. Upon complex formation (after 30 min. incubation), increasing amounts of heparin (0, 0.5, 1.25, 2.5, 5, 10, 20, 40, 80 μg) was added to the complexes and incubated for 30 min. At the end of the incubation time, complexes treated with varying amounts of heparin were loaded into agarose gel. Gels (3%) have been runed (100 V, 25 min.) and imaged (UV illumination) as same before. A low-range DNA ladder and naked siRNA (same concentration used in complex formation) was also loaded to the wells.

3.3.8. Determination of Polymer Toxicity

The cyto-toxicity of polymers was investigated on different cell lines, namely, MDA-MB-231 (human ovarian cancer cell line), H460 (human lung cancer cell line), NIH/3T3 (mouse fibroblast cell line) and Raw 264.7 (mouse macrophage cell line). MTT assay was employed to determine the effects of the polymer on cell viability. Briefly, cells were seeded to 96-well plate at a concentration of 10.000 per well. After 24 h incubation, medium was discarded and 95 μl of fresh media was added into the wells. Then 5 μl of polymer solutions (in 10 mM phosphate buffer pH 6.0) added to the wells (final polymer concentration in the wells: 20, 10, 5, 2.5, 1.25 μM). Cells were incubated with polymers for 24 h and at the end of the incubation period, medium was discarded. 100 μl of fresh medium including MTT reagent (10 % (v/v)) was added to the wells and microplates were incubated in the cell culture incubator (5% CO_2, dark and humidified atmosphere)

for 3 h and 30 min. At the end of the incubation period, supernatants were removed, and formazan crystals were dissolved in 100µl DMSO. The absorbance at 570 nm was determined using a microplate reader. Cells incubated with only phosphate buffer was used as control and viability of these accepted as 100 % after blank measurements were subtracted. Assay was performed in triplicate.

3.3.9. Investigation of Cell Association of Polymers and Polyplexes

Flow cytometer was used to determine the association of the linear block copolymers with cells. For this aim, cells (MDA-MB-231 and H460-luc2) were seeded to 24-well plate at the concentration of 10^5/well (in 500 µl). After 24 h incubation period, medium was discarded, 285 µl fresh media was added to the wells. Afterwards, 15 µl of Cy5-labeled polymers (0.067 nmole polymer per well) were added to the wells. Polymers were incubated with cells for 30 min. or 4 h in cell culture incubator. After incubation periods, media was discarded. Wells were washed with 500 µl of PBS. PBS was removed and cells were detached by trypsinization (200 µl). Afterwards, 800 µl of complete media was added to the wells and harvested cells were centrifuged for 5 min. at 1000 rpm. Then media was discarded, and cell pellet was dissolved in 200 µl of PBS (including PI at a concentration of 0.01 mg/ 20 ml). Cell solutions were transferred to the flow cytometer tubes. Cells treated with only buffer were used as controls. Assay was performed in triplicate.

Cellular association of polymer-siRNA complexes was also investigated. In this case, cells (MDA-MB-231 and H460-luc2) were seeded to 24-well plate at the concentration of $5x10^4$/well. Alexa Fluor-488 labeled siRNA was complexed with the non-labeled polymers (linear and star polymers) at N/P of 2 or 50 as described before. Complexes (25 µl) were incubated with the cells for 24 h (total volume of media + complexes in one well was 500 µl and siRNA concentration was 50 nM). Afterwards, the same procedure was applied as described above. Only Alexa Fluor-488 labeled siRNA (without polymer) was used as control. Assay was performed in triplicate.

3.3.10. Investigation of Intracellular Distribution of Polyplexes

Cellular uptake of the complexes was further investigated using confocal microscopy. Fluorescently labeled siRNA and Cy-5 labeled block copolymers were used to track intracellular fate of the complexes. Hoeschst 33342 was used as nuclear dye. Lysosomes/endosomes were labeled using LysoTracker^{TM} to determine the localization of the vesicles inside the cell.

A classical imaging procedure was performed as follows. First, cells (MDA-MB-231) were seeded (300 µl for each well) to 8-well chamber slides (ibiTreat) at a concentration of 10^4/ well. Next day, medium was removed, and fresh media (200 µl) was pipetted to the wells. Complexes (5 µl) prepared at N/P 2 or 50 was added to the wells (final concentration of the siRNA in one well was 50 nM). Cells were treated with complexes for 24 h and at the end of the incubation period, media was discarded. Wells were washed with 300 µl of HBSS for 3 times. Then, 200 µl of Hoechst (diluted to the concentration of 1 µg/ml with HBSS) was pipetted to the wells and chamber was covered with aluminum foil and incubated for 10 min. in the cell culture incubator. After the incubation, media was removed, and cells were washed with HBSS at room temperature for 2-3 times. 200 µl of LysoTracker Red (diluted to the concentration of 100 nM with HBSS) was applied to the wells. Cells were incubated in the cell culture incubator for 1h in the dark atmosphere. At the end of the incubation, media was removed, and cells were washed with HBSS (at least three times) and then serum containing fresh RPMI was added to the wells. Afterwards, live cell imaging was performed directly.

3.3.11. Determination of Gene Silencing Efficiency and Toxicity of the Polyplexes

MDA-MB-231-luc2-gfp (human mammary gland cancer cell line) and H460-luc2 (human lung cancer cell line) were used for the investigation of gene silencing efficiency and toxicity of the polyplexes. A commercial transfection reagent Lipofectamine RNAi max was used as a control. A negative control siRNA which is not targeting the luciferase sequence was also employed to determine non-specific gene silencing effects.

MDA-MB-231-luc2-gfp was cultured in 10% FBS containing high glucose DMEM (with l-glutamine, HEPES and phenol red) and H460-luc2 was cultured in 10% FBS containing RPMI 1640 media (with l-glutamine, HEPES and phenol red). When they reached to enough confluency, cells were seeded to 96-well plates at a concentration of 10^4 cells/well. After 24 h, medium was discarded, and fresh media was added. Lipofectamine-siRNA complexes were prepared based on manufacturer's recommendations. Polymer-siRNA complexes (at varied siRNA doses and N/P ratios) were prepared as described before. Cells were treated with complexes for 24 h. After 24 h incubation, cells were incubated for further 24 h in fresh media -without nanoparticles- before measurements. To determine the cell viability MTT assay was employed and performed as described before. To determine the gene silencing ability, luciferase assay was performed. For this aim, 48 h post-treatment with nanoparticles, media of the cells were discarded. Cells were washed with 100 µl of PBS. Afterwards, 20 µl lysis reagent was pipetted to the wells. After 20 min. incubation luminescence intensity was measured using the pre-programed plate reader. 100 µl of luciferase reagent was distributed to the wells by dispenser of the instrument and measurements were recorded (after reagent distribution immediately) for 10 seconds after 2 seconds delay time. The assay was performed in triplicate.

In addition to luciferase reporter assay, RT-qPCR was also used to examine the transfection efficiency. An intermediate filament protein, vimentin, was targeted on MDA-MB-231 cell line. siRNA targeting the luciferase gene was used as the negative control. Cells were seeded to 6-well plates at a concentration of 30 x 10^4 cells/well. After 48 h, medium was discarded, and fresh media was added. Polymer-siRNA complexes at N/P of 50 was prepared as described before and added to the cells (final siRNA concentration in the wells was 50 nM). After 24 h, medium was removed, and fresh medium was added. Cells were further incubated for 24 h. At the end of the total 48 h of incubation period, total RNA was isolated using Monarch Total RNA Miniprep Kit. RevertAid First Strand cDNA Synthesis Kit was used to synthesize cDNA from 1 µg of total RNA. Vimentin mRNA level was determined by qPCR and normalized to housekeeping gene, TBP. (Primers: vimentin 5′-GCTAACCAACGACAAAGCCC-3′, 5′-CGTTCAAGGTCAAGACGTGC-3′). The vimentin expression of non-treated cells was assumed to be 100% and the expression in polyplex-treated cells was calculated accordingly. Results are presented as average ± standard deviation (n=3).

CHAPTER 4

RESULTS AND DISCUSSION

4.1. Synthesis and Characterization of Monomers

4.1.1. Synthesis of BocAEAEMA

Boc-protected, amine containing monomer, BocAEAEMA, was synthesized by adapting a previously reported procedure (Kurtulus et al., 2014). In the first step of the synthesis, N-(2-hydroxyethyl) ethylenediamine was reacted with di-tert-butyl dicarbonate. With the reaction, amine groups of the N-(2-hydroxyethyl) ethylenediamine has been blocked by tert-butyloxy carbonyl groups. After the reaction, sample was taken from the crude and analyzed by ^{1}H-NMR in $CDCl_3$ (Figure 4.1).

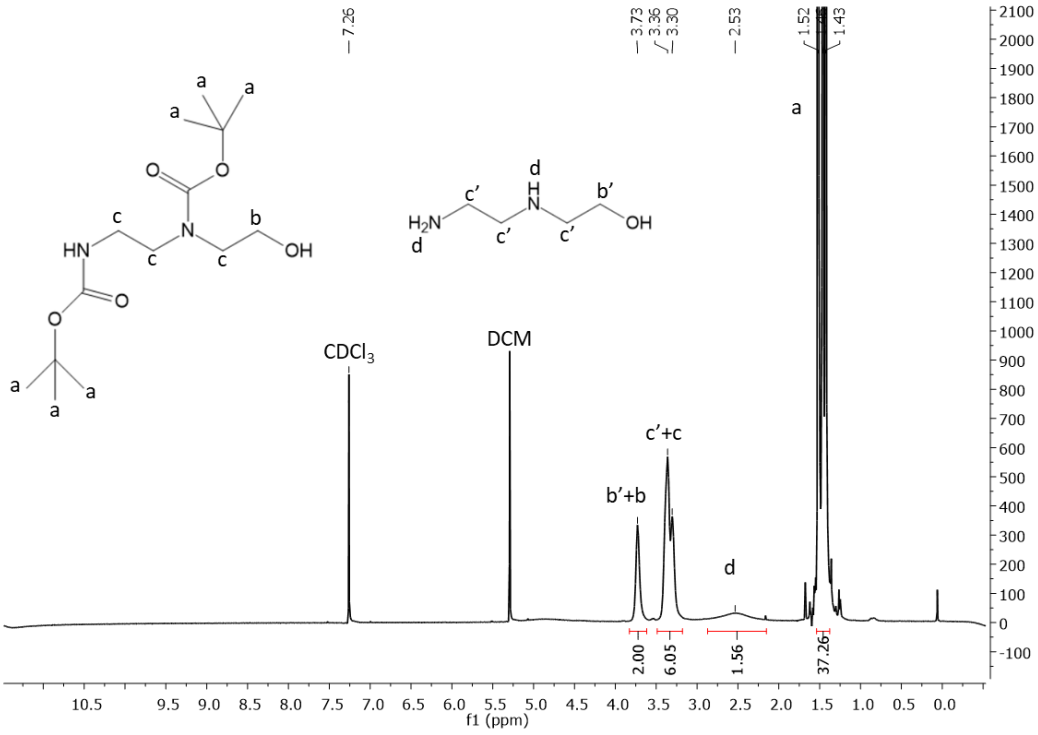

Figure 4.1. ^{1}H-NMR spectrum of the reaction mixture (1st step-before purification).

The characteristic signals of Boc groups were observed between 1.43 and 1.52 ppm on the spectrum. Protons belonging the amine groups of the starting material (N-(2-hydroxyethyl) ethylenediamine) was also observed at 2.53 ppm indicating the presence of the unreacted compound after the reaction. Percent yield could be calculated using the integral of the peaks at 3.73 and 2.53 ppm as shown in below equation (Equation 4.1). The yield of the reaction was found to be 48% by NMR.

$$\%\,Yield\ = \frac{I_{3.73ppm}/_2 - I_{2.53\,ppm}/_3}{I_{3.73ppm}/_2}\ x\ 100 \qquad (4.1)$$

To purify the BocAEAE from the reaction mixture, Water-DCM extraction was performed. Mixture was extracted with water at least for 4 times. After the extraction, solvent was evaporated using rotary evaporator then air dried for further drying. NMR sample was taken and analyzed in $CDCl_3$ (Figure 4.2)

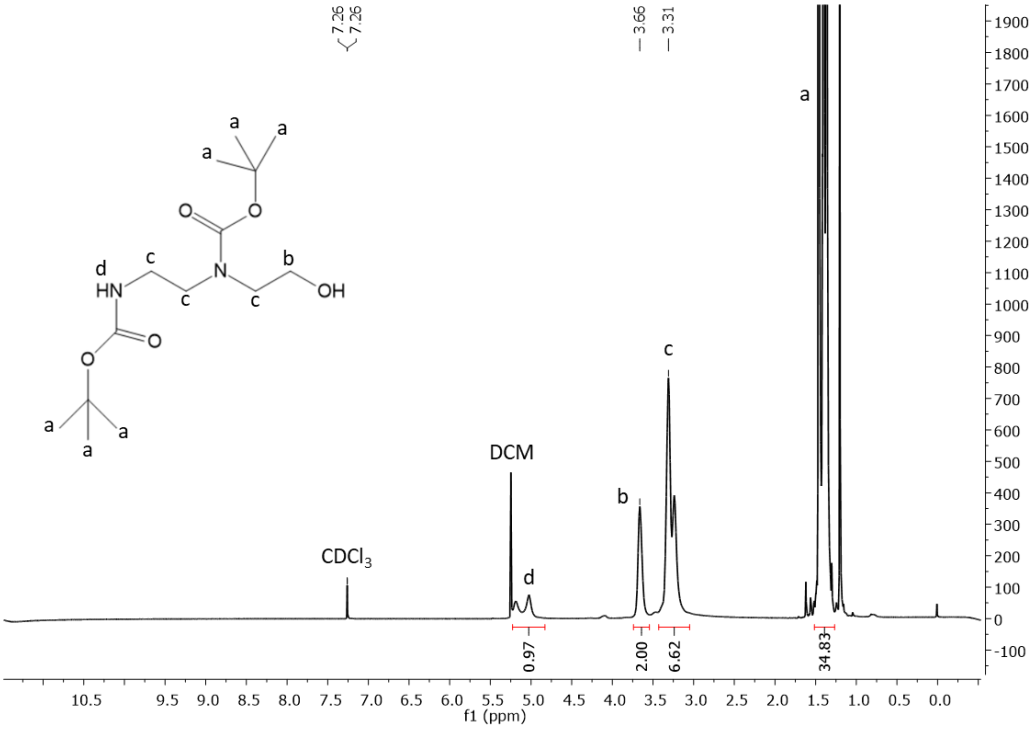

Figure 4.2. ^{1}H-NMR spectrum of the reaction (1st step) mixture after water-DCM extraction.

By extraction water soluble N-(2-hydroxyethyl) ethylenediamine could be removed from the mixture. The disappearance of the signals coming from the amine groups of N-(2-hydroxyethyl) ethylenediamine at 2.53 ppm proved the successful purification of BocAEAE. However, the integral values belonging the Boc groups (1.43-1.52 ppm) was found the be almost same before and after extraction. This showed that the reaction mixture still includes excess di-tert-butyl dicarbonate after extraction. To remove unreacted di-tert-butyl decarbonate, flash chromatography was performed. After flash chromatography, the obtained fraction was analyzed by ^{1}H-NMR (Figure 4.3). A significant decrease at the integral value of characteristic Boc groups (at 1.43-1.52 ppm) proved the success of the purification. All the integral and chemical shift values matched with expected chemical structure and showed that pure BocAEAE could be obtained successfully.

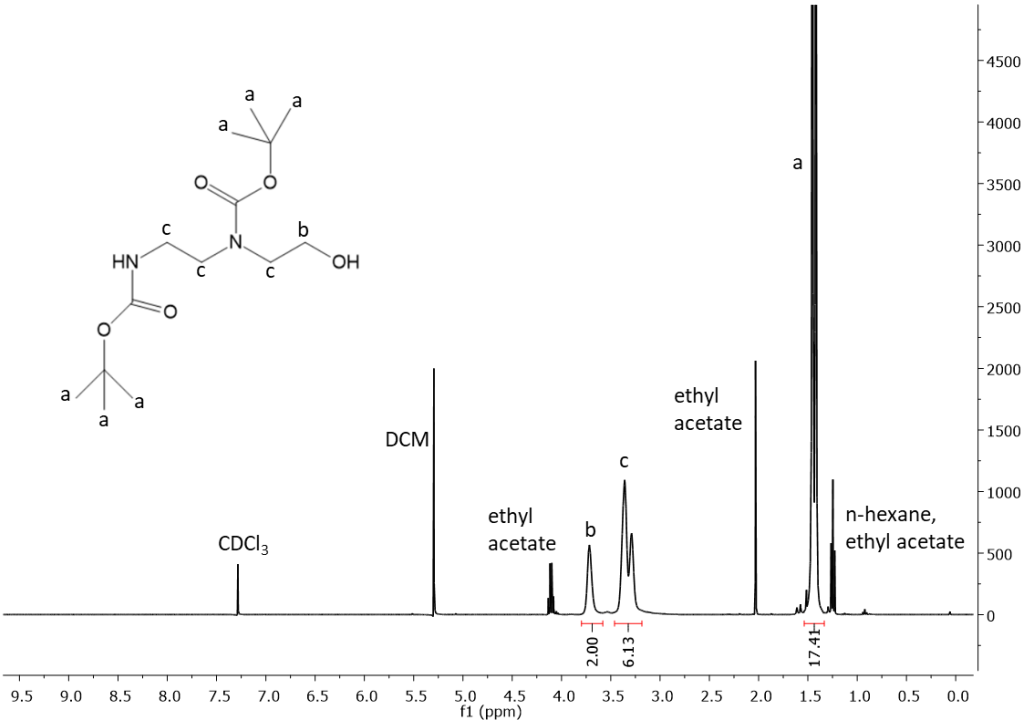

Figure 4.3. ^{1}H-NMR spectrum of reaction (1st step) mixture after flash chromatography.

At the second step of the synthesis, pure BocAEAE was reacted with methacrylic anhydride to yield methacrylated monomer, BocAEAEMA, (Figure 4.4).

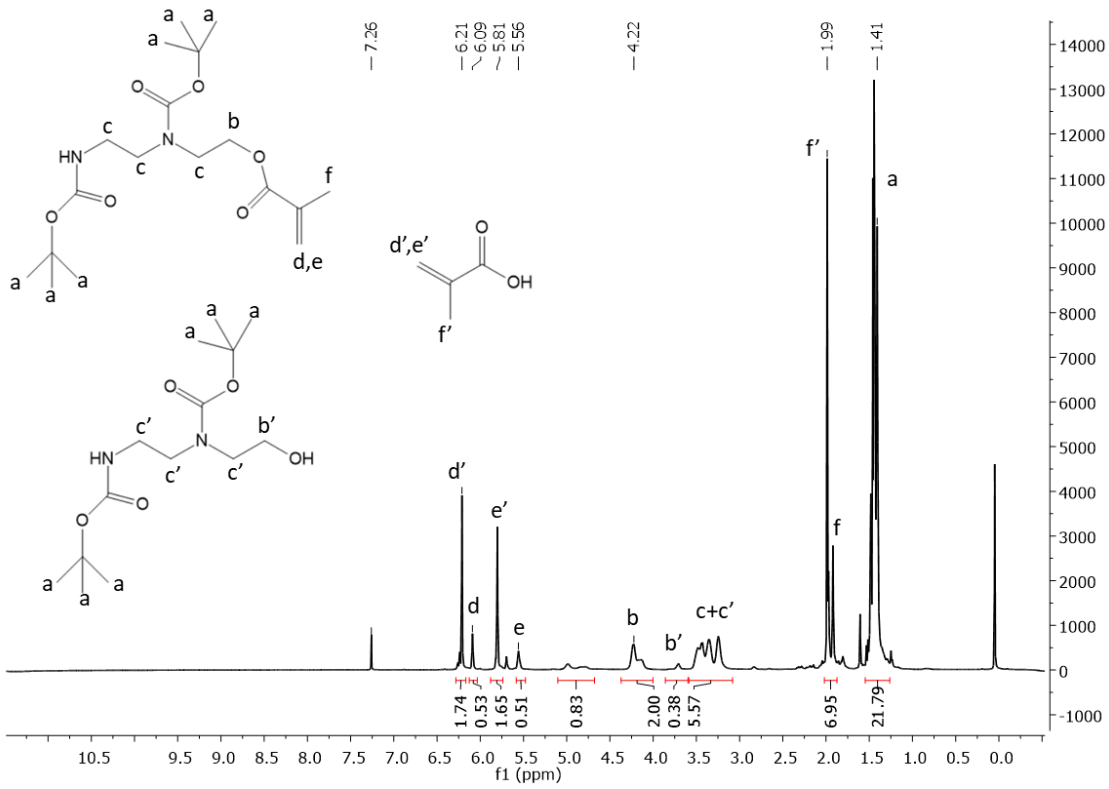

Figure 4.4. ^{1}H-NMR spectrum of reaction mixture (2nd step-before purification).

^{1}H-NMR analysis of the 2nd step reaction mixture showed the formation of ester bond (at 4.22 ppm) which has proved the formation of final monomer structure successfully. The yield was calculated according to the given Equation (Equation 4.2).

$$\%\, Yield = \frac{I_{4.22\ ppm}/_{2}}{I_{3.78ppm}/_{2} + I_{4.22\ ppm}/_{2}}\ x\ 100 \qquad (4.2)$$

The yield of the 2nd reaction was found to be 84% by NMR. For purification, the reaction mixture was extracted with water then brine (3 times for each) then further purified by flash chromatography using gradient mixture of petroleum benzine and ethyl acetate. Collected fractions were analyzed by thin layer chromatography (TLC) and ^{1}H-

NMR. As evidenced by ^{1}H-NMR, pure monomer fraction could be obtained after performing flash chromatography (Figure 4.5). Consequently, BocAEAEMA could be successfully synthesized and purified.

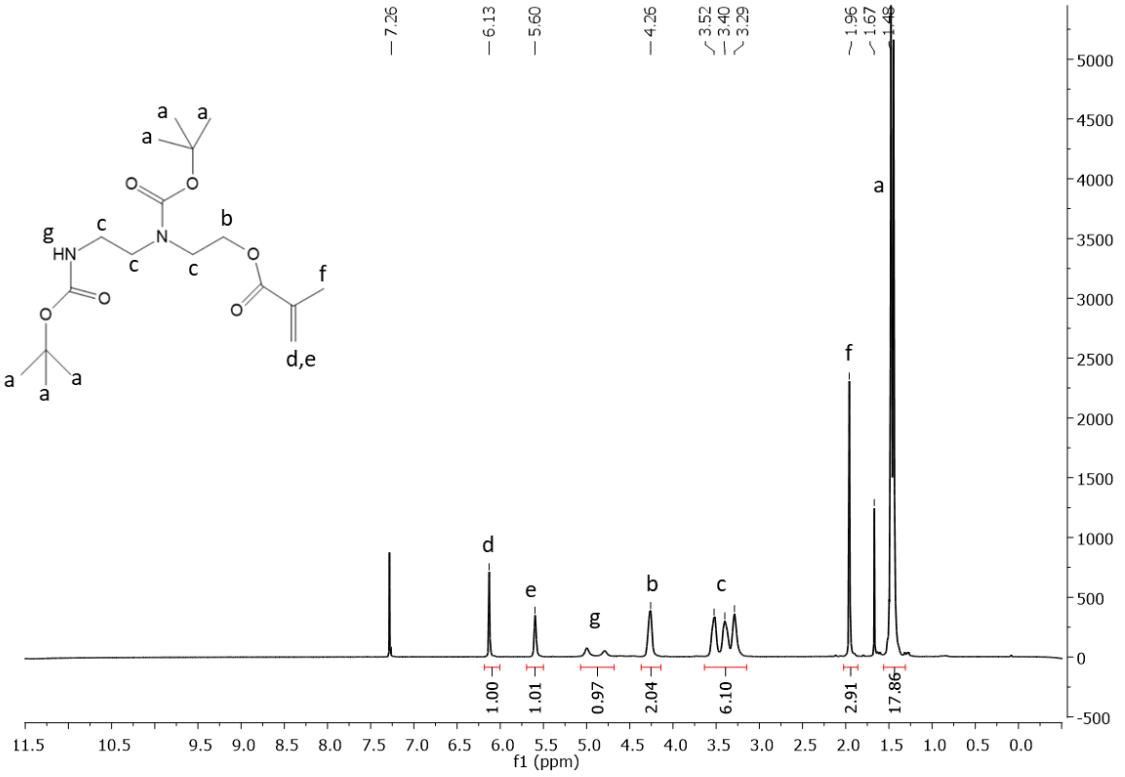

Figure 4.5. ^{1}H-NMR spectrum of pure BocAEAEMA (2nd step-after purification).

4.1.2. Synthesis of OEtOxMA

With the discovery of immunogenicity of PEG and anti-PEG antibodies, the research to find PEG alternatives has gained great importance. Hydrophilic POx (poly(2-oxazoline) stands out as a good candidate since these polymers, -similar to PEG- show stealth properties and are also considered as non-toxic and low immunogenic. Additionally, they can show desired biodistribution and excretion profile which makes them perfect candidate for drug delivery applications. Moreover, the availability of

versatile oxazoline monomers (such as methyl, ethyl or propyl oxazoline) allows to tune the solubility, aggregation tendency and hydrophobicity as demanded. Furthermore, the selection of suitable initiator and terminating agents together with monomer can lead to the formation of differed functionalized structures that can be modified for further applications and used for broad range of applications. By considering all these, OEtOxMA has been synthesized and afterwards used for the preparation of P(AEAEMA)-*b*-P(OEtOxMA) block copolymer as an alternative to P(OEGMA) containing P(OEGMA)-*b*-P(AEAEMA) block copolymer. The effect of the POEGMA replacement has been discussed and the effect of this replacement on siRNA delivery has been investigated throughout this work.

OEtOx, has been synthesized by CROP and the polymerization was terminated by methacrylic acid to obtain methacrylate end functionalized OEtOxMA. Methyl tosylate (MeTos) was used as initiator and the molar ratio of monomer (EtOx, 2-Ethyl-2-oxazoline) to MeTos was set to 8 to obtain OEtOx having approximately same DP with commercially obtained OEGMA (Mn: 450 g/mol; DP: 8-9). Polymerization of EtOx was performed in acetonitrile in the oil bath set to 80 °C. Direct end-capping method was used as described elsewhere (Weber et al., 2009). Living oxazolinium groups that are located at the end of the chain were attacked with nucleophilic methacrylate anions and this leaded to formation of OEtOx with methacrylate unit (OEtOxMA). The reaction mixture was analyzed by ^{1}H-NMR (Figure 4.6). The presence of vinyl protons at 5.57 and 6.07 ppm proved the formation of OEtOxMA.

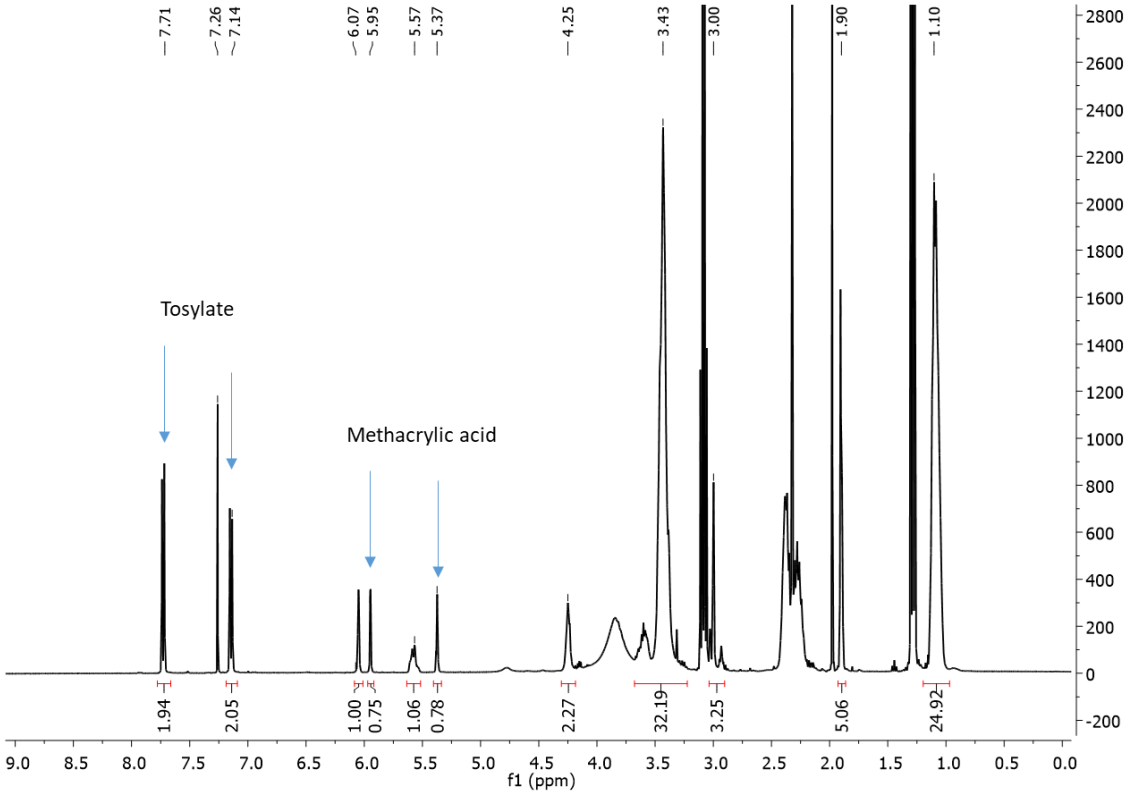

Figure 4.6. ^{1}H-NMR spectrum of OEtOxMA polymerization mixture before purification.

Excess methacrylic acid, initiator and TEA was removed by extraction. After purification, ^{1}H-NMR analysis was carried out and the disappearance of the tosylate and methacrylic acid was observed in the spectrum (Figure 4.7). The integrals of the vinyl protons at 5.59 and 6.07 ppm and methyl protons at 3.02 ppm showed great consistency demonstrating that functionalization of the OEtOxMA could be done at high efficiency. In other words, considering the usual errors seen in NMR analysis in general, it can be said that all living OEtOx species could be capped with methacrylate units.

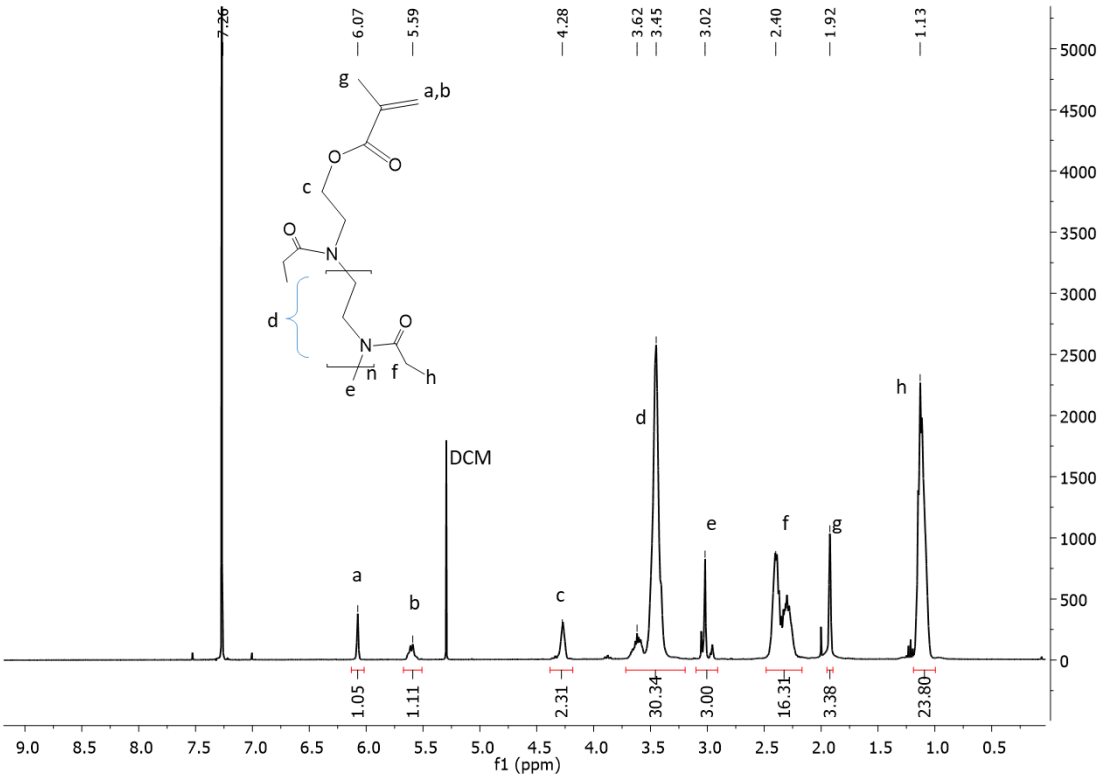

Figure 4.7. ^{1}H-NMR spectrum of pure OEtOxMA.

DP of the macromonomer was calculated according to Equation 4.3 and found to be 8.16.

$$DP = \frac{I_{3.2-3.7ppm} + I_{4.2-4.4ppm}}{4} \quad (4.3)$$

Pure OEtOxMA was analyzed by SEC for further characterization and, Mn and Đ values were determined (Figure 4.8). SEC trace showed that the well-defined macromonomer could be obtained with dispersity of 1.10 and Mn of 1440 g/mol. Mn obtained from the SEC was found to be higher than theorical Mn which is acceptable and expectable due to relative determination of Mn via SEC-RI detector and calibration curve.

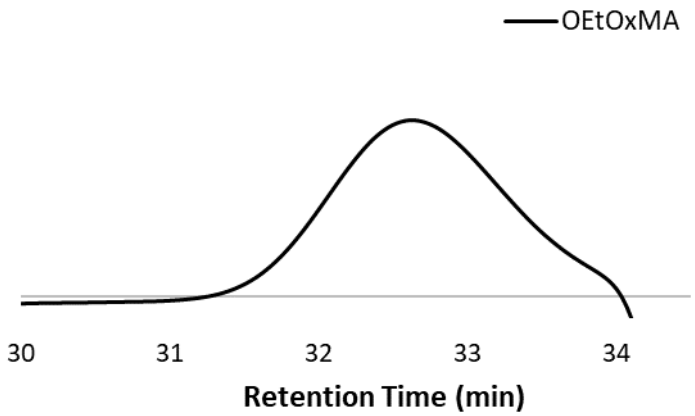

Figure 4.7. SEC trace of OEtOxMA.

The properties of the OEtOxMA macromonomer was given in the Table 4.1.

Table 4.1. The properties of the synthesized OEtOxMA.

[M]/ [I][a]	**DP[b]**	**Mn (g/mol)[a]**	**Mn (g/mol)[c]**	**Đ[c]**
8	8.16	900	1440	1.10

a: determined theoretically, b: determined by NMR c: determined by SEC.

4.2. Synthesis and Characterization of Linear Block Copolymers

4.2.1. Synthesis of P(OEGMA)-*b*-P(AEAEMA)

To yield P(OEGMA)-*b*-P(AEAEMA) block copolymers, first P(OEGMA)s having varied molecular weights have been synthesized by RAFT polymerization and used as Macro-RAFT agents later. Percentage OEGMA (monomer) conversions were

determined by analyzing the P(OEGMA) polymerization mixture by ^{1}H-NMR (Figure 4.8, Equation 4.4)

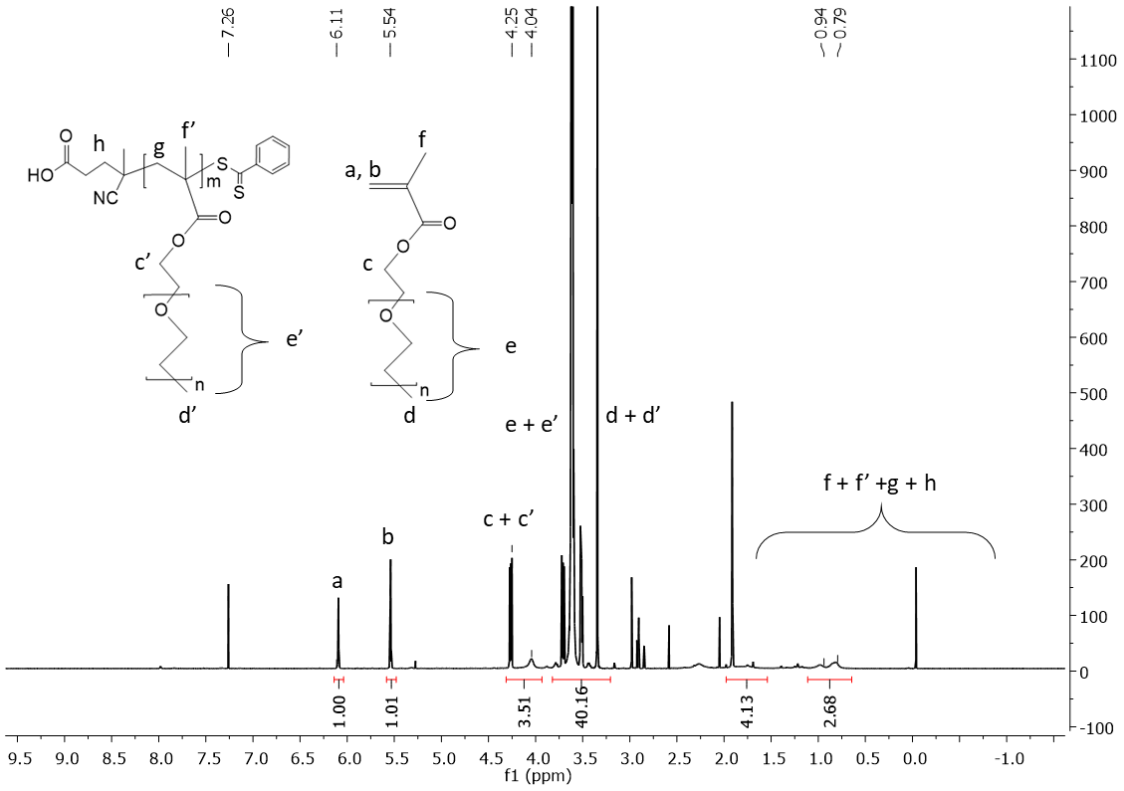

Figure 4.8. Representative ^{1}H-NMR spectrum of P(OEGMA) polymerization mixture (before purification).

$$\text{Conversion (\%)} = \frac{\left(\frac{I_{4.00-4.4\ ppm}}{2}\right)-\left(\frac{I_{6.13ppm}+I_{5.58ppm}}{2}\right)}{\left(\frac{I_{4.00-4.4\ ppm}}{2}\right)}\ x\ 100 \qquad (4.4)$$

$P(OEGMA)_{13}$(5K) was purified by dialysis against water, $P(OEGMA)_{20}$ and $P(OEGMA)_{43}$ were purified by precipitating in cold diethyl ether. Characteristic vinyl peaks of monomer (6.13 and 5.57 ppm) disappeared in the spectrum after purification as

verified by ^{1}H-NMR (Figure 4.9) Molar mass and dispersity of P(OEGMA) Macro-RAFT agents were determined by SEC (SEC curves of the macro-RAFT agents are presented on the next pages on the same graph along with the corresponding block copolymer curves). Properties of the synthesized P(OEGMA)s are given in Table 4.2.

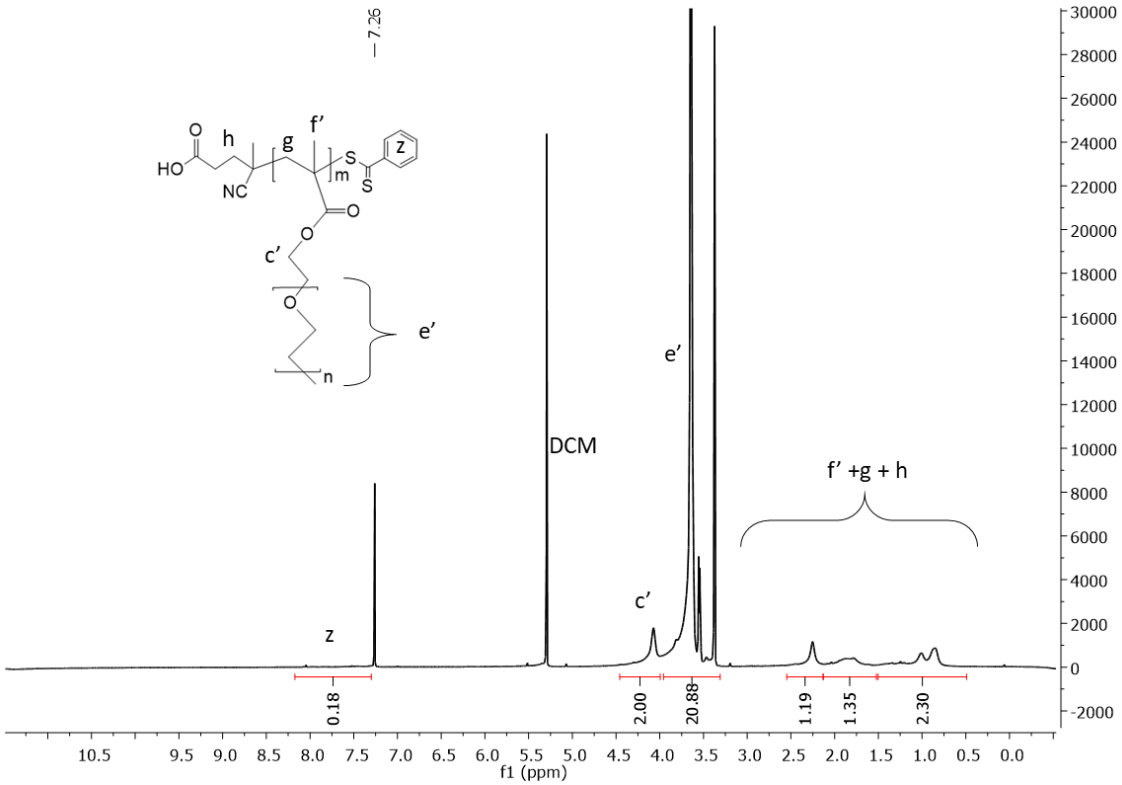

Figure 4.9. Representative ^{1}H-NMR spectrum of pure P(OEGMA).

Table 4.2. The properties of the synthesized P(OEGMA)s.

[M]/ [R]/[I]	**M_n[a] (g/mol)**	**Đ[a]**	**DP[b]**	**Conversion[c] (%)**
50/1/0.25	5400	1.15	13	N/A
100/1/0.25	10000	1.14	20	40
100/1/0.25	15000	1.17	43	43

a: determined by SEC, b: calculated theoretically using NMR conversion data, when conversion data not applicable, integral values of RAFT Z-group and methylene protons of oligoethylene glycol unit adjacent to ester bond in pure NMR spectrum was used, c: determined by NMR.

Purified P(OEGMA) macro-RAFT agents were used to obtain block copolymers, P(OEGMA)-*b*-P(BocAEAEMA). AIBN as initiator, BocAEAEMA as monomer were added to reaction vessel together with the corresponding macro-RAFT agent and polymerized at 65°C under nitrogenous atmosphere for determined times. Samples were taken from polymerization mixtures and analyzed by ^{1}H-NMR to calculate monomer conversions (Figure 4.10)

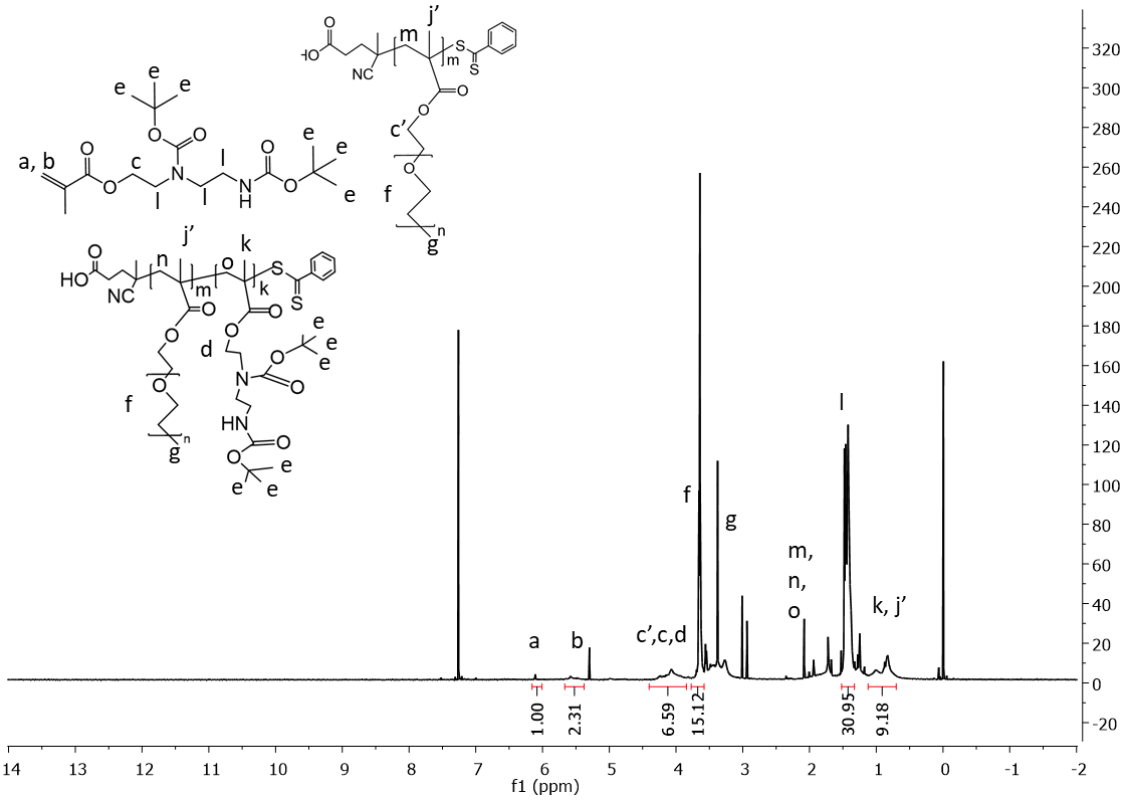

Figure 4.10. Representative ^{1}H-NMR spectrum of P(OEGMA)-*b*-P(BocAEAEMA) polymerization mixture (before purification).

Monomer conversions were calculated according to Equations 4.5 and 4.6.

$$I_{3,80-4,32\ ppm}=\left[2*\left(\frac{I_{3,65\ ppm}}{28}\right)\right]+I_{copolymer}+\left[2*\left(I_{6.12ppm}\right)\right] \quad (4.5)$$

$$Conversion\ (\%)\ =\ \frac{I_{copolymer}/_2}{I_{copolymer}/_2\ +\left(I_{6.12ppm}\right)}\ *\ 100 \quad (4.6)$$

P(OEGMA)-*b*-P(BocAEAEMA) block copolymers were purified by precipitating into hexane. Characteristic vinyl peaks of monomer (6.13 and 5.57 ppm) disappeared in the spectrum after purification as verified by ^{1}H-NMR (Figure 4.11)

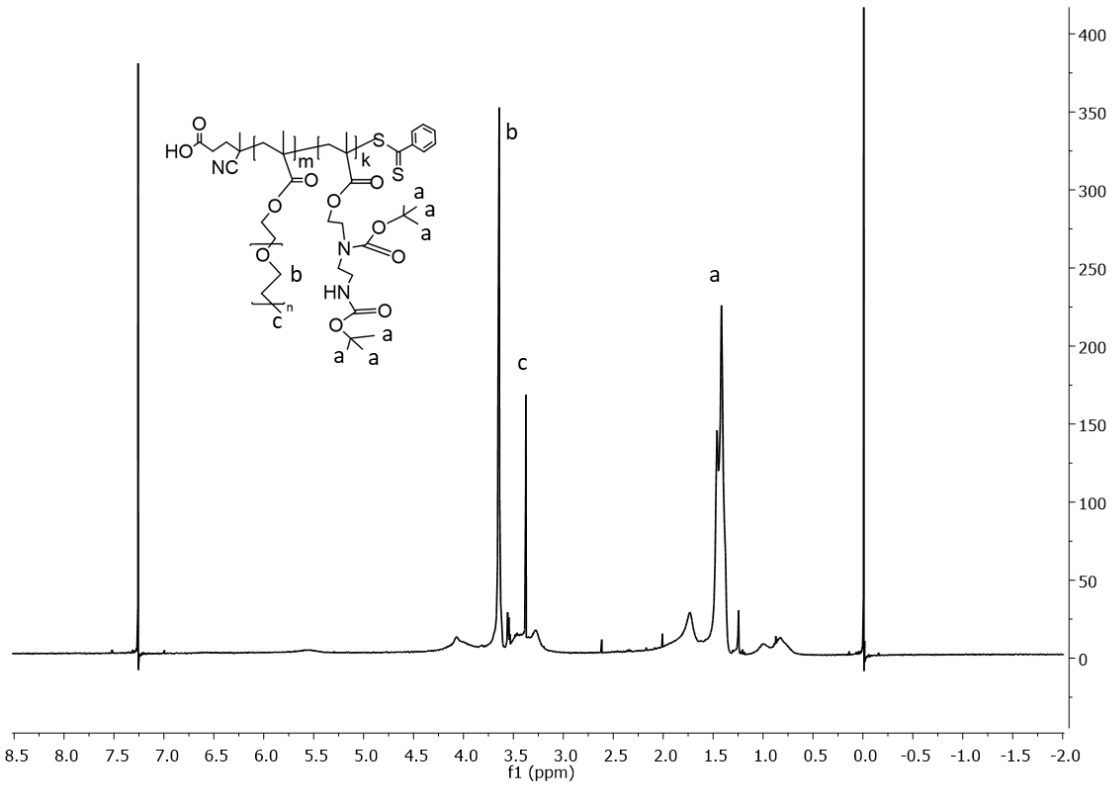

Figure 4.11. Representative ^{1}H-NMR spectrum of pure P(OEGMA)-*b*-P(BocAEAEMA)

Molar mass and dispersity of the block copolymers was determined by SEC (Figure 4.12). The shift in the SEC curve toward the lower retention times showed the increase in molecular weight which is attributed to formation of block copolymers or in other words chain extension of P(OEGMA) polymers with BocAEAEMA.

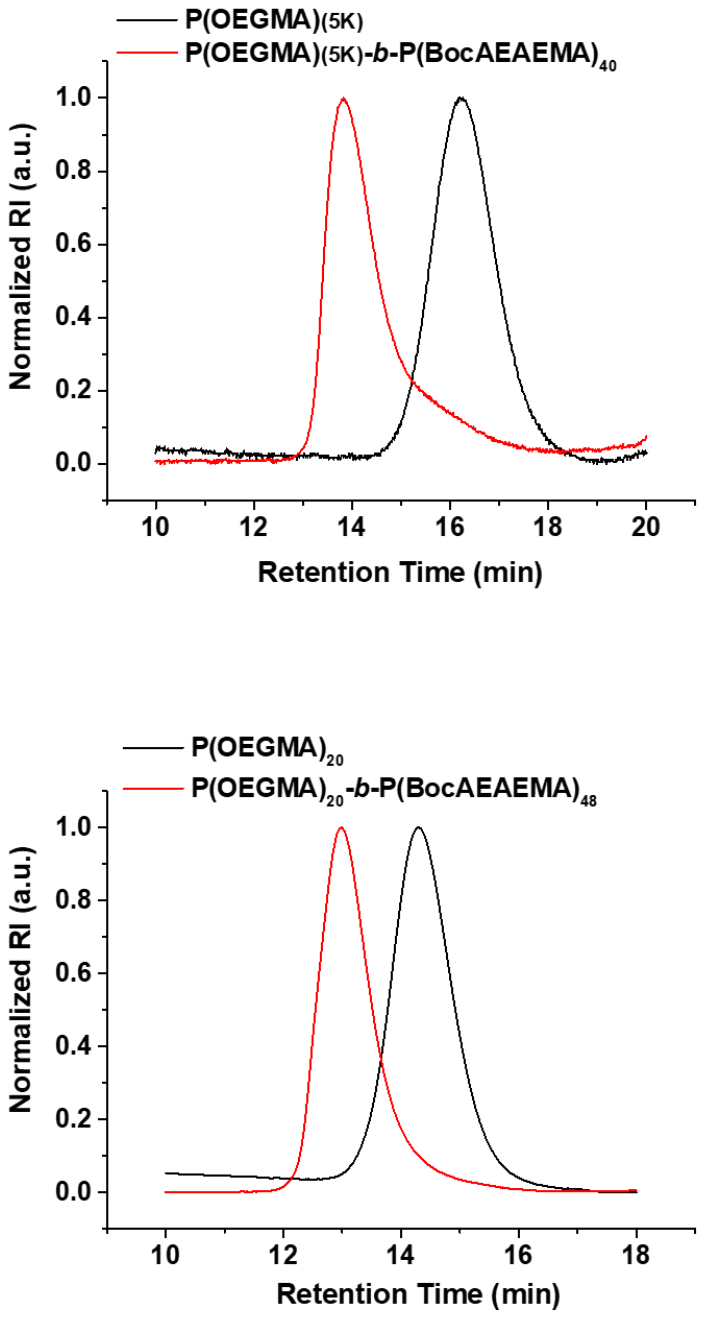

Figure 4.12. SEC curves of P(OEGMA) macroRAFT agents and P(OEGMA)-*b*-P(BocAEAEMA) block copolymers.

(Cont. on next page)

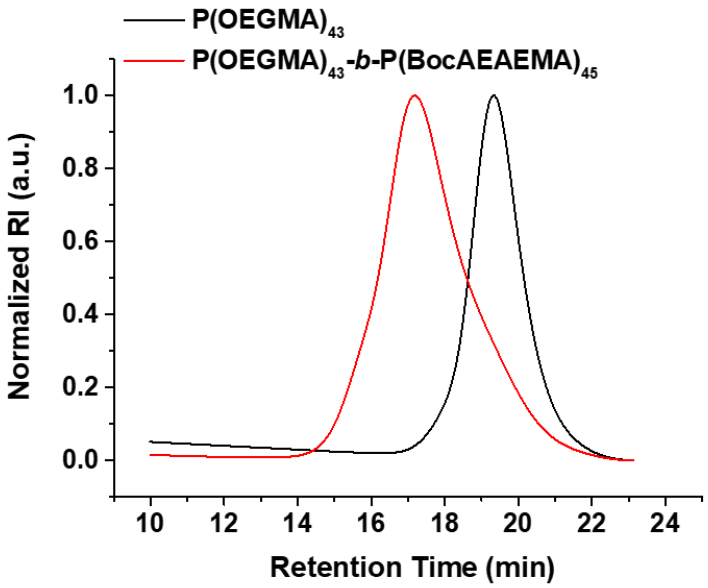

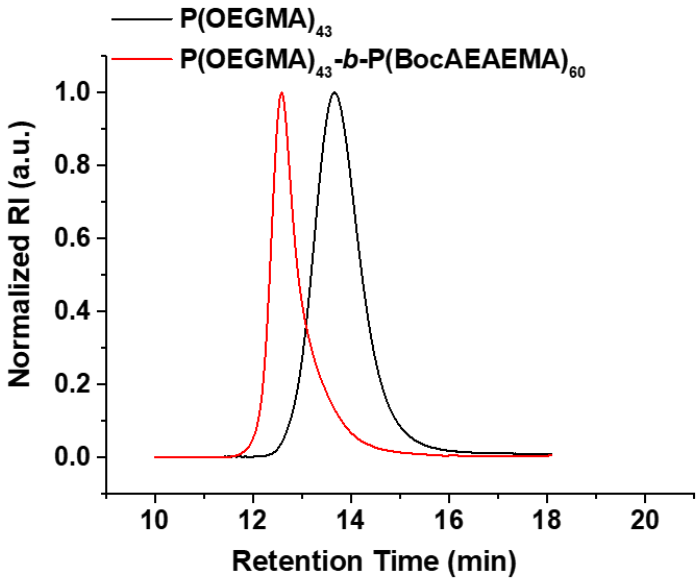

Figure 4.12. (Cont.)

The analytics of P(OEGMA)-*b*-P(BocAEAEMA) block copolymers are presented in Table 4.3.

Table 4.3. The properties of the synthesized P(OEGMA)-*b*-P(BocAEAEMA).

M_n[a] (g/mol)	**Đ[a]**	**DP[b] P(OEGMA)**	**DP[b] P(BocAEAEMA)**	**Conversion[d] (%)**
17500	1.60	13	40[b,c]	N/A
23700	1.34	20	48	48
26300	1.60	43	45	45
34000	1.31	43	60	60

a: determined by SEC, b: calculated theoretically using NMR conversion data, c: DP assumed to be 40 since the macro-CTA and block copolymer molar mass of this sample was found to be same with PEGylated counterpart, d: determined by NMR.

The controlled RAFT copolymerization mechanism is also demonstrated by a kinetic study (Figure 4.13, Figure 4.14, and Table 4.4). For this purpose, $P(OEGMA)_{43}$ macro-RAFT agent was used ([M]/[R]/[I] = 100/1/0.25, [M] = 1 M). As shown in Figure 4.13, $Ln([M]_0/[M])$ increased proportionally with time. Mn values increased in direct proportion to the conversions (%). Đ values were found to be less than 1.45. All these results indicate that copolymerization kinetic data has showed good harmony with the characteristics of controlled RAFT polymerization.

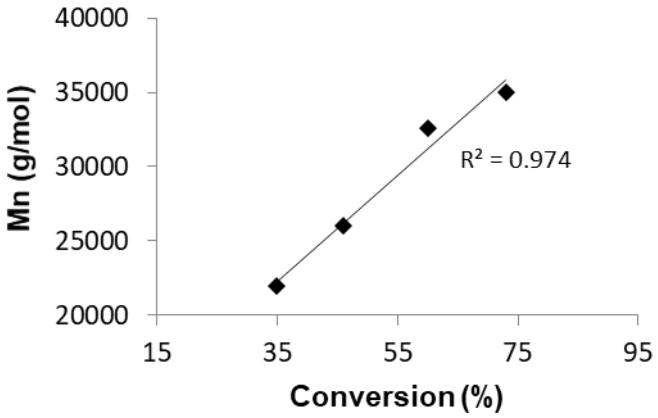

Figure 4.13. RAFT kinetic graphs of block copolymers, P(OEGMA)-*b*-P(BocAEAEMA) (macro-RAFT: 15 kDa, [M]/[R]/[I] = 100/1/0.25, [M] = 1 M).

(Cont. on next page)

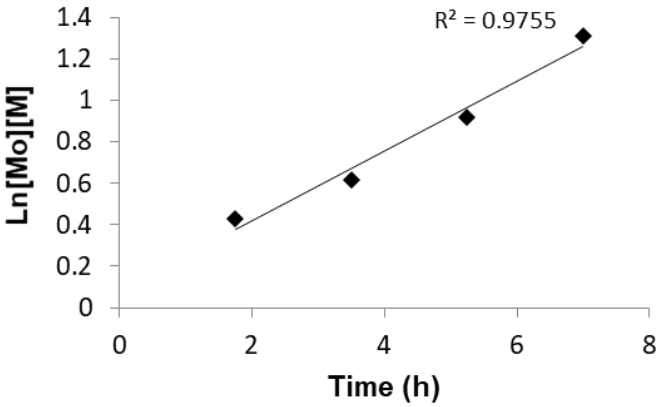

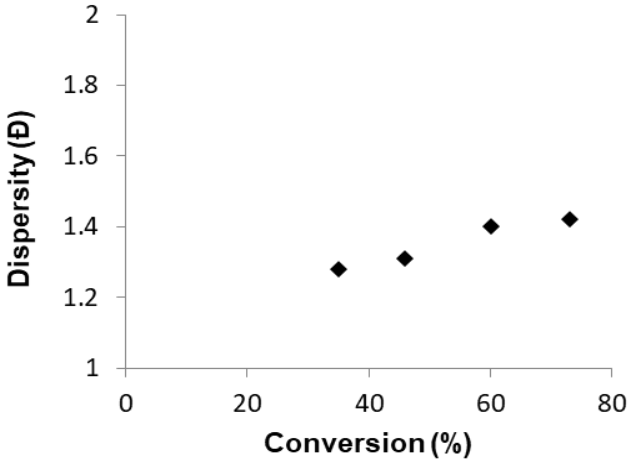

Figure 4.13. (Cont.)

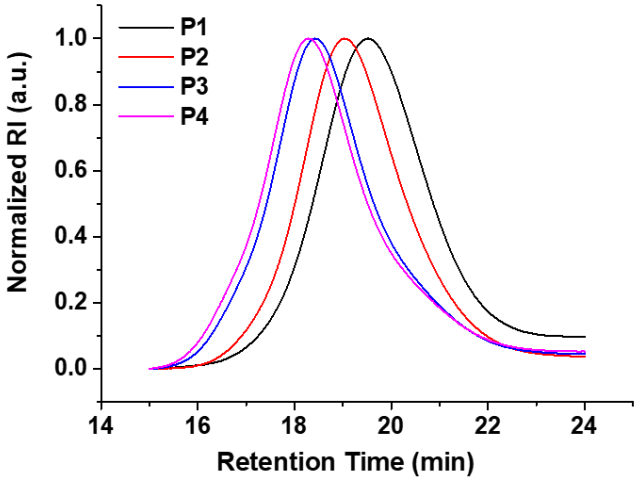

Figure 4.14. SEC curves of P(OEGMA)-*b*-P(BocAEAEMA) block copolymers synthesized for kinetic studies.

Table 4.4. The properties of the P(OEGMA)-*b*-P(BocAEAEMA) polymers synthesized for kinetic studies.

Polymer Code	**M_n[a] (g/mol)**	**Đ[a]**	**Conversion[b] (%)**
P1	22000	1.28	35
P2	26000	1.31	46
P3	32600	1.40	60
P4	35000	1.42	73

a: determined by SEC, b: determined by NMR.

The protecting Boc groups of P(OEGMA)-*b*-P(BocAEAEMA) polymers were removed prior to siRNA complexation studies. For this aim, polymers were treated with trifluoroacetic acid and purified by precipitating in diethyl ether. With the removal of Boc groups, the hydrophobicity of the polymers was dramatically changed as polymers became soluble in water. The characteristic signals of these groups (1.35 – 1.45 ppm) were disappeared after deprotection as evidenced by ^{1}H-NMR (Figure 4.15).

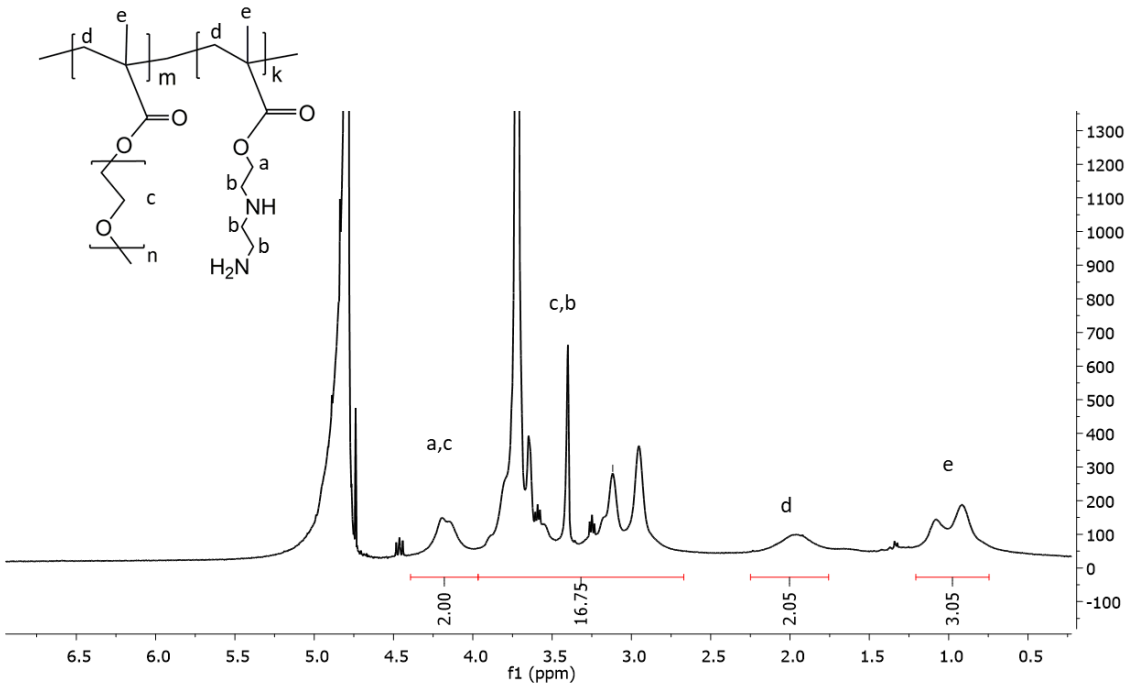

Figure 4.15. Representative ^{1}H-NMR spectrum of pure P(OEGMA)-*b*-P(AEAEMA).

Prior to cell culture studies, to avoid possible toxic effects of RAFT end group, aminolysis reaction was performed. Polymers were reacted with hexylamine and triethylamine in the presence of methyl methacrylate. Afterwards polymers were purified by precipitating in diethyl ether and further purified by dialyzing against water for three days. At the end of the dialysis, polymers were collected and freeze-dried.

4.2.2. Synthesis of PEG-*b*-P(AEAEMA)

In addition to P(OEGMA)-*b*-P(AEAEMA) polymers, pegylated P(AEAEMA), PEG-*b*-P(AEAEMA), was also synthesized to discuss the architectural effect of PEG and P(OEGMA) to siRNA delivery. Even though P(OEGMA) (comb-type PEG) is known to display similar pharmacokinetic and pharmacodynamic properties with PEG, it is anticipated that the siRNA complex formation can potentially differ due to significant structural difference of P(OEGMA) and PEG. For the synthesis, RAFT functionalized PEG (Poly(ethylene glycol) methyl ether (4-cyano-4-pentanoate dodecyl trithiocarbonate) (Mn 5400, Đ ≤1.1) was used and RAFT polymerized in the presence of monomer, BocAEAEMA and initiator, AIBN. The block copolymer, PEG-*b*-P(AEAEMA), was characterized, purified and deprotected as described in P(OEGMA)-*b*-P(AEAEMA) synthesis section. SEC and NMR data were presented in Figure 4.16 and Figure 4.17, respectively. The properties of obtained PEG-*b*-P(AEAEMA) is presented at Table 4.5.

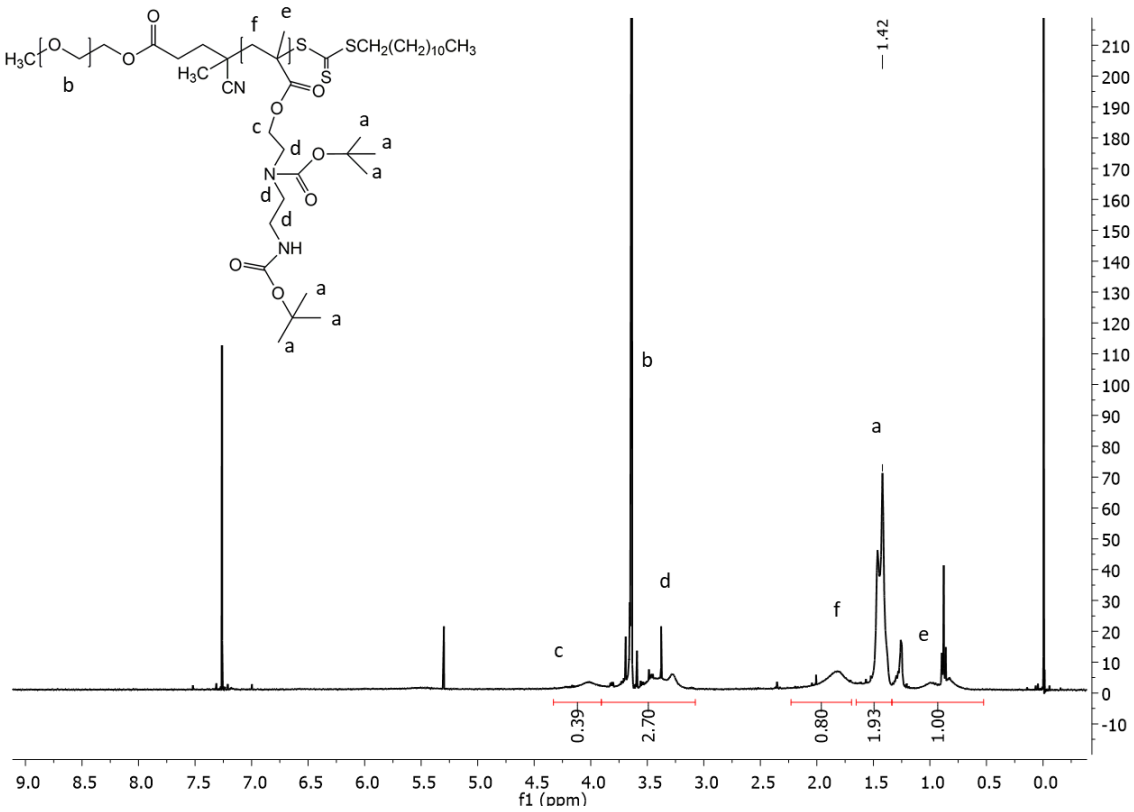

Figure 4.16. ^{1}H-NMR spectrum of pure PEG-*b*-P(BocAEAEMA).

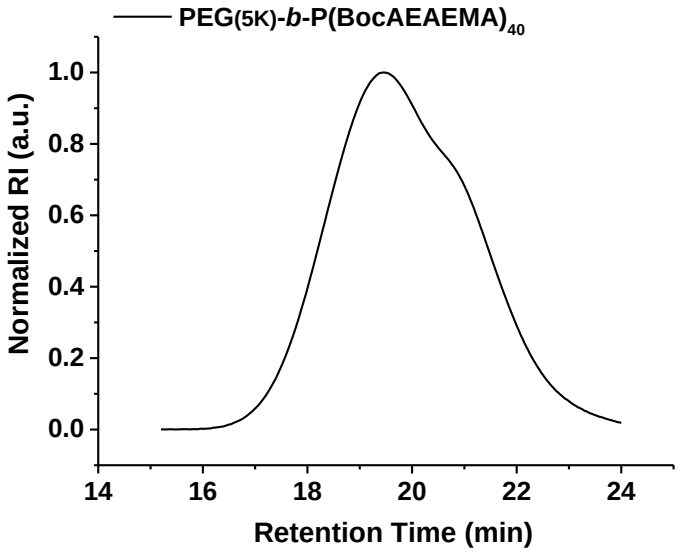

Figure 4.17. SEC curve of PEG-*b*-P(BocAEAEMA).

Table 4.5. The properties of the synthesized PEG-*b*-P(BocAEAEMA).

M_n[a] (g/mol)	Đ[a]	DP[b] P(OEGMA)	DP[c] P(BocAEAEMA)	Conversion[c] (%)
18500	1.39	122	40	40

a: determined by SEC, b: calculated theoretically, c: determined by NMR.

4.2.3. Synthesis of P(AEAEMA)-*b*-P(OEtOxMA)

Poly(2-oxazoline) (POx) is known to be one of the strong 'stealth polymer' candidates as an alternative to PEG. With the discovery of anti-PEG antibodies, PEG replaceability has begun to be questioned especially in the field of pharmaceutical sciences. Although PEGylated and POXylated polymers have been compared in many studies, the siRNA delivery potential of PEG or POX including block copolymers have not been studied and reported in comparison. By considering this, a new block copolymer, P(AEAEMA)-*b*-P(OEtOxMA), has been synthesized as an alternative to $P(OEGMA)_{43}$-*b*-$P(AEAEMA)_{45}$ polymer. To be able to compare the potential different effects of P(OEtOxMA) and P(OEGMA), degree of branching (DP) values of the OEtOxMA macromonomer and P(OEtOxMA) block kept the same with OEGMA macromonomer and $P(OEGMA)_{43}$ block, respectively. DP of P(AEAEMA) was also aimed to be the same for both block copolymers only to evaluate the effects of stealth blocks.

To yield P(AEAEMA)-*b*-P(OEtOxMA); first amine containing monomer, BocAEAEMA, was polymerized by RAFT polymerization. Initiator (AIBN) concentration was kept at minimum to yield high amounts of polymer chains with living RAFT end groups. At the same time, targeted DP was attempted to be obtained at low monomer conversion (below 70%) to avoid termination reactions that might cause the formation of dead-end chains. Accordingly, [M]/ [R] ratio and reaction time was determined, and the polymerization was carried out in a proper solvent (toluene). Monomer conversion was calculated by using ^{1}H-NMR spectrum of reaction mixture (Figure 4.18). Monomer signal at 6.11 ppm and the sum of monomer and polymer signals at 3.8-4.3 ppm was used to calculate the monomer conversion (67%).

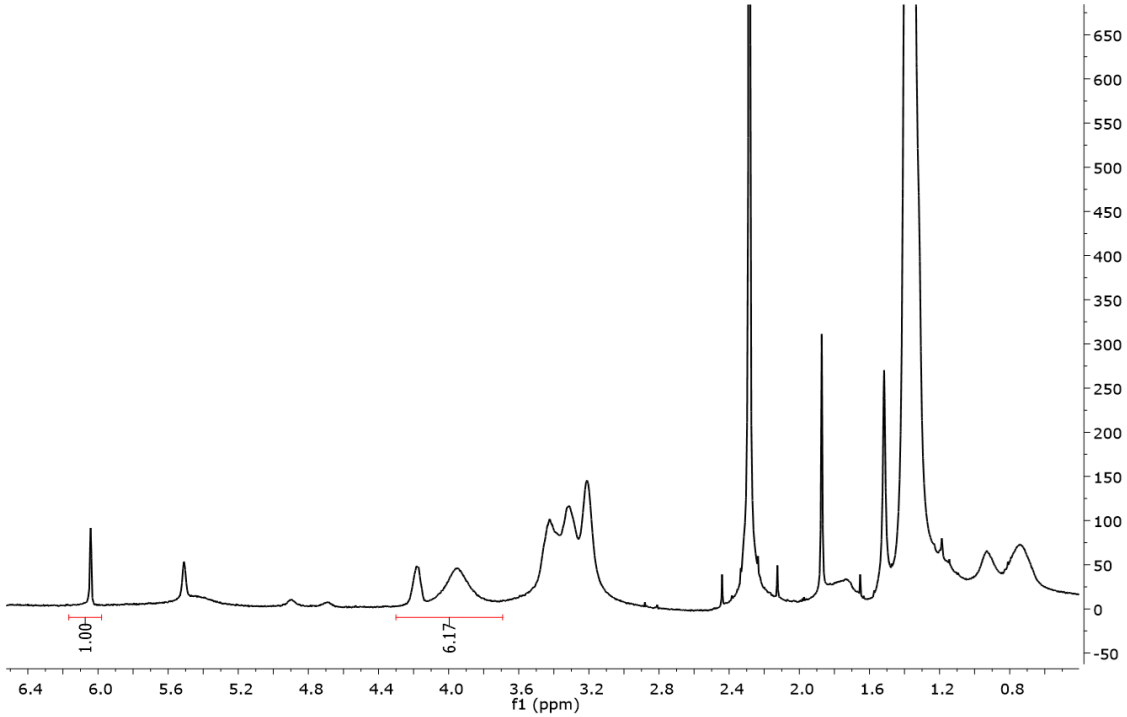

Figure 4.18. H-NMR spectrum of Boc(AEAEMA) polymerization mixture before purification.

Polymer was purified by precipitating into petroleum benzine. After purification, molecular weight and dispersity of the polymer was investigated by SEC and was found to be 14.1 kDa and 1.11, respectively (SEC curve is presented on the same plot with corresponding block copolymer curve on the following pages). P(BocAEAEMA) having targeted DP could be obtained with suitable monomer conversion and narrow dispersity which makes synthesized P(BocAEAEMA) convenient for chain extension reactions.

Chain extension of the P(BocAEAEMA) was performed in the presence of pre-synthesized OEtOxMA, macromonomer. Targeted DP could be obtained at selected monomer concentration (0.37 M) and , [M]/ [R]/ [I] ([50]/ [1]/ [0.25)] by RAFT copolymerization for 3h 40 min. A reference material (anisole) was added to the polymerization mixture and NMR sample was taken before and after polymerization. The integral of reference material was proportioned to the integral of vinyl protons (coming from the macromonomer) in each spectrum to find out the monomer conversion. Monomer conversion was found to be 76%. Block copolymer, P(BocAEAEMA)-*b*-P(OEtOxMA), was purified from unreacted macromonomer and macroRAFT agent by

precipitating into diethyl ether and further washing with ether. ^{1}H-NMR of the pure block copolymer was examined to determine the composition of the block copolymer (Figure 4.18). Different from P(OEGMA) block copolymers, the unreacted macroRAFT could also be removed during purification therefore composition was also calculated by using the signals coming from Boc groups of P(BocAEAEMA) block at 1.42 ppm and terminal methyl group of P(OEtOxMA) block at 3.02 ppm. According to the ^{1}H-NMR analysis, the percentage of P(BocAEAEMA) and P(OEtOxMA) was found to be 46 and 54, respectively. The composition of the block copolymer showed good agreement with the theoretical DP values of the blocks (DP $_{P(BocAEAEMA)}$: 40, DP $_{P(OEtOxMA)}$: 38).

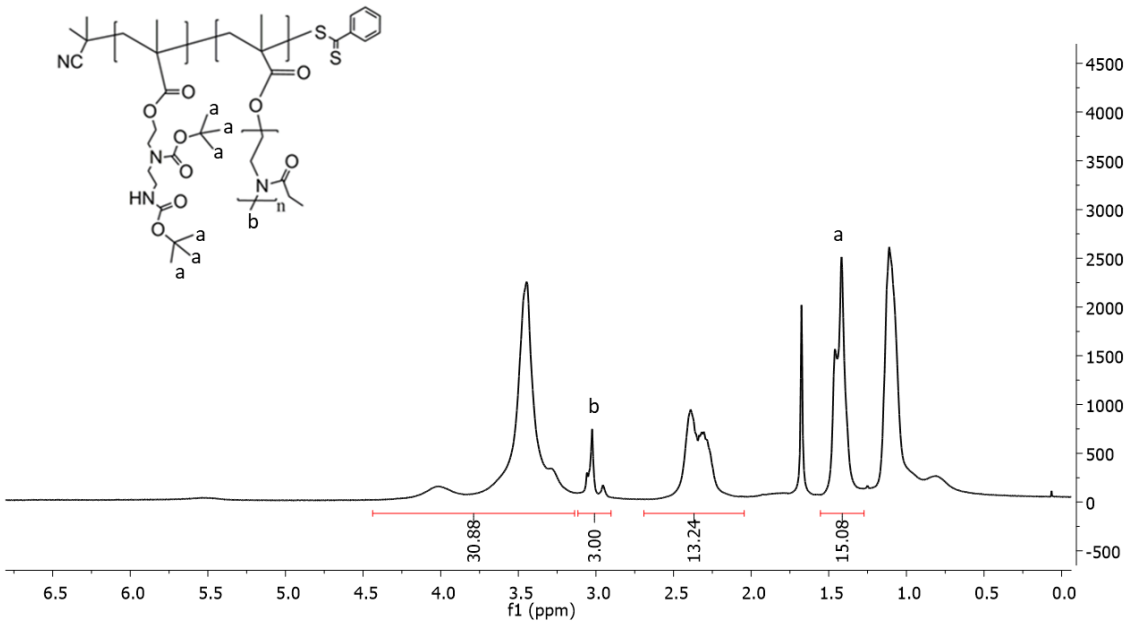

Figure 4.19. ^{1}H-NMR spectrum of pure P(BocAEAEMA)-*b*-P(OEtOxMA).

After purification, molecular weight and dispersity of the block copolymer was determined by SEC (Figure 4.20). Mn and Đ was found to be 34.7 kDa and 1.29, respectively. SEC displayed monomodal and equally distributed curve implying that block copolymer could be obtained via RAFT polymerization successfully with low dispersity. The properties of P(BocAEAEMA)-*b*-P(OEtOxMA) block copolymer is presented in Table 4.6.

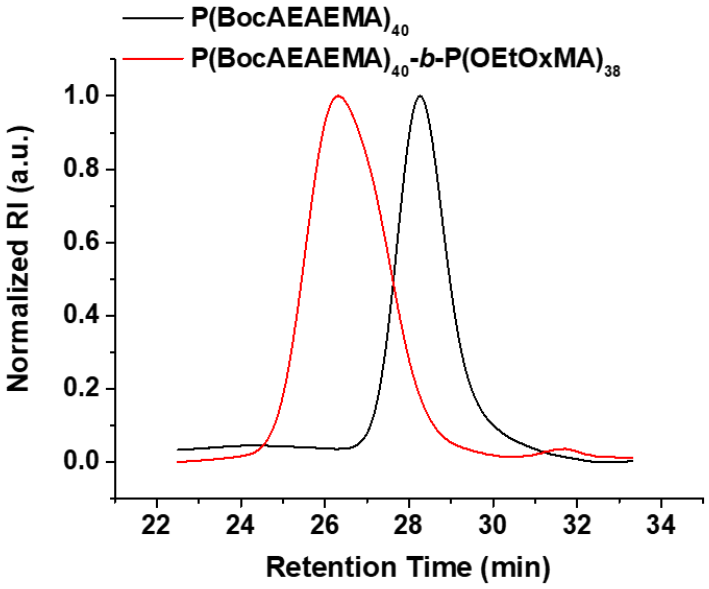

Figure 4.20. SEC trace of P(BocAEAEMA)-*b*-P(OEtOxMA).

Table 4.6. The properties of the synthesized P(BocAEAEMA)-*b*-P(OEtOxMA).

M_n[a] (g/mol)	**Đ[a]**	**DP[b] P(OEtOxMA)**	**DP[b] P(BocAEAEMA)**	**Conversion[c] (%)**
34700	1.29	38	40	76

a: determined by SEC, b: calculated theoretically using NMR conversion data, c: determined by NMR.

Boc groups of the polymer was removed using TFA as described before. Purified polymer was analyzed by ^{1}H-NMR (Figure 4.21). The protecting Boc groups could have been removed from the structure entirely as evidenced by ^{1}H-NMR.

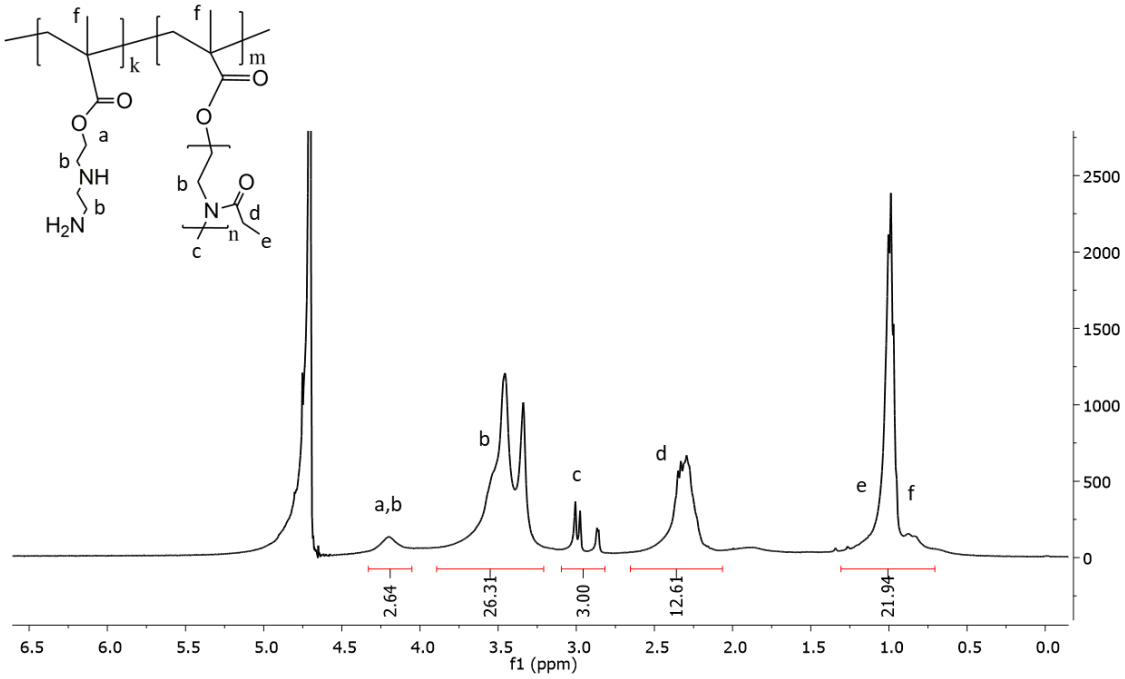

Figure 4.21. ^{1}H-NMR spectrum of pure P(AEAEMA)-*b*-P(OEtOxMA).

4.3. Synthesis and Characterization of Star Polymers

To investigate the effect of polymeric architecture, miktoarm star polymers have been synthesized. siRNA delivery potential of these structures was also evaluated and compared to linear copolymers. The cationic (AEAEMA) and neutral (OEGMA) structures used for block copolymers were used for star polymer preparation as well.

Arm-first approach has been followed for miktoarm star polymer synthesis. For this aim, first; arms (P(BocAEAEMA) and P(OEGMA)) were synthesized via RAFT polymerization. Then, purified arms were cross-linked in the presence of a monomer and cross-linker; namely butyl acrylate and N,N'-bis(acryloyl)cystamine, respectively. For the star synthesis, varied reaction solvents (toluene, anisole, chlorobenzene), macroRAFT agents with different RAFT end group (CPADB, CDTPA) and acrylate/methacrylate based monomers with different hydrophobicity (butyl acrylate, butyl methacrylate, methyl methacrylate) were employed and it has been found that, especially the RAFT agent and reaction solvent directly effects the efficiency of star formation (data not shown). Based on these, anisole and CDTPA was chosen as reaction solvent and RAFT

agent, respectively as they provided the best yield. A hydrophobic monomer, butyl acrylate, was chosen as core forming unit in order to obtain stabile, amphiphilic star polymers (and star polymer-siRNA complexes) that can potentially interact with cell and/or endosome membranes.

DP of P(OEGMA) and P(BocAEAEMA) was approximately kept same with DP values of $P(OEGMA)_{43}$-*b*-$P(AEAEMA)_{45}$ block copolymer in order to observe the effect of architecture without the effect of chain length. P(OEGMA) and P(BocAEAEMA) was synthesized and characterized as described before. Unlike block copolymer synthesis, CDTPA was used as RAFT agent in this case. The properties of the characterized polymers were given in Table 4.7.

Table 4.7. The properties of arms used for star synthesis.

Polymer	**M_n[a] (g/mol)**	**M_n[b] (g/mol)**	**Đ [a]**	**DP[b]**	**Conversion[c] (%)**
P(BocAEAEMA)	12700	15645	1.14	42	85
P(OEGMA)	14300	18000	1.21	36	52

a: determined by SEC, b: determined theoretically, c: determined by NMR

Purified arms were cross-linked in the presence of butyl acrylate. Mole ratio of arms to each other at feed was kept either equal or 4:1 (P(BocAEAEMA):P(OEGMA)) to yield miktoarm stars having different amount of cationic arm. Since star polymers were prepared to interact with siRNA through electrostatic interactions, in order to keep the interaction strong, the percentage of cationic arm in the star polymer was targeted to be 50% or higher. Two miktoarm star polymers with different amount of cationic arm were synthesized to investigate the possible differed behaviors of star polymers in terms of stealth properties, toxicity, cell interactions, physicochemical properties etc. A homoarm star polymer made of P(OEGMA) was also synthesized as a control polymer. The molar equivalent of arm : core was kept same for all star polymers. After synthesis, star polymers were purified by precipitating into petroleum benzine (for miktoarm stars) or into diethyl ether (for homoarm P(OEGMA) star). To remove unreacted arms, precipitates were dissolved in methanol and further purified using centrifugal

concentrator (MWCO: 100 kDa). Mn and Đ of the pure star polymers were determined by SEC (Figure 4.22, Table 4.8). SEC proved that arms remained after polymerization could be removed from star polymers completely. Miktoarm stars (SP1 and SP2) showed very narrow distribution profile with a Đ of ≤1.17 indicating that predicted well-defined star-shaped structures could be obtained with the chosen reaction conditions. P(OEGMA) homoarm star polymer (SP3), showed slightly larger Đ compared to miktoarm star polymers. This can be attributed to the difficulty of crosslinking the same species due to the differed interchain interactions and differed solubility of the reactants in the homoarm star synthesis medium compared to miktoarm star synthesis environment. Also, although the same arm: core molar equivalents were used for all polymers, the molecular weight of the homoarm star polymer was found to be quite lower than the miktoarm star polymers, possibly due to the described cross-linking difficulty of the same species.

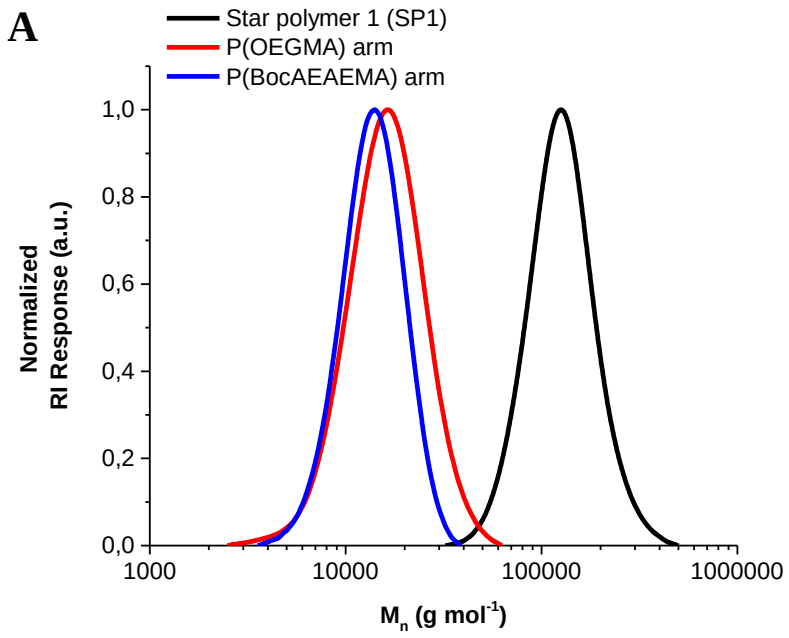

Figure 4.22. SEC traces of P(OEGMA)/P(BocAEAEMA) miktoarm star polymer-1 (SP1) (A), P(OEGMA)/P(BocAEAEMA) miktoarm star polymer-2 (SP2) (B), P(OEGMA) homoarm star polymer-3 (SP3) (C).

(Cont. on next page)

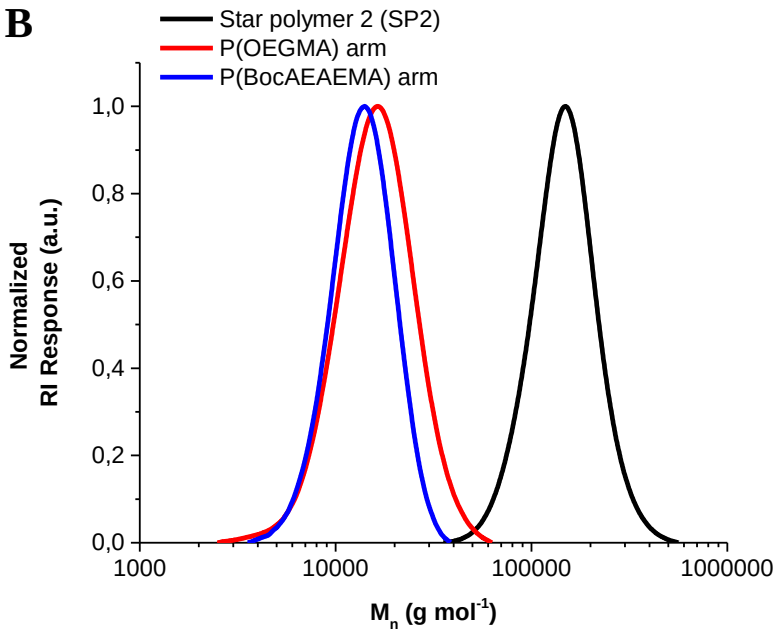

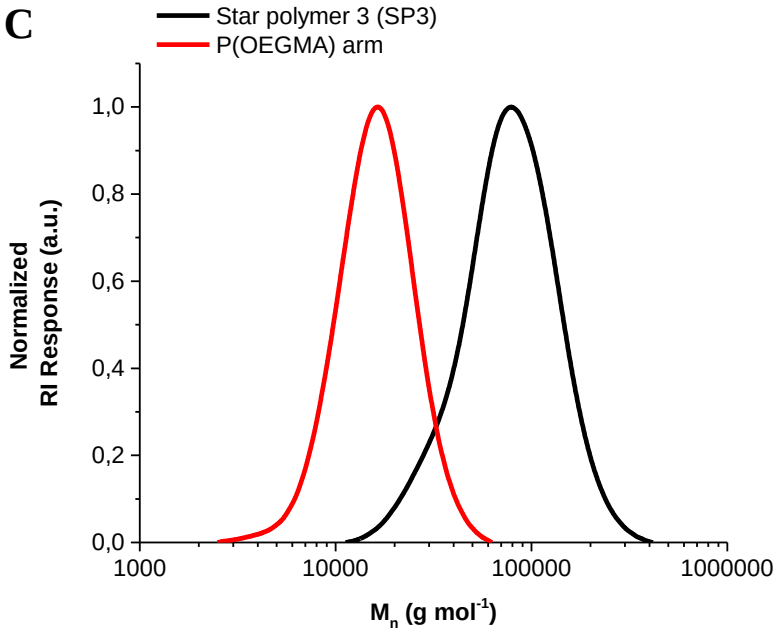

Figure 4.22. (Cont.)

Table 4.8 The properties of star polymers.

Polymer	**M_n[a] (g/mol)**	**Đ [a]**	**Arm composition[b] (Percentage of P(BocAEAEMA) (%))**	**Arm number[c] (P(BocAEAEMA)-P(OEGMA))**
SP1	116000	1.17	≈50	4.3 - 4.3
SP2	136000	1.16	≈80	2.1 - 8.4
SP3	64000	1.36	0	0.0 - 4.5

a: determined by SEC-RI, b: determined by NMR, c: calculated theoretically.

Pure star polymers were analyzed by ^{1}H-NMR and percent arm composition of the SP1 and SP2 were determined via signals of Boc groups and ethylene glycol units (Figure 4.23, Table 4.8). The signals of the BA and BAC that are located at the core of the star couldn't be observed in the spectrum meaning that it didn't interfere with the arm composition calculation. Arm number was also theoretically calculated via Mn and arm composition obtained from SEC and ^{1}H-NMR, respectively (Table 4). The initial molar ratio of the arms and the arm composition obtained after polymerization showed a perfect correlation with each other. This indicates that the desired final composition could be precisely targeted only by fixing the initial moles of arms to targeted values.

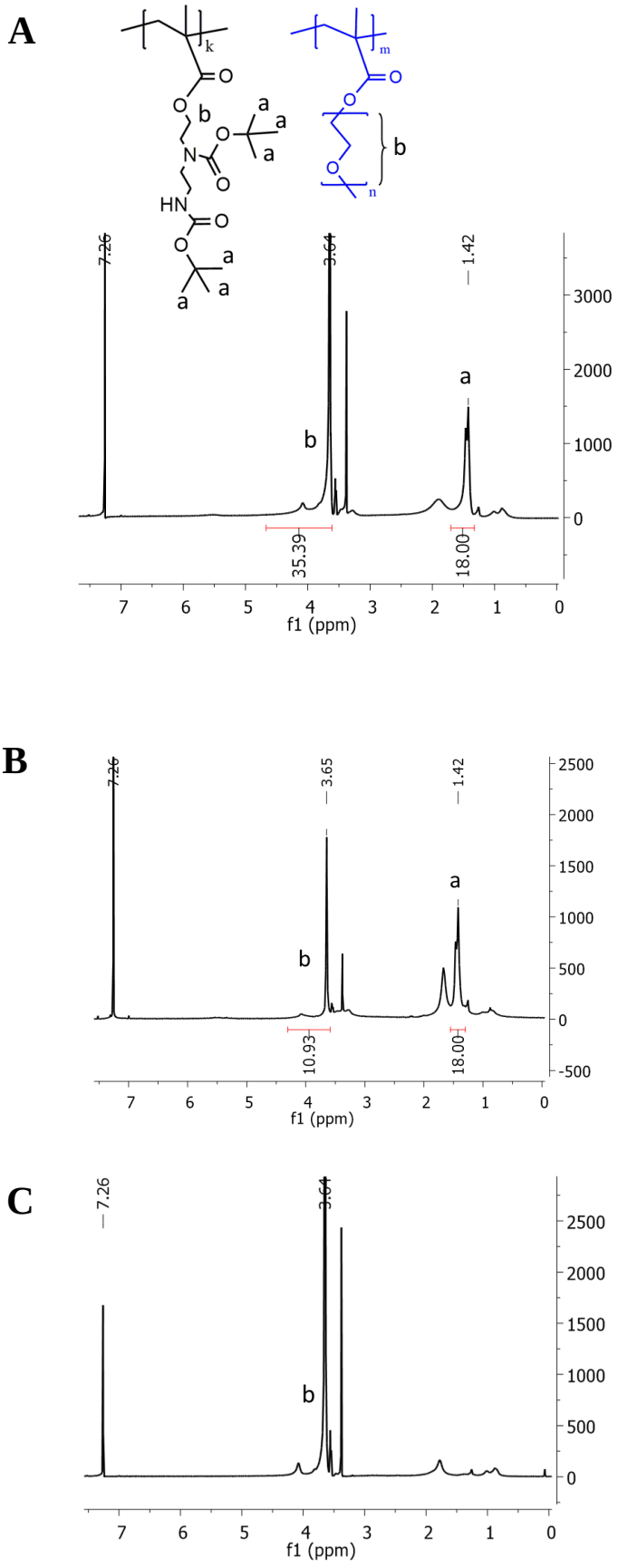

Figure 4.23. [1]HNMR spectrum of pure SP1 (A), SP2 (B) and SP3 (C).

To reveal amine groups, SP1 and SP2 were deprotected using TFA as described before and afterwards polymers were purified by precipitating into diethyl ether (x3). The removal of Boc protecting groups were confirmed by ^{1}H-NMR analysis.

After deprotection star polymers were characterized by DLS and hydrodynamic diameters were determined (Figure 4.24, Table 4.9). Polymers were dissolved in PBS and sizes were directly recorded after 2 min incubation period. Monomodal size distribution was observed for all star polymers. The average size of SP2 was found to be highest with diameter of 22.8 nm and SP3 was found to be lowest with diameter of 15.18 nm. Sizes obtained with DLS fitted well with the Mn determined by SEC. Again, similar to SEC results, homoarm star polymer (SP3) showed the highest PDI (0.44). SP2 showed lower PDI than SP1 (0.29 and 0.37, respectively), possibly due to charge difference/cationic arm density of two miktoarm star polymers. It is highly likely that SP2 stars could better repelled each other because of high cationic arm content and displayed lower PDI particularly after deprotection. In summary, DLS results showed that even after deprotection star polymers could preserve their well-defined structures without showing significant aggregation tendency.

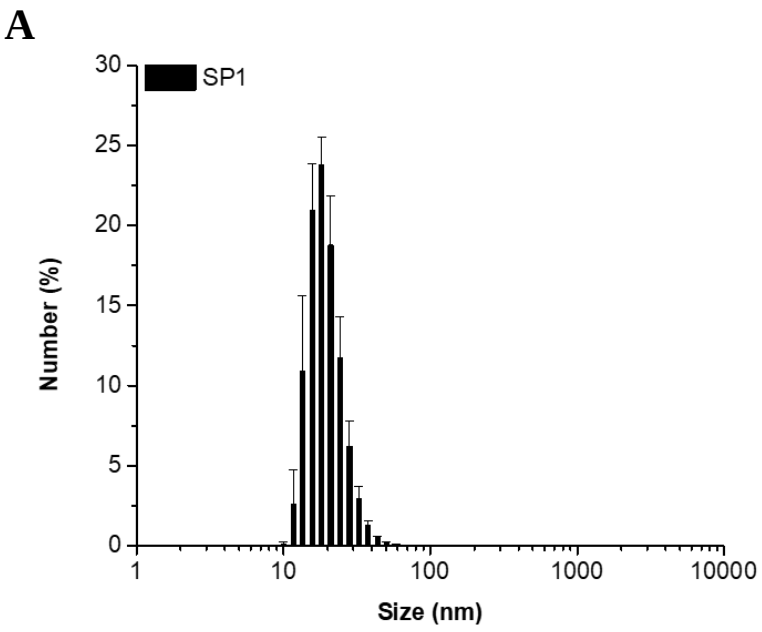

Figure 4.24. Hydrodynamic size distribution of star polymers in PBS.

(Cont. on next page)

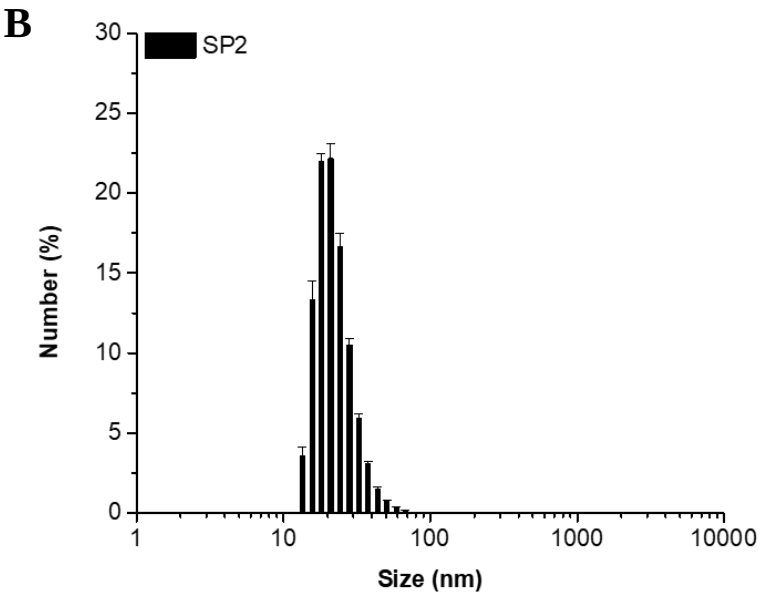

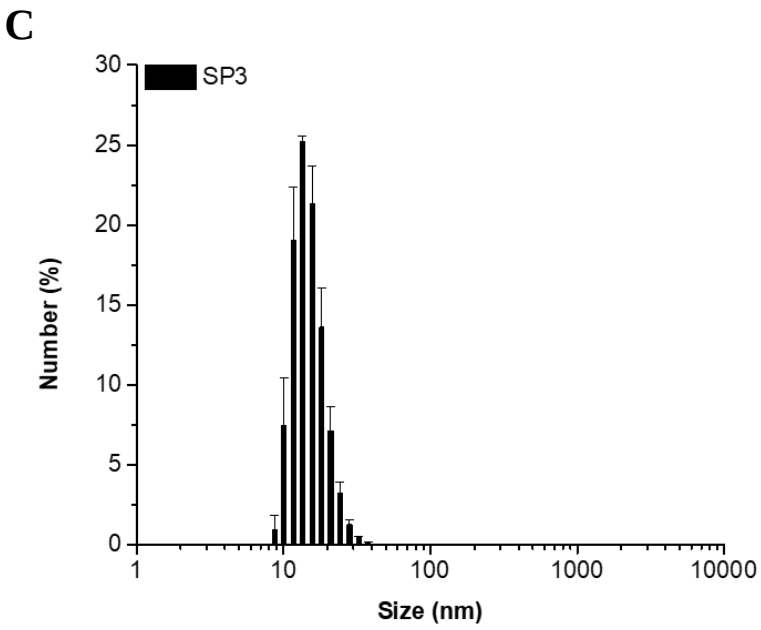

Figure 4.24. (Cont.)

Table 4.9. Average hydrodynamic diameters and PDI values of star polymers in PBS.

Polymer	Diameters[a] (nm)	PDI[a]
SP1	19.76±1.03	0.369±0.007
SP2	22.79±0.19	0.289±0.032
SP3	15.18±0.60	0.437±0.064

a: Results are given as average ± standard deviation of three measurements.

4.4. Polyplex Formation and Characterization

4.4.1. siRNA Complexation

Cationic polymers could form complexes known as polyplexes with siRNA via electrostatic interactions. The amount of polymer required to fully complex with siRNA could be determined by analyzing the polymer/siRNA polyplexes prepared at different ratios. Since the interaction occurs between positively charged amino groups of the polymers and negatively charged phosphate groups of siRNAs, the polymer/ siRNA ratio is frequently described as a N/P (Nitrogen/Phosphate). To determine the complex forming ability of the polymers, polymers at different amounts were added to fixed amounts of siRNA so that polyplexes with varied N/P were obtained. The prepared polyplexes were visualized on agarose gel and by determining N/P where siRNA band is disappeared, the minimum amount of polymer required to form complexes with siRNA was determined.

Linear block copolymers, P(OEGMA)$_{(5K)}$-*b*-P(AEAEMA)$_{40}$, PEG$_{(5K)}$-*b*-P(AEAEMA)$_{40}$, P(OEGMA)$_{20}$-*b*-P(AEAEMA)$_{48}$, P(OEGMA)$_{43}$-*b*-P(AEAEMA)$_{60}$, P(OEGMA)$_{43}$-*b*-P(AEAEMA)$_{45}$ and P(AEAEMA)$_{40}$-*b*-P(OEtOxMA)$_{38}$ and star polymers (SP1 and SP2) were complexed with siRNA at varied N/P ratios (1, 2, 3, 4, 5, 10, 30 or 50) and after vigorous mixing complexes incubated at room temperature for 30 min-1 h. Varied amount of polymers were always added to pre-pipetted siRNA and formulations were always freshly prepared throughout this thesis. In addition, the

incubation time of the mixtures was always kept between 30 min-1h to ensure the reproducibility of the formulation preparations.

All block copolymers could form complexes with siRNA efficiently as can be seen in electropherograms (Figure 4.25, Figure A1, A2 and A3). $P(OEGMA)_{43}$-*b*-$P(AEAEMA)_{46}$ and $P(AEAEMA)_{40}$-*b*-$P(OEtOxMA)_{38}$, were able to start forming complexes at N/P of 2 (Figure 4.25). However free siRNA band and/or smear was also still observable at this N/P ratio indicating that not all siRNA molecules in the media were complexed with polymer. When N/P is increased to 3, in other words when more polymers were used in the complex formation, the free siRNA band completely disappeared showing that entire siRNA molecules in the media complexed with added $P(OEGMA)_{43}$-*b*-$P(AEAEMA)_{46}$ or $P(AEAEMA)_{40}$-*b*-$P(OEtOxMA)_{38}$ at N/P of 3. This result showed that the different neutral blocks with approximately same DP ($P(OEGMA)_{43}$ and $P(OEtOxMA)_{38}$) exhibited similar behavior in siRNA complexation.

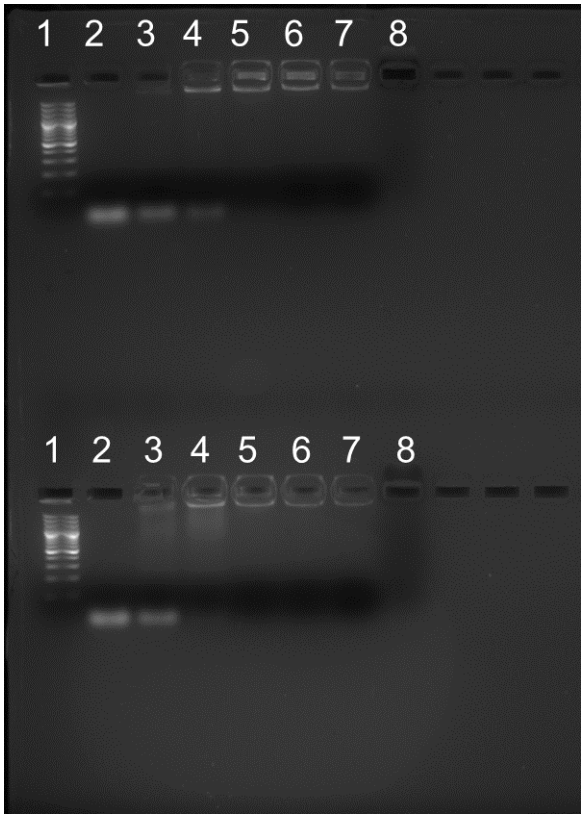

Figure 4.25. Agarose gel electropherogram of $P(OEGMA)_{43}$-b-$P(AEAEMA)_{45}$-siRNA (samples at the top) and $P(AEAEMA)_{40}$-b-$P(OEtOxMA)_{38}$-siRNA (samples at the bottom) complexes. Lane 1: DNA marker; Lane 2: naked siRNA; Lanes 3-8: complexes prepared at N/P of 1, 2, 3, 4, 5, and 50, respectively.

$PEG_{(5K)}$-*b*-$P(AEAEMA)_{40}$ was the most efficient polymer in siRNA complexation as it was able to bind entire siRNA molecules only at N/P of 1 (Figure A1). Whereas, comb-type (or brush-type) PEG counterpart of this polymer, namely $P(OEGMA)_{(5K)}$-*b*-$P(AEAEMA)_{40}$, could bind the siRNA at N/P of 2 completely (Figure A2). The results demonstrated that incorporation of linear PEG (instead of comb-type PEG) to the block copolymer structure might be favorable for efficient siRNA complexation. Another block copolymer with longer P(OEGMA) block length, $P(OEGMA)_{20}$-*b*-$P(AEAEMA)_{48}$, could fully complex the siRNA at N/P of 3 similar to $P(OEGMA)_{43}$-*b*-$P(AEAEMA)_{45}$ (Figure A3). Both block copolymers, $P(OEGMA)_{20}$-*b*-$P(AEAEMA)_{48}$ and $P(OEGMA)_{43}$-*b*-$P(AEAEMA)_{45}$, were less efficient at complexation compared to $P(OEGMA)_{(5K)}$-*b*-$P(AEAEMA)_{40}$ having shorter P(OEGMA) block length. This showed that P(OEGMA) slightly affects the complexation in a negative manner especially at block lengths higher than 5 kDa. $P(OEGMA)_{43}$-*b*-$P(AEAEMA)_{60}$ (polymer with longest cationic block) could bind all siRNA in the media at N/P of 4 (almost fully complexed at N/P of 3 though) (Figure A3). Slightly weaker complexation performance of this polymer was attributed to the relatively low solubility in aqueous media due to increased molecular weight leading to increased interchain and intrachain hydrogen bonding.

All in all, linear block polymers were able to efficiently bind siRNA at low N/P ratios without needing the excess polymer.

Two different miktoarm star polymers, P(OEGMA)/P(AEAEMA) miktoarm star polymer-1 (SP1) and P(OEGMA)/P(AEAEMA) miktoarm star polymer-2 (SP2), with varied cationic block arm number (SP1= 50% cationic arm, SP2= 80% cationic arm) were used in the complex formation assays. Since N/P ratio is employed for the determination of complex formation, even though the polymers have different cationity same amount of amine groups for both polymers have been complexed with fixed amount of siRNA. Gel electrophoresis results revealed that, SP1 was slightly better at complexing siRNA since the free siRNA band was disappeared at N/P of 5 completely when SP1 was used (Figure 4.26). However free siRNA band was still visible in some extent at N/P of 5 when SP2 was used. This might be attributed to increased amount of polymer since more SP1 was required compared to SP2 to reach the same amine density. Homo-arm star polymer (SP3, arms: P(OEGMA)) was used as a control polymer and as seen in the electropherogram it did not interact with siRNA indicating that the core structure of the star polymers not playing important role at complexing siRNA.

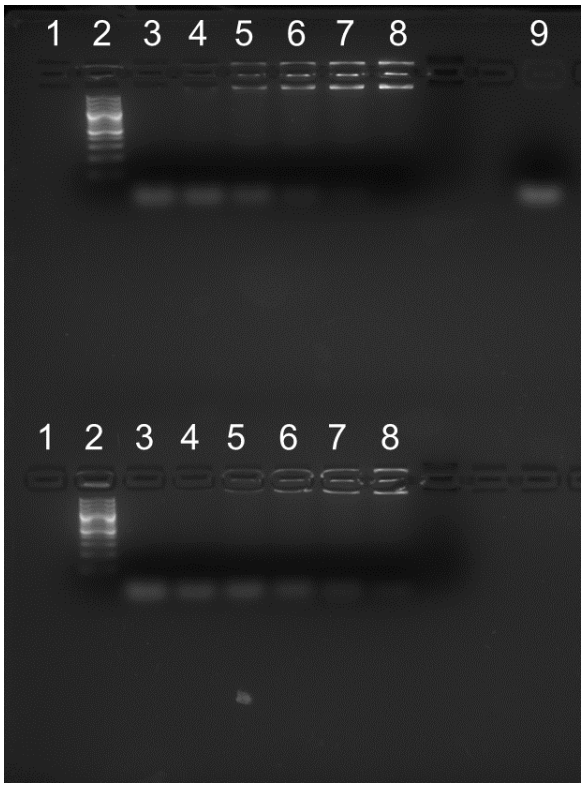

Figure 4.26. Agarose gel electropherogram of SP1-siRNA (samples at the top) and SP2-siRNA (samples at the bottom) complexes. Lane 1: DNA marker; Lane 2: naked siRNA; Lanes 3-8: complexes prepared at N/P of 1, 2, 3, 4, 5, and 50, respectively. Lane 9: control (SP3-siRNA mixture).

Linear block structures were better at complexing siRNA compared to star architecture (Table 4.10). This is showing that the linear blocks could easily interacted with siRNA and could wrapped it effectively due to their flexible structure. In contrast to this, star polymers have displayed more hindered interaction with siRNA possibly because of lower steric availability of cationic amine groups. However, still star architecture was also able to complex entire siRNA molecules in the media relatively at low N/P ratios.

Table 4.10. Lowest N/P values where polymers fully complexed entire siRNA molecules in the media.

Polymer	**Lowest N/P value for full complexation**
$PEG_{(5K)}$-*b*-$P(AEAEMA)_{40}$	1
$P(OEGMA)_{(5K)}$-*b*-$P(AEAEMA)_{40}$	2
$P(OEGMA)_{20}$-*b*-$P(AEAEMA)_{48}$	3
$P(OEGMA)_{43}$-*b*-$P(AEAEMA)_{45}$	3
$P(OEGMA)_{43}$-*b*-$P(AEAEMA)_{60}$	4
$P(AEAEMA)_{40}$-*b*-$P(OEtOxMA)_{38}$	3
SP1	5
SP2	>5

4.4.2. Size of the Polyplexes

Four different block copolymers, $P(OEGMA)_{(5K)}$-*b*-P(AEAEMA), $PEG_{(5K)}$-*b*-$P(AEAEMA)_{40}$, $P(OEGMA)_{43}$-*b*-$P(AEAEMA)_{45}$ and $P(AEAEMA)_{40}$-*b*-$P(OEtOxMA)_{38}$, were complexed with siRNA at three different N/P ratios (2, 10 and 50) and the hydrodynamic sizes of the prepared polyplexes were investigated in PBS by dynamic light scattering (Figure 4.27 and Table 4.11). These polymers were chosen to examine the effect of P(OEGMA), PEG and P(OEtOxMA) blocks on colloidal stability together with the effect of N/P ratio.

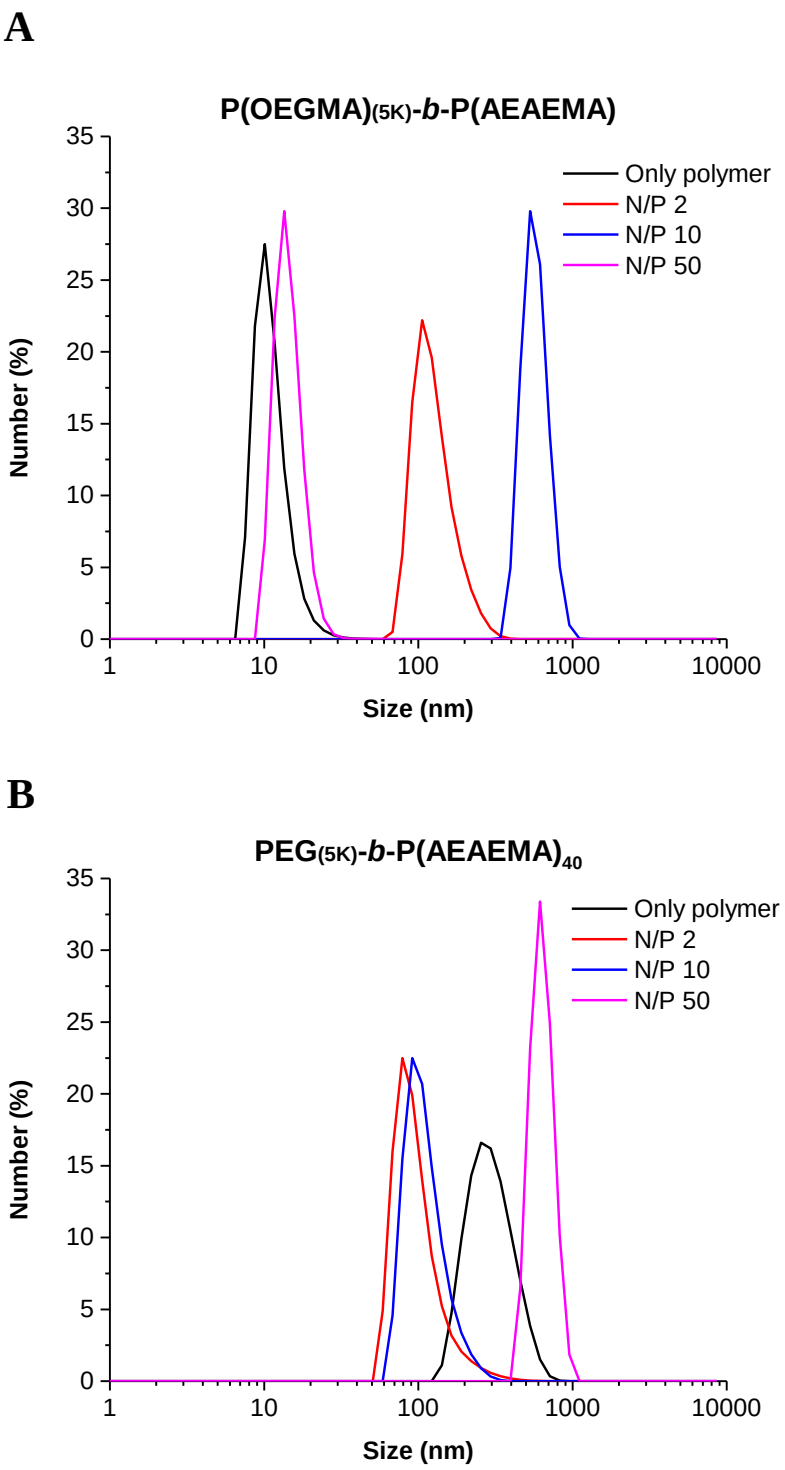

Figure 4.27. Hydrodynamic size distribution of block copolymers and block copolymer-siRNA complexes at varied N/P in PBS.

(Cont. on next page)

C

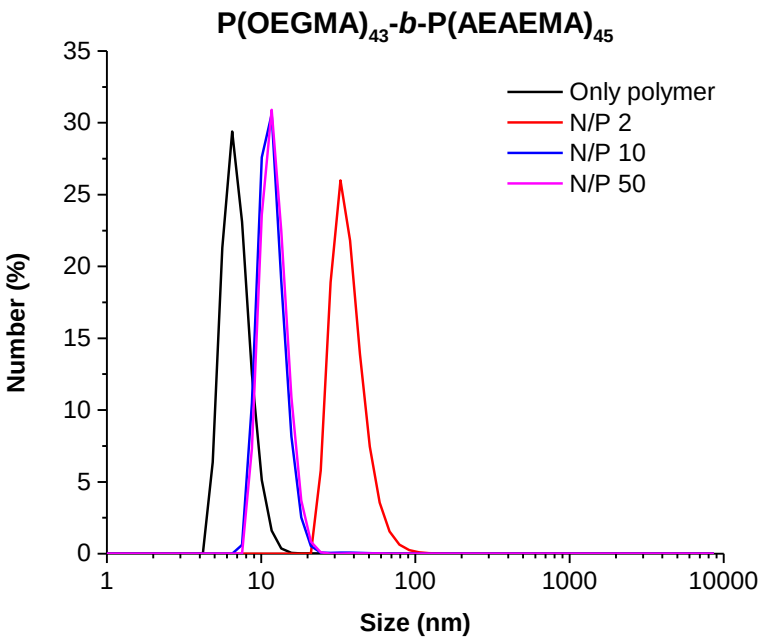

D

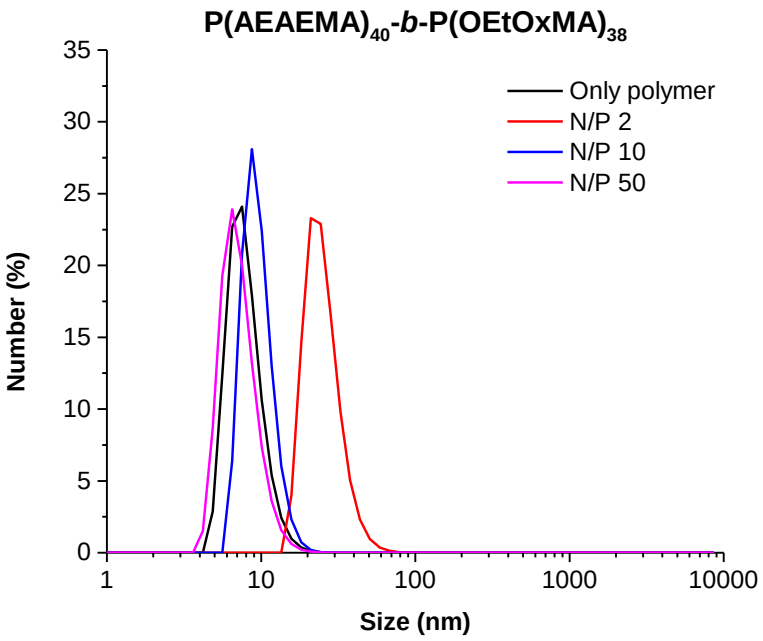

Figure 4.27. (Cont.)

Table 4.11. The number average hydrodynamic diameters (nm) (A) and PDI values (B) of linear block copolymers and their siRNA complexes at varied N/P in PBS (pH 7.4).

A

Polymer	Only polymer	N/P 2	N/P 10	N/P 50
P(OEGMA)$_{(5K)}$-*b*-P(AEAEMA)	6.41±1.71	132.00±8.55	628.50±41	10.68±1.91
PEG$_{(5K)}$-*b*-P(AEAEMA)	268.43±44.52	102.54±5.90	109.73±5.42	799.70±277.28
P(OEGMA)$_{43}$-*b*-P(AEAEMA)$_{45}$	7.91±2.39	35.74±1.46	14.84±3.02	11.75±0.60
P(AEAEMA)$_{40}$-*b*-P(OEtOxMA)$_{38}$	7.84±0.14	25.04±0.89	9.28±0.21	7.60±0.23

Results are given as average ± standard deviation of three measurements.

B

Polymer	Only polymer	N/P 2	N/P 10	N/P 50
P(OEGMA)$_{(5K)}$-*b*-P(AEAEMA)	0.399±0.034	0.178±0.012	0.370±0.081	0.777±0.164
PEG$_{(5K)}$-*b*-P(AEAEMA)	0.375±0.027	0.205±0.011	0.098±0.014	0.374±0.063
P(OEGMA)$_{43}$-*b*-P(AEAEMA)$_{45}$	0.439±0.015	0.350±0.025	0.439±0.016	0.507±0.034
P(AEAEMA)$_{40}$-*b*-P(OEtOxMA)$_{38}$	0.387±0.025	0.339±0.039	0.682±0.040	0.429±0.034

Results are given as average ± standard deviation of three measurements.

P(OEGMA)$_{(5K)}$-*b*-P(AEAEMA) block copolymer formed nanoparticles with diameter of 132 nm at N/P of 2 indicating that block copolymers (with diameter of ≈6 nm) were assembled and formed micelle-like nanostructures (often called polyion complex (PIC) nanoparticle) in the presence of siRNA molecules. It is most likely that the cationic P(AEAEMA) block electrostatically interacted with negatively charged

siRNA molecules and formed the core and this core is shielded by the hydrophilic P(OEGMA) block that is located at the corona. With the increase in N/P ratio (at N/P of 10), or in other words, when more polymer was complexed with same amount of siRNA, nanoparticles formed aggregates having diameters of ≈628 nm. When N/P ratio increased to 50, formation of more stable and compact structures has been observed possibly due to increased amount of charged polymer that can potentially lead to charge repulsion and support the colloidal stability. It is likely that at this N/P ratio only one or few polymers were complexed with one siRNA molecule since the diameter at this N/P was found to be ≈11 nm.

Linear PEG block copolymer, $PEG_{(5K)}$-*b*-$P(AEAEMA)_{40}$, displayed a different profile than all other block copolymers. This block copolymer was able to form nanostructures with diameter of ≈268 nm even without siRNA. This is directly attributed to the structure of linear PEG block which is more hydrophilic than P(OEGMA) since it lacks the methacrylate-based long -CH_2-CH_2- chain. The relative difference in the hydrophobicity of P(AEAEMA) and PEG and increased amount of hydrogen bonds could possibly triggered the formation of polymeric supramolecular structures whereas this has not been observed in the cases of P(OEGMA) block copolymers. At N/P of 2 and 10, the diameters of the $PEG_{(5K)}$-*b*-$P(AEAEMA)_{40}$-siRNA complexes was found to be approximately 103 and 110 nm, respectively. This is indicating that in the presence of siRNA more compact structures formed due to complex formation and PICs could be obtained at significantly decreased diameters. Compared to $P(OEGMA)_{(5K)}$ block copolymer-siRNA complexes, $PEG_{(5K)}$ block copolymer could form complexes with decreased diameters possibly due to differed hydrodynamic behavior of linear PEG compared to comb-type/brush PEG (P(OEGMA)). At N/P of 10, in contrast to $P(OEGMA)_{(5K)}$, $PEG_{(5K)}$ block copolymer was still able to form nanostructures which is showing that incorporation of linear PEG blocks to the polyplex structure is sterically more convenient than brush PEG. However, aggregation tendency was observed when N/P increased to 50.

The diameter of the $P(OEGMA)_{43}$-*b*-$P(AEAEMA)_{45}$ was found to be slightly higher than $P(OEGMA)_{(5K)}$-*b*-P(AEAEMA) with ≈8 nm. This is expected since $P(OEGMA)_{43}$-*b*-$P(AEAEMA)_{45}$ consists of P(OEGMA) with higher Mn. However, when $P(OEGMA)_{43}$-*b*-$P(AEAEMA)_{45}$ was complexed with siRNA (N/P of 2) the sizes of the polyplexes was found to be significantly lower than $P(OEGMA)_{(5K)}$-*b*-P(AEAEMA)-

siRNA complexes suggesting that Mn of P(OEGMA) directly affected the hydrodynamic sizes of the complexes. The sizes of P(OEGMA)$_{43}$-*b*-P(AEAEMA)$_{45}$-siRNA complexes at N/P of 2 was found to be ≈36 nm indicating that more compact/small PIC nanoparticles formed with the increase in P(OEGMA) block length. This is possibly due to steric hinderance/bulkiness of high Mn P(OEGMA) which is preventing the incorporation of high amount of polymer chains to the PIC structure. When N/P is increased to 10 and 50 sizes were decreased to ≈15 and ≈12 nm, respectively. This is showing that the increase in N/P resulted in formation of smaller nanoparticles. In this case possibly one siRNA molecule is complexed with one or few polymer chains due to presence of excess amount of polymer with respect to siRNA.

P(OEtOxMA) block copolymer, P(AEAEMA)$_{40}$-*b*-P(OEtOxMA)$_{38}$, was displayed similar size profile (≈8 nm) with P(OEGMA)$_{43}$-*b*-P(AEAEMA)$_{45}$. This is expected since DP values of these two block copolymers was approximately same. However, sizes of P(AEAEMA)$_{40}$-*b*-P(OEtOxMA)$_{38}$-siRNA complexes (25 nm, 10 nm and 8 nm for N/P 2, 10 and 50, respectively) were found to be considerably smaller than P(OEGMA)$_{43}$-*b*-P(AEAEMA)$_{45}$-siRNA complexes at all tested N/P values. This is possibly due to bulkiness of ethyl oxazoline units obstructing the polymer-siRNA interaction sterically and leading to formation of complexes consisting of one/few siRNA molecule(s) and one/few polymer chain(s).

Generally, PDI values of the block copolymer-siRNA complexes at N/P of 2 were found to be ≈0.2-0.3 indicating the relative narrow size distribution. When N/P ratio was increased to 20 and 50 usually an increase in the PDI was observed. This is suggesting that with the increase in polymer amount, complexes consisting of different amount of polymer and siRNA was began to form. It is also likely that free/uncomplexed (excess) polymer chains were also contributed to the PDI at high N/P ratios which was not the case at low N/P ratios as there is not much free polymer chains at N/P of 2.

Miktoarm star polymers SP1 and SP2 were complexed with siRNA at different N/P ratios (2, 10 and 50) and sizes were determined after complex formation (Figure 4.28 and Table 4.12). Both star polymers formed aggregates at N/P of 2 possibly due to neutralization of total charge. When polymer amount was increased (at N/P of 10 and 50), sizes decreased as expected due to charge repulsion. At N/P of 50, similar size distribution was observed with only polymer size distribution indicating that either one star polymer

could complex with one siRNA molecule in the media, or one siRNA molecule was complexed at the interface of few star polymers.

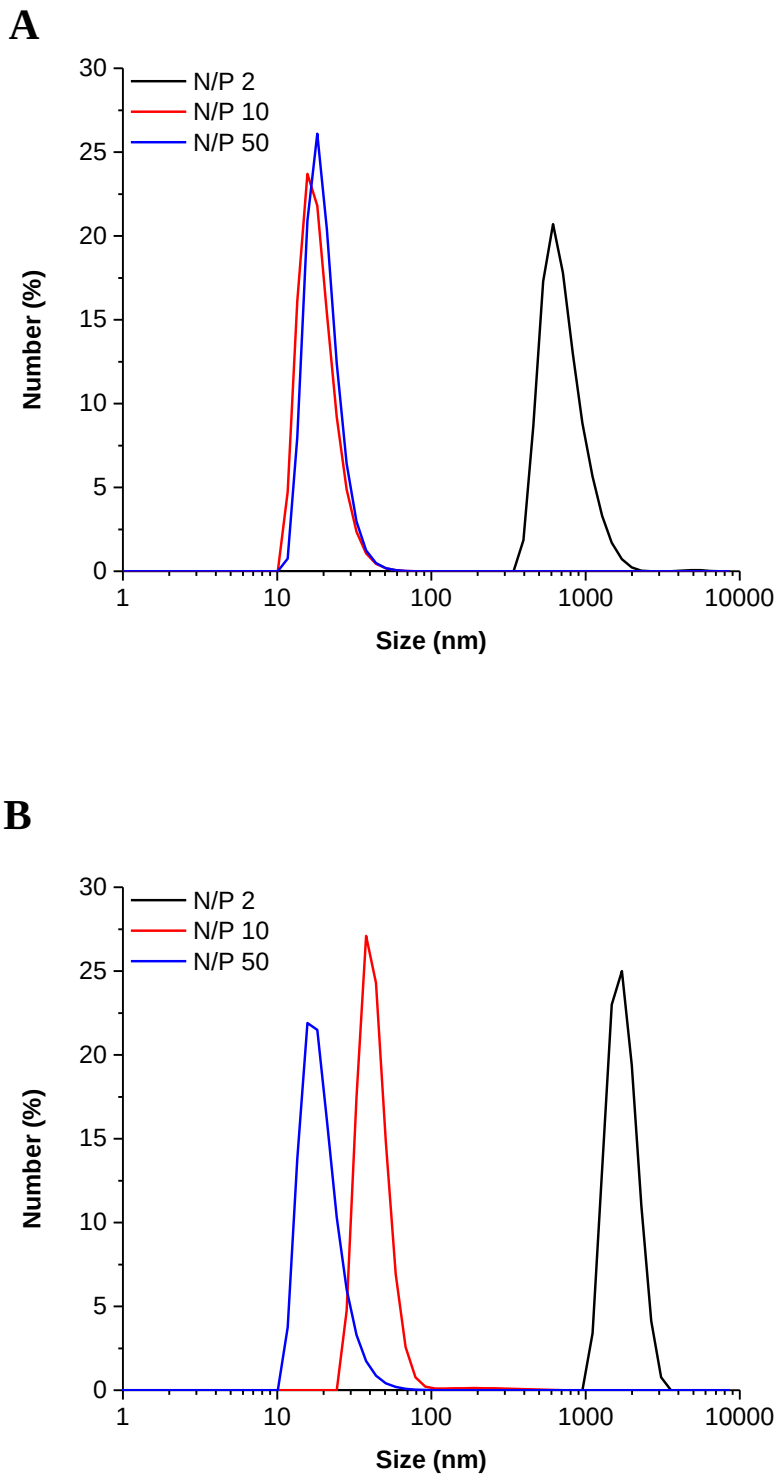

Figure 4.28. Hydrodynamic size distribution of SP1-siRNA **(A)** and SP2-siRNA complexes **(B)** at varied N/P in PBS.

Table 4.12 The number average hydrodynamic diameters (nm) (A) and PDI values (B) of star polymers and their siRNA complexes at varied N/P in PBS (pH 7.4).

A

Polymer	Only polymer	N/P 2	N/P 10	N/P 50
SP1	19.76±1.03	849.33±91.29	19.28±4.04	19.38±0.78
SP2	22.79±0.19	1734.00±76.71	97.03±57.87	22.15±1.77
SP3	15.18±0.60	-	-	-

Results are given as average ± standard deviation of three measurements.

B

Polymer	Only polymer	N/P 2	N/P 10	N/P 50
SP1	0.369±0.007	0.226±0.030	0.558±0.059	0.473±0.067
SP2	0.289±0.032	0.276±0.037	0.268±0.013	0.275±0.029
SP3	0.437±0.064	-	-	-

Results are given as average ± standard deviation of three measurements.

Electron microscopy techniques, Scanning Electron Microscopy (SEM), Transmission Electron Microscopy (TEM), were also employed to verify the DLS results and examine the morphology of the polyplexes in detail. TEM images of P(OEGMA)$_{43}$-*b*-P(AEAEMA)$_{45}$-siRNA complexes showed that at N/P of 2 polyplex sizes are larger; in contrast, at N/P of 50 more defined and smaller particles were observable (Figure B1). These results showed good harmony with the DLS results. The size of this same polymer-siRNA complexes was investigated by SEM as well (Figure B2). SEM showed that at N/P of 50 siRNA complexes of P(OEGMA)$_{43}$-*b*-P(AEAEMA)$_{45}$ have diameters around 58-160 nm based on ImageJ software analysis. In comparison, P(AEAEMA)$_{40}$-b-P(OEtOxMA)$_{38}$-siRNA complexes at the same N/P exhibited significantly higher particle diameters (200-600 nm) (Figure B3). SEM of star polymer complexes, SP1-siRNA at N/P 50, was also investigated and the diameters were found to be between 80-100 nm (Figure B4). However, it should be noted that, the employed SEM sample preparation technique was not the most suitable technique as it can cause to unintended aggregations which lead to misinterpretation of the data. In addition, electron microscopy data are limited to the under-investigation area of the specimen. There is always the possibility that other parts of the specimen may contain particles of different sizes and has not been imaged by the

microscope analyst. Also, the relatively low resolution of SEM might not allow the imaging of smaller particles. Under these constraints, Cryo-TEM might be recommended to better reveal the size and morphology profile of these complexes.

4.4.3. Zeta Potential of the Polyplexes

Surface charge of the complexes can provide important vision regarding the cellular interaction of the delivery systems. Even positively charged nanoparticles are known to be more favorable in terms of cell association and cell uptake, negatively charged or neutral systems are often desirable especially at clinical translation stage since positively charged materials known to activate the immune system, complement pathways and exhibit cytotoxicity (Akinc et al., 2019). Additionally, charge of the particles also often affects the colloidal stability.

For the stated reasons, surface charge of the complexes was investigated by zeta potential measurements. Linear block copolymer-siRNA complexes P(OEGMA)$_{43}$-*b*-P(AEAEMA)$_{45}$, P(AEAEMA)$_{40}$-*b*-P(OEtOxMA)$_{38}$, P(OEGMA)$_{(5K)}$-*b*-P(AEAEMA)$_{40}$ and PEG$_{(5K)}$-*b*-P(AEAEMA)$_{40}$, were prepared at N/P of 50 and N/P of 2 in PBS and zeta potential values were determined by electrophoretic light scattering (Figure 8 and Table 1). Generally, all polyplexes displayed slightly negative charge indicating that neutral blocks were effective at masking the charge. Among all block copolymer-siRNA complexes prepared at N/P of 50, only PEG$_{(5K)}$-*b*-P(AEAEMA)$_{40}$ complexes was found to be neutral. This finding is also in good agreement with DLS result, as PEG$_{(5K)}$-*b*-P(AEAEMA)$_{40}$ complexes tend to form aggregates at this N/P ratio. In contrast to this, P(OEGMA)$_{(5K)}$-*b*-P(AEAEMA)$_{40}$-siRNA complexes showed the highest negative charge with -2.02 ±1.70 mV indicating that linear PEG might be more effective at charge masking compared to comb-type PEG. P(OEGMA)$_{43}$-*b*-P(AEAEMA)$_{45}$-siRNA complexes showed lower negativity compared to P(OEGMA)$_{(5K)}$-*b*-P(AEAEMA)$_{40}$-siRNA complexes suggesting that higher P(OEGMA) block length could mask the charge better. P(AEAEMA)$_{40}$-*b*-P(OEtOxMA)$_{38}$-siRNA complexes (-0.78 mV) exhibited very similar zeta potential value with P(OEGMA)$_{43}$-*b*-P(AEAEMA)$_{45}$-siRNA complexes (-0.97 mV) indicating that these two comb-type blocks with same DP led to formation of very similar polyplex structures. It should be noted that, the size of polyplexes formed of

P(AEAEMA)$_{40}$-*b*-P(OEtOxMA)$_{38}$ and P(OEGMA)$_{43}$-*b*-P(AEAEMA)$_{45}$ was also approximately same with each other as evidenced by DLS. At N/P of 2, the zeta potential values were higher compared to N/P of 50 of the same block copolymer-siRNA complexes. This was probably due to presence of lower polymer amount in the media and differed complexation profile as shown by DLS and gel electrophoresis.

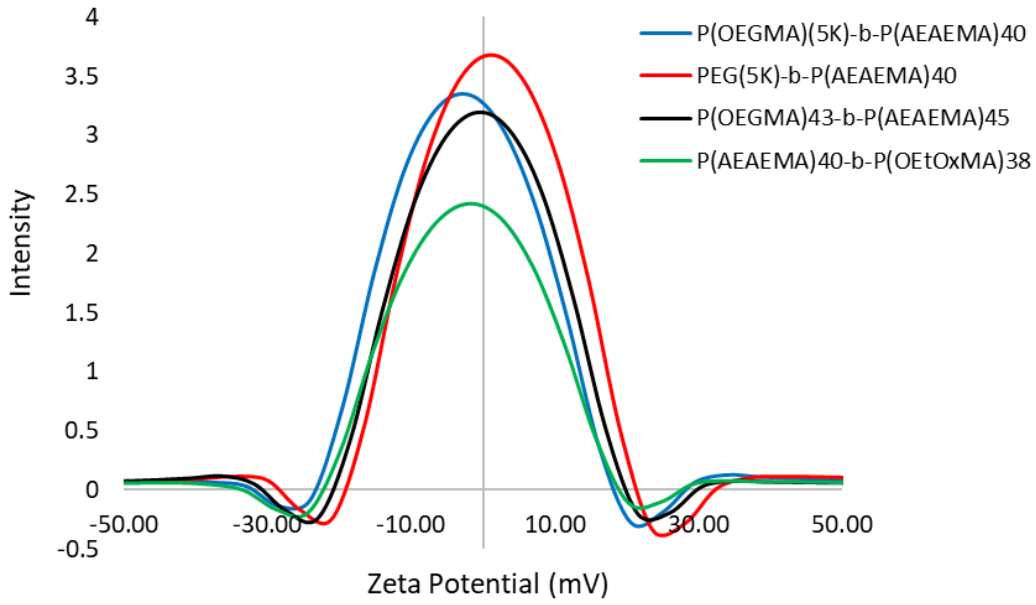

Figure 4.29. Representative zeta potential curves of block copolymer-siRNA complexes at N/P of 50 in PBS.

Table 4.13. Zeta potential (mV) of block copolymer-siRNA complexes in PBS.

Polymer	**N/P 2**	**N/P 50**
P(OEGMA)$_{(5K)}$-*b*-P(AEAEMA)$_{40}$	N/A	-2.02 ±1.70
PEG$_{(5K)}$-*b*-P(AEAEMA)$_{40}$	-3.19 ± 0.49	0.05 ± 0.77
P(OEGMA)$_{43}$-*b*-P(AEAEMA)$_{45}$	-1.34 ± 0.60	-0.97 ± 0.79
P(AEAEMA)$_{40}$-*b*-P(OEtOxMA)$_{38}$	N/A	-0.78 ± 0.90

4.5. Serum Stability of siRNA

Nucleic acid carriers are known to protect their cargos against serum nucleases. To provide better insight into the effect of stealth polymers (P(OEGMA) and P(OEtOxMA)) and different star polymers (SP1, SP2) on siRNA stability, the siRNA protecting ability of linear block copolymers, $P(OEGMA)_{43}$-*b*-$P(AEAEMA)_{45}$ and $P(AEAEMA)_{40}$-*b*-$P(OEtOxMA)_{38}$, and miktoarm P(OEGMA)/P(AEAEMA) star polymers, SP1 and SP2, was determined. For this, complexes were prepared at N/P of 50 and incubated in FBS at 37 °C. At predetermined times, aliquots were taken, the nuclease activity was stopped by EDTA treatment, and samples were frozen and kept at -20 °C until analysis. Before running the samples on agarose gel, heparin was added to disassemble the complexes. As expected, degradation of naked siRNA has begun in minutes and entire siRNA molecules in the media were degraded completely within hours (Figure 4.30). Naked siRNA was mostly degraded within 2 h and almost complete degradation was observed by the time reached to 8h (Figure 4.31). After 24 h there was no visible band on the gel indicating the complete degradation of entire siRNA molecules in the media by serum nucleases.

Figure 4.30. Agarose gel electropherogram of naked siRNA incubated at 50% FBS (v/v) for varying times. Lane 1: Marker, Lane 2-6: naked siRNA after incubation in serum containing media for 0 h, 0.5 h, 2 h, 8 h, and 24 h, respectively.

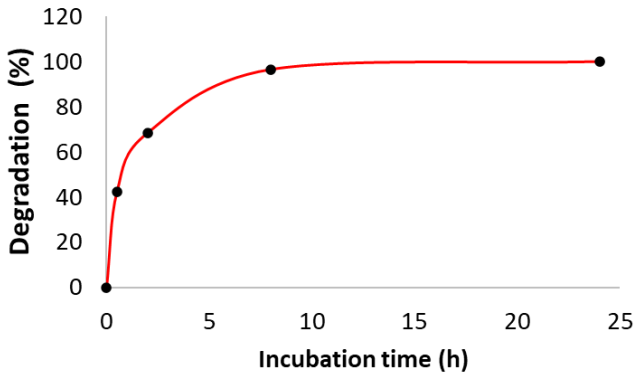

Figure 4.31. ImageJ analysis results of gel electropherogram of naked siRNA incubated at 50% FBS (v/v) for varying times.

Together with naked siRNA, serum interaction of block copolymer-siRNA complexes and star polymer-siRNA complexes was also determined under the same experimental conditions (Figure 4.32, 4.33, 4.34 and 4.35). The electropherograms showed that approximately complete protection of siRNA was achived up to 8 h when siRNA is complexed to linear block or star polymers. By the time 24 h, the siRNA bands were still highly visible however the intensity was generally weaker compared to first 8 h. This is showing that some siRNA might be released from the complexes by time and degraded in serum. Another scenerio might be the slowed down degradation of siRNA even when it is still complexed to polymers. When siRNA is complexed by the polymers, the serum nuclease-siRNA interaction is sterically blocked. This pevents the rapid degradation of siRNA however still some amount of siRNA might be still accesible in some extent which might cause to the slower degradation by the nucleases with respect to time.

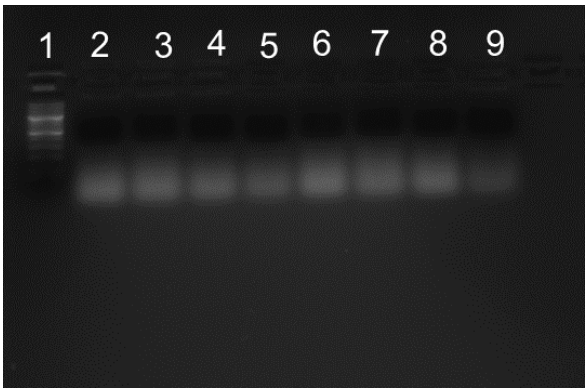

Figure 4.32. Agarose gel electropherogram of linear block copolymer-siRNA complexes, P(OEGMA)$_{43}$-*b*-P(AEAEMA)$_{46}$-siRNA and P(AEAEMA)$_{40}$-*b*-P(OEtOxMA)$_{38}$-siRNA, at N/P of 50, incubated at 50% FBS (v/v) for varying times. Lane 1: Marker, Lane 2-5: P(OEGMA)$_{43}$-*b*-P(AEAEMA)$_{46}$-siRNA complexes after incubation in serum containing media for 0 h, 2 h, 8 h, and 24 h, respectively. Lane 6-9: P(AEAEMA)$_{40}$-*b*-P(OEtOxMA)$_{38}$-siRNA complexes after incubation in serum containing media for 0 h, 2 h, 8 h, and 24 h, respectively.

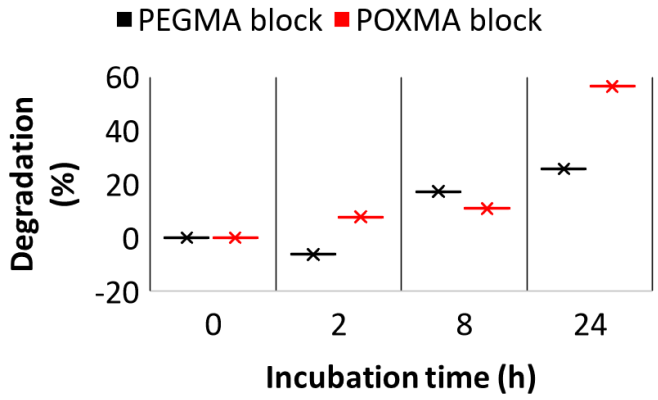

Figure 4.33. ImageJ analysis results of gel electropherogram of block copolymer-siRNA complexes, P(OEGMA)$_{43}$-*b*-P(AEAEMA)$_{46}$-siRNA (PEGMA block) and P(AEAEMA)$_{40}$-*b*-P(OEtOxMA)$_{38}$-siRNA (POXMA block), at N/P of 50, incubated at 50% FBS (v/v) for varying times.

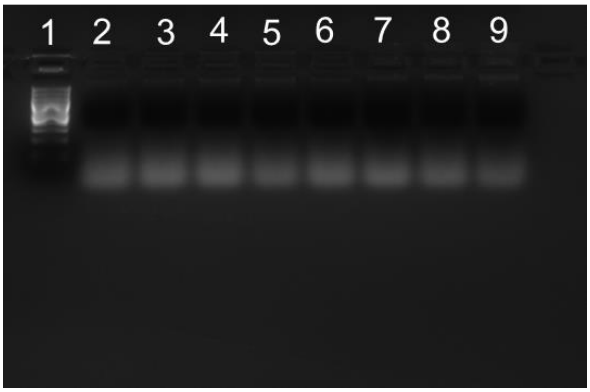

Figure 4.34. Agarose gel electropherogram of star polymer-siRNA complexes, SP1 and SP2, at N/P of 50, incubated at 50% FBS (v/v) for varying times. Lane 1: Marker, Lane 2-5: SP1-siRNA complexes after incubation in serum containing media for 0 h, 2 h, 8 h, and 24 h, respectively. Lane 6-9: SP2-siRNA complexes after incubation in serum containing media for 0 h, 2 h, 8 h, and 24 h, respectively.

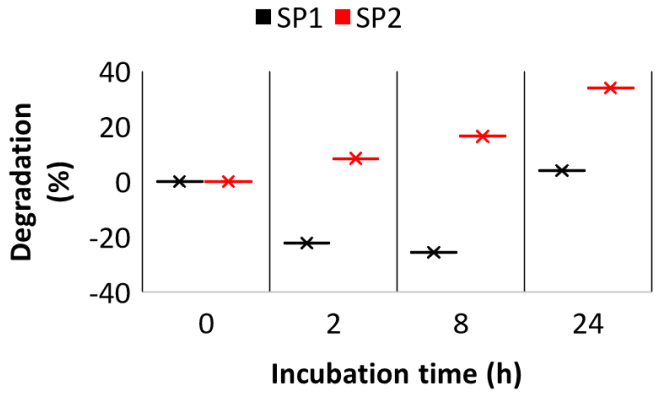

Figure 4.35. ImageJ analysis results of gel electropherogram of star polymer-siRNA complexes, SP1-siRNA and SP2-siRNA, at N/P of 50, incubated at 50% FBS (v/v) for varying times.

Based on ImageJ analysis result of 24 h incubation period, PEGMA block copolymer, P(OEGMA)$_{43}$-*b*-P(AEAEMA)$_{45}$, was able to prevent the degradation of siRNA at higher extent compared to POXMA block copolymer, P(AEAEMA)$_{40}$-*b*-P(OEtOxMA)$_{38}$ (Figure 4.36). This might be attributed to the differed serum interaction behavior of these two different stealth polymers, PEGMA and P(OEtOxMA). As can be seen in the next section (Release of siRNA), these block copolymers show different relase

profile even they have similar complexation ability (both fully complexed at N/P of 3). Collectively, these results show that the neutral blocks play a significantly different role in polymer-siRNA-serum interactions. Among star polymers, SP1 was found to be better at protecting siRNA against serum nucleases. The fact that SP1 contains more P(OEGMA) compared to SP2 (SP1: 50% P(OEGMA); SP2: 20% P(OEGMA)) might be the reason for this result since P(OEGMA) is known to be protein-repellent.

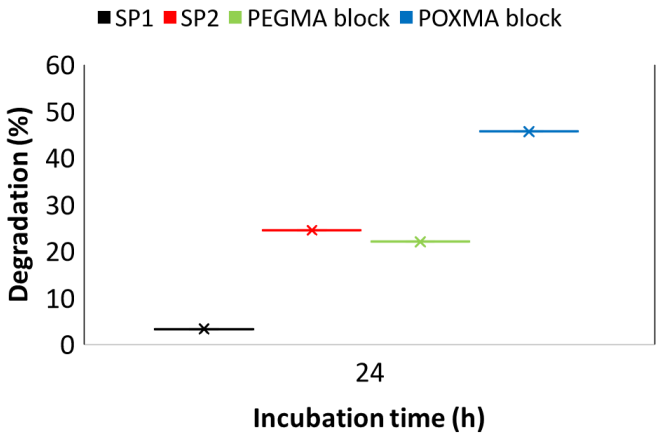

Figure 4.36. ImageJ analysis results of polymer-siRNA complexes at N/P of 50, incubated at 50% FBS (v/v) for 24 h.

All in all, all block and star polymers were able to protect siRNA in FBS containing medium leading to increased stability of the siRNA which is necessary for successful nucleic acid delivery applications.

4.6. Release of siRNA

For successful transfection applications, siRNA must be released from the complex once it is inside the cytosol. At the same time, siRNA should not be released when the complexes are in the extracellular matrix. Therefore, the carriers should be able to bind siRNA in some extent.

In order to investigate the effect of stealth polymers (P(OEGMA) and P(OEtOxMA)) and different star polymers (SP1, SP2) on siRNA release, heparin competition assay was performed. Complexes of two different block polymers, $P(OEGMA)_{43}$-*b*-$P(AEAEMA)_{45}$-siRNA $P(AEAEMA)_{40}$-*b*-$P(OEtOxMA)_{38}$-siRNA, or star polymers, SP1 and SP2, have been prepared at the same N/P ratios (N/P of 50) and different amounts of heparin (0 μg, 0.5 μg, 1.25 μg, 2.5 μg, 5 μg, 10 μg, 20 μg, 40 μg, 80 μg) was added to complexes in order to displace the siRNA. The heparin amount required to fully displace the siRNA was determined by gel electrophoresis (Figure 4.37).

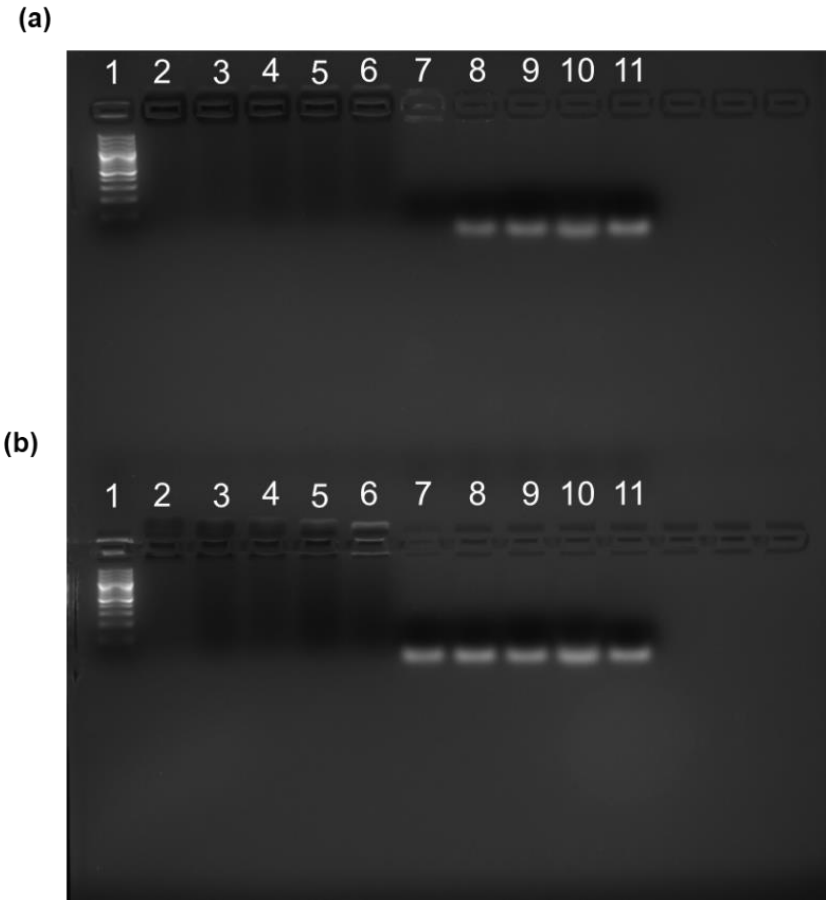

Figure 4.37. Agarose gel electropherogram showing the release profile of linear $P(OEGMA)_{43}$-*b*-$P(AEAEMA)_{45}$-siRNA (a) $P(AEAEMA)_{40}$-*b*-$P(OEtOxMA)_{38}$-siRNA (b) and miktoarm star SP1-siRNA (c) and SP2-siRNA (d) complexes prepared at N/P of 50 and treated with varying amounts of heparin. Lane 1: Marker, Lane 2-10: 0 μg, 0.5 μg, 1.25 μg, 2.5 μg, 5 μg, 10 μg, 20 μg, 40 μg, 80 μg heparine added complexes, respectively, Lane 11: Only siRNA.

(Cont. on next page)

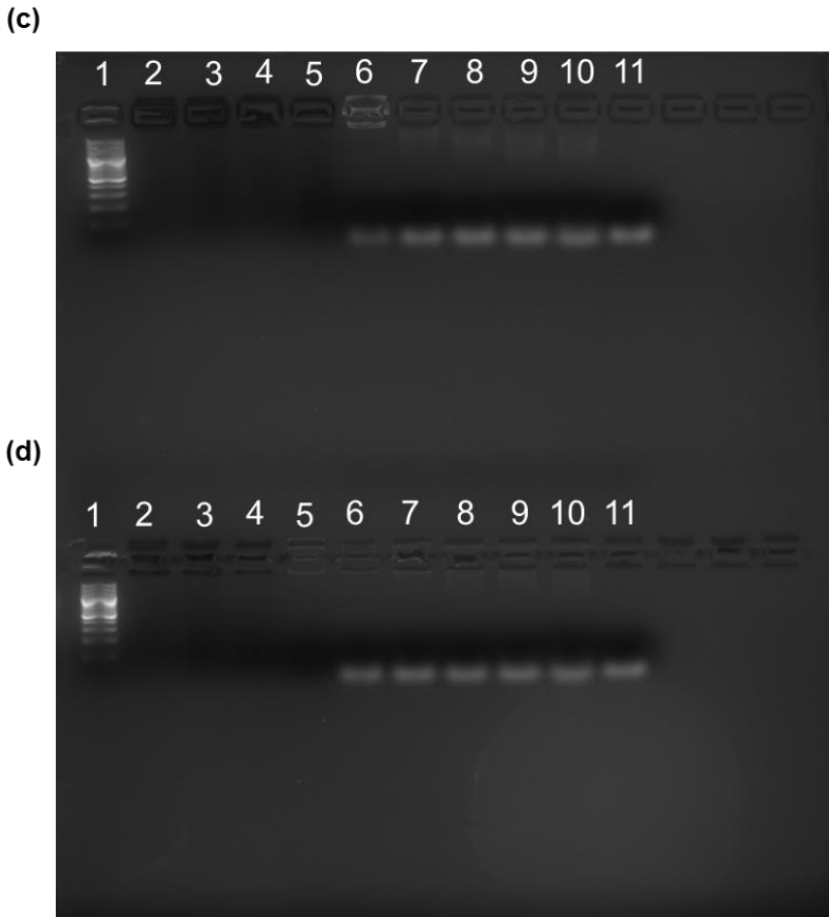

Figure 4.37. (Cont.)

Interestingly, block copolymers have displayed different release profiles even though the cationic block length was approximately same for both block copolymers. P(OEGMA)$_{43}$-*b*-P(AEAEMA)$_{46}$ was able to release siRNA when 20 μg of heparin was added to the complexes whereas only 10 μg of heparin was enough to displace siRNA from P(AEAEMA)$_{40}$-*b*-P(OEtOxMA)$_{38}$ – siRNA complexes. This is showing that the neutral blocks, P(OEGMA) or P(OEtOxMA), have important roles and interfering with the heparin interactions. It is likely that the neutral blocks have varied shielding effects therefore allowing the heparin interference/competition at different extents.

The siRNA release of star polymer-siRNA complexes has also been determined at the same conditions. Different from linear block copolymers, both star polymers released siRNA when 5 μg of heparin was added to the complexes. However, siRNA band intensity was slightly weaker with SP1-siRNA complexes at 5 μg of heparin

indicating that not all siRNA was released at this heparin amount. These results showed good harmony with the complex formation results since SP1 was able to bind siRNA at lower N/P ratios compared to SP2. This is showing that SP1 could bind siRNA tighter even though the cationic arm density was less than SP2. However, it should be noted that since N/P ratio was employed at these assays, the cationic charge amount (quantity) in the complex formation media was balanced for all formulations.

Collectively, due to their flexible structures, block copolymers were able to bind siRNA easier and form complexes tighter. Compared to this star polymers could release siRNA at lower heparin amounts and could form complexes at higher N/P ratios likely due to architectural differences.

4.7. Cytotoxicity of Polymers

The cytotoxicity of polymers was investigated by MTT Assay. Polymers (linear block copolymers: P(OEGMA)$_{43}$-*b*-P(AEAEMA)$_{45}$, P(AEAEMA)$_{40}$-*b*-P(OEtOxMA)$_{38}$, P(OEGMA)$_{(5K)}$-*b*-P(AEAEMA)$_{40}$ and PEG$_{(5K)}$-*b*-P(AEAEMA)$_{40}$ star polymers: SP1, SP2 and SP3) were prepared at different concentrations in PBS and treated with cells (3T3/NIH mouse fibroblast cell line, RAW 264.7 mouse macrophage cell line, MDA-MB-231-luc2-gfp human mammary cancer cell line or H460-luc2 lung cancer cell line) for 24 h. After 24h, absorbance of wells was measured using a microplate reader. The viability of only PBS treated cells was accepted as 100% and percent cell viability of the polymer treated cells was calculated in according to PBS treated wells.

It is known that each cell type behaves uniquely depending on its function therefore, the degree of interaction with nanocarriers or nanoparticles differs from one cell line to another. Therefore, different cell lines were employed to assess the cytotoxicity of different polymers. MDA-MB-231-luc2-gfp human mammary cancer cell line and H460-luc2 lung cancer cell line was the model cell lines that utilized throughout this study therefore, the cytotoxicity was also employed on these cell lines. In addition, NIH/3T3 mouse fibroblast cell line was also employed since it is one of the most commonly utilized cell lines for nanoparticle-based cytotoxicity assays and the cell type and the organism is same with BALB/3T3 clone A31 which is one of the recommended

cell lines according to ISO 10993-5 standards (biological evaluation of medical devices-part 5: tests for *in vitro* cytotoxicity). As a last cell line, RAW 264.7 mouse macrophage cell line was employed. Macrophages are important cell types since they take role in immune response and nanoparticles tend to create immunological effects and inflammatory responses (Manke, Wang, & Rojanasakul, 2013; Pandey & Prajapati, 2018). Therefore, assessing the effects of nanoparticles on macrophage cell line might give some information regarding the differences of evaluated nanoparticles/molecules. Moreover, macrophages present in all tissues and might exhibit enhanced sensitivity to molecules due to their scavenger duty (Dalzon et al., 2017). Furthermore, macrophage malfunction might cause unintended immunological responses (immune deficiency, autoimmunity) or tissues damages (G. Y. Chen & Nuñez, 2010; Navegantes et al., 2017). Because of all these reasons the toxicity of the polymers was tested on a macrophage cell line as well.

In general, the viability of polymer-treated cells decreased with increased amount of polymer in a dose-dependent manner (Figure 6). P(OEGMA)$_{43}$-*b*-P(AEAEMA)$_{45}$ did not profoundly affect the viability of tested cell lines except Raw 264.7. Interestingly this polymer showed significant toxicity on macrophage cells in an increasing trend with respect to polymer concentration. However, this special case was only valid for P(OEGMA)$_{43}$-*b*-P(AEAEMA)$_{45}$ meaning that other block copolymers displayed similar levels of toxicity on different cell lines including macrophage cells. POX analog of P(OEGMA)$_{43}$-*b*-P(AEAEMA)$_{45}$, namely P(AEAEMA)$_{40}$-*b*-P(OEtOxMA)$_{38}$, was generally found to be less toxic at all tested concentrations for all tested cell lines. This might be due to unique/enhanced interaction of ethylene glycol units with cell (membranes). Another reason that contributes to this situation might be the high dispersity of P(OEGMA) block copolymer and slightly longer cationic block of the P(OEGMA) block copolymer compared to POX block copolymer. Additionally, another P(OEGMA) block copolymer, P(OEGMA)$_{(5K)}$-*b*-P(AEAEMA)$_{40,}$ also showed higher toxicity compared to P(AEAEMA)$_{40}$-*b*-P(OEtOxMA)$_{38}$. This result also might be considered as another finding supporting the possible differed interaction of P(OEGMA) containing block polymers with cells.

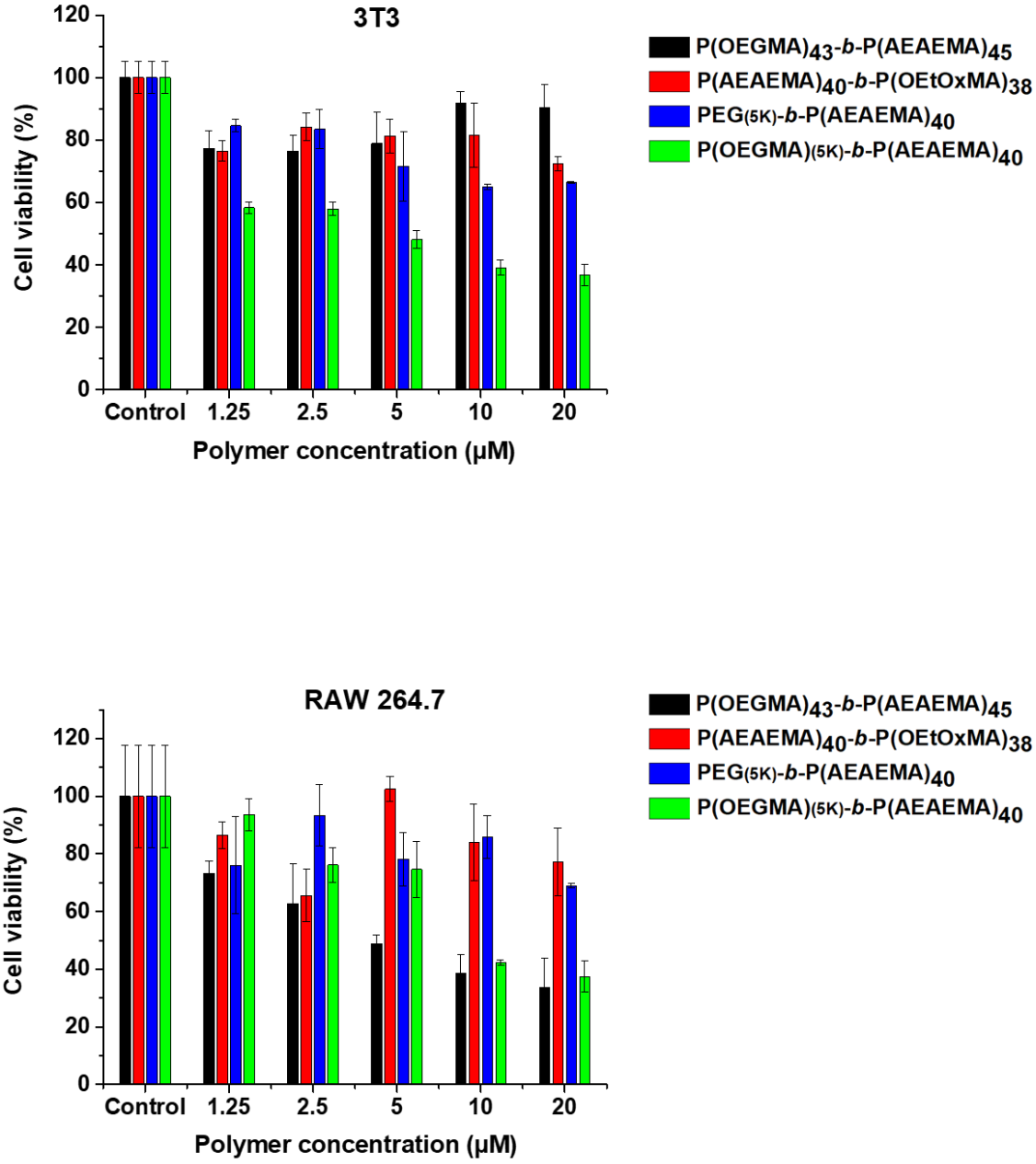

Figure 4.38. The effect of block copolymers on cell viability (24 h incubation).

(Cont. on next page)

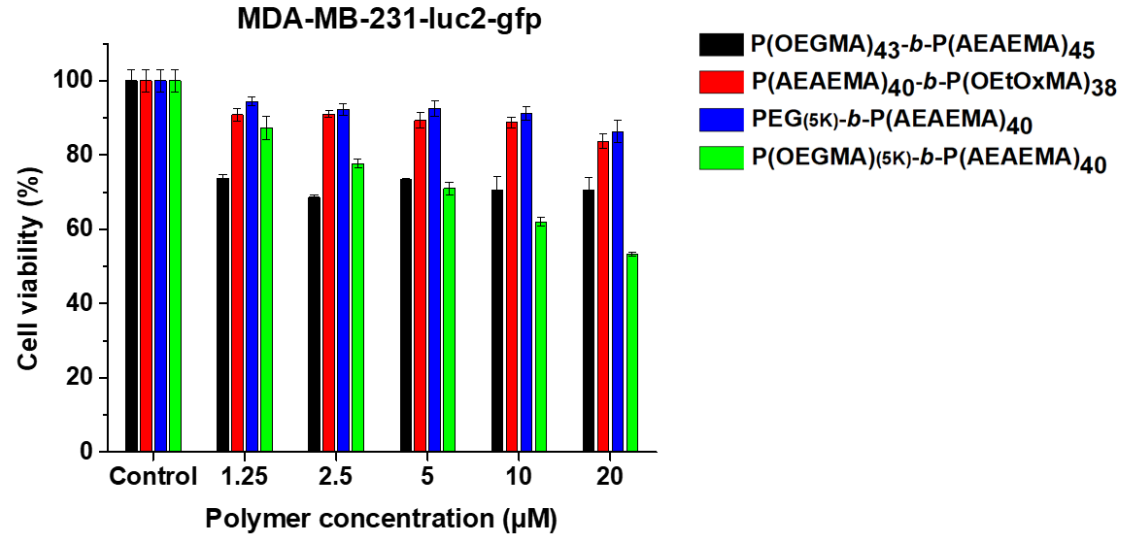

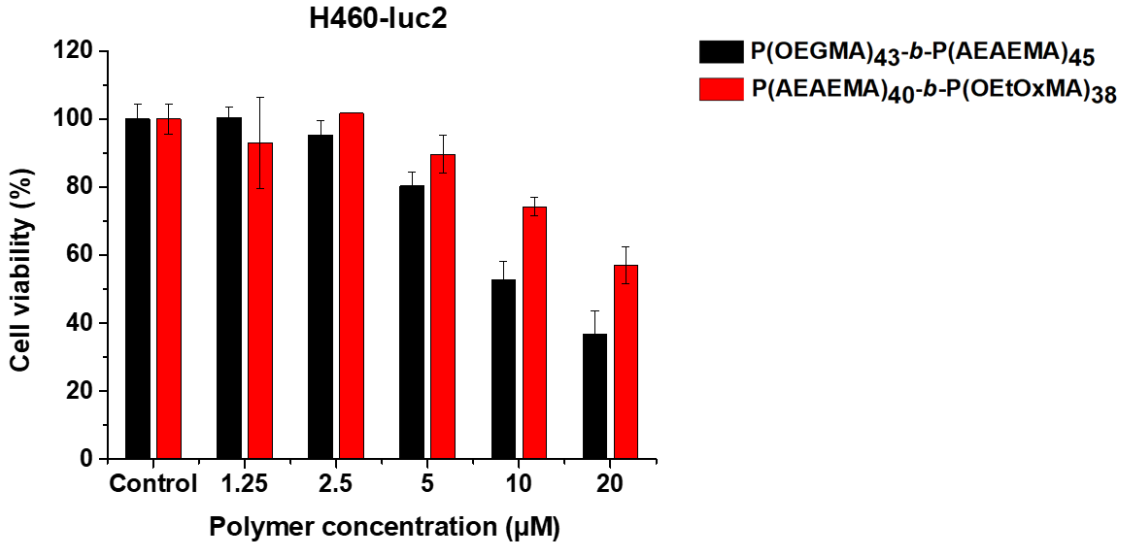

Figure 4.38. (Cont.)

The effect of P(OEGMA) block length on cell viability was also determined with the comparison of $P(OEGMA)_{43}$-*b*-$P(AEAEMA)_{45}$ and $P(OEGMA)_{(5K)}$-*b*-$P(AEAEMA)_{40}$ block copolymers. Based on NIH/3T3 fibroblast cell results it can be said that the increase in P(OEGMA) chain length led to the higher cell viability. P(OEGMA) is known to be biocompatible polymer that brings stealth properties to the structures in which it is conjugated or formulated. Longer P(OEGMA) block might provide better shielding

properties which might be affecting the cell viability in a positive manner in return. However, there were no certain differences between P(OEGMA)$_{43}$-*b*-P(AEAEMA)$_{45}$ and P(OEGMA)$_{(5K)}$-*b*-P(AEAEMA)$_{40}$ on cancer cell lines (MDA-MB-231 and H460) and Raw 264.7 macrophages. On these cell lines, either polymers showed similar effects, or the effect differed with the change in polymer concentration.

The possible effect of architectural difference arising from linear PEG and comb-type PEG, P(OEGMA), was also evaluated. Block copolymers with same molecular weights, different PEG architecture, P(OEGMA)$_{(5K)}$-*b*-P(AEAEMA)$_{40}$ and PEG$_{(5K)}$-*b*-P(AEAEMA)$_{40}$, have showed different effects on cell viability. P(OEGMA)$_{(5K)}$-*b*-P(AEAEMA)$_{40}$ was found to be significantly toxic on all tested cell lines in a dose-dependent manner. In contrast to this PEG$_{(5K)}$-*b*-P(AEAEMA)$_{40}$ did not affect the viability significantly even at high polymer concentrations. However, it should be noted that the solubility of PEG$_{(5K)}$-*b*-P(AEAEMA)$_{40}$ was a bit low and aggregation tendency was observed for this polymer solution, whereas P(OEGMA)$_{(5K)}$-*b*-P(AEAEMA)$_{40}$ appeared crystal-clear in PBS solution. The strong intrachain and interchain hydrogen bonding causing from PEG might be responsible for the reduced solubility whereas this might not be the case for P(OEGMA)$_{(5K)}$-*b*-P(AEAEMA)$_{40}$ consisting of PEG with relatively hydrophobic methacrylate backbone.

Overall, all block copolymer-treated cells showed %50 or better viability even at high polymer concentrations like 5 μM indicating that the block copolymers could be well-tolerated by different cell lines and could be used for bio-applications.

The cytotoxicity of star polymers was also determined (Figure 4.39). P(OEGMA) homoarm star polymer (SP3) was used as control polymer and as expected it did not affect the cell viability. Even at the highest polymer concentration (10 μM), SP3 treated cells showed approximately 100% or higher cell viability. This also showed that the hydrophobic core of the star polymer did not significantly affect the behavior of the star polymers in viability-wise. In contrast to SP3, miktoarm star polymers, SP1 and SP2, were slightly more toxic to MDA-MB-231 and H460. Both miktoarm star polymers showed similar toxicity profile on MDA-MB-231 and viability was found to be 80% or better at the highest polymer concentration. Unlike MDA-MB-231, on H460 slight differences in toxicity was observed between SP1 and SP2. SP2 decreased the cell viability more compared to SP1 and this is attributed to the higher cationic arm density of SP2. It is known that cationic polymers tend to affect the stability of the cell membrane,

interact with proteins and other macromolecules in the cell and eventually create more toxicity. Therefore, the increased toxicity of the SP2 compared to SP1 was expected. This trend was also observed on Raw 264.7 macrophage cell line. On NIH/3T3 cells, both miktoarm star polymers showed very similar toxicity profile. Based on these results, it can be said that SP1 and SP2 exhibited different toxicity profiles depending on the cell line.

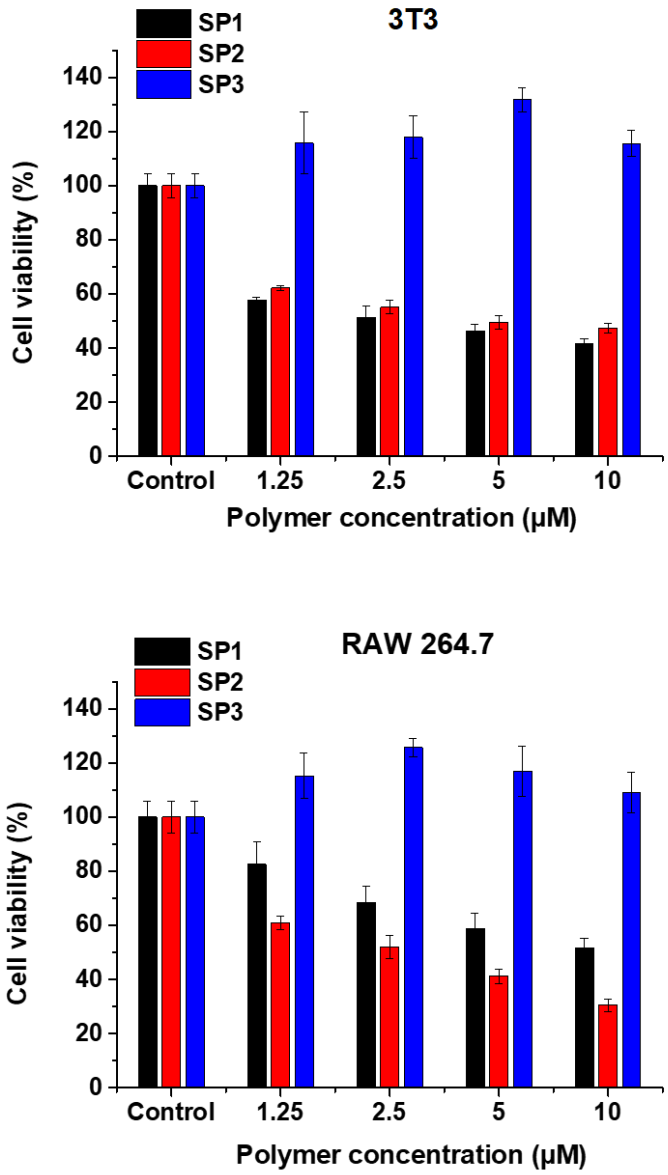

Figure 4.39. The effect of star polymers on cell viability (24 h incubation).

(Cont. on next page)

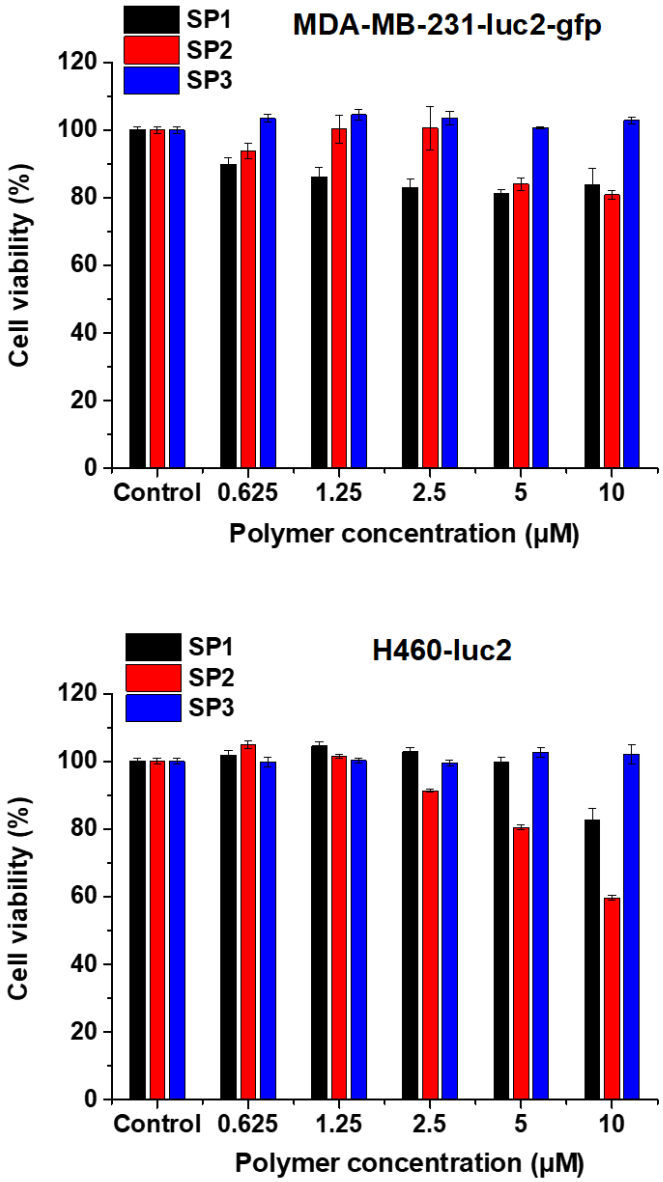

Figure 4.39. (Cont.)

Even though star polymers were very well tolerated by cancer cell lines (MDA-MB-231-luc2-gfp breast cancer and H460 lung cancer), they showed significant toxicity on NIH/3T3 fibroblast cells and Raw 264.7 macrophage cells even at the lowest polymer concentration (1.25 μM). Also compared to linear block copolymers, miktoarm star polymers were generally more toxic at the same polymer concentrations. However, it

should be noted that since the polymer molarity kept same for toxicity assays, in case of star polymers, cells had been treated with higher quantity of polymer (or in other words higher cationic charge) due to high molecular weight of star polymers. This potentially might be responsible for the reduced viability of star polymer-treated cells.

The differences in the toxicity of different miktoarm star polymers also have shown that by incorporating and tuning the P(OEGMA) arm number in the star structure, the toxicity of these miktoarm star polymers could be balanced and kept within the desired range. This is showing that the miktoarm strategy is also effective at decreasing the cytotoxicity of polymer-based carriers.

In conclusion, star polymers showed moderate to low toxicity depending on the cell line and polymer concentration. The toxicity of these systems might be tuned for desired aims and applications.

4.8. Cell Association of Linear Block Copolymers

To examine the effect of stealth polymers, P(OEGMA) and P(OEtOxMA), on cell association, P(OEGMA)$_{43}$-*b*-P(AEAEMA)$_{45}$ and P(AEAEMA)$_{40}$-*b*-P(OEtOxMA)$_{38}$ were labeled with Cy5-NHS ester and cell association of these block copolymers was determined. Cells (MDA-MB-231 and H460) were incubated with the polymers for 30 min or 4 h and cell association profile of the polymers was investigated using flow cytometer instrument (Figure 4.40). As evidenced by MTT Assay, for both cell lines, polymers at the concentration of 2.5 μM did not affect the viability significantly, even so, lower polymer concentrations were used for cell association experiments to be sure that experiments were performed at safe/well-tolerated polymer dosage. Moreover, to avoid the possible interference of death cells, PI (propidium iodide) was added to the samples and the contribution of death cells were eliminated when data were analyzed. The fluorescence intensity of Cy5 labeled polymers was measured by fluorescence spectrometer and mean fluorescence intensity (MFI) values obtained by flow cytometer was normalized based on the fluorescence spectrometer measurements.

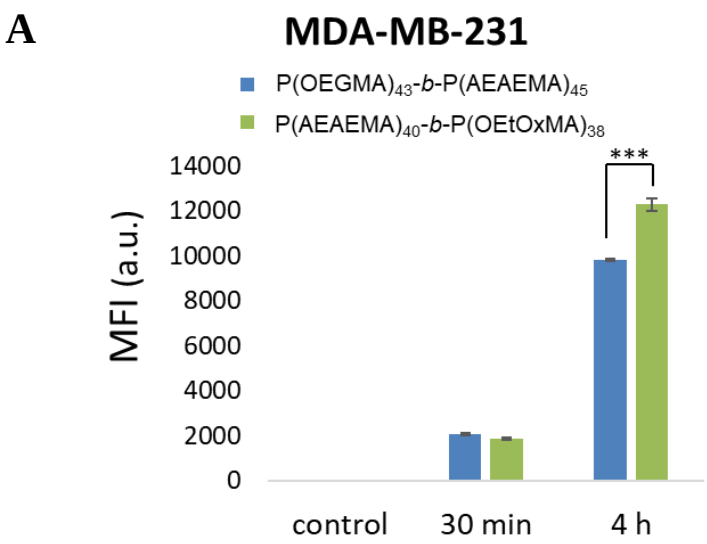

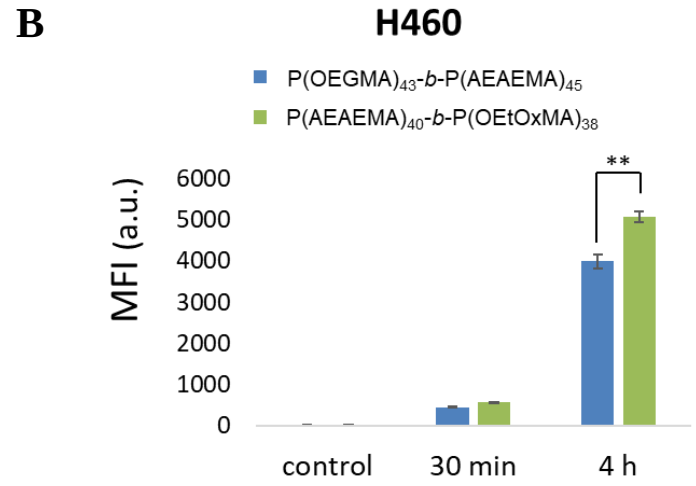

Figure 4.40. Cell association of Cy5-labeled $P(OEGMA)_{43}$-*b*-$P(AEAEMA)_{45}$ and $P(AEAEMA)_{40}$-*b*-$P(OEtOxMA)_{38}$ with H460 (A) and MDA-MB-231 (B). Data was presented as mean ± standard deviation (n=3). Student's t-test was used for statistical analysis: *$p \leq 0.05$; **$p \leq 0.01$; ***$p \leq 0.001$.

As shown in the Figure 4.40, even after 30 min incubation period, a strong MFI signal was observed compared to control cell group indicating that polymers highly and rapidly associated with both cell lines, MDA-MB-231 and H460 cells. Both polymers showed similar association profile at this incubation time. After 4 h incubation, fluorescent intensity increased more suggesting the increased association of the polymers

with cells at the longer incubation period. MFI values of both polymers was found to be approximately 9-fold higher for 4 h incubation time compared to 30 min incubation for H460 cells indicating that association of the polymers might have exhibited a linear trend with respect to time. MFI values obtained for MDA-MB-231 was generally found to be higher than H460. The increase with respect to time is also found to be less (4.7 and 6.5-fold for P(OEGMA) and P(EtOxMA) block copolymer, respectively) which might be suggesting that polymers were able to associate with MDA-MB-231 faster.

For both cell lines and 30 min incubation, both block copolymers displayed approximately same association profile. When incubation time increased to 4 h, P(EtOxMA) block copolymer showed higher MFI for both cell lines. High dispersity of P(OEGMA) block copolymer might be the reason for this profile as cellular uptake/association of P(OEGMA) copolymer might be affected by the variance/difference at polymer chain lengths.

4.9. Cell Uptake of Polyplexes

To investigate the effect of P(OEGMA) and P(OEtOxMA) blocks on siRNA uptake, $P(OEGMA)_{43}$-*b*-$P(AEAEMA)_{45}$-siRNA complexes and $P(AEAEMA)_{40}$-*b*-$P(OEtOxMA)_{38}$-siRNA complexes were prepared at N/P of 50 using Alexa Fluor 488-labeled siRNA. Cellular uptake of linear block copolymer-siRNA complexes was evaluated by flow cytometer (Figure 4.41). Complexes were incubated with cells for 24 h and siRNA dose was kept at 50 nM to mimic the conditions used with the transfection assay. Only siRNA (Alexa Fluor 488-labeled) was used as control and as shown in the figure, naked siRNA was not able to be taken up by cells. Gating was performed based on the plot of only siRNA sample and accordingly Alexa Fluor 488 positive cell percentage of polyplex treated wells was determined and presented in the corresponding graphs.

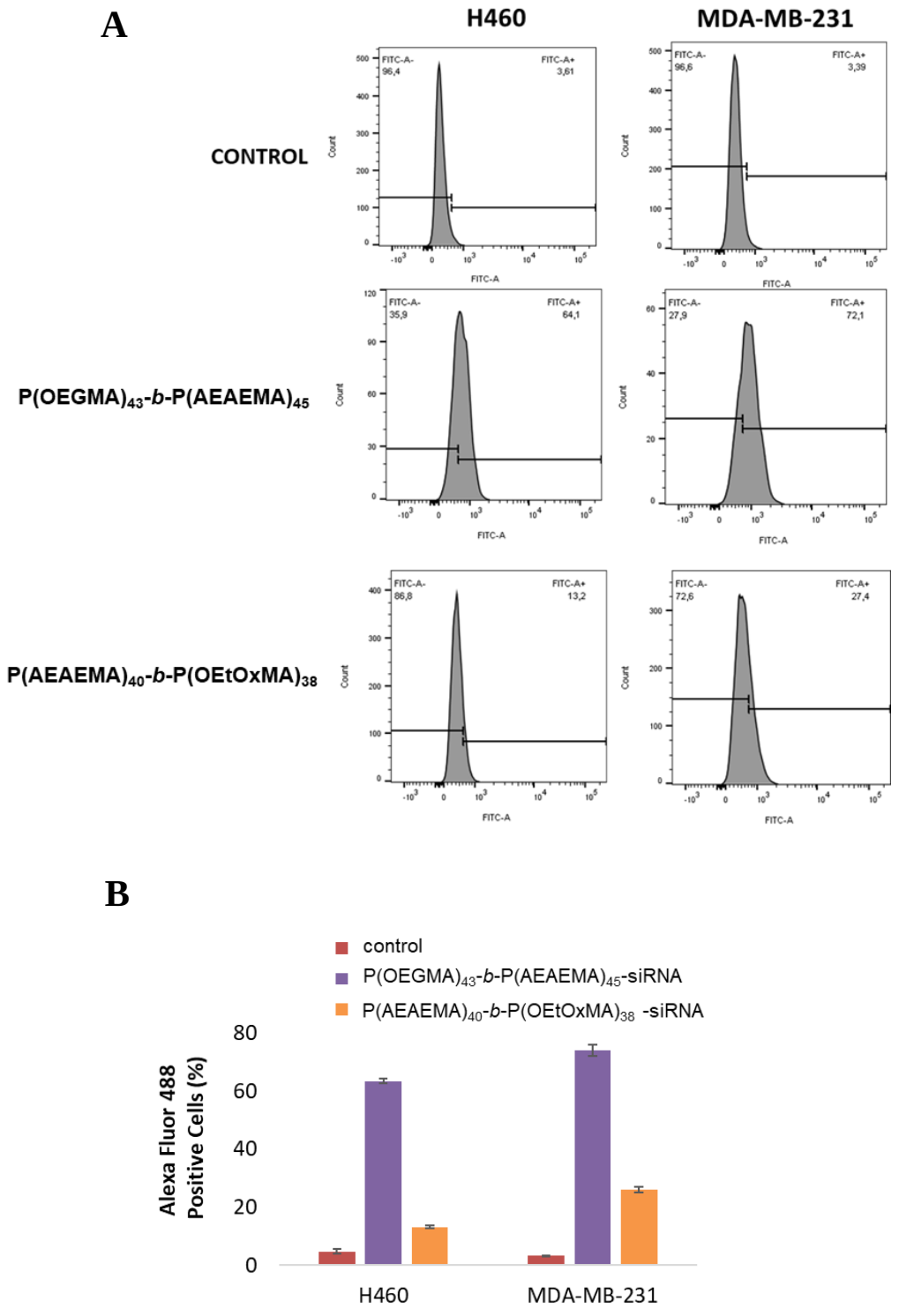

Figure 4.41. Cell uptake of Alexa Fluor 488-siRNA complexed with linear block copolymers, $P(OEGMA)_{43}$-*b*-$P(AEAEMA)_{45}$, $P(AEAEMA)_{40}$-*b*-$P(OEtOxMA)_{38}$, at N/P of 50. Representative flow cytometer plots (A), the percent uptake of siRNA (B) and corresponding MFI values (C).

(Cont. on next page)

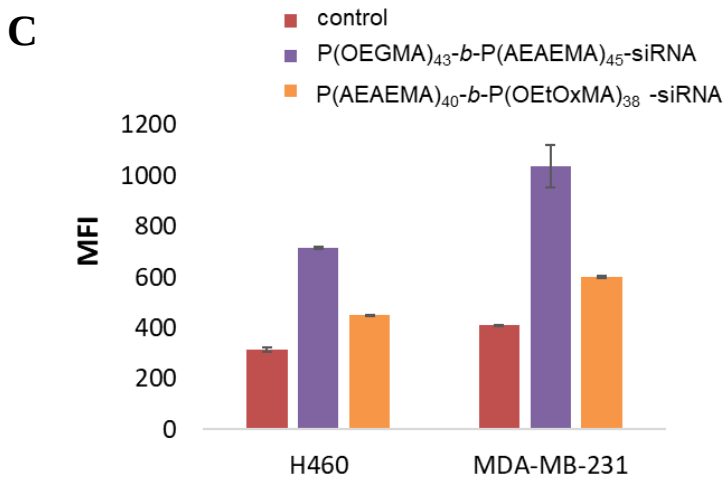

Figure 4.41. (Cont.)

Both polymers were able to carry siRNA into the cells at the chosen conditions. However, a significant difference was observed at siRNA delivery with P(OEGMA) and P(OEtOxMA) block copolymers for both cell lines. When cells were treated with P(OEGMA) block copolymer-siRNA complexes, after 24 h, the average percentage of siRNA positive cells was found to be 63.5 % and 74.1 % for H460 and MDA-MB-231 cell lines, respectively. Compared to this, P(OEtOxMA) block copolymer-siRNA complexes were able to carry the siRNA to 13.1 % and 26.2 % of H460 and MDA-MB-231 cell lines, respectively. This is indicating that under the same conditions (N/P= 50 and siRNA dose=50nM), P(OEGMA) block copolymers could deliver the siRNA into cells in much higher amounts than P(OEtOxMA) block copolymers. Even though, the cellular association of only block copolymers (without siRNA) was found to be similar to each other, the uptake of complexes was found to be significantly different. It is likely that, the uptake/association of only linear block copolymers was driven mostly by the cationic block since the negatively charged cell membrane tend to interact with cationic charges more than the neutral/negative charges due to charge attraction. Whereas the uptake of siRNA complexed with block copolymers might be affected by the directly neutral blocks (P(OEGMA) or P(OEtOxMA)) since the cationic block of the polymers were occupied with siRNA due to complex formation. Because the siRNA was labeled and traced instead of polymers, the interference of the uptake of free (uncomplexed) polymer chains has also been eliminated. Because of the stated reasons, observed siRNA uptake should have been determined as a result of P(OEGMA) or P(EtOxMA) block-cell

membrane interaction. The difference might be arising of the unique interaction of ethylene glycol units with cells which possibly can lead to higher cell uptake. In addition to this, the size, charge and behavior of these block copolymer-siRNA complexes in serum containing media might also be affecting the uptake of the complexes.

Although the chosen cell lines (H460 and MDA-MB-231) have showed approximately similar results in the uptake of siRNA, a slight difference could still be observed. This might be related to the differed doubling time of the cell lines as the cells were seed at the equal amount and incubated for 48 h (24 h incubation after seeding and further 24 h incubation with complexes) although H460 has higher doubling time than MDA-MB-231.

In order to investigate the effect of N/P ratio on cell uptake, siRNA-block copolymer complexes were prepared at N/P of 2 and the cell uptake of the complexes was investigated (Figure 4.42). As can be seen from the flow cytometer plots, in this case very limited siRNA uptake was observed for both block copolymers and both cell lines. This might be attributed to the possible alteration in the physicochemical properties of the complexes at N/P of 2 as proved by DLS measurements. Additionaly, the release and/or degradation profile of siRNA might be significantly differed when low polymer amount was employed for the formulations. It should also be noted that, according to gel electrophoresis results, most of the siRNA was complexed at N/P of 2 however full complexation was seen at N/P of 3.

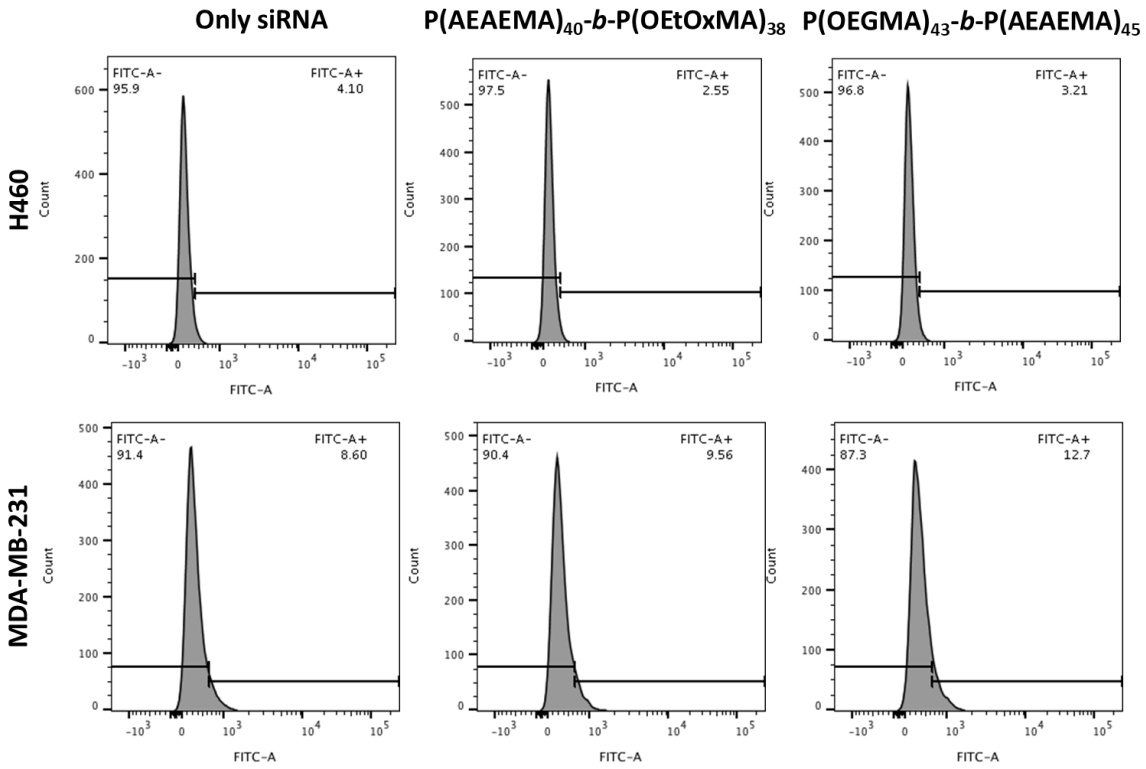

Figure 4.42. Representative flow cytometer plots of Alexa Fluor 488-siRNA complexed with linear block copolymers, $P(OEGMA)_{43}$-*b*-$P(AEAEMA)_{45}$, $P(AEAEMA)_{40}$-*b*-$P(OEtOxMA)_{38}$, at N/P of 2.

siRNA delivery potential of star polymers was also investigated (Figure 4.43 and 4.44). Same N/P ratios (50 and 2) with block copolymers were employed for star polymers as well. Both star polymers could deliver siRNA to cells at N/P of 50 and displayed very similar profile even though their cationic arm density is significantly different from each other. SP1 and SP2 were able to deliver siRNA to the approximately 69% and 65% of H460 cells, respectively. For MDA-MB-231, approximately 54% and 50% of the cells was found at the positive gate when cells were transfected with SP1 and SP2, respectively. At N/P of 2, a significant uptake could not be observed possibly due to aggregation at this N/P ratio as shown by DLS before.

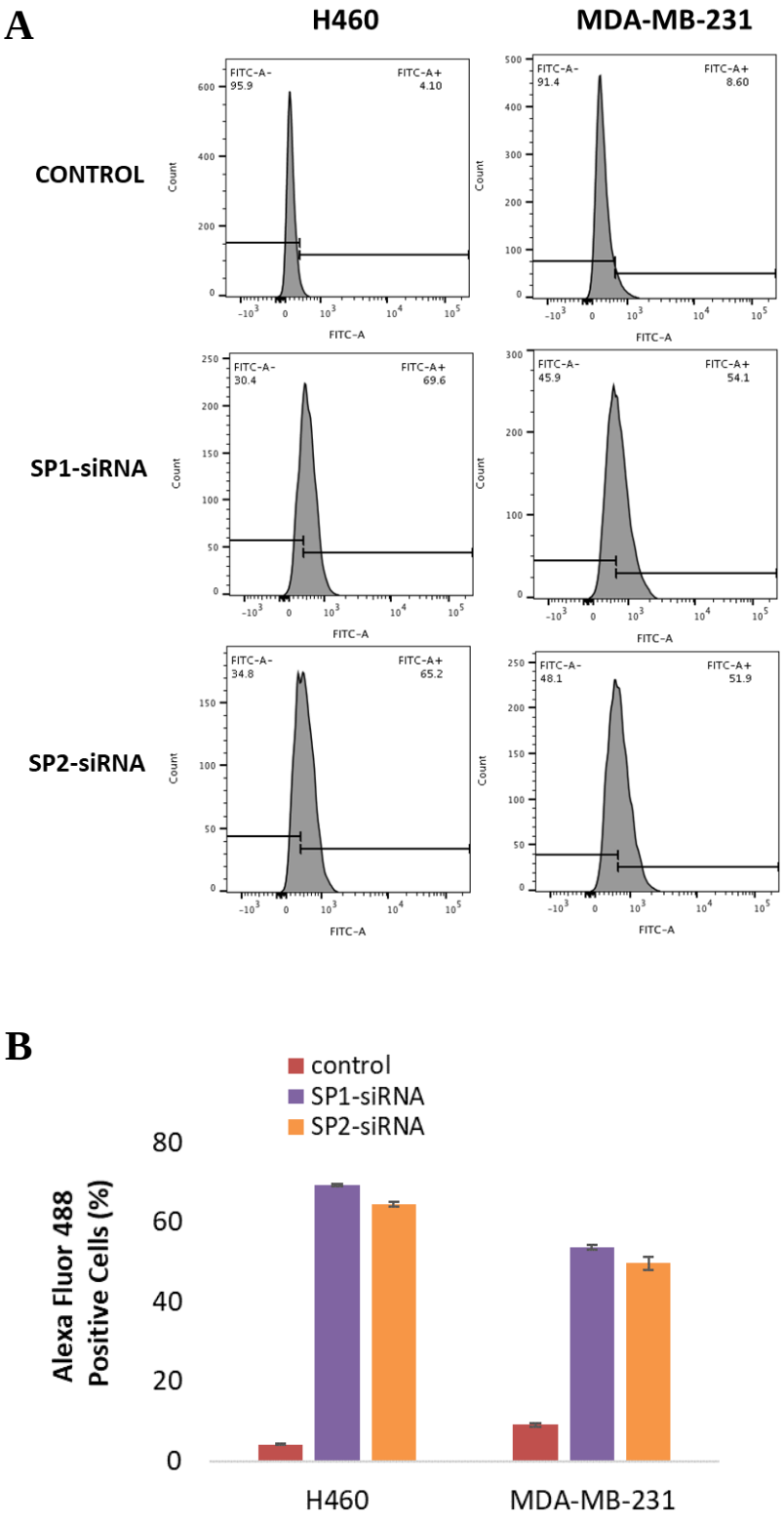

Figure 4.43. Cell uptake of Alexa Fluor 488-siRNA complexed with star polymers, SP1 and SP2, at N/P of 50. Representative flow cytometer plots (A), the percent uptake of siRNA (B) and corresponding MFI values (C).

(Cont. on next page)

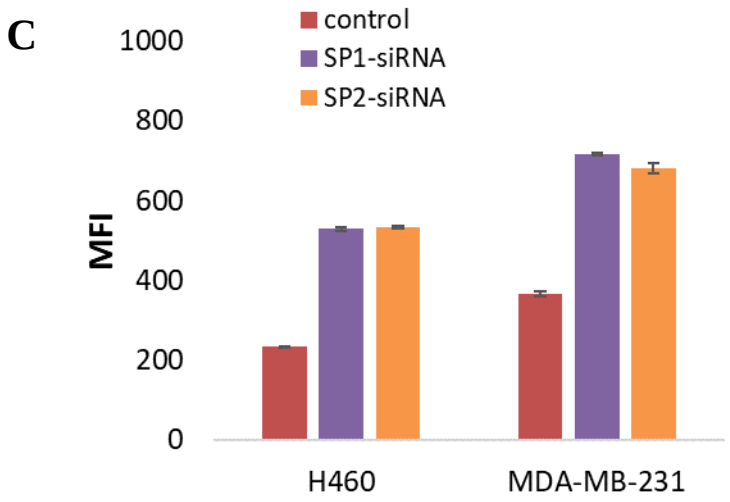

Figure 4.43. (Cont.)

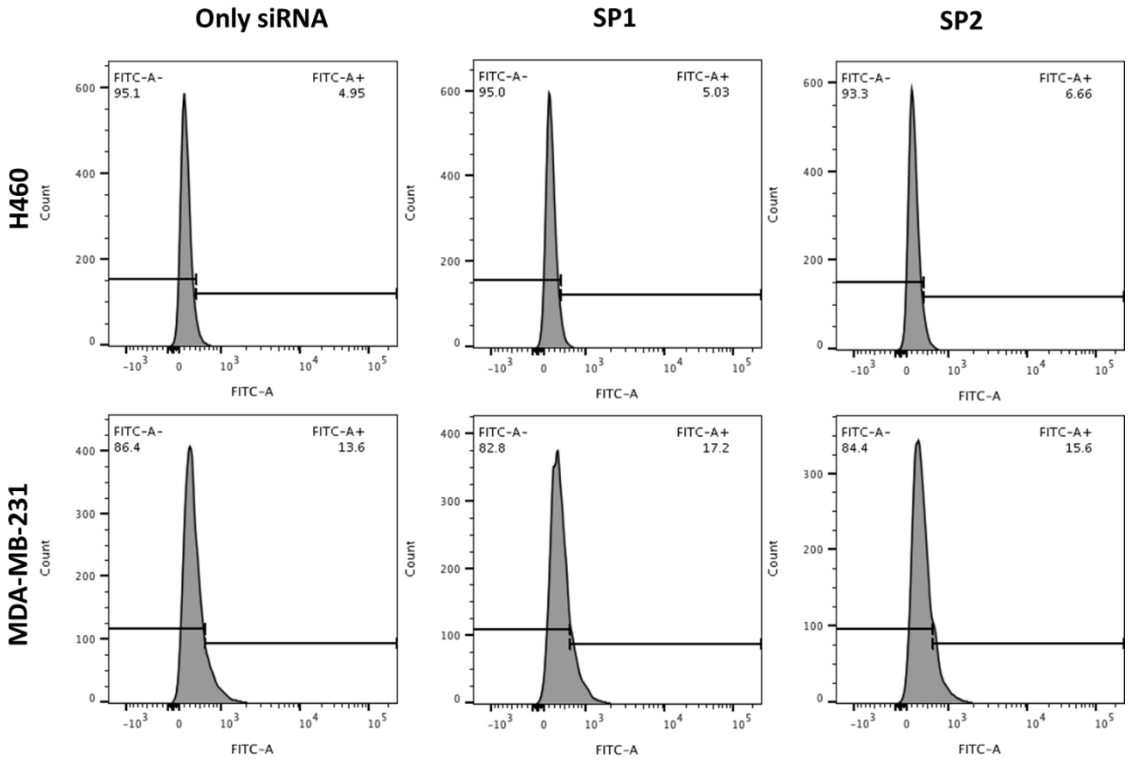

Figure 4.44. Representative flow cytometer plots of Alexa Fluor 488-siRNA complexed with star polymers, SP1 and SP2, at N/P of 2.

4.10. Intracellular Distribution of Polyplexes

In order to determine the intracellular fate of the polyplexes, confocal laser scanning microscopy (CLSM) was employed. According to transfection and siRNA uptake results, P(OEGMA)$_{43}$-*b*-P(AEAEMA)$_{45}$ at N/P of 50 was able to efficiently deliver siRNA to the cells. Therefore, this block copolymer and its POx counterpart, P(AEAEMA)$_{40}$-*b*-P(OEtOxMA)$_{38}$, were chosen for the confocal studies (Figure 4.45). MDA-MB-231 cells were employed for the assay since P(OEGMA)$_{43}$-*b*-P(AEAEMA)$_{45}$ was able to transfect this cell line.

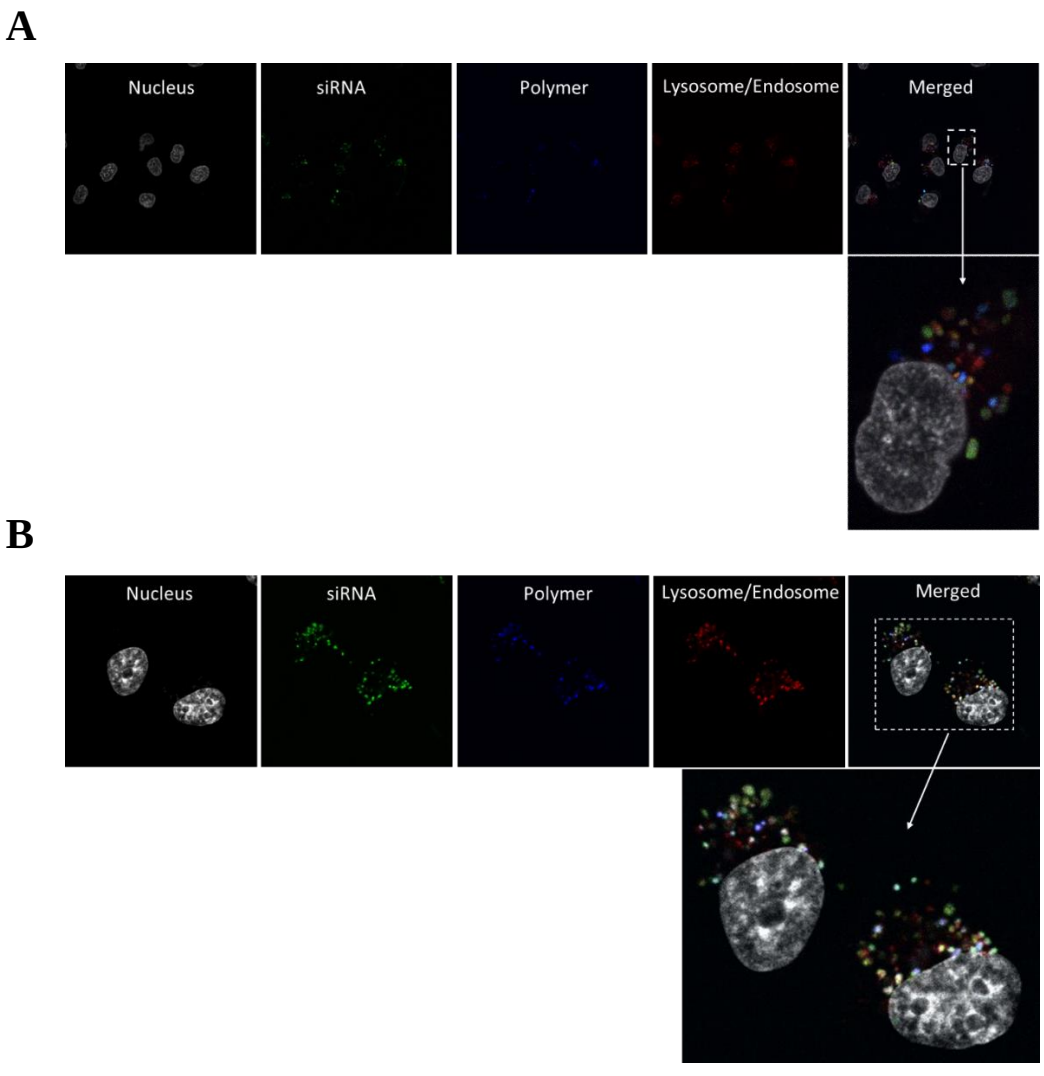

Figure 4.45. Confocal microscopy images of MDA-MB-231 cells incubated with P(OEGMA)$_{43}$-*b*-P(AEAEMA)$_{45}$-siRNA complexes (A) and P(AEAEMA)$_{40}$-*b*-P(OEtOxMA)$_{38}$-siRNA complexes (B) at N/P of 50 for 24 h.

For CLSM, the nucleus of the cells was labeled using Hoeschst 33342. Cy5 labeled polymers and Alexa Fluor 488-labeled siRNA was used for the preparation of block copolymer-siRNA complexes. Moreover, cells were stained with LysoTracker red to visualize the acidic cell organelles (endosomes and lysosomes). The experimental procedure (siRNA dose, N/P ratio, incubation time etc.) used for CLSM studies was kept same with transfection and cell uptake assays to create comparable conditions. The cellular uptake of siRNA and possible localization of the polymer, siRNA, and endosome/lysosome with respect to each other has been investigated.

As can be seen from the images, both siRNA and polymers were taken up by the cells indicating that polymers and siRNA not only associate with the cells but also were able to be internalized by the cells. Obtained CLSM results showed good agreement with the flow cytometer data as both block copolymers (P(OEGMA)$_{43}$-*b*-P(AEAEMA)$_{45}$ and P(AEAEMA)$_{40}$-*b*-P(OEtOxMA)$_{38}$) could deliver siRNA to the cells at N/P ratio of 50. Polymers and siRNA were localized inside the cytoplasm and none of them has been observed in the nucleus indicating that prepared delivery system is highly suitable for the chosen application since RNAi mechanism takes place in the cytoplasm of the cells.

Generally, a homogeneous distribution of polymer and siRNA in the cell cytoplasm could not be observed in the confocal images. It was observed that each cell behaved differently in terms of uptake amount of both carrier and drug. This was attributed to the possible different behavior of cells being in the differed growth state. Also, the uptake and distribution profile of the polymer and siRNA was differed significantly based on the cell confluency of the imaged area indicating that the presence and the density of neighbor cells directly affecting the intracellular profile.

The merged confocal images showed that, siRNA (colored green) could also possibly escape from the endo/lysosomes which is essential for the successful siRNA transfection. Also, it can be stated that some of the internalized siRNA colocalized with the endo/lysosomes (can be seen as orange/yellow color in the merged images). The polymer itself was found to be mostly colocalized with siRNA and/or endo/lysosomes especially in the case of P(AEAEMA)$_{40}$-*b*-P(OEtOxMA)$_{38}$ block copolymer (colored cyan/white in the merged images). However, it is also reported that siRNA might also incorporate with RISC without being released by the carrier. Besides all this, it should be noted that in many cases only very small amount of siRNA (less than 1%) is able to escape from endosomes and trigger the RNAi mechanism, therefore CLSM may not be the

perfect tool for making a final statement about the endosomal escape and transfection efficiency.

As shown by flow cytometer before, the uptake of block copolymer-siRNA complexes at N/P of 2 was very limited. This was also proved by CLSM images (Figure 4.46). As can be seen from the images, mostly only red color (endosomes and lysosomes) could be observed due to absence of siRNA (green) and polymer (blue) in the cell cytosol. The yellow color was also observed indicating that the limited siRNA in the cell cytosol was colocalized with endosomes/lysosomes.

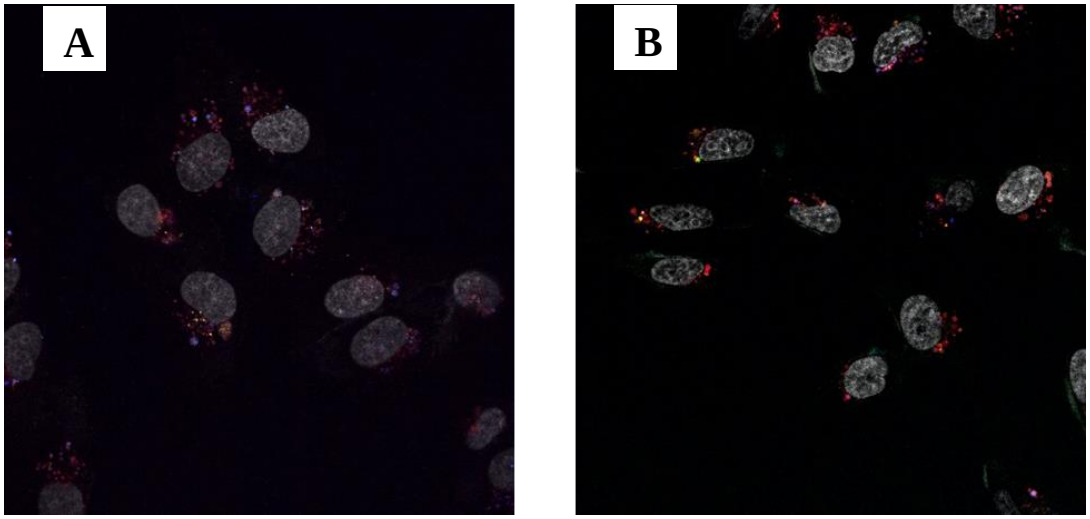

Figure 4.46. Confocal microscopy images (merged) of MDA-MB-231 cells incubated with $P(OEGMA)_{43}$-*b*-$P(AEAEMA)_{45}$-siRNA complexes (A) and $P(AEAEMA)_{40}$-*b*-$P(OEtOxMA)_{38}$-siRNA complexes (B) at N/P of 2 for 24 h.

Intracellular profile of the star polymer-siRNA complexes has also been investigated. Star polymers (SP1 and SP2) were complexed with siRNA at N/P of 2 or 50. Similar to linear block copolymer confocal microscopy studies, Alexa Fluor 488-labeled siRNA, LysoTracker red and Hoeschst 33342 was employed as labeled drug (green), endosome/lysosome stain (red) and nuclear dye (blue), respectively. Non-labeled star polymers were used for the assay. As shown by flow cytometer, both star polymers were able to carry siRNA to the cell cytosol at N/P of 50. This also has been proved by CLSM (Figure 4.47 and 4.48). As seen in the figures, siRNA molecules were found to be

in the cell cytoplasm when cells (MDA-MB-231) were transfected with star polymer-siRNA complexes prepared at N/P of 50. However, it has been observed that large amount of siRNA molecules (colored green) heavily colocalized with lysosomes/endosomes (colored red). Entrapped drug inside the acidic vesicles were appeared mostly as yellow in merged images indicating the equal contribution of drug and vesicles. In addition, many red colors were also observed indicating the presence of vesicles that are not containing drug. Still, some green dots could also be seen in the merged images suggesting the possible presence of free siRNA.

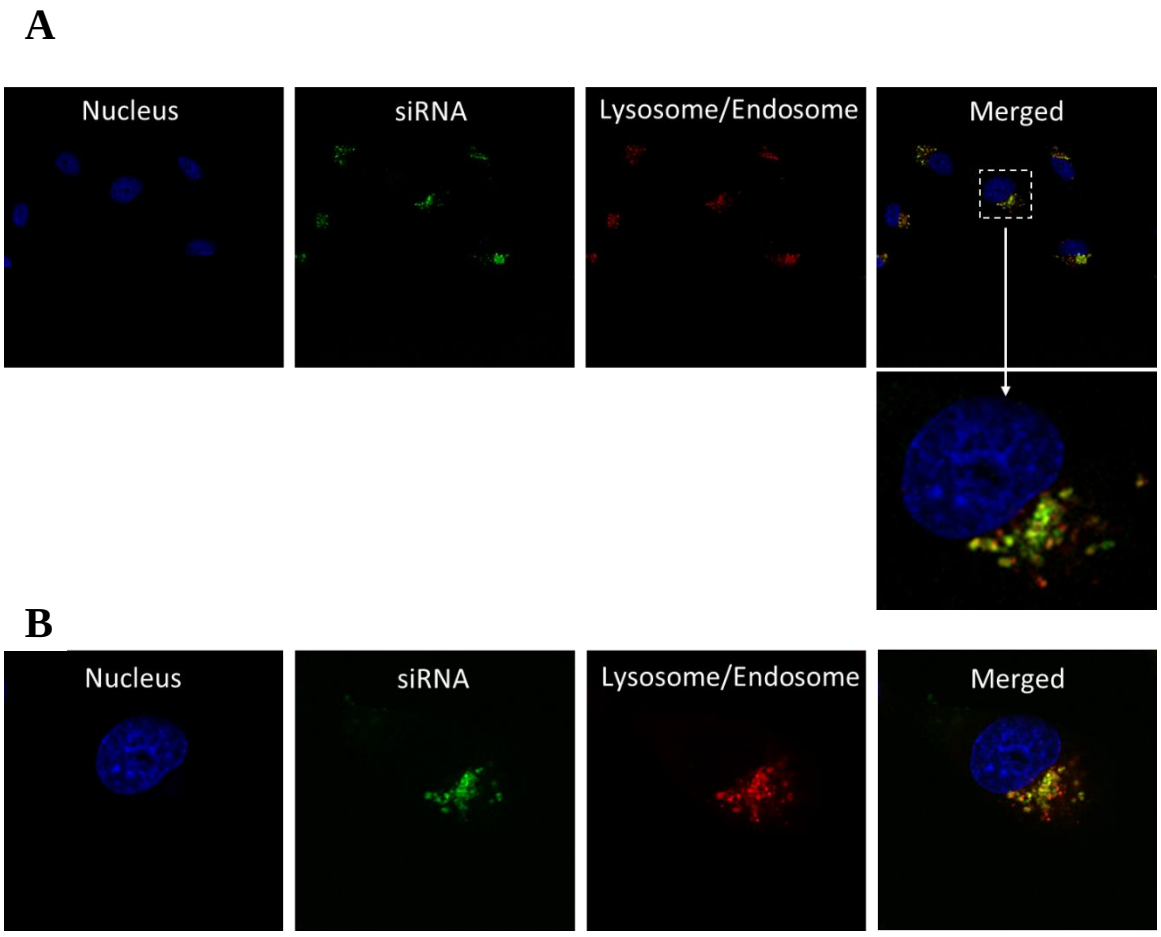

Figure 4.47. Confocal microscopy images of MDA-MB-231 cells incubated with SP1-siRNA complexes at N/P of 50 for 24 h. Images showing the multiple cells (A) and single cell (B).

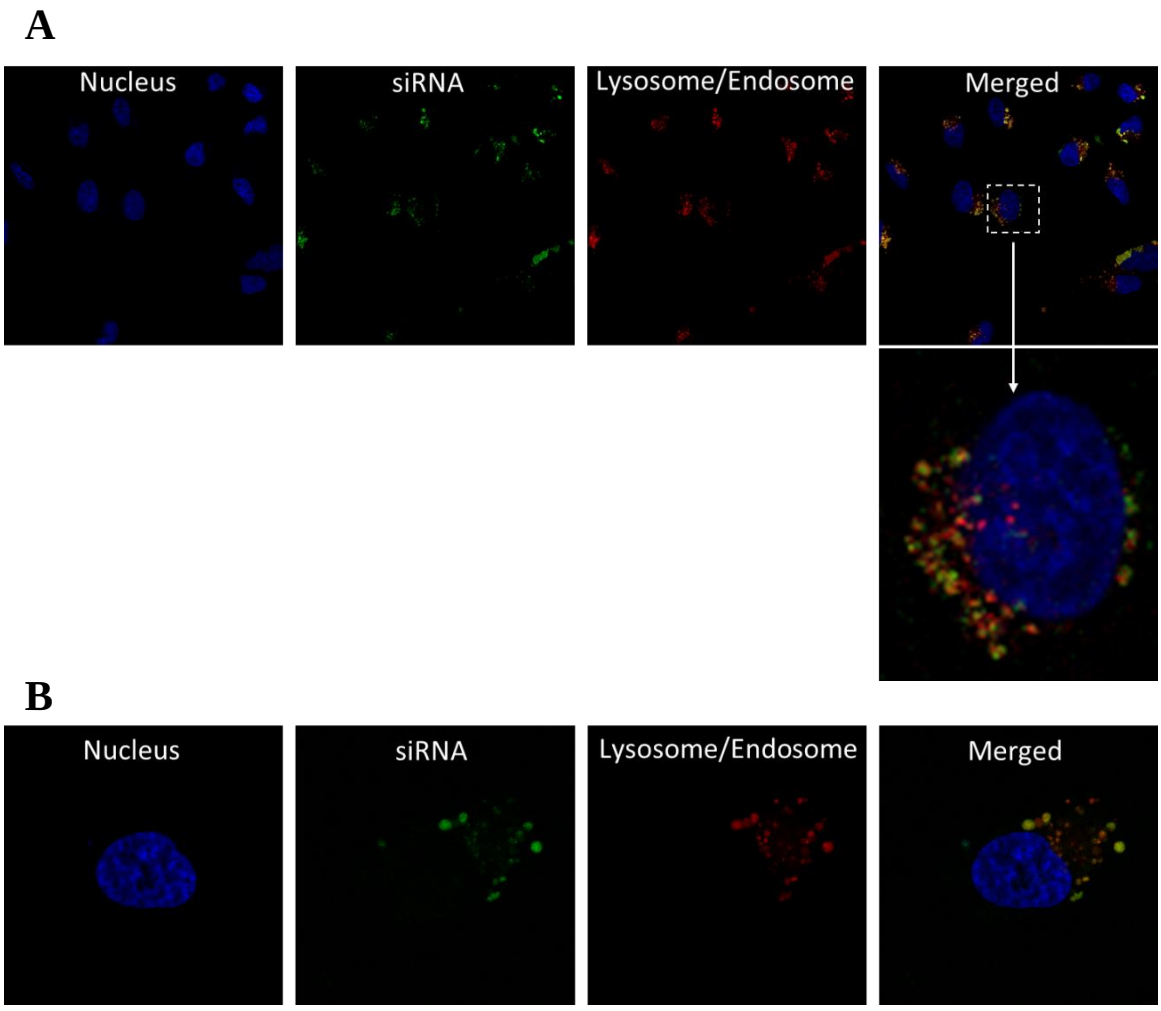

Figure 4.48. Confocal microscopy images of MDA-MB-231 cells incubated with SP1-siRNA complexes at N/P of 50 for 24 h. Images showing the multiple cells (A) and single cell (B).

Although it has known that star polymers were not successful to deliver siRNA at N/P of 2, this was also further proved by CLSM. This was expected since star polymer-siRNA complexes at N/P of 2 showed aggregation tendency as shown by DLS. Additionally, flow cytometer results also showed that the uptake of siRNA was very significantly low at N/P of 2. Consequently, as can be seen in CLSM images, siRNA (colored green) was barely observable in the merged images (Figure 4. 49). siRNA uptake was highly limited in this case and all siRNAs taken up by the cells colocalized with endosomes/lysosomes as seen orange/yellow in merged images.

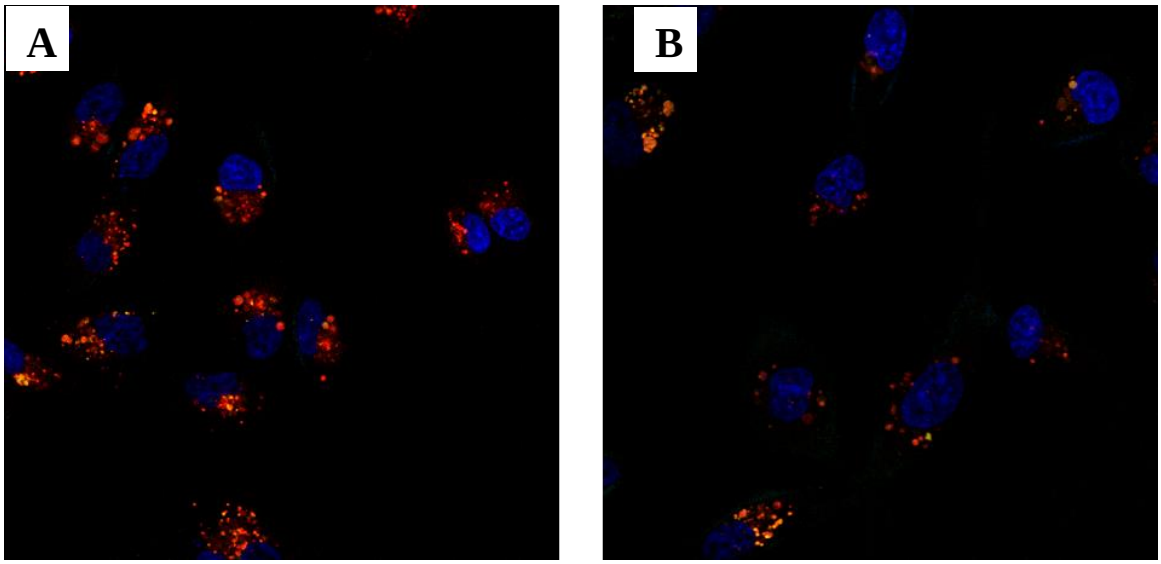

Figure 4.49. Confocal microscopy images (merged) of MDA-MB-231 cells incubated with SP1-siRNA complexes (A) and SP2-siRNA complexes (B) at N/P of 2 for 24 h.

4.11. Transfection Efficiency and Toxicity of Polyplexes

siRNA transfection ability of the polymers was firstly evaluated on stably luciferase expressing MDA-MB-231-luc2-gfp cell line. An siRNA sequence targeting the firefly luciferase (Luc-siRNA) and another siRNA sequence not targeting any gene (Nt-siRNA) was used as positive and negative control siRNAs, respectively. A lipid-based commercial siRNA transfection reagent Lipofectamine RNAimax (Lipo) was used as a control as well. The luciferase expression levels of the cells were determined by measuring the luminescence with Promega Luciferase Assay Kit. The luciferase expression of non-treated cells was accepted as 100% and sample-treated wells were calculated accordingly.

Before determining the transfection ability of the polymers, Lipo-siRNA complexes were tested (Figure 4.50). For this, complexes were prepared at siRNA doses of 20 and 50 nM based on manufacturer's recommendations. Cells were treated with the complexes for 24 h and the luminescence intensity was determined 48 h post-transfection. The viability of the cells was determined by MTT assay in parallel to transfection experiments. As can be seen in the figure, lipo-Luc-siRNA complexes showed potent

gene silencing efficiency. Complexes were able to decrease the luciferase expression approximately to 20% at both siRNA doses without showing any toxicity. In contrast, lipo-Nt-siRNA complexes did not decrease the gene expression. This showed that the employed Luc-siRNA is able to target the luciferase mRNA successfully in a specific manner.

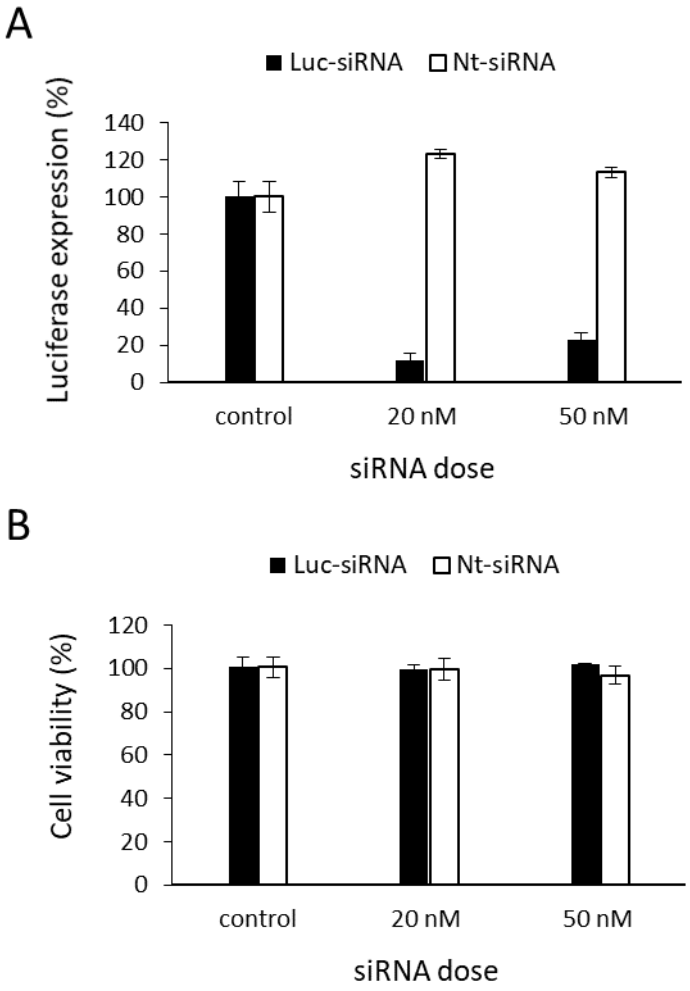

Figure 4.50. The effect of Lipo-siRNA complexes on luciferase expression (A) and viability (B) of MDA-MB-231-luc2-gfp cells.

Using the same method, the transfection efficiency of various linear block copolymers and star polymers were also determined. First, siRNA dose was fixed to 100 nM (frequently used siRNA dose in the literature) and the transfection efficiency of $P(OEGMA)_{43}$-*b*-$P(AEAEMA)_{45}$ and $PEG_{(5K)}$-*b*-$P(AEAEMA)_{40}$ was evaluated in the first place (Figure 4.51). Since higher P(OEGMA) block length is known to provide higher

stability and protein-repellent properties to the nanoparticles, this polymer was chosen among other P(OEGMA) block copolymers with same cationic block lengths. Although based on DLS results, $PEG_{(5K)}$-*b*-$P(AEAEMA)_{40}$ has showed aggregation tendency at higher N/P ratios, this polymer was also tested to better reveal the differences between comb-type and linear PEG block copolymers.

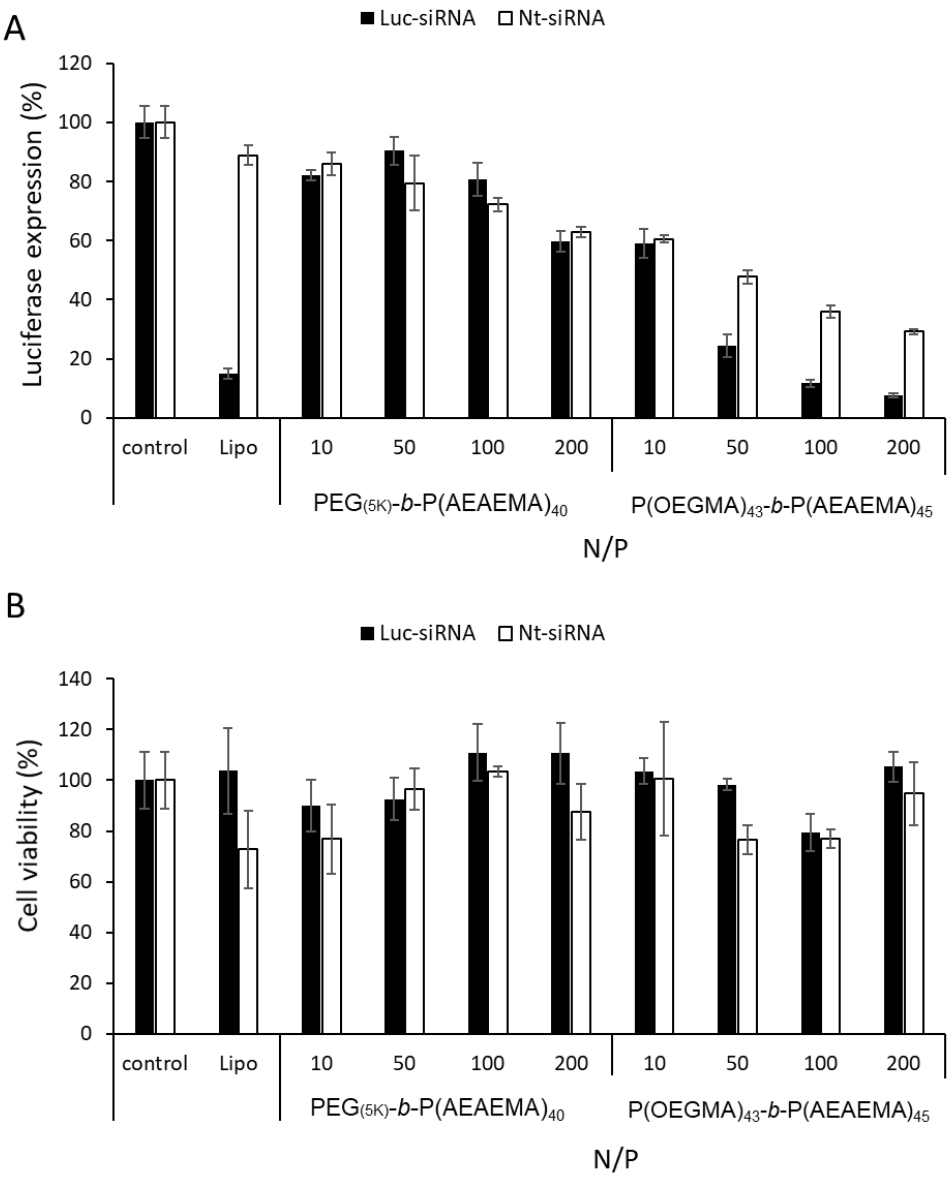

Figure 4.51. The effect of $PEG_{(5K)}$-*b*-$P(AEAEMA)_{40}$- and $P(OEGMA)_{43}$-*b*-$P(AEAEMA)_{45}$-siRNA complexes on luciferase expression (A) and viability (B) of MDA-MB-231-luc2-gfp cells (siRNA dose= 100 nM).

As can be seen in Figure 4.51, $PEG_{(5K)}$-*b*-$P(AEAEMA)_{40}$-siRNA complexes at varying N/P ratios have showed very same profile regardless of used siRNA sequence indicating that this polymer was not able to show any transfection efficiency. In contrast, $P(OEGMA)_{43}$-*b*-$P(AEAEMA)_{45}$-Luc-siRNA and $P(OEGMA)_{43}$-*b*-$P(AEAEMA)_{45}$-Nt-siRNA complexes displayed significantly different luciferase expression profile at all N/P ratios higher than 10. This result showed that $P(OEGMA)_{43}$-*b*-$P(AEAEMA)_{45}$ was able to reduce the luciferase expression level in an N/P dependent manner without showing significant toxicity. Although $P(OEGMA)_{43}$-*b*-$P(AEAEMA)_{45}$-Luc-siRNA complexes decreased the luciferase expression to significantly lower levels compared to $P(OEGMA)_{43}$-*b*-$P(AEAEMA)_{45}$-Nt-siRNA complexes, non-specific silencing was observed at the tested siRNA dose. Therefore, siRNA dose was reduced to 50, 25 or 10 nM and complexes of $P(OEGMA)_{43}$-*b*-$P(AEAEMA)_{45}$ at varying N/P ratios have been prepared and tested (Figure 4.52). Generally, N/P dependent decrease in luciferase expression was observed. $P(OEGMA)_{43}$-*b*-$P(AEAEMA)_{45}$-Luc-siRNA complexes was found to be effective even at the lowest siRNA dose (10 nM). At N/P of 400, luciferase expression was found to be significantly low (22%) however, cell viability was also found to be decreasing at this N/P ratio (< %80). When siRNA dose was increased to 25 nM, complexes could be able to reduce the protein expression to 46% (at N/P of 100) without compromising from safety (cell viability > 80%). At siRNA dose of 50 and N/P of 50, luciferase expression and cell viability were found to be 28% and 86%, respectively. At this siRNA dose and N/P ratio, there was neither non-specific silencing effects nor significant cytotoxicity. In other words, the formulation was able to show potent gene silencing effect without showing detrimental effects on cell viability. Based on *t*-test, the difference between Luc-siRNA and Nt-siRNA complexes of $P(OEGMA)_{43}$-*b*-$P(AEAEMA)_{45}$ was statistically highly significant ($p \leq 0.001$) (three independent experiments -each in triplicate- was performed and average values ± standard deviation of the results was presented in the figure). Therefore, these conditions were determined to be optimal and used also in further experiments (cellular uptake/distribution, release, stability assays etc.).

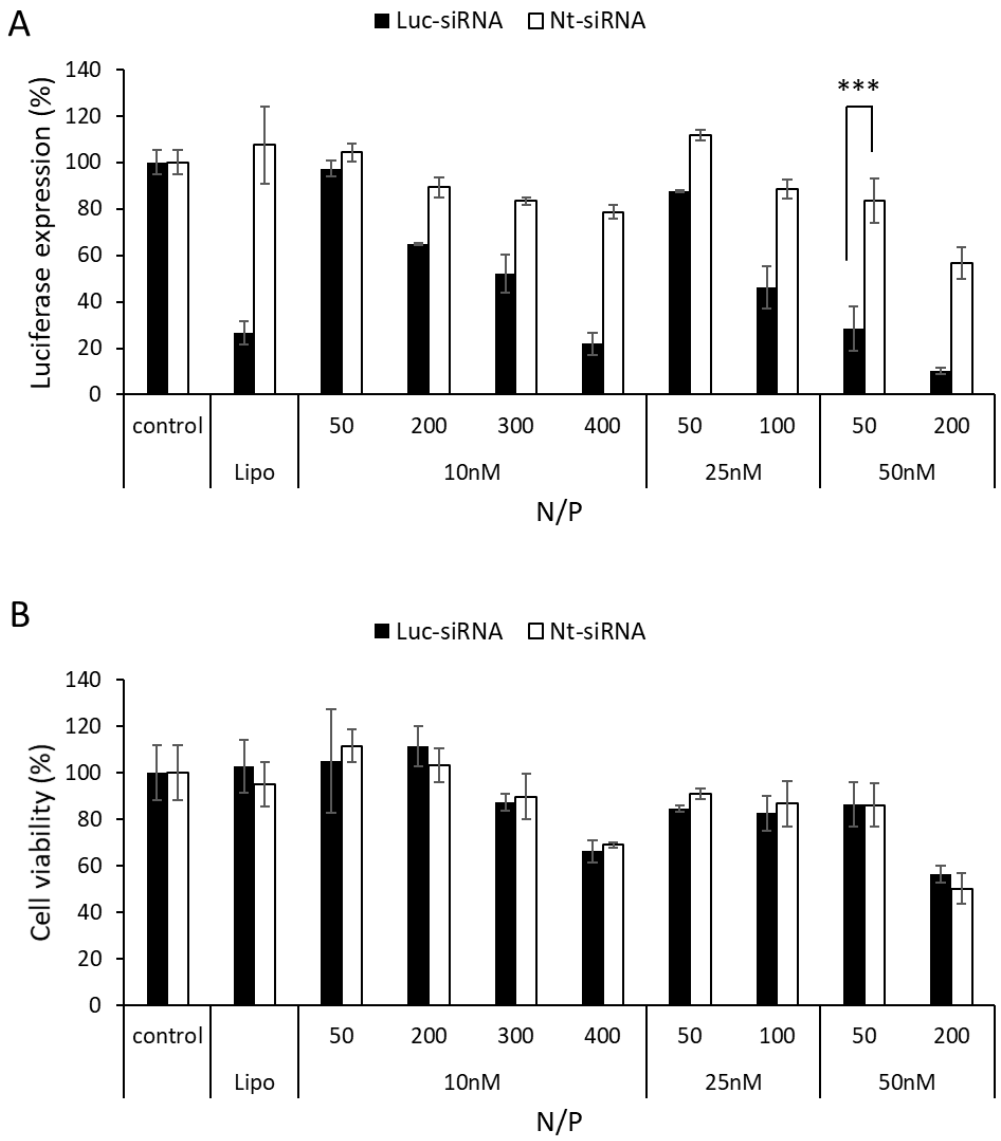

Figure 4.52. The effect of P(OEGMA)$_{43}$-*b*-P(AEAEMA)$_{45}$-siRNA complexes on luciferase expression (A) and viability (B) of MDA-MB-231-luc2-gfp cells (siRNA dose= 10, 25 or 50 nM). Data was presented as mean ± standard deviation (n=3). Student's t-test was used for statistical analysis: *$p \leq 0.05$; **$p \leq 0.01$; ***$p \leq 0.001$.

To determine the effect of cationic block length on siRNA delivery, P(OEGMA)$_{43}$-*b*-P(AEAEMA)$_{60}$-siRNA complexes were prepared at two different N/P ratios and siRNA doses and tested under the same experimental conditions. Although there was statistically significant difference between positive and negative control siRNA complexes of P(OEGMA)$_{43}$-*b*-P(AEAEMA)$_{60}$, the transfection efficiency was lower

compared to P(OEGMA)$_{43}$-*b*-P(AEAEMA)$_{45}$-siRNA complexes indicating that the cationic block length significantly affects the siRNA transfection efficiency of the linear block copolymers possibly due to differed siRNA complexation and release profile.

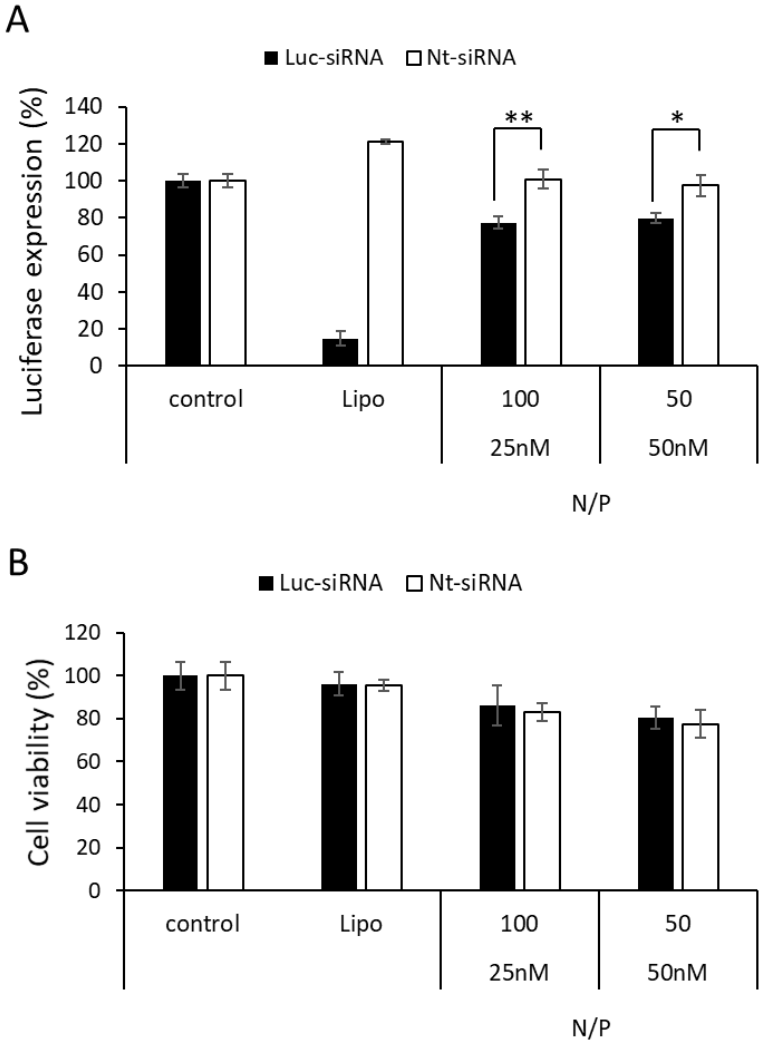

Figure 4.53. The effect of P(OEGMA)$_{43}$-*b*-P(AEAEMA)$_{60}$-siRNA complexes on luciferase expression (A) and viability (B) of MDA-MB-231-luc2-gfp cells (siRNA dose= 25 or 50 nM). Data was presented as mean ± standard deviation (n=3). Student's t-test was used for statistical analysis: *$p \leq 0.05$; **$p \leq 0.01$; ***$p \leq 0.001$.

It is known that transfection reagents usually exhibit cell line-dependent performance. To further evaluate the efficacy of the polymer-siRNA complexes, another cell line, stably luciferase expressing H460-luc2 lung cancer, was employed. The luciferase silencing efficiency of the polymers was evaluated using the same procedure and experimental conditions utilized in MDA-MB-231-luc2-gfp transfection experiments. Prior to polymers, the commercial transfection reagent, Lipofectamine RNAimax (Lipo), was tested again on this cell line. For this aim, lipofectamine-siRNA complexes having varied doses of siRNA (10, 50 and 100 nM) were prepared and incubated with cells for 24 h. Afterwards, luciferase expression and viability was checked using the microplate-reader (Figure 4.54).

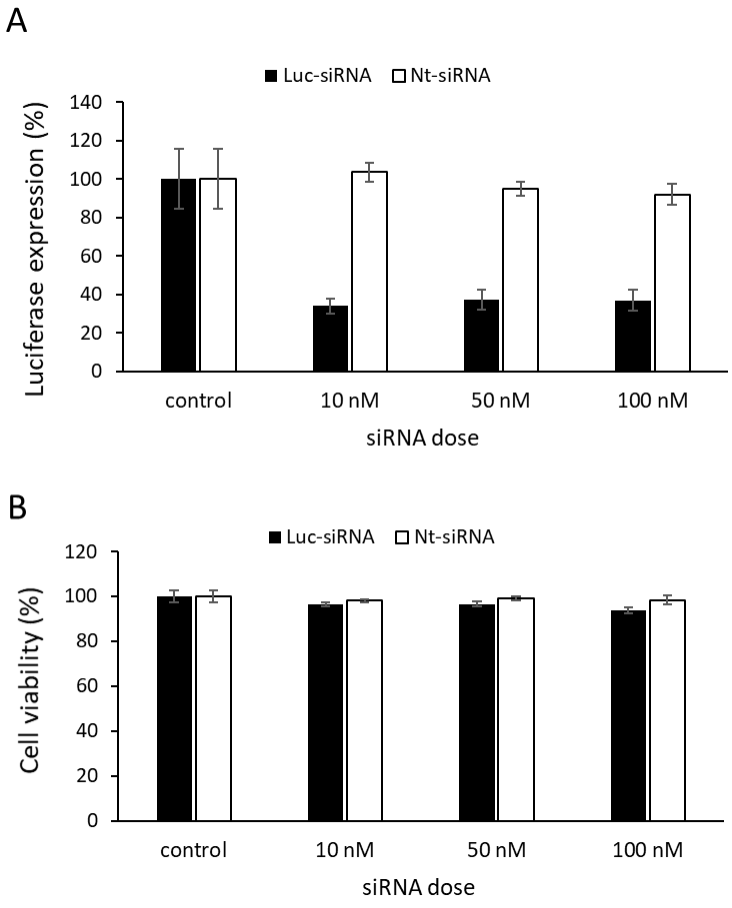

Figure 4.54. The effect of Lipo-siRNA complexes on luciferase expression (A) and viability (B) of H460-luc2.

As seen in the Figure 4.54, lipofectamine-luc-siRNA complexes were able to decrease the luciferase expression to approximately 30% without showing any significant toxicity. The increase in siRNA concentration did not lead to further decrease in gene expression indicating that the maximum silencing efficiency that can be obtained without toxicity has been reached for lipofectamine-siRNA complexes.

Next, the effect of P(OEGMA)$_{43}$-*b*-P(AEAEMA)$_{45}$ block copolymer-siRNA complexes on gene expression and cell viability was investigated using different siRNA doses (10, 25 and 50 nM) and N/P ratios (50, 100 and 200) (Figure 4.55). Gene expression was decreased to approximately 50% when 50 nM siRNA was used (at N/P of 50). It should be noted that this was the optimal formulation based on Mda-md-231-luc2-gfp luciferase assays. At this N/P ratio and siRNA dose, even though there was no significant cytotoxic effect, the gene expression level was found to be same for both positive and negative control siRNA complexes indicating that the reduction in gene expression is non-specific and could not be the direct result of RNAi mechanism. To avoid non-specific silencing, siRNA dose was reduced to 25 nM and two different N/P ratio, 100 and 200, has been tested. However, at these conditions either cell viability significantly decreased (at N/P of 200) or luciferase expression remained approximately at the same levels (at N/P of 100).

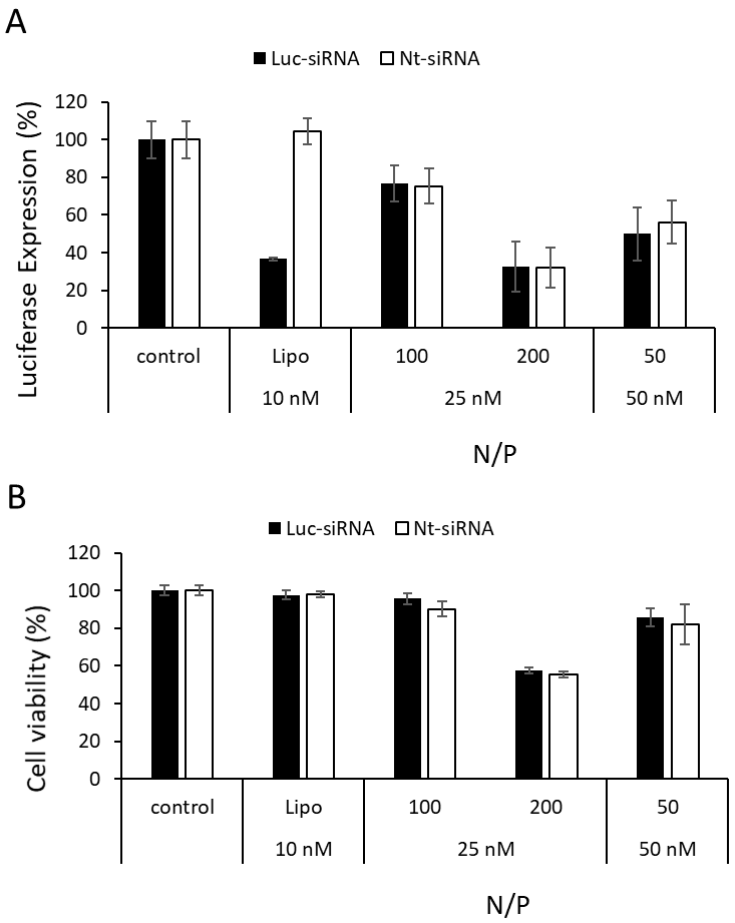

Figure 4.55. The effect of P(OEGMA)$_{43}$-*b*-P(AEAEMA)$_{45}$-siRNA complexes on luciferase expression (A) and viability (B) of H460-luc2 cells (siRNA dose= 10, 25 or 50 nM).

To see the effect of oxazoline polymer block, P(AEAEMA)$_{40}$-*b*-P(OEtOxMA)$_{38}$-siRNA complexes were prepared at N/P of 50 and 100 and the transfection efficiency of this block copolymer was also determined (Figure 4.56). siRNA concentration was kept at 50 nM to avoid possible non-specific silencing effects. As shown by AlamarBlue assay, formulations did not show any cytotoxicity effect on H460 at the prepared concentrations. Even though there is no detectable toxicity, complexes prepared with negative control siRNA was also decreased the gene expression to a certain level. Polymer-Luc-siRNA complexes were able to decrease the luciferase expression to 61% and 42% at N/P of 50 and 100, respectively without showing any toxicity.

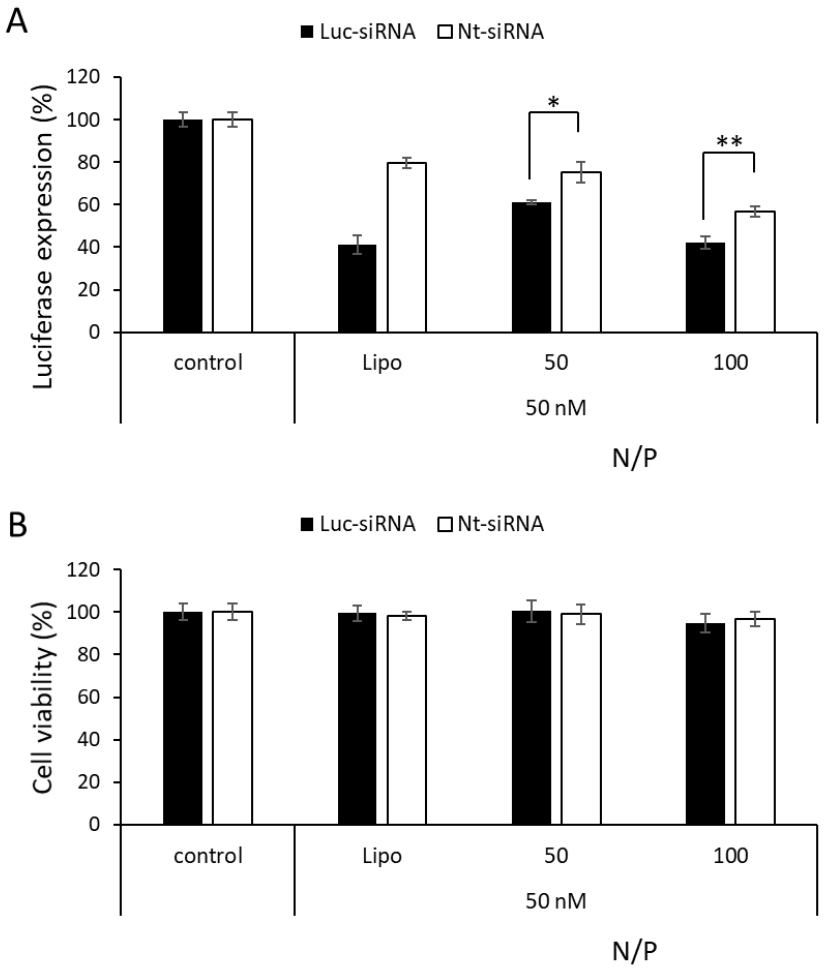

Figure 4.56. The effect of P(AEAEMA)$_{40}$-*b*-P(OEtOxMA)$_{38}$-siRNA complexes on luciferase expression (A) and viability (B) of H460-luc2 cells (siRNA dose= 50 nM). Data was presented as mean ± standard deviation (n=3). Student's t-test was used for statistical analysis: *$p \leq 0.05$; **$p \leq 0.01$; ***$p \leq 0.001$.

Transfection efficiency of P(OEGMA)/P(AEAEMA) miktoarm star polymers (SP1 and SP2) was also determined (Figure 4.57 and 4.58). Two different siRNA concentration (50 and 100 nM) and two different N/P ratio (5 and 50; or 50 and 100) was used to investigate the effect of siRNA dose and polymer amount. Both miktoarm stars did not significantly affect the luciferase expression at siRNA concentration of 50 nM except SP1-siRNA complexes at N/P of 50. SP1 was able to decrease the luciferase expression to 74%. None of the prepared formulations showed toxicity on H460 cell line therefore siRNA concentration was increased to 100 nM (Figure 4.58). When N/P was also increased to 100, some cytotoxic effects began to be observed. At the same time,

luciferase expression was also decreased due to observed toxicity. However, the luciferase expression levels of SP2-Luc-siRNA and SP2-Nt-siRNA complexes was found to be statistically significantly different from each other (at N/P of 100, siRNA dose=100 nM). Overall, star polymers were able to show moderate transfection efficiency at certain N/P values and siRNA doses.

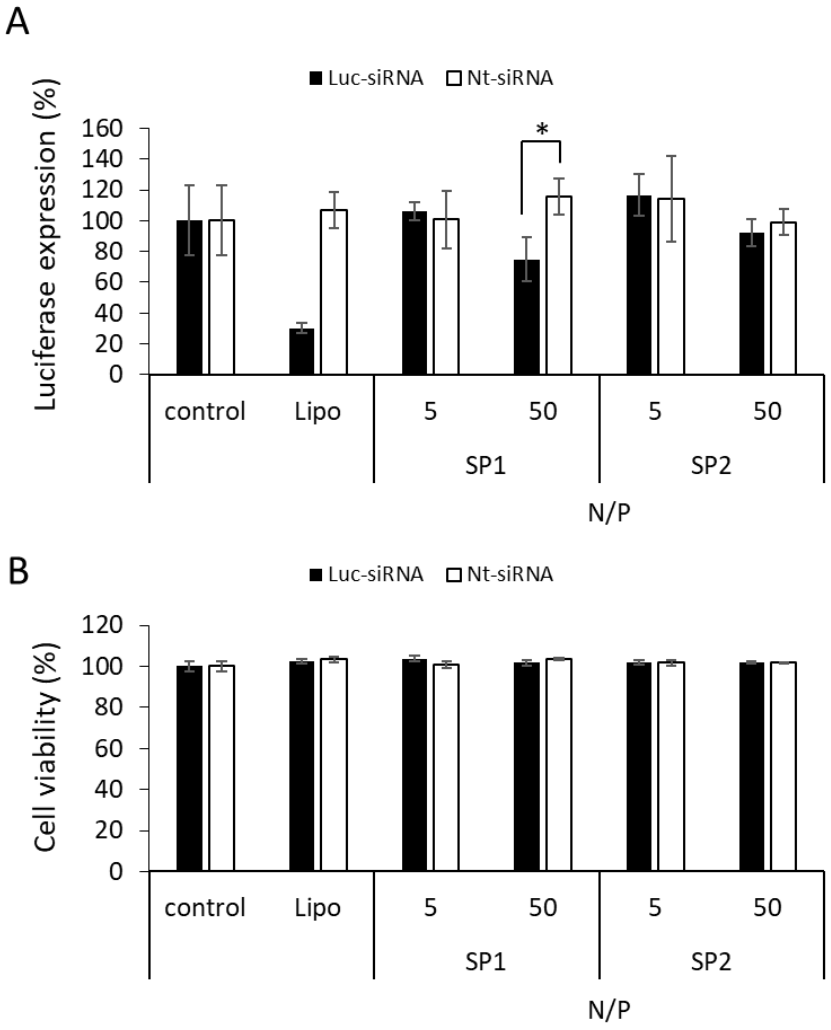

Figure 4.57. The effect of star polymer-siRNA complexes on luciferase expression (A) and viability (B) of H460-luc2 cells (siRNA dose= 50 nM). Data was presented as mean ± standard deviation (n=3). Student's t-test was used for statistical analysis: *$p \leq 0.05$; **$p \leq 0.01$; ***$p \leq 0.001$.

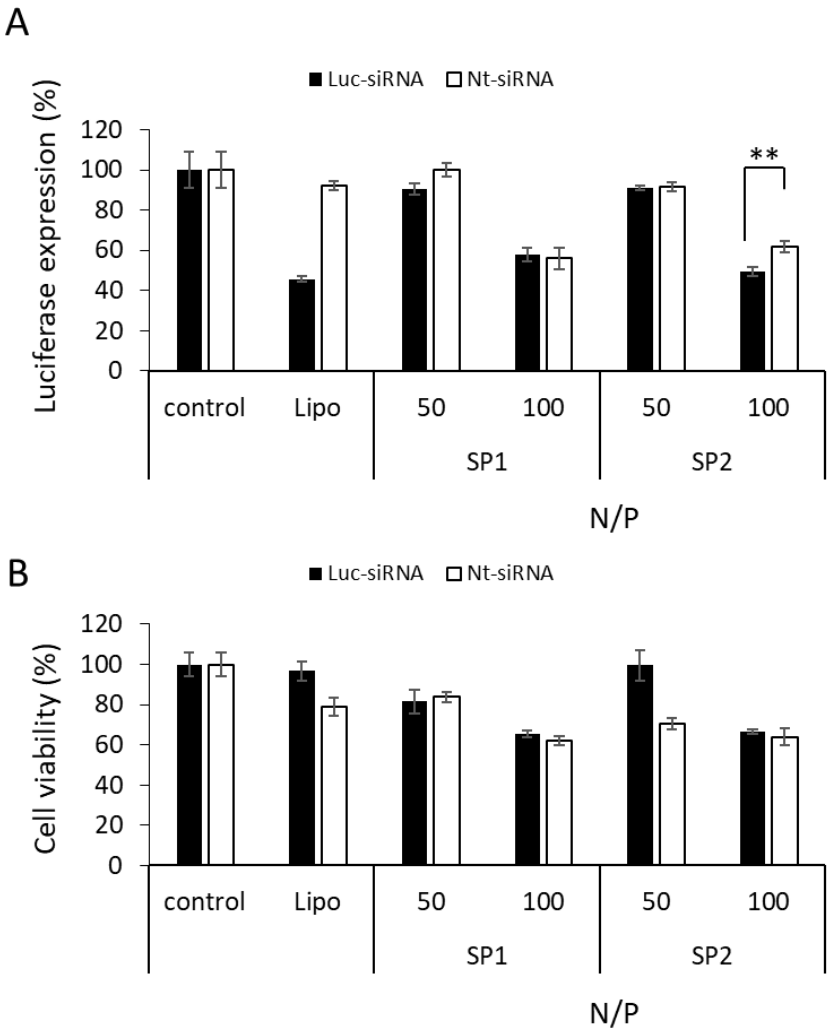

Figure 4.58. The effect of star polymer-siRNA complexes on luciferase expression (A) and viability (B) of H460-luc2 cells (siRNA dose= 100 nM). Data was presented as mean ± standard deviation (n=3). Student's t-test was used for statistical analysis: *$p \leq 0.05$; **$p \leq 0.01$; ***$p \leq 0.001$.

Overall, when luciferase assay data for both cell lines were considered, P(OEGMA)$_{43}$-*b*-P(AEAEMA)$_{45}$ block copolymer was found to be the most effective siRNA transfection agent since it showed potent gene silencing ability on MDA-MB-231-luc2-gfp. However, this polymer did not demonstrate specific silencing effect on H460-luc2. Therefore, it was attempted to confirm the efficacy of this polymer on breast cancer cell line. For this aim, instead of stably luciferase expressing MDA-MB-231-luc2-gfp cell line, native (not-transfected) form of this cell line, MDA-MB-231, was used and vimentin was selected as the target protein for several reasons. In literature, it has been shown that

vimentin can be silenced on MDA-MB-231 cells using siRNA-transfection reagent systems (Francart et al., 2020). Additionally, the overexpression of this intermediate filament has been shown to be associated with tumor growth and metastasis, thus becoming a potential target for cancer therapy (Francart et al., 2020; Satelli & Li, 2011). MDA-MB-231 cells were transfected with polymer-siRNA complexes and vimentin mRNA expression level was determined by RT-qPCR (Figure 4.59). An siRNA sequence targeting vimentin (Vim-siRNA) and another siRNA sequence targeting firefly luciferase (Luc-siRNA) was used as positive and negative control siRNAs, respectively. siRNA dose was fixed to 50 nM and complexes prepared at N/P of 50 as these conditions were determined to be optimal by luciferase assay. Together with P(OEGMA)$_{43}$-*b*-P(AEAEMA)$_{45}$, the transfection efficiency of P(AEAEMA)$_{40}$-*b*-P(OEtOxMA)$_{38}$, and P(OEGMA)/P(AEAEMA) miktoarm star polymers (SP1 and SP2) were also investigated to reveal the effect of stealth polymer block and polymeric architecture. As seen in the Figure 4.59, P(OEGMA)$_{43}$-*b*-P(AEAEMA)$_{45}$-Vim-siRNA complexes was able to reduce the mRNA expression to 41% in contrast, non-targeting siRNA complex of this polymer (P(OEGMA)$_{43}$-*b*-P(AEAEMA)$_{45}$-Luc-siRNA) only slightly affected the mRNA expression (mRNA expression = 80%). P(AEAEMA)$_{40}$-*b*-P(OEtOxMA)$_{38}$ and star polymers did not exhibit transfection efficiency at the tested conditions possibly due to low cellular uptake and poor siRNA binding/release ability of these polymers as shown by flow cytometry and gel electrophoresis, respectively. None of the polyplexes showed toxic effects on MDA-MB-231 cells as shown by MTT assay. Overall, this result verified the siRNA transfection ability of P(OEGMA)$_{43}$-*b*-P(AEAEMA)$_{45}$ on MDA-MB-231 breast cancer cell line.

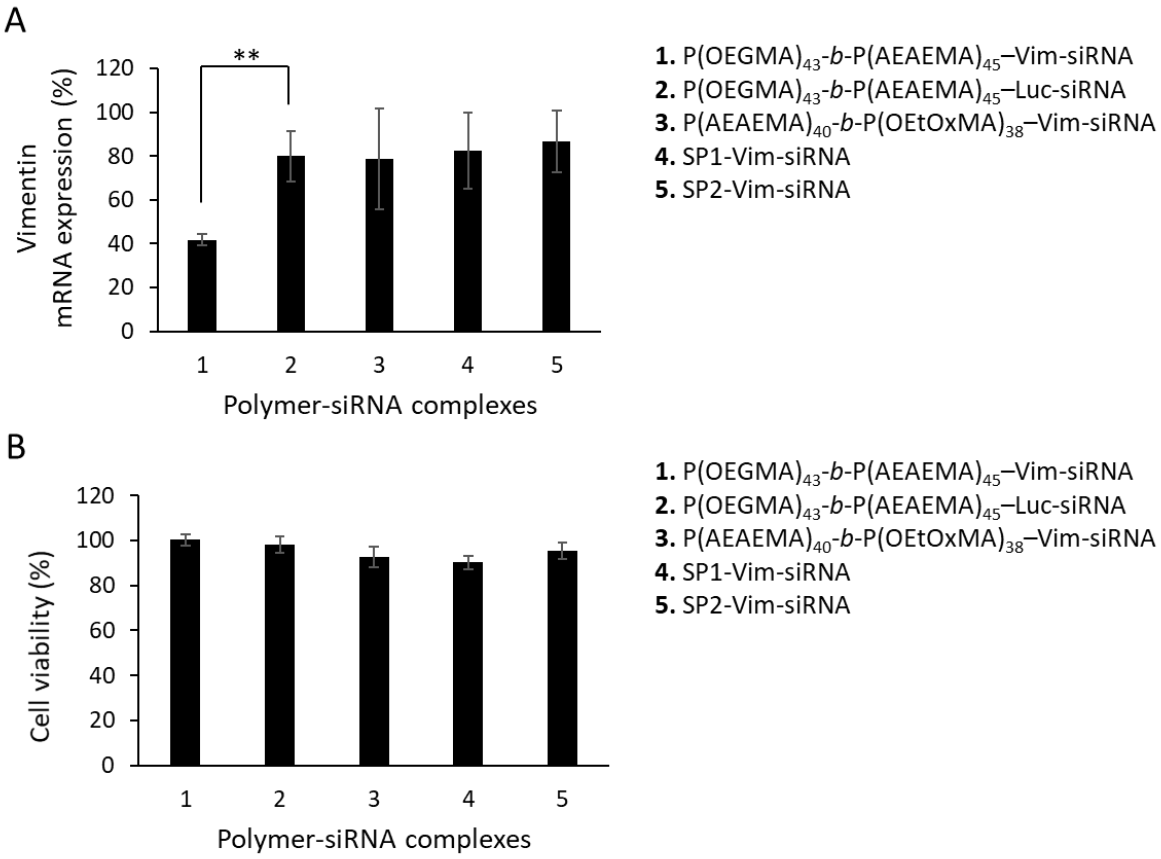

Figure 4.59. The effect of polymer-siRNA complexes on vimentin expression (A) and viability (B) of MDA-MB-231 cells (siRNA dose= 50 nM). Data was presented as mean ± standard deviation (n=3). Student's t-test was used for statistical analysis: *$p \leq 0.05$; **$p \leq 0.01$; ***$p \leq 0.001$.

CHAPTER 5

CONCLUSION

Effective delivery of siRNA molecules into cells is of great importance in the field of gene therapy. In this thesis, new polymeric carriers, P(OEGMA)-*b*-P(AEAEMA), PEG-*b*-P(AEAEMA) and P(AEAEMA)-*b*-P(OEtOxMA) block copolymers and P(OEGMA)/P(AEAEMA) miktoarm star polymers, have been prepared and their siRNA delivery potential has been investigated.

P(OEGMA) chain length of P(OEGMA)-*b*-P(AEAEMA) block copolymers was found to be an important parameter in siRNA delivery. The increase in P(OEGMA) block length led to decrease in toxicity, polyplex sizes and complex forming ability as shown by MTT assay, DLS and gel electrophoresis, respectively.

Stealth polymer blocks, P(OEGMA) and P(OEtOxMA), drastically affected the intracellular uptake of siRNA. P(OEGMA) block copolymer-siRNA complexes ($P(OEGMA)_{43}$-*b*-$P(AEAEMA)_{45}$-siRNA) were taken up by MDA-MB-231 and H460 cells at considerably higher quantity compared to its P(OEtOxMA) counterpart, $P(AEAEMA)_{40}$-*b*-$P(OEtOxMA)_{38}$, possibly due to differed serum/cell interactions of two different stealth polymers.

The effect of polymer architecture on siRNA delivery was determined by comparing P(OEGMA)-*b*-P(AEAEMA) linear block copolymer with P(OEGMA)/P(AEAEMA) miktoarm star polymer. Star polymers released siRNA easier, formed complexes at higher N/P and generally were more toxic compared to linear block copolymers.

Importantly, $P(OEGMA)_{43}$-*b*-$P(AEAEMA)_{45}$-siRNA complexes was able to show potent transfection efficiency in MDA-MB-231 cells as shown by luciferase assay and RT-qPCR. Whereas other polymers did not show significant efficiency due to limited uptake or unfavorable complexation.

Overall, this study reported the siRNA delivery potential of new polymeric systems and revealed some important design criteria and parameters in polymer-based siRNA delivery. The following suggestions can be made to improve this study:

1. The formulation medium and the way the formulations are prepared may be investigated further as they affect the transfection efficiency. Different buffers (e.g., HEPES, NaCl) or formulation preparation techniques (e.g., adding siRNA to polymer instead of adding polymer to siRNA) may be tested. Microfluidic systems may be used in formulation preparation to reproducibly obtain well-defined polyplexes.
2. As the use of modified nucleic acids leads to improved stability and higher transfection efficiency, polymers may be complexed with modified siRNA instead of unmodified siRNA for higher transfection efficiency.
3. Amine groups of P(AEAEMA) block may be modified with a targeting ligand and hydrophobic/lipophilic units for higher stability, cell uptake, endosomal escape, and transfection efficiency.
4. Zwitterionic stealth polymers may be incorporated to P(AEAEMA) as an alternative stealth polymer block.
5. Miktoarm star polymers with cationic core may be prepared to obtain star polymers with tighter siRNA complexing capability.

REFERENCES

Akinc, A., Maier, M. A., Manoharan, M., Fitzgerald, K., Jayaraman, M., Barros, S., . . . Madden, T. D. (2019). The Onpattro story and the clinical translation of nanomedicines containing nucleic acid-based drugs. *Nature Nanotechnology, 14*(12), 1084-1087.

Alconcel, S. N., Baas, A. S., & Maynard, H. D. (2011). FDA-approved poly (ethylene glycol)–protein conjugate drugs. *Polymer Chemistry, 2*(7), 1442-1448.

Amoozgar, Z., & Yeo, Y. (2012). Recent advances in stealth coating of nanoparticle drug delivery systems. *Wiley Interdisciplinary Reviews: Nanomedicine and Nanobiotechnology, 4*(2), 219-233.

Armstrong, J. (2009). PEGylated Protein Drugs: Basic Science and Clinical Applications. *Veronese, FM., editor*, 147-169.

Arnold, A. E., Czupiel, P., & Shoichet, M. (2017). Engineered polymeric nanoparticles to guide the cellular internalization and trafficking of small interfering ribonucleic acids. *Journal of Controlled Release, 259*, 3-15.

Averick, S. E., Paredes, E., Irastorza, A., Shrivats, A. R., Srinivasan, A., Siegwart, D. J., . . . Averick, A. A. (2012). Preparation of cationic nanogels for nucleic acid delivery. *Biomacromolecules, 13*(11), 3445-3449.

Bass, B. L. (2000). Double-stranded RNA as a template for gene silencing. *Cell, 101*(3), 235-238.

Behzadi, S., Serpooshan, V., Tao, W., Hamaly, M. A., Alkawareek, M. Y., Dreaden, E. C., . . . Mahmoudi, M. (2017). Cellular uptake of nanoparticles: journey inside the cell. *Chemical society reviews, 46*(14), 4218-4244.

Bernards, R. (2006). Exploring the uses of RNAi—gene knockdown and the Nobel Prize. *New England journal of medicine, 355*(23), 2391-2393.

Bernstein, E., Caudy, A. A., Hammond, S. M., & Hannon, G. J. (2001). Role for a bidentate ribonuclease in the initiation step of RNA interference. *Nature, 409*(6818), 363-366.

Bertrand, N., Wu, J., Xu, X., Kamaly, N., & Farokhzad, O. C. (2014). Cancer nanotechnology: the impact of passive and active targeting in the era of modern cancer biology. *Advanced drug delivery reviews, 66*, 2-25.

Beyerle, A., Irmler, M., Beckers, J., Kissel, T., & Stoeger, T. (2010). Toxicity pathway focused gene expression profiling of PEI-based polymers for pulmonary applications. *Molecular pharmaceutics, 7*(3), 727-737.

Bholakant, R., Qian, H., Zhang, J., Huang, X., Huang, D., Feijen, J., . . . Chen, W. (2020). Recent Advances of Polycationic siRNA Vectors for Cancer Therapy. *Biomacromolecules, 21*(8), 2966-2982.

Birmingham, A., Anderson, E. M., Reynolds, A., Ilsley-Tyree, D., Leake, D., Fedorov, Y., . . . Karpilow, J. (2006). 3′ UTR seed matches, but not overall identity, are associated with RNAi off-targets. *Nature methods, 3*(3), 199-204.

Blanco, E., Shen, H., & Ferrari, M. (2015). Principles of nanoparticle design for overcoming biological barriers to drug delivery. *Nature biotechnology, 33*(9), 941.

Blencowe, A., Tan, J. F., Goh, T. K., & Qiao, G. G. (2009). Core cross-linked star polymers via controlled radical polymerisation. *Polymer, 50*(1), 5-32.

Bono, N., Ponti, F., Mantovani, D., & Candiani, G. (2020). Non-viral in vitro gene delivery: it is now time to set the bar! *Pharmaceutics, 12*(2), 183.

Boussif, O., Lezoualc'h, F., Zanta, M. A., Mergny, M. D., Scherman, D., Demeneix, B., & Behr, J.-P. (1995). A versatile vector for gene and oligonucleotide transfer into cells in culture and in vivo: polyethylenimine. *Proceedings of the National Academy of Sciences, 92*(16), 7297-7301.

Bramsen, J. B., Laursen, M. B., Nielsen, A. F., Hansen, T. B., Bus, C., Langkjær, N., . . . Van Aerschot, A. (2009). A large-scale chemical modification screen identifies design rules to generate siRNAs with high activity, high stability and low toxicity. *Nucleic acids research, 37*(9), 2867-2881.

Brokowski, C., & Adli, M. (2019). CRISPR ethics: moral considerations for applications of a powerful tool. *Journal of molecular biology, 431*(1), 88-101.

Buyens, K., Meyer, M., Wagner, E., Demeester, J., De Smedt, S. C., & Sanders, N. N. (2010). Monitoring the disassembly of siRNA polyplexes in serum is crucial for predicting their biological efficacy. *Journal of Controlled Release, 141*(1), 38-41.

Byrne, P., Cullinan, J., Mintzes, B., & Smith, S. M. (2020). UK deal over inclisiran. In: British Medical Journal Publishing Group.

Cabral, H., Miyata, K., Osada, K., & Kataoka, K. (2018). Block copolymer micelles in nanomedicine applications. *Chemical reviews, 118*(14), 6844-6892.

Caracciolo, G., Cardarelli, F., Pozzi, D., Salomone, F., Maccari, G., Bardi, G., . . . Laganà, A. (2013). Selective targeting capability acquired with a protein corona adsorbed on the surface of 1, 2-dioleoyl-3-trimethylammonium propane/DNA nanoparticles. *ACS applied materials & interfaces, 5*(24), 13171-13179.

Carrstensen, H., Mueller, R. H., & Müller, B. (1992). Particle size, surface hydrophobicity and interaction with serum of parenteral fat emulsions and model drug carriers as parameters related to RES uptake. *Clinical nutrition, 11*(5), 289-297.

Cavallaro, G., Sardo, C., Craparo, E. F., Porsio, B., & Giammona, G. (2017). Polymeric nanoparticles for siRNA delivery: Production and applications. *International journal of pharmaceutics, 525*(2), 313-333.

Chandradoss, S. D., Schirle, N. T., Szczepaniak, M., MacRae, I. J., & Joo, C. (2015). A dynamic search process underlies microRNA targeting. *Cell, 162*(1), 96-107.

Chapman, R. G., Ostuni, E., Takayama, S., Holmlin, R. E., Yan, L., & Whitesides, G. M. (2000). Surveying for surfaces that resist the adsorption of proteins. *Journal of the American Chemical Society, 122*(34), 8303-8304.

Chen, G. Y., & Nuñez, G. (2010). Sterile inflammation: sensing and reacting to damage. *Nature Reviews Immunology, 10*(12), 826-837.

Chen, X., Mangala, L. S., Rodriguez-Aguayo, C., Kong, X., Lopez-Berestein, G., & Sood, A. K. (2018). RNA interference-based therapy and its delivery systems. *Cancer and Metastasis Reviews, 37*(1), 107-124.

Cheng, Q., Du, L., Meng, L., Han, S., Wei, T., Wang, X., . . . Zheng, S. (2016). The promising nanocarrier for doxorubicin and siRNA co-delivery by PDMAEMA-based amphiphilic nanomicelles. *ACS applied materials & interfaces, 8*(7), 4347-4356.

Chew, W. L., Tabebordbar, M., Cheng, J. K., Mali, P., Wu, E. Y., Ng, A. H., . . . Church, G. M. (2016). A multifunctional AAV–CRISPR–Cas9 and its host response. *Nature methods, 13*(10), 868-874.

Cho, H. Y., Averick, S. E., Paredes, E., Wegner, K., Averick, A., Jurga, S., . . . Matyjaszewski, K. (2013). Star polymers with a cationic core prepared by ATRP for cellular nucleic acids delivery. *Biomacromolecules, 14*(5), 1262-1267.

Choi, Y. H., Liu, F., Kim, J.-S., Choi, Y. K., Park, J. S., & Kim, S. W. (1998). Polyethylene glycol-grafted poly-L-lysine as polymeric gene carrier. *Journal of Controlled Release, 54*(1), 39-48.

Cifuentes, D., Xue, H., Taylor, D. W., Patnode, H., Mishima, Y., Cheloufi, S., . . . Lawson, N. D. (2010). A novel miRNA processing pathway independent of Dicer requires Argonaute2 catalytic activity. *Science, 328*(5986), 1694-1698.

Collingwood, M. A., Rose, S. D., Huang, L., Hillier, C., Amarzguioui, M., Wiiger, M. T., . . . Behlke, M. A. (2008). Chemical modification patterns compatible with high potency dicer-substrate small interfering RNAs. *Oligonucleotides, 18*(2), 187-200.

Cong, L., Ran, F. A., Cox, D., Lin, S., Barretto, R., Habib, N., . . . Marraffini, L. A. (2013). Multiplex genome engineering using CRISPR/Cas systems. *Science, 339*(6121), 819-823.

Convertine, A. J., Diab, C., Prieve, M., Paschal, A., Hoffman, A., Johnson, P., & Stayton, P. S. (2010). pH-responsive polymeric micelle carriers for siRNA drugs. *Biomacromolecules, 11*(11), 2904-2911.

Cooley, M., Sarode, A., Hoore, M., Fedosov, D. A., Mitragotri, S., & Gupta, A. S. (2018). Influence of particle size and shape on their margination and wall-adhesion: implications in drug delivery vehicle design across nano-to-micro scale. *Nanoscale, 10*(32), 15350-15364.

Crooke, S. T., Wang, S., Vickers, T. A., Shen, W., & Liang, X.-h. (2017). Cellular uptake and trafficking of antisense oligonucleotides. *Nature biotechnology, 35*(3), 230-237.

D'souza, A. A., & Shegokar, R. (2016). Polyethylene glycol (PEG): a versatile polymer for pharmaceutical applications. *Expert opinion on drug delivery, 13*(9), 1257-1275.

Da Silva-Candal, A., Brown, T., Krishnan, V., Lopez-Loureiro, I., Ávila-Gómez, P., Pusuluri, A., . . . Castillo, J. (2019). Shape effect in active targeting of nanoparticles to inflamed cerebral endothelium under static and flow conditions. *Journal of Controlled Release, 309*, 94-105.

Dalzon, B., Aude-Garcia, C., Collin-Faure, V., Diemer, H., Béal, D., Dussert, F., . . . Carrière, M. (2017). Differential proteomics highlights macrophage-specific responses to amorphous silica nanoparticles. *Nanoscale, 9*(27), 9641-9658.

de Ilarduya, C. T., Sun, Y., & Düzgüneş, N. (2010). Gene delivery by lipoplexes and polyplexes. *European journal of pharmaceutical sciences, 40*(3), 159-170.

de Paula Brandão, P. R., Titze-de-Almeida, S. S., & Titze-de-Almeida, R. (2020). Leading RNA interference therapeutics part 2: silencing delta-aminolevulinic acid synthase 1, with a focus on givosiran. *Molecular diagnosis & therapy, 24*(1), 61-68.

Dias, N., & Stein, C. (2002). Antisense oligonucleotides: basic concepts and mechanisms. *Molecular cancer therapeutics, 1*(5), 347-355.

Doherty, E. A., & Doudna, J. A. (2001). Ribozyme structures and mechanisms. *Annual review of biophysics and biomolecular structure, 30*(1), 457-475.

Dong, Y., Siegwart, D. J., & Anderson, D. G. (2019). Strategies, design, and chemistry in siRNA delivery systems. *Advanced drug delivery reviews, 144*, 133-147.

Doudna, J. A., & Charpentier, E. (2014). The new frontier of genome engineering with CRISPR-Cas9. *Science, 346*(6213).

Dowdy, S. F. (2017). Overcoming cellular barriers for RNA therapeutics. *Nature biotechnology, 35*(3), 222-229.

Dunbar, C. E., High, K. A., Joung, J. K., Kohn, D. B., Ozawa, K., & Sadelain, M. (2018). Gene therapy comes of age. *Science, 359*(6372).

Duong, H. T., Jung, K., Kutty, S. K., Agustina, S., Adnan, N. N. M., Basuki, J. S., . . . Boyer, C. (2014). Nanoparticle (star polymer) delivery of nitric oxide effectively negates Pseudomonas aeruginosa biofilm formation. *Biomacromolecules, 15*(7), 2583-2589.

Dykxhoorn, D. M., Novina, C. D., & Sharp, P. A. (2003). Killing the messenger: short RNAs that silence gene expression. *Nature reviews Molecular cell biology, 4*(6), 457-467.

Elbashir, S. M., Lendeckel, W., & Tuschl, T. (2001). RNA interference is mediated by 21-and 22-nucleotide RNAs. *Genes & development, 15*(2), 188-200.

Fam, S. Y., Chee, C. F., Yong, C. Y., Ho, K. L., Mariatulqabtiah, A. R., & Tan, W. S. (2020). Stealth coating of nanoparticles in drug-delivery systems. *Nanomaterials, 10*(4), 787.

Fire, A., Xu, S., Montgomery, M. K., Kostas, S. A., Driver, S. E., & Mello, C. C. (1998). Potent and specific genetic interference by double-stranded RNA in Caenorhabditis elegans. *Nature, 391*(6669), 806-811.

Foroozandeh, P., & Aziz, A. A. (2018). Insight into cellular uptake and intracellular trafficking of nanoparticles. *Nanoscale research letters, 13*(1), 1-12.

Francart, M.-E., Vanwynsberghe, A. M., Lambert, J., Bourcy, M., Genna, A., Ancel, J., . . . Struman, I. (2020). Vimentin prevents a miR-dependent negative regulation of tissue factor mRNA during epithelial–mesenchymal transitions and facilitates early metastasis. *Oncogene, 39*(18), 3680-3692.

Frank, M. M., & Fries, L. F. (1991). The role of complement in inflammation and phagocytosis. *Immunology today, 12*(9), 322-326.

Frazier, K. S. (2015). Antisense oligonucleotide therapies: the promise and the challenges from a toxicologic pathologist's perspective. *Toxicologic pathology, 43*(1), 78-89.

Gao, H., & Matyjaszewski, K. (2009). Synthesis of functional polymers with controlled architecture by CRP of monomers in the presence of cross-linkers: From stars to gels. *Progress in polymer science, 34*(4), 317-350.

Gao, S., Dagnaes-Hansen, F., Nielsen, E. J. B., Wengel, J., Besenbacher, F., Howard, K. A., & Kjems, J. (2009). The effect of chemical modification and nanoparticle formulation on stability and biodistribution of siRNA in mice. *Molecular therapy, 17*(7), 1225-1233.

Garay, R. P., El-Gewely, R., Armstrong, J. K., Garratty, G., & Richette, P. (2012). Antibodies against polyethylene glycol in healthy subjects and in patients treated with PEG-conjugated agents. *Expert opinion on drug delivery, 9*(11), 1319-1323. doi:10.1517/17425247.2012.720969

Garber, K. (2018). Alnylam launches era of RNAi drugs. In: Nature Publishing Group.

Gaspar, V. M., Baril, P., Costa, E. C., de Melo-Diogo, D., Foucher, F., Queiroz, J. A., . . . Correia, I. J. (2015). Bioreducible poly (2-ethyl-2-oxazoline)–PLA–PEI-SS triblock copolymer micelles for co-delivery of DNA minicircles and Doxorubicin. *Journal of Controlled Release, 213*, 175-191.

Gehr, P., & Zellner, R. (2019). *Biological Responses to Nanoscale Particles*: Springer.

Georgiou, T. K. (2014). Star polymers for gene delivery. *Polymer international, 63*(7), 1130-1133.

Gessner, A., Waicz, R., Lieske, A., Paulke, B.-R., Mäder, K., & Müller, R. (2000). Nanoparticles with decreasing surface hydrophobicities: influence on plasma protein adsorption. *International journal of pharmaceutics, 196*(2), 245-249.

Gheysen, G., & Vanholme, B. (2007). RNAi from plants to nematodes. *Trends in biotechnology, 25*(3), 89-92.

Glassner, M., Vergaelen, M., & Hoogenboom, R. (2018). Poly (2-oxazoline) s: A comprehensive overview of polymer structures and their physical properties. *Polymer international, 67*(1), 32-45.

Golan, T., Khvalevsky, E. Z., Hubert, A., Gabai, R. M., Hen, N., Segal, A., . . . Raskin, S. (2015). RNAi therapy targeting KRAS in combination with chemotherapy for locally advanced pancreatic cancer patients. *Oncotarget, 6*(27), 24560.

Gordon, K. H., & Waterhouse, P. M. (2007). RNAi for insect-proof plants. *Nature biotechnology, 25*(11), 1231-1232.

Grayson, A. C. R., Doody, A. M., & Putnam, D. (2006). Biophysical and structural characterization of polyethylenimine-mediated siRNA delivery in vitro. *Pharmaceutical research, 23*(8), 1868-1876.

Gref, R., Minamitake, Y., Peracchia, M. T., Trubetskoy, V., Torchilin, V., & Langer, R. (1994). Biodegradable long-circulating polymeric nanospheres. *Science, 263*(5153), 1600-1603.

Grishok, A., Pasquinelli, A. E., Conte, D., Li, N., Parrish, S., Ha, I., . . . Mello, C. C. (2001). Genes and mechanisms related to RNA interference regulate expression of the small temporal RNAs that control C. elegans developmental timing. *Cell, 106*(1), 23-34.

Gu, J., Al-Bayati, K., & Ho, E. A. (2017). Development of antibody-modified chitosan nanoparticles for the targeted delivery of siRNA across the blood-brain barrier as a strategy for inhibiting HIV replication in astrocytes. *Drug delivery and translational research, 7*(4), 497-506.

Hadjesfandiari, N., & Parambath, A. (2018). Stealth coatings for nanoparticles: Polyethylene glycol alternatives. In *Engineering of Biomaterials for Drug Delivery Systems* (pp. 345-361): Elsevier.

Hamil, A. S., & Dowdy, S. F. (2016). Synthesis and conjugation of small interfering ribonucleic neutral SiRNNs. In *SiRNA Delivery Methods* (pp. 1-9): Springer.

Hannon, G. J. (2002). RNA interference. *Nature, 418*(6894), 244-251.

Harada-Shiba, M., Yamauchi, K., Harada, A., Takamisawa, I., Shimokado, K., & Kataoka, K. (2002). Polyion complex micelles as vectors in gene therapy–pharmacokinetics and in vivo gene transfer. *Gene therapy, 9*(6), 407-414.

Helms, B., Guillaudeu, S. J., Xie, Y., McMurdo, M., Hawker, C. J., & Fréchet, J. M. (2005). One-pot reaction cascades using star polymers with core-confined catalysts. *Angewandte Chemie International Edition, 44*(39), 6384-6387.

Hoang Thi, T. T., Pilkington, E. H., Nguyen, D. H., Lee, J. S., Park, K. D., & Truong, N. P. (2020). The importance of poly (ethylene glycol) alternatives for overcoming PEG immunogenicity in drug delivery and bioconjugation. *Polymers, 12*(2), 298.

Hohjoh, H. (2004). Enhancement of RNAi activity by improved siRNA duplexes. *FEBS letters, 557*(1-3), 193-198.

Hoshyar, N., Gray, S., Han, H., & Bao, G. (2016). The effect of nanoparticle size on in vivo pharmacokinetics and cellular interaction. *Nanomedicine, 11*(6), 673-692.

Hutvágner, G., & Zamore, P. D. (2002). A microRNA in a multiple-turnover RNAi enzyme complex. *Science, 297*(5589), 2056-2060.

Ipsaro, J. J., & Joshua-Tor, L. (2015). From guide to target: molecular insights into eukaryotic RNA-interference machinery. *Nature structural & molecular biology, 22*(1), 20.

Itaka, K., & Kataoka, K. (2009). Recent development of nonviral gene delivery systems with virus-like structures and mechanisms. *European Journal of Pharmaceutics and Biopharmaceutics, 71*(3), 475-483.

Iwamoto, N., Butler, D. C., Svrzikapa, N., Mohapatra, S., Zlatev, I., Sah, D. W., . . . Frank-Kamenetsky, M. (2017). Control of phosphorothioate stereochemistry substantially increases the efficacy of antisense oligonucleotides. *Nature biotechnology, 35*(9), 845-851.

Jackson, A. L., Bartz, S. R., Schelter, J., Kobayashi, S. V., Burchard, J., Mao, M., . . . Linsley, P. S. (2003). Expression profiling reveals off-target gene regulation by RNAi. *Nature biotechnology, 21*(6), 635-637.

Jackson, A. L., Burchard, J., Schelter, J., Chau, B. N., Cleary, M., Lim, L., & Linsley, P. S. (2006). Widespread siRNA "off-target" transcript silencing mediated by seed region sequence complementarity. *Rna, 12*(7), 1179-1187.

Janas, M. M., Schlegel, M. K., Harbison, C. E., Yilmaz, V. O., Jiang, Y., Parmar, R., . . . Shulga-Morskaya, S. (2018). Selection of GalNAc-conjugated siRNAs with limited off-target-driven rat hepatotoxicity. *Nature communications, 9*(1), 1-10.

Joh, D. Y., Zimmers, Z., Avlani, M., Heggestad, J. T., Aydin, H. B., Ganson, N., . . . Hershfield, M. S. (2019). Architectural Modification of Conformal PEG-Bottlebrush Coatings Minimizes Anti-PEG Antigenicity While Preserving Stealth Properties. *Advanced healthcare materials, 8*(8), 1801177.

Kanasty, R., Dorkin, J. R., Vegas, A., & Anderson, D. (2013). Delivery materials for siRNA therapeutics. *Nature materials, 12*(11), 967-977.

Kargaard, A., Sluijter, J. P., & Klumperman, B. (2019). Polymeric siRNA gene delivery–transfection efficiency versus cytotoxicity. *Journal of Controlled Release, 316*, 263-291.

Kaul, G., & Amiji, M. (2002). Long-circulating poly (ethylene glycol)-modified gelatin nanoparticles for intracellular delivery. *Pharmaceutical research, 19*(7), 1061-1067.

Key, J., Palange, A. L., Gentile, F., Aryal, S., Stigliano, C., Di Mascolo, D., . . . Singh, J. (2015). Soft discoidal polymeric nanoconstructs resist macrophage uptake and enhance vascular targeting in tumors. *ACS nano, 9*(12), 11628-11641.

Khutoryanskiy, V. V. (2018). Beyond PEGylation: alternative surface-modification of nanoparticles with mucus-inert biomaterials. *Advanced drug delivery reviews, 124*, 140-149.

Khvalevsky, E. Z., Gabai, R., Rachmut, I. H., Horwitz, E., Brunschwig, Z., Orbach, A., . . . Yavin, E. (2013). Mutant KRAS is a druggable target for pancreatic cancer. *Proceedings of the National Academy of Sciences, 110*(51), 20723-20728.

Khvorova, A., Reynolds, A., & Jayasena, S. D. (2003). Functional siRNAs and miRNAs exhibit strand bias. *Cell, 115*(2), 209-216.

Khvorova, A., & Watts, J. K. (2017). The chemical evolution of oligonucleotide therapies of clinical utility. *Nature biotechnology, 35*(3), 238-248.

Kim, B., Park, J. H., & Sailor, M. J. (2019). Rekindling RNAi therapy: materials design requirements for in vivo siRNA delivery. *Advanced materials, 31*(49), 1903637.

Kim, B. S., Kim, H. J., Osawa, S., Hayashi, K., Toh, K., Naito, M., . . . Kataoka, K. (2019). Dually stabilized triblock copolymer micelles with hydrophilic shell and hydrophobic interlayer for systemic antisense oligonucleotide delivery to solid tumor. *ACS Biomaterials Science & Engineering, 5*(11), 5770-5780.

Kim, B. S., Osawa, S., Yum, J., Naito, M., & Miyata, K. (2020). Installation of a Thermoswitchable Hydrophobic Domain into a Unimer Polyion Complex for Enhanced Cellular Uptake of siRNA. *Bioconjugate chemistry, 31*(5), 1320-1326.

Kim, D.-H., Behlke, M. A., Rose, S. D., Chang, M.-S., Choi, S., & Rossi, J. J. (2005). Synthetic dsRNA Dicer substrates enhance RNAi potency and efficacy. *Nature biotechnology, 23*(2), 222-226.

Kim, H. J., Kim, A., Miyata, K., & Kataoka, K. (2016). Recent progress in development of siRNA delivery vehicles for cancer therapy. *Advanced drug delivery reviews, 104*, 61-77.

Kim, S. J., Ramsey, D. M., Boyer, C., Davis, T. P., & McAlpine, S. R. (2013). Effectively delivering a unique Hsp90 inhibitor using star polymers. *ACS medicinal chemistry letters, 4*(10), 915-920.

Kleinman, M. E., Yamada, K., Takeda, A., Chandrasekaran, V., Nozaki, M., Baffi, J. Z., . . . Pan, Y. (2008). Sequence-and target-independent angiogenesis suppression by siRNA via TLR3. *Nature, 452*(7187), 591-597.

Kotterman, M. A., Chalberg, T. W., & Schaffer, D. V. (2015). Viral vectors for gene therapy: translational and clinical outlook. *Annual review of biomedical engineering, 17*, 63-89.

Kou, L., Bhutia, Y. D., Yao, Q., He, Z., Sun, J., & Ganapathy, V. (2018). Transporter-guided delivery of nanoparticles to improve drug permeation across cellular barriers and drug exposure to selective cell types. *Frontiers in pharmacology, 9*, 27.

Kurtulus, I., Yilmaz, G., Ucuncu, M., Emrullahoglu, M., Becer, C. R., & Bulmus, V. (2014). A new proton sponge polymer synthesized by RAFT polymerization for intracellular delivery of biotherapeutics. *Polymer Chemistry, 5*(5), 1593-1604.

Ledford, H. (2018). Gene-silencing technology gets first drug approval after 20-year wait. *Nature, 560*(7718), 291-293.

Lee, H. Y., Zhou, K., Smith, A. M., Noland, C. L., & Doudna, J. A. (2013). Differential roles of human Dicer-binding proteins TRBP and PACT in small RNA processing. *Nucleic acids research, 41*(13), 6568-6576.

Lee, P. W., Isarov, S. A., Wallat, J. D., Molugu, S. K., Shukla, S., Sun, J. E., . . . Konkolewicz, D. (2017). Polymer structure and conformation alter the antigenicity of virus-like particle–polymer conjugates. *Journal of the American Chemical Society, 139*(9), 3312-3315.

Lewis, B. P., Burge, C. B., & Bartel, D. P. (2005). Conserved seed pairing, often flanked by adenosines, indicates that thousands of human genes are microRNA targets. *Cell, 120*(1), 15-20.

Li, J., & Kataoka, K. (2020). Chemo-physical Strategies to Advance the in Vivo Functionality of Targeted Nanomedicine: The Next Generation. *Journal of the American Chemical Society*.

Li, M., Al-Jamal, K. T., Kostarelos, K., & Reineke, J. (2010). Physiologically based pharmacokinetic modeling of nanoparticles. *ACS nano, 4*(11), 6303-6317.

Liang, X.-h., Sun, H., Shen, W., & Crooke, S. T. (2015). Identification and characterization of intracellular proteins that bind oligonucleotides with phosphorothioate linkages. *Nucleic acids research, 43*(5), 2927-2945.

Lila, A. S. A., Kiwada, H., & Ishida, T. (2013). The accelerated blood clearance (ABC) phenomenon: clinical challenge and approaches to manage. *Journal of Controlled Release, 172*(1), 38-47.

Lima, W. F., Prakash, T. P., Murray, H. M., Kinberger, G. A., Li, W., Chappell, A. E., . . . Seth, P. P. (2012). Single-stranded siRNAs activate RNAi in animals. *Cell, 150*(5), 883-894.

Liu, J., Carmell, M. A., Rivas, F. V., Marsden, C. G., Thomson, J. M., Song, J.-J., . . . Hannon, G. J. (2004). Argonaute2 is the catalytic engine of mammalian RNAi. *Science, 305*(5689), 1437-1441.

Liu, M., Johansen, P., Zabel, F., Leroux, J.-C., & Gauthier, M. A. (2014). Semi-permeable coatings fabricated from comb-polymers efficiently protect proteins in vivo. *Nature communications, 5*(1), 1-8.

Luxenhofer, R., Han, Y., Schulz, A., Tong, J., He, Z., Kabanov, A. V., & Jordan, R. (2012). Poly (2-oxazoline) s as Polymer Therapeutics. *Macromolecular rapid communications, 33*(19), 1613-1631.

Luxenhofer, R., & Jordan, R. (2016). Poly (2-oxazoline) s (POx) in Biomedical Applications. *Material Matters, Aldrich, 8*(3), 70.

Malcolm, D. W., Freeberg, M. A., Wang, Y., Sims Jr, K. R., Awad, H. A., & Benoit, D. S. (2017). Diblock copolymer hydrophobicity facilitates efficient gene silencing and cytocompatible nanoparticle-mediated siRNA delivery to musculoskeletal cell types. *Biomacromolecules, 18*(11), 3753-3765.

Manke, A., Wang, L., & Rojanasakul, Y. (2013). Mechanisms of nanoparticle-induced oxidative stress and toxicity. *BioMed research international, 2013*.

Matsumura, Y., & Maeda, H. (1986). A new concept for macromolecular therapeutics in cancer chemotherapy: mechanism of tumoritropic accumulation of proteins and the antitumor agent smancs. *Cancer research, 46*(12 Part 1), 6387-6392.

Meade, B. R., Gogoi, K., Hamil, A. S., Palm-Apergi, C., Van Den Berg, A., Hagopian, J. C., . . . Dowdy, C. F. (2014). Efficient delivery of RNAi prodrugs containing reversible charge-neutralizing phosphotriester backbone modifications. *Nature biotechnology, 32*(12), 1256.

Mitchell, M. J., Billingsley, M. M., Haley, R. M., Wechsler, M. E., Peppas, N. A., & Langer, R. (2020). Engineering precision nanoparticles for drug delivery. *Nature reviews Drug discovery*, 1-24.

Miyata, K., Oba, M., Nakanishi, M., Fukushima, S., Yamasaki, Y., Koyama, H., . . . Kataoka, K. (2008). Polyplexes from poly (aspartamide) bearing 1, 2-diaminoethane side chains induce pH-selective, endosomal membrane destabilization with amplified transfection and negligible cytotoxicity. *Journal of the American Chemical Society, 130*(48), 16287-16294.

Moghimi, S. M., Hunter, A. C., & Murray, J. C. (2001). Long-circulating and target-specific nanoparticles: theory to practice. *Pharmacological reviews, 53*(2), 283-318.

Moreadith, R. W., Viegas, T. X., Bentley, M. D., Harris, J. M., Fang, Z., Yoon, K., . . . Li, X. (2017). Clinical development of a poly (2-oxazoline)(POZ) polymer therapeutic for the treatment of Parkinson's disease–Proof of concept of POZ as a versatile polymer platform for drug development in multiple therapeutic indications. *European Polymer Journal, 88*, 524-552.

Nair, J. K., Attarwala, H., Sehgal, A., Wang, Q., Aluri, K., Zhang, X., . . . Schofield, S. (2017). Impact of enhanced metabolic stability on pharmacokinetics and pharmacodynamics of GalNAc–siRNA conjugates. *Nucleic acids research, 45*(19), 10969-10977.

Navarro, G., Pan, J., & Torchilin, V. P. (2015). Micelle-like nanoparticles as carriers for DNA and siRNA. *Molecular pharmaceutics, 12*(2), 301-313.

Navegantes, K. C., de Souza Gomes, R., Pereira, P. A. T., Czaikoski, P. G., Azevedo, C. H. M., & Monteiro, M. C. (2017). Immune modulation of some autoimmune diseases: the critical role of macrophages and neutrophils in the innate and adaptive immunity. *Journal of translational medicine, 15*(1), 1-21.

Nelson, C. E., Kintzing, J. R., Hanna, A., Shannon, J. M., Gupta, M. K., & Duvall, C. L. (2013). Balancing cationic and hydrophobic content of PEGylated siRNA polyplexes enhances endosome escape, stability, blood circulation time, and bioactivity in vivo. *ACS nano, 7*(10), 8870-8880.

Neun, B. W., Barenholz, Y., Szebeni, J., & Dobrovolskaia, M. A. (2018). Understanding the role of anti-PEG antibodies in the complement activation by doxil in vitro. *Molecules, 23*(7), 1700.

Nielsen, P. E., Egholm, M., & Buchardt, O. (1994). Peptide nucleic acid (PNA). A DNA mimic with a peptide backbone. *Bioconjugate chemistry, 5*(1), 3-7.

Nykänen, A., Haley, B., & Zamore, P. D. (2001). ATP requirements and small interfering RNA structure in the RNA interference pathway. *Cell, 107*(3), 309-321.

Owens III, D. E., & Peppas, N. A. (2006). Opsonization, biodistribution, and pharmacokinetics of polymeric nanoparticles. *International journal of pharmaceutics, 307*(1), 93-102.

Pafiti, K. S., Mastroyiannopoulos, N. P., Phylactou, L. A., & Patrickios, C. S. (2011). Hydrophilic cationic star homopolymers based on a novel diethanol-N-methylamine dimethacrylate cross-linker for siRNA transfection: synthesis, characterization, and evaluation. *Biomacromolecules, 12*(5), 1468-1479.

Pandey, R. K., & Prajapati, V. K. (2018). Molecular and immunological toxic effects of nanoparticles. *International journal of biological macromolecules, 107*, 1278-1293.

Park, K. (2018). Impact of anti-PEG antibodies on PEGylated nanoparticles fate in vivo. *Journal of controlled release: official journal of the Controlled Release Society, 287*, 257-257.

Parmar, R., Willoughby, J. L., Liu, J., Foster, D. J., Brigham, B., Theile, C. S., . . . Pei, Y. (2016). 5′-(E)-Vinylphosphonate: A Stable Phosphate Mimic Can Improve the RNAi Activity of siRNA–GalNAc Conjugates. *ChemBioChem, 17*(11), 985-989.

Patil, M. L., Zhang, M., & Minko, T. (2011). Multifunctional triblock nanocarrier (PAMAM-PEG-PLL) for the efficient intracellular siRNA delivery and gene silencing. *ACS nano, 5*(3), 1877-1887.

Peng, L., & Wagner, E. (2019). Polymeric carriers for nucleic acid delivery: current designs and future directions. *Biomacromolecules, 20*(10), 3613-3626.

Pezzoli, D., Giupponi, E., Mantovani, D., & Candiani, G. (2017). Size matters for in vitro gene delivery: investigating the relationships among complexation protocol, transfection medium, size and sedimentation. *Scientific reports, 7*(1), 1-11.

Prasad, V. (2018). Tisagenlecleucel—the first approved CAR-T-cell therapy: implications for payers and policy makers. *Nature Reviews Clinical Oncology, 15*(1), 11-12.

Qi, Y., Simakova, A., Ganson, N. J., Li, X., Luginbuhl, K. M., Ozer, I., . . . Chilkoti, A. (2016). A brush-polymer/exendin-4 conjugate reduces blood glucose levels for up to five days and eliminates poly (ethylene glycol) antigenicity. *Nature biomedical engineering, 1*(1), 1-12.

Ray, K. K., Landmesser, U., Leiter, L. A., Kallend, D., Dufour, R., Karakas, M., . . . Visseren, F. L. (2017). Inclisiran in patients at high cardiovascular risk with elevated LDL cholesterol. *N Engl J Med, 376*, 1430-1440.

Ren, J. M., McKenzie, T. G., Fu, Q., Wong, E. H., Xu, J., An, Z., . . . Qiao, G. G. (2016). Star polymers. *Chemical reviews, 116*(12), 6743-6836.

Rennick, J. J., Johnston, A. P., & Parton, R. G. (2021). Key principles and methods for studying the endocytosis of biological and nanoparticle therapeutics. *Nature Nanotechnology*, 1-11.

Rettig, G. R., & Behlke, M. A. (2012). Progress toward in vivo use of siRNAs-II. *Molecular therapy, 20*(3), 483-512.

Reynolds, A., Leake, D., Boese, Q., Scaringe, S., Marshall, W. S., & Khvorova, A. (2004). Rational siRNA design for RNA interference. *Nature biotechnology, 22*(3), 326-330.

Reyon, D., Tsai, S. Q., Khayter, C., Foden, J. A., Sander, J. D., & Joung, J. K. (2012). FLASH assembly of TALENs for high-throughput genome editing. *Nature biotechnology, 30*(5), 460.

Richter, A. W., & Åkerblom, E. (1984). Polyethylene glycol reactive antibodies in man: titer distribution in allergic patients treated with monomethoxy polyethylene glycol modified allergens or placebo, and in healthy blood donors. *International Archives of Allergy and Immunology, 74*(1), 36-39.

Rideau, E., Dimova, R., Schwille, P., Wurm, F. R., & Landfester, K. (2018). Liposomes and polymersomes: a comparative review towards cell mimicking. *Chemical society reviews, 47*(23), 8572-8610.

Robb, G. B., & Rana, T. M. (2007). RNA helicase A interacts with RISC in human cells and functions in RISC loading. *Molecular cell, 26*(4), 523-537.

Robbins, M., Judge, A., Liang, L., McClintock, K., Yaworski, E., & MacLachlan, I. (2007). 2′-O-methyl-modified RNAs act as TLR7 antagonists. *Molecular therapy, 15*(9), 1663-1669.

Romano, N., & Macino, G. (1992). Quelling: transient inactivation of gene expression in Neurospora crassa by transformation with homologous sequences. *Molecular microbiology, 6*(22), 3343-3353.

Roser, M., Fischer, D., & Kissel, T. (1998). Surface-modified biodegradable albumin nano-and microspheres. II: effect of surface charges on in vitro phagocytosis and biodistribution in rats. *European Journal of Pharmaceutics and Biopharmaceutics, 46*(3), 255-263.

Salmaso, S., & Caliceti, P. (2013). Stealth properties to improve therapeutic efficacy of drug nanocarriers. *Journal of drug delivery, 2013*.

Salomon, W. E., Jolly, S. M., Moore, M. J., Zamore, P. D., & Serebrov, V. (2015). Single-molecule imaging reveals that Argonaute reshapes the binding properties of its nucleic acid guides. *Cell, 162*(1), 84-95.

Sano, M., Sierant, M., Miyagishi, M., Nakanishi, M., Takagi, Y., & Sutou, S. (2008). Effect of asymmetric terminal structures of short RNA duplexes on the RNA interference activity and strand selection. *Nucleic acids research, 36*(18), 5812-5821.

Satelli, A., & Li, S. (2011). Vimentin in cancer and its potential as a molecular target for cancer therapy. *Cell Mol Life Sci, 68*(18), 3033-3046. doi:10.1007/s00018-011-0735-1

Schallon, A., Jérôme, V., Walther, A., Synatschke, C. V., Müller, A. H., & Freitag, R. (2010). Performance of three PDMAEMA-based polycation architectures as gene delivery agents in comparison to linear and branched PEI. *Reactive and Functional Polymers, 70*(1), 1-10.

Scholz, C., & Wagner, E. (2012). Therapeutic plasmid DNA versus siRNA delivery: common and different tasks for synthetic carriers. *Journal of Controlled Release, 161*(2), 554-565.

Schroeder, A., Levins, C. G., Cortez, C., Langer, R., & Anderson, D. G. (2010). Lipid-based nanotherapeutics for siRNA delivery. *Journal of internal medicine, 267*(1), 9-21.

Schwarz, D. S., Hutvágner, G., Haley, B., & Zamore, P. D. (2002). Evidence that siRNAs function as guides, not primers, in the Drosophila and human RNAi pathways. *Molecular cell, 10*(3), 537-548.

Scott, L. J. (2020). Givosiran: first approval. *Drugs, 80*(3), 335-339.

Sebak, A. (2018). Limitations of PEGylated nanocarriers: unfavourable physicochemical properties, biodistribution patterns and cellular and subcellular fates. *Int. J. Pharm, 10*, 6-12.

Setten, R. L., Rossi, J. J., & Han, S.-p. (2019). The current state and future directions of RNAi-based therapeutics. *Nature reviews Drug discovery, 18*(6), 421-446.

Shemi, A., Khvalevsky, E. Z., Gabai, R. M., Domb, A., & Barenholz, Y. (2015). Multistep, effective drug distribution within solid tumors. *Oncotarget, 6*(37), 39564.

Shen, W., Wang, H., Ling-Hu, Y., Lv, J., Chang, H., & Cheng, Y. (2016). Screening of efficient polymers for siRNA delivery in a library of hydrophobically modified polyethyleneimines. *Journal of Materials Chemistry B, 4*(39), 6468-6474.

Shibata, T., Kanaoka, S., & Aoshima, S. (2006). Quantitative synthesis of star-shaped poly (vinyl ether) s with a narrow molecular weight distribution by living cationic polymerization. *Journal of the American Chemical Society, 128*(23), 7497-7504.

Siegwart, D. J., Oh, J. K., & Matyjaszewski, K. (2012). ATRP in the design of functional materials for biomedical applications. *Progress in polymer science, 37*(1), 18-37.

Smith, D., Holley, A. C., & McCormick, C. L. (2011). RAFT-synthesized copolymers and conjugates designed for therapeutic delivery of siRNA. *Polymer Chemistry, 2*(7), 1428-1441.

Snead, N. M., Wu, X., Li, A., Cui, Q., Sakurai, K., Burnett, J. C., & Rossi, J. J. (2013). Molecular basis for improved gene silencing by Dicer substrate interfering RNA compared with other siRNA variants. *Nucleic acids research, 41*(12), 6209-6221.

Song, J.-J., Smith, S. K., Hannon, G. J., & Joshua-Tor, L. (2004). Crystal structure of Argonaute and its implications for RISC slicer activity. *Science, 305*(5689), 1434-1437.

Soucek, L., Whitfield, J. R., Sodir, N. M., Massó-Vallés, D., Serrano, E., Karnezis, A. N., . . . Evan, G. I. (2013). Inhibition of Myc family proteins eradicates KRas-driven lung cancer in mice. *Genes & development, 27*(5), 504-513.

Spiniello, M., Blencowe, A., & Qiao, G. G. (2008). Synthesis and characterization of fluorescently labeled core cross-linked star polymers. *Journal of Polymer Science Part A: Polymer Chemistry, 46*(7), 2422-2432.

Suk, J. S., Xu, Q., Kim, N., Hanes, J., & Ensign, L. M. (2016). PEGylation as a strategy for improving nanoparticle-based drug and gene delivery. *Advanced drug delivery reviews, 99*, 28-51.

Sulistio, A., Widjaya, A., Blencowe, A., Zhang, X., & Qiao, G. (2011). Star polymers composed entirely of amino acid building blocks: a route towards stereospecific, biodegradable and hierarchically functionalized stars. *Chemical Communications, 47*(4), 1151-1153.

Sun, P., Huang, W., Kang, L., Jin, M., Fan, B., Jin, H., . . . Gao, Z. (2017). siRNA-loaded poly (histidine-arginine) 6-modified chitosan nanoparticle with enhanced cell-penetrating and endosomal escape capacities for suppressing breast tumor metastasis. *International journal of nanomedicine, 12*, 3221.

Teo, J., McCarroll, J. A., Boyer, C., Youkhana, J., Sagnella, S. M., Duong, H. T., . . . Davis, T. P. (2016). A rationally optimized nanoparticle system for the delivery of RNA interference therapeutics into pancreatic tumors in vivo. *Biomacromolecules, 17*(7), 2337-2351.

Teo, P. Y., Yang, C., Hedrick, J. L., Engler, A. C., Coady, D. J., Ghaem-Maghami, S., . . . Yang, Y. Y. (2013). Hydrophobic modification of low molecular weight polyethylenimine for improved gene transfection. *Biomaterials, 34*(32), 7971-7979.

Terashima, T., Nomura, A., Ito, M., Ouchi, M., & Sawamoto, M. (2011). Star-Polymer-Catalyzed Living Radical Polymerization: Microgel-Core Reaction Vessel by Tandem Catalyst Interchange. *Angewandte Chemie, 123*(34), 8038-8041.

Tunca, U., Ozyurek, Z., Erdogan, T., & Hizal, G. (2004). Novel miktofunctional initiator for the preparation of an ABC-type miktoarm star polymer via a combination of controlled polymerization techniques. *Journal of Polymer Science Part A: Polymer Chemistry, 42*(17), 4228-4236.

Uhl, C., Gao, Y., Zhou, S., & Liu, Y. (2018). The shape effect on polymer nanoparticle transport in a blood vessel. *RSC advances, 8*(15), 8089-8100.

Vandamme, C., Adjali, O., & Mingozzi, F. (2017). Unraveling the complex story of immune responses to AAV vectors trial after trial. *Human gene therapy, 28*(11), 1061-1074.

Vermeulen, A., Behlen, L., Reynolds, A., Wolfson, A., Marshall, W. S., Karpilow, J., & Khvorova, A. (2005). The contributions of dsRNA structure to Dicer specificity and efficiency. *Rna, 11*(5), 674-682.

Veronese, F. M., & Pasut, G. (2005). PEGylation, successful approach to drug delivery. *Drug discovery today, 10*(21), 1451-1458.

Victor, R. (2014). Poly (2-oxazoline) s as materials for biomedical applications. *Journal of Materials Science: Materials in Medicine, 25*(5), 1211-1225.

von Roemeling, C., Jiang, W., Chan, C. K., Weissman, I. L., & Kim, B. Y. (2017). Breaking down the barriers to precision cancer nanomedicine. *Trends in biotechnology, 35*(2), 159-171.

Wang, F., Zuroske, T., & Watts, J. K. (2020). RNA therapeutics on the rise. *Nat. Rev. Drug Discov, 19*, 441-442.

Wang, Y., Juranek, S., Li, H., Sheng, G., Wardle, G. S., Tuschl, T., & Patel, D. J. (2009). Nucleation, propagation and cleavage of target RNAs in Ago silencing complexes. *Nature, 461*(7265), 754-761.

Weber, C., Becer, C. R., Hoogenboom, R., & Schubert, U. S. (2009). Lower critical solution temperature behavior of comb and graft shaped poly [oligo (2-ethyl-2-oxazoline) methacrylate] s. *Macromolecules, 42*(8), 2965-2971.

Wilhelm, S., Tavares, A. J., Dai, Q., Ohta, S., Audet, J., Dvorak, H. F., & Chan, W. C. (2016). Analysis of nanoparticle delivery to tumours. *Nature reviews materials, 1*(5), 1-12.

Willoughby, J. L., Chan, A., Sehgal, A., Butler, J. S., Nair, J. K., Racie, T., . . . Yucius, K. (2018). Evaluation of GalNAc-siRNA conjugate activity in pre-clinical animal models with reduced asialoglycoprotein receptor expression. *Molecular therapy, 26*(1), 105-114.

Wood, H. (2018). FDA approves patisiran to treat hereditary transthyretin amyloidosis. In: Nature Publishing Group.

Wu, W., Wang, W., & Li, J. (2015). Star polymers: Advances in biomedical applications. *Progress in polymer science, 46*, 55-85.

Xu, F., Zhang, Z., Ping, Y., Li, J., Kang, E., & Neoh, K. (2009). Star-shaped cationic polymers by atom transfer radical polymerization from β-cyclodextrin cores for nonviral gene delivery. *Biomacromolecules, 10*(2), 285-293.

Yang, C., Gao, S., Dagnæs-Hansen, F., Jakobsen, M., & Kjems, J. (2017). Impact of PEG chain length on the physical properties and bioactivity of PEGylated chitosan/siRNA nanoparticles in vitro and in vivo. *ACS applied materials & interfaces, 9*(14), 12203-12216.

Yang, Q., Jones, S. W., Parker, C. L., Zamboni, W. C., Bear, J. E., & Lai, S. K. (2014). Evading immune cell uptake and clearance requires PEG grafting at densities substantially exceeding the minimum for brush conformation. *Molecular pharmaceutics, 11*(4), 1250-1258.

Zamore, P. D., Tuschl, T., Sharp, P. A., & Bartel, D. P. (2000). RNAi: double-stranded RNA directs the ATP-dependent cleavage of mRNA at 21 to 23 nucleotide intervals. *Cell, 101*(1), 25-33.

Zhang, P., Sun, F., Liu, S., & Jiang, S. (2016). Anti-PEG antibodies in the clinic: Current issues and beyond PEGylation. *Journal of Controlled Release, 244*, 184-193.

Zhang, P., Zhang, Z., Wang, D., Hao, J., & Cui, J. (2020). Monodispersity of Poly (ethylene glycol) Matters for Low-Fouling Coatings. *ACS Macro Letters, 9*(10), 1478-1482.

Zintchenko, A., Philipp, A., Dehshahri, A., & Wagner, E. (2008). Simple modifications of branched PEI lead to highly efficient siRNA carriers with low toxicity. *Bioconjugate chemistry, 19*(7), 1448-1455.

Zlatev, I., Castoreno, A., Brown, C. R., Qin, J., Waldron, S., Schlegel, M. K., . . . Gupta, S. (2018). Reversal of siRNA-mediated gene silencing in vivo. *Nature biotechnology, 36*(6), 509-511.

Zuckerman, J. E., & Davis, M. E. (2015). Clinical experiences with systemically administered siRNA-based therapeutics in cancer. *Nature reviews Drug discovery, 14*(12), 843-856.

APPENDIX A

siRNA COMPLEX FORMATION

Figure A1. Agarose gel electropherogram of PEG$_{(5K)}$-b-P(AEAEMA)$_{40}$-siRNA complexes. Lane 1: DNA marker; Lane 2: naked siRNA; Lanes 3-7: complexes prepared at N/P of 1, 2, 3, 4 and 5, respectively.

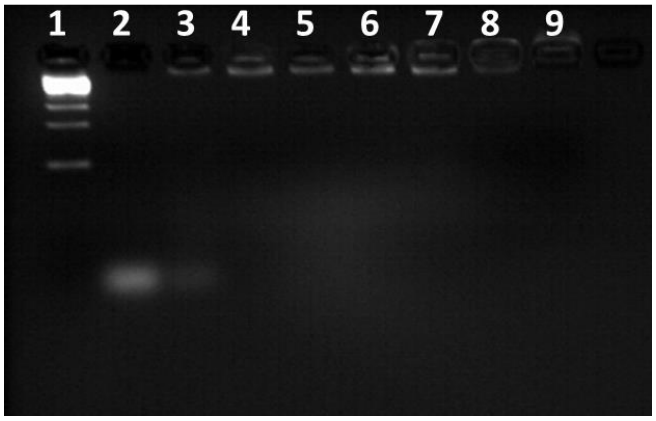

Figure A2. Agarose gel electropherogram of P(OEGMA)$_{(5K)}$-b-P(AEAEMA)$_{40}$-siRNA complexes. Lane 1: DNA marker; Lane 2: naked siRNA; Lanes 3-9: complexes prepared at N/P of 1, 2, 3, 4, 5, 10 and 30, respectively.

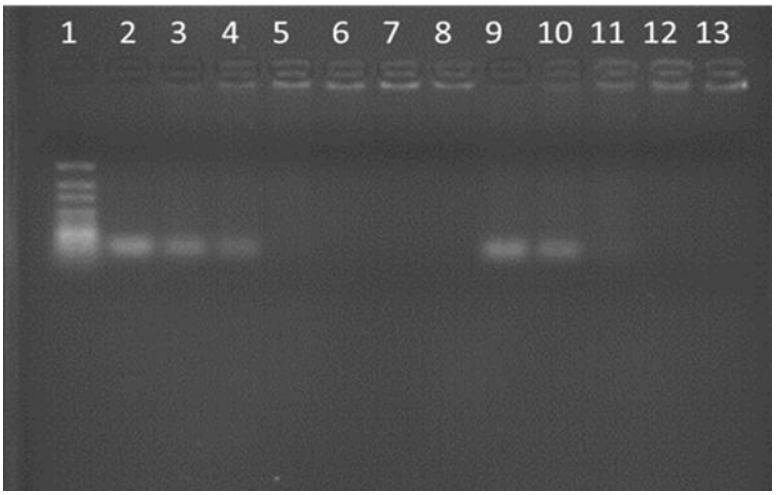

Figure A3. Agarose gel electropherogram of $P(OEGMA)_{20}$-b-$P(AEAEMA)_{48}$-siRNA and $P(OEGMA)_{43}$-b-$P(AEAEMA)_{60}$-siRNA complexes. Lane 1: DNA marker; Lane 2: naked siRNA; Lanes 3-8: $P(OEGMA)_{20}$-b-$P(AEAEMA)_{48}$-siRNA complexes prepared at N/P of 1, 2, 3, 4, 5, 10 and 30, respectively. Lane 9-13: $P(OEGMA)_{43}$-b-$P(AEAEMA)_{60}$-siRNA complexes prepared at N/P of 1, 2, 3, 4 and 5, respectively.

APPENDIX B

ELECTRON MICROSCOPY IMAGES

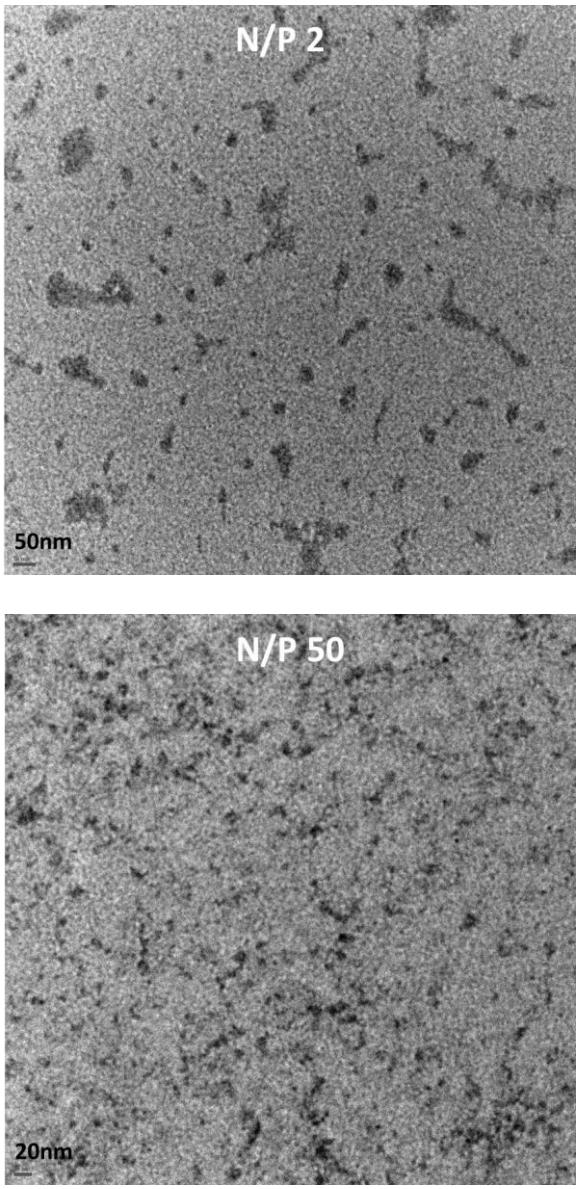

Figure B1. TEM images of $P(OEGMA)_{43}$-*b*-$P(AEAEMA)_{45}$-siRNA complexes at N/P of 2 and 50.

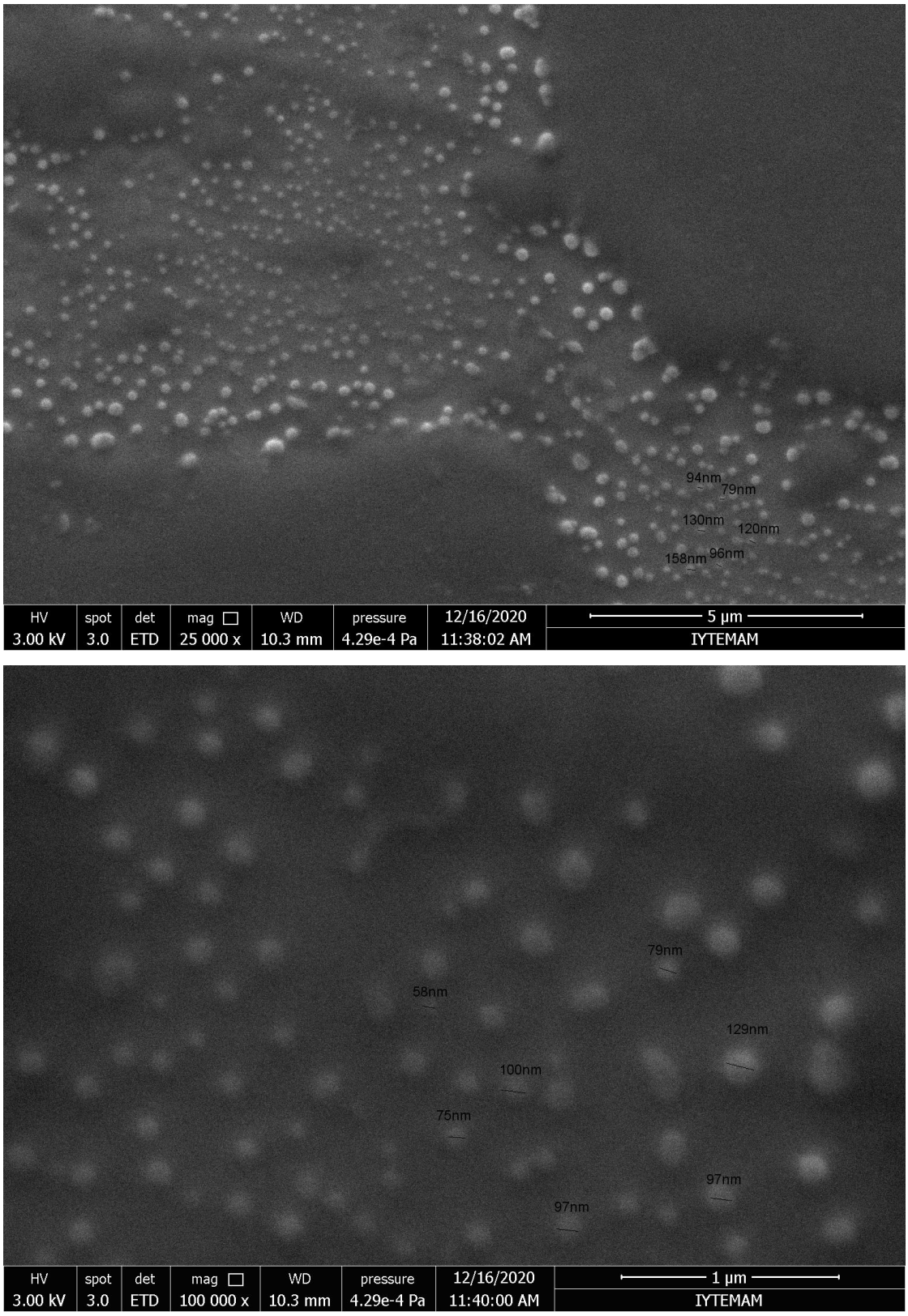

Figure B2. SEM images of P(OEGMA)$_{43}$-*b*-P(AEAEMA)$_{45}$-siRNA complexes at N/P of 50.

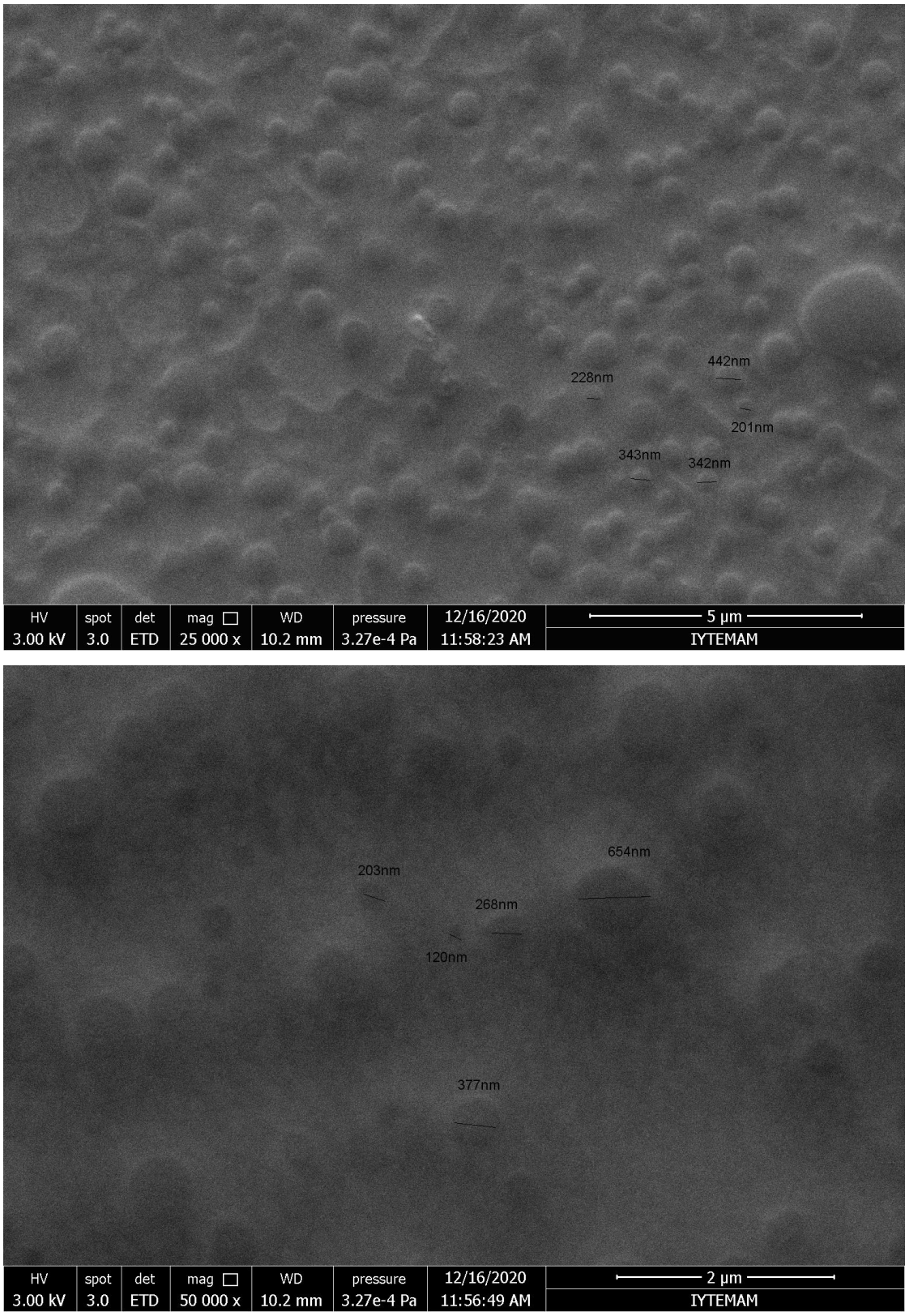

Figure B3. SEM images of P(AEAEMA)$_{40}$-b-P(OEtOxMA)$_{38}$-siRNA complexes at N/P of 50.

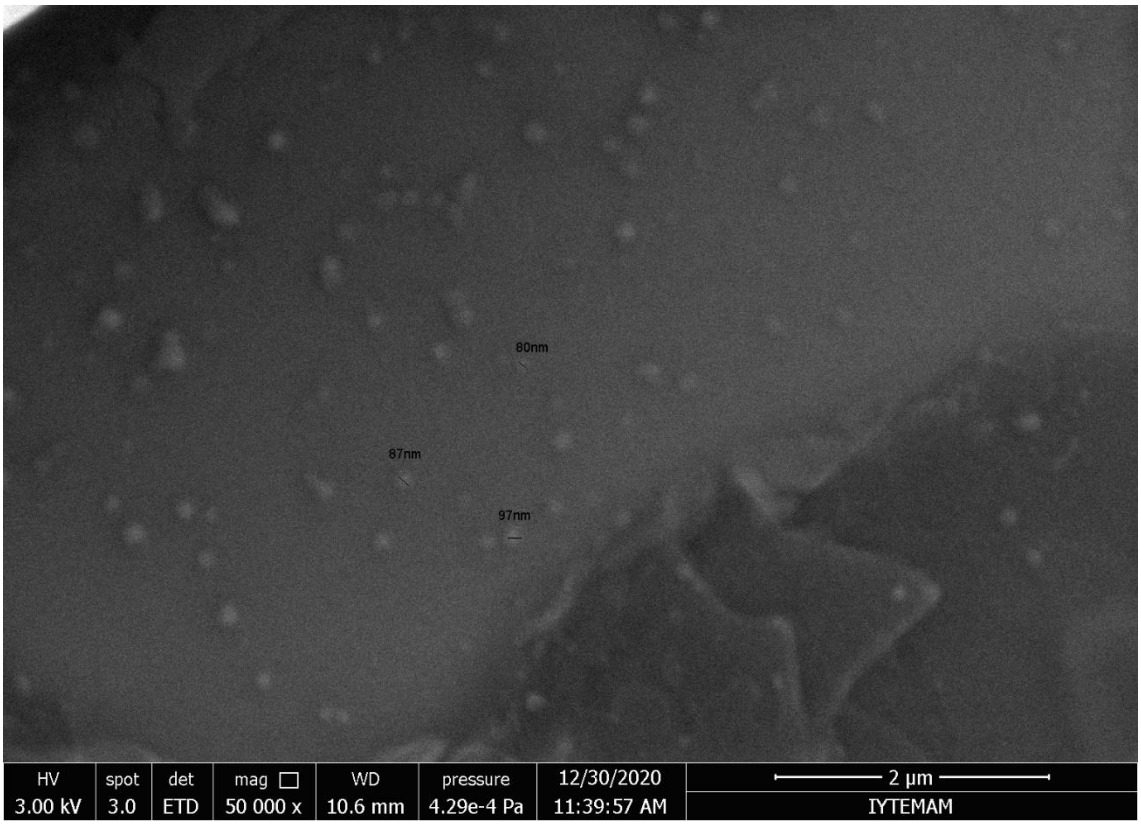

Figure B4. SEM images of SP1-siRNA complexes at N/P of 50.